INSTITUTIONEN FÖR TEKNISK VATTENRESURSLÄRA
LUNDS UNIVERSITET, TEKNISKA OCH NATURVETENSKAPLIGA HÖGSKOLAN

DEPARTMENT OF WATER RESOURCES ENGINEERING
LUND UNIVERSITY, INSTITUTE OF SCIENCE AND TECHNOLOGY

QUANTIFICATION OF
BEACH PROFILE CHANGE

by

Magnus Larson

DTIC
ELECTE
S D
MAY 1 9 1988
H

Report No. 1008

Lund, Sweden, 1988

QUANTIFICATION OF BEACH PROFILE CHANGE

by
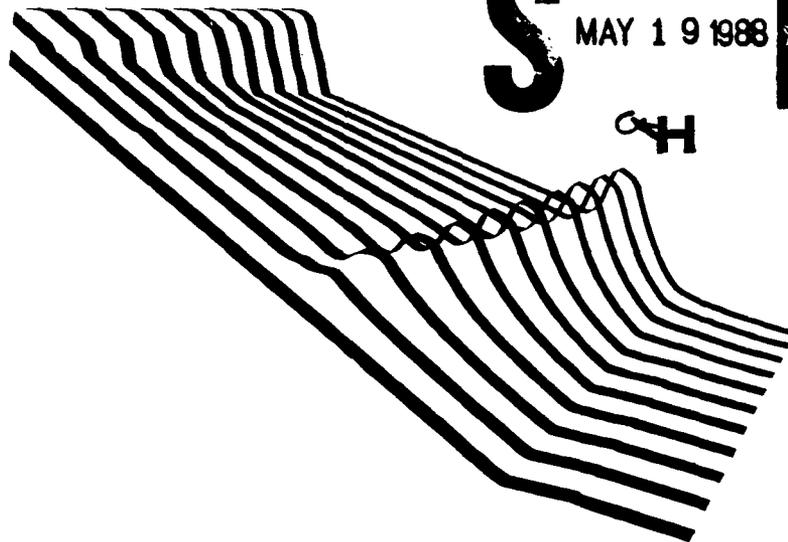
Magnus Larson

DTIC
ELECTE
MAY 1 9 1988
S D
H

88 5 17 005

ABSTRACT

An engineering numerical model is presented for simulating beach
profile change in the surf zone produced by wave-induced cross-
shore sand transport. The model simulates the dynamics of
macroscale profile change, such as growth and movement of
breakpoint bars and berms.

The foundation for the development of the numerical model was two
large wave tank experiments consisting altogether of 42 cases
with different incident wave conditions, median grain size, and
initial beach shape. An extensive analysis was made to define and
quantify parameters describing profile change and relate these
parameters to wave and sand characteristics.

The model was developed using transport rate relationships
inferred from profile change measured in the large wave tanks.
Distributions of the net transport rate were obtained by in-
tegrating the sand conservation equation across pairs of profiles
separated in time. Semi-empirical transport rate relationships
were developed for different regions of the profile.

The beach profile change model was calibrated and verified with
the prototype-scale laboratory data. The model was also applied
to simulate field beach profile change measured in five storm
events and good agreement was found. Beach profile evolution in
the vicinity of a seawall and the adjustment of a beach fill to
incident waves were other cases studied with the model.

Keywords: Beach profile change, cross-shore sand transport,
          numerical model, bar formation, large wave tank,
          seawall, beach fill

PREFACE

This study was conducted in part at the Coastal Engineering Research Center (CERC), U.S. Army Engineer Waterways Experiment Station, Vicksburg, Mississippi, and in part at the Department of Water Resources Engineering, Institute of Science and Technology, University of Lund, Lund, Sweden.

The work at the University of Lund was performed under the supervision of Professor Dr. Gunnar Lindh, Department of Water Resources Engineering, whereas the portion of the study performed at CERC was under the supervision of Dr. Nicholas C. Kraus, Senior Research Scientist, Research Division.

The study at CERC was conducted from 23 June 1986 through 31 July 1987 under the work unit Surf Zone Sediment Transport Processes, Shore Protection and Restoration Program. The work was funded through the U.S. Army Research, Development and Standardization Group, UK, under contract No. DAJA-86-C-0046. The CERC portion of the investigation was under the general direction of Dr. James R. Houston, Chief, CERC; Mr. H. Lee Butler, Chief, Research Division (CR), CERC.

The following is a list of technical articles written as an outcome of this investigation. These articles constitute to a varying degree the foundation of the work contained herein and were written simultaneously with this thesis. Accordingly, most are in the process of being published.

Larson, M., and Kraus, N. C. 1988a. "Beach Profile Change, 1: Morphology," submitted for publication.

Larson, M., and Kraus, N. C. 1988b. "Beach Profile Change, 2: Net Cross-Shore Sand Transport Rate," submitted for publication.

Larson, M., and Kraus, N. C. 1988c. "Beach Profile Change, 3: Numerical Model," submitted for publication.

1

Larson, M., Kraus, N. C., and Sunamura, T. 1988. "Beach Profile Change: Morphology, Transport Rate, and Numerical Simulation," Proceedings of the 21th Coastal Engineering Conference, American Society of Civil Engineers, in preparation.

Kraus, N. C., and Larson, M. 1988a. "Beach Profile Change Measured in the Tank for Large Waves, 1956-1957 and 1962," Technical Report CERC-88-00 , Coastal Engineering Research Center, U.S. Army Engineer Waterways Experiment Station, Vicksburg, MS, in press.

Kraus, N. C., and Larson, M. 1988b. "Prediction of Initial Profile Adjustment of Nourished Beaches to Wave Action," Proceedings of Beach Preservation Technology '88, American Shore and Beach Preservation Association, in press.

ACKNOWLEDGEMENTS

3

4

CONTENTS

7

LIST OF FIGURES

9

10

11

12

14

LIST OF TABLES

QUANTIFICATION OF BEACH PROFILE CHANGE

PART I: INTRODUCTION

Problem Statement and Objectives

The study of beach profile change in the broad sense
encompasses nearshore processes that shape the beach on all
spatial and temporal scales. Beach profile change is a phenome-
non of fundamental interest and, as such, has been studied by
geologists, oceanographers, and coastal engineers.

In coastal engineering, quantitative understanding of beach
profile change is pursued mainly to allow prediction of beach
evolution in the vicinity of planned or existing engineering
projects. Two types of coastal engineering problems of par-
ticular importance for which predictive tools are needed are
beach and dune erosion that occurs under storm waves and high
water levels, and adjustment of beach fill to long-term wave
action. The time scale associated with storm-induced erosion is
on the order of 1 to 3 days and depends on the level and duration
of the storm surge as well as the waves, whereas the time scale
of beach fill adjustment is several weeks to several months and
depends on season of placement, fill material, and wave climate
at the coast.

It is often convenient to separate nearshore sediment
movement into two components, longshore sediment transport and
cross-shore sediment transport, although this separation is not
always valid in a strict sense. Longshore sediment transport
figures prominently in situations involving loss of sediment
supply, such of damming of rivers, and in impoundment at struc-
tures such as groins and jetties. In these cases longshore

16

transport is the major process governing nearshore topography change and cannot be neglected.

For beaches located away from structures, inlets, and river mouths, it may be appropriate to neglect longshore transport as a first approximation, i.e., assume the gradient of the longshore transport rate is negligibly small at the site. In this case, cross-shore transport will determine the change in beach profile contours. This assumption will be made in this investigation: longshore sediment transport is neglected and profile change produced solely by cross-shore sediment transport is considered.

The ultimate goal of this investigation is development of a numerical model to predict beach profile change produced by wave action. Numerous such models have been reported in the literature; however, apart from the present work only one highly schematized numerical model has been considered sufficiently accurate to be of engineering use. Most efforts appear to have failed because the level of detail attempted was beyond the state of knowledge of the physical processes involved. At present, knowledge is very limited on the collective motion of sediment particles in spatially varying flows of oscillatory currents, wave-induced mean current, and turbulence fields of breaking waves. Numerous other complicating factors, such as the complex fluid motion over an irregular bottom, and absence of rigorous descriptions of broken waves and sediment-sediment interaction, also make the problem of computing sediment transport and resultant beach profile change essentially impossible if a first-principles approach at the microscale is taken.

On the other hand, despite the incredibly complex and diverse processes and factors involved, beach profile change if viewed on the macroscale is remarkably smooth and simple. Certain prominent features, such as bars, troughs, and berms go through cycles of formation, growth, movement, and erasure with a morphodynamic pattern that has been reasonably well described by a number of qualitative conceptual models. The question can then

17

be asked whether it is not possible to develop a quantitative (numerical) model of beach profile change based on empirically determined global relations for the wave-induced net cross-shore sediment (sand) transport rate that can be inferred from the smooth and regular change observed to occur during beach profile evolution. Development of such a model is the subject of this investigation.

Procedure Used

The principal physical mechanisms which determine beach profile change must be quantitatively described to model the profile response numerically. For this purpose it is necessary to study profile evolution under varying waves, sand characteristics, and profile shape. However, to establish cause and effect relationships between the governing factors and the profile response, it must be possible to clearly delineate these relationships. Laboratory facilities provide an environment where such investigations may be carried out efficiently, while allowing for data sampling at almost any spatial or temporal scale. The difficult problem of transforming observations made under scale distortion is eliminated if experiments are performed at the scale of the prototype, i.e., at a sufficiently large scale as to satisfactorily represent the interaction between fluid forces and sand grains that produces significant sand transport in the field.

Use of field profile data as a basis for developing a numerical model is extremely difficult due to the complexity and randomness of naturally occurring conditions and cost of data collection. Ultimately a numerical model must be verified against field data but in the process of development of the model laboratory data can provide considerably more insight into the relative influence of the factors producing the profile change.

18

Study of these individual factors implicitly assumes the validity
of the superposition principle for application of the model to
the general case. For example, examination of the effect of
water level variation on profile evolution under fixed incident
waves isolates the influence of this factor and allows under-
standing of the related physical processes involved. A combina-
tion of such observations constitute the foundation for a
numerical model which is used in a predictive mode for varying
water level and wave conditions, even though these factors have
been evaluated separately. Consequently, careful data analysis
is the basis for many assumptions and empirical relationships
employed in the numerical model developed here and the first
logical step towards understanding beach profile change by this
procedure.

From an engineering point of view it is of considerable
importance to quantify properties related to beach profile
change. This regards both geometric parameters such as bar
volume and depth to bar crest, as well as more complex quantities
such as net cross-shore sand transport rates. Any structure or
activity extending into the nearshore region is influenced by and
influences the evolution of the beach profile, thus requiring
quantitative estimates of profile change under various environ-
mental and design conditions. A thorough analysis of different
geometric characteristics of the profile and their dependence on
the wave and sand properties is in this respect valuable.
Through this analysis the important processes shaping the beach
and generating different morphologic features may be clarified,
forming the conceptual framework for a numerical model.

A fundamental assumption of this study is that beach profile
change is mainly governed by breaking of short-period waves (in
the approximate range of 3-20 sec). No attempt has been made to
include the effect of long-period waves, such as partially
standing waves or infragravity waves, regarding profile evolu-
tion, as no adequate data on profile change are available that

permit firm conclusions to be made. Recent field investigations have indicated that, in some cases, infragravity or long-period wave energy can be larger near the shoreline than that of the existing short-period waves. This dominance of the wave energy spectrum in very shallow water by long-period waves is expected to play an important role in beach profile processes on the shore face and, possibly, the inner surf zone. However, no relationship between beach profile change and infragravity waves exists at present due to lack of data. When such data become available, superposition should allow calculation of profile change under both short- and long-period waves.

The main purpose of the data analysis is not to derive widely applicable relationships for geometric properties of the profile, but to identify the important factors governing profile change. These factors will be integral parts in the conceptual foundation underlying the numerical model development. In some cases however, empirical relationships derived from the data are used directly in the model if general conclusions about the behavior of the quantity can be made.

Basic Terminology

Nomenclature associated with the beach profile and nearshore region is presented which is used throughout the report. Terms defined in the Shore Protection Manual (SPM 1984) have been adapted to a large extent. However, for some quantities a slightly different description is employed that is better suited for nearshore processes as related to beach profile change. Figures 1a and 1b are definition sketches pertaining to beach profile morphology and nearshore wave dynamics, respectively. The portion of the beach profile of interest here spans across-shore from the dunes to the seaward end of the nearshore zone.

20

A

COASTAL AREA

NEARSHORE ZONE

COAST | BEACH OR SHORE | |

BACKSHORE | INSHORE | OFFSHORE

DUNE

—FORESHORE

BERM | STEP | BREAKERS

HWL

LWL

BAR

TROUGH

HWL HIGH WATER LEVEL
LWL LOW WATER LEVEL

B

SWASH ZONE | SURF ZONE | OFFSHORE ZONE

LIMIT OF UPRUSH

BROKEN WAVES

INNER BREAKERS | OUTER BREAKERS

RE-FORMED WAVES

RUNUP | RP | PP | BP | RP | PP | BP | STILL-WATER LEVEL

BACKRUSH

BREAKER-DEPTH

BEACH FACE | INNER BAR | OUTER BAR | DEEP BAR

BP BREAK POINT
PP PLUNGE POINT
RP REFORMATION POINT

Figure 1. Definition sketch of the beach profile: (a) morphology, and (b) nearshore wave dynamics (after Shore Protection Manual 1984)

21

Profile morphology

As waves approach the beach from deep water they enter the nearshore zone. The seaward boundary of the nearshore zone is dynamic and for our purpose is considered to be the depth at which waves begin to shoal upward. The shoreward boundary of wave action is also dynamic and is at the limit of wave runup, located at the intersection between the maximum water level and the beach profile. A gently sloping bottom will cause a gradual shoaling of the waves, leading to an increase in wave height and finally to breaking at a point where the wave height is about equal to the water depth. The region seaward of wave breaking is denoted as the offshore; the inshore encompasses the surf zone, i.e., that portion of the profile exposed to breaking and broken waves. The broken waves propagate with large energy dissipation through turbulence, initiating and maintaining sand movement. At the beach face, the remaining wave energy is expended by a runup bore as water rushes up the profile.

The flat area shoreward of the beach face is called the backshore and is only exposed during severe wave conditions or when the water level is unusually high. On the backshore one or several berms may exist, which are accretionary features where material has been deposited by wave action. The term "accretionary" refers to features generated by sand transport directed onshore. A step often develops immediately seaward of a berm where the slope depends on the properties of the runup bore and the sand grains. Under storm wave action a scarp may also form; here, the term "step" will be used to denote both a scarp and a step. On many beaches a line of dunes is present shoreward of the backshore which consists of large ridges of unconsolidated sand that have been transported by wind from the backshore.

A bar is a depositional feature formed by sand that was transported from neighboring areas. Several bars may appear along a beach profile, often having a distinct trough on the

22

shoreward side. Bars are highly dynamic features that respond to
the existing wave climate by changing form and translating
across-shore, but at the same time bars influence the waves
incident upon them. If a bar was created during an episode of
high waves, it may be located at such great depth that very
little or almost no sand transport activity takes place until
another period of high waves occurs. Some transport from the bar
caused by shoaling waves may take place, but the time scale of
this process is considerably longer than if the bar is located
close to the surf zone and breaking or broken waves.

Nearshore waves

The above-discussed terminology is mainly related to the
various regions and features of the beach profile. Nearshore
waves are also described by specialized terminology (Figure 1b).
Again, some definitions are not unique and describe quantities
that change in space and time. The region between the break
point and the limit of the backrush where broken waves prevail is
called the surf zone. The swash zone extends approximately from
the limit of the backrush to the maximum point of uprush,
coinciding with the beach face. As waves break and propagate
toward shore, reformation may occur depending on the profile
shape; that is, the translatory broken wave form reverts to an
oscillatory wave. This oscillatory wave will break again as it
reaches sufficiently shallow water, transforming into a broken
wave with considerable energy dissipation. The region where
broken waves have reformed to oscillatory waves is called the
reformation zone, and the point where this occurs is the wave
reformation point.

The break point is located where the maximum particle
velocity of the wave exceeds the wave celerity and the front face
of the wave becomes vertical. As a wave breaks, the crest falls
over into the base of the wave accompanied by large amount of

energy dissipation. If the breaking waves are of the plunging type (Galvin 1972), the point of impingement is easily recognized and denoted as the plunge point. For spilling breakers, however, the plunge point concept is not commonly used but such a point could be defined using the location of maximum energy dissipation. This definition is in accordance with the conditions prevailing at the plunge point for a plunging breaker.

A beach profile exposed to constant wave and water level conditions over a sufficiently long time interval will attain a fairly stable shape known as the equilibrium profile. On a beach in nature, where complex wave and water level variations exist, an equilibrium profile may never develop or, if so, only for a short time before the waves or water level again change. However, the equilibrium concept remains useful since it provides information of the amount of sand that has to be redistributed within the profile to attain the natural shape for a specific set of wave conditions. The equilibrium profile is in general considered to be a function of sand and wave characteristics.

24

PART II: LITERATURE REVIEW

From the earliest investigations of beach morphology, the study of profile change has focused to a large extent upon the properties of bars. A wide range of morphologic features have been classified as bar formations by different authors, and different terminology is used to denote the same feature. The literature on beach profile change is vast, and this chapter is intended to give a chronological survey of results relevant to the present work.

Literature

Many of the first contributions to the study of bars were made by German researchers around the beginning of this century. Lehmann (1884) noted the role of breaking waves in suspending sand and found that profile change could occur very rapidly with respect to offshore bar movement. Otto (1911) and Hartnack (1924) measured geometric properties of bars in the Baltic Sea, such as depth to bar crest, distance from shoreline to bar crest, and bar slopes. Hartnack (1924) pointed out the importance of breaking waves in the process of bar formation and noted that the distance between bar crests increased with distance from shore for multiple bars and that the depth to bar crest increased correspondingly.

Systematic laboratory modeling of beach profile evolution appears to have been first applied by Meyer (1936), who mainly investigated scaling effects in movable bed experiments. He also derived an empirical relationship between beach slope and wave steepness. Waters (1939) performed pioneering work on the characteristic response of the beach profile to wave action, and classified profiles as ordinary or storm type. He concluded that wave steepness can be used to determine the type of beach profile

25

that developed under a set of specific wave conditions. The process of sediment sorting along the profile was demonstrated in the experiments, in which the coarser material remained near the plunge point and finer material moved offshore.

Bagnold (1940) studied beach profile evolution in small-scale laboratory experiments by use of rather coarse material (0.5-7.0 mm), resulting in accretionary profiles with berm build-up. He found that foreshore slope was independent of the wave height and mainly a function of grain size. However, the equilibrium height of the berm was linearly related to wave height. The effect of a seawall on the beach profile was investigated by allowing waves to reach the end of the tank. By varying the water level, a tide was simulated, and in other experiments a varying wave height was employed.

Evans (1940) studied bars and troughs (named balls and lows by Evans) along the eastern shore of Lake Michigan and concluded these features to be the result of plunging breakers. He regarded the bar and trough to form a unit with the trough always located shoreward of the bar. If the profile slope was mild so that several break points appeared, a series of bars and troughs would develop. Also, a change in wave conditions could result in a change in bar shape and a migration of the bar seaward or shoreward. A decreasing water level would cause the inner-most bar to migrate onshore and take the form of a subaqueous dune, whereas an increase in water level would allow a new bar system to develop inshore and the most seaward bars would become fossilized.

In connection with amphibious landing operations during World War II, Keulegan (1945) experimentally obtained simple relations for predicting depth to bar crest and trough depth. He found the ratio between trough and crest depths to be approximately constant and independent of wave steepness. Important contributions to the basic understanding of the physics of beach profile change were also made through further laboratory experi-

26

ments by Keulegan (1948). The objective of the study was to determine the shape and characteristics of bars and how they were molded by the incident waves. He recognized the surf zone as being the most active area of beach profile change and the breaking waves as the cause of bar formation. The location of the maximum sand transport rate, measured by trap, was found to be close to the break point, and the transport rate showed a good correlation with the wave height envelope. Keulegan (1948) noted three distinct regions along the profile where the transport properties were different from a morphologic perspective. A gentler initial beach slope implied a longer time before the equilibrium profile was attained for fixed wave conditions. For a constant wave steepness, an increase in wave height moved the bar seaward, whereas for a constant wave height an increase in wave steepness (decrease in wave period) moved the bar shoreward. He noted that bars developed in the laboratory experiments were shorter and more peaked than bars in the field and attributed this difference to variability in the wave climate on natural beaches.

King and Williams (1949), in work also connected with the war effort, distinguished between bars generated on non-tidal beaches and bars occurring on beaches with a marked tidal variation (called ridge and runnel systems by them). They assumed that non-breaking waves moved sand shoreward and broken waves moved sand seaward. Field observations from the Mediterranean confirmed the main ideas of this conceptualization. In laboratory experiments the cross-shore transport rate was measured with traps, showing a maximum transport rate located around the break point. Furthermore, the term "breakpoint bar" was introduced whereas berm formations were denoted as "swash bars." The slope of the berm was related to the wavelength, where a longer wave period produced a more gentle slope. King and Williams (1949) hypothesized that ridge and runnel systems

27

were not created by breaking waves, but were a result of swash processes.

Johnson (1949) gave an often-cited review of scale effects in movable-bed modeling and referenced the criterion for distinguishing ordinary and storm profiles given by Waters (1939).

Shepard (1950) made profile surveys along the pier at Scripps Institution of Oceanography, La Jolla, California, in 1937 and 1938, and discussed the origin of troughs. He suggested that the combination of plunging breakers and longshore currents were the primary causes. He also showed that the trough and crest depths depended on breaker height. Large bars formed somewhat seaward of the plunge point of the larger breakers, and the ratios for the trough to crest depth were smaller than those found by Keulegan (1948) in laboratory experiments. Shepard (1950) also observed the time scale of beach profile response to the incident wave climate and concluded that the profile change was better related to the existing wave height than to the greatest wave height from the preceding five days.

Bascom (1951) studied the slope of the foreshore along the Pacific coast and attempted to relate it to grain size. A larger grain size implied a steeper foreshore slope. He also determined a trend in variation in grain size across the profile that is much cited in the literature. A bimodal distribution was found with peaks at the summer berm and at the step of the foreshore. The largest particles were found on the beach face close to the limit of the backrush, and the grain size decreased in the seaward direction.

Scott (1954) modified the wave steepness criterion of Waters (1939) for distinguishing between ordinary (summer) and storm profiles, based on his laboratory experiments. He also found that the rate of profile change was greater if the initial profile was further from equilibrium shape, and he recognized the importance of wave-induced turbulence for promoting bar forma-

tion. Some analysis of sediment stratification and packing along the profile was carried out.

Rector (1954) investigated the shape of the equilibrium beach profile in a laboratory study. Equations were developed for profile shapes in two sections separated at the base of the foreshore. Coefficients in the equilibrium profile equation were a function of deepwater wave steepness and grain size normalized by the deepwater wavelength. An empirical relationship was derived for determining the maximum depth of profile adjustment as a function of the two parameters. These parameters were also used to predict net sand transport direction.

Watts (1954) and Watts and Dearduff (1954) studied the effect on the beach profile of varying wave period and water level, respectively. A varying wave period reduced the bar and trough system as compared to waves of constant period, but only slightly affected beach slope in the foreshore and offshore. The influence of the water level variation for the range tested (at most 20% variation in water level with respect to the tank depth in the horizontal portion) was small, producing essentially the same foreshore and offshore slopes. However, the active profile translated landward for the tidal variation, allowing the waves to attack at a higher level and thus activating a larger portion of the profile.

Bruun (1954) developed a predictive equation for the equilibrium beach profile by studying beaches along the Danish North Sea coast and the California coast. The equilibrium shape (depth) followed a power curve with distance offshore, with the power evaluated as 2/3.

Ippen and Eagleson (1955) experimentally and theoretically investigated sorting of sediments by wave shoaling on a plane beach. The movement of single spherical particles was investigated and a "null point" was found on the beach where the particle was stable for the specific grain size.

3   29

Saville (1957) was the first to employ a large wave tank capable of reproducing near-prototype wave and beach conditions, and he studied equilibrium beach profiles and model scale effects. Waves with very low steepness were found to produce storm profiles, contrary to results from small-scale experiments (Waters 1939, Scott 1954). Comparisons were made between the large wave tank studies and small-scale experiments, but no reliable relationship between prototype and model was obtained. The data set from this experiment is used extensively in the present work.

Caldwell (1959) presented a summary of the effects of storm (northeaster) and hurricane wave attack on natural beach profiles for a number of storm events.

McKee and Sterrett (1961) investigated cross-stratification patterns in bars by spreading layers of magnetite over the sand.

Kemp (1961) introduced the concept of "phase difference," referring to the relation between time of uprush and wave period. He assumed the transition from a step (ordinary) to a bar (storm) profile to be a function of the phase difference and to occur roughly if the time of uprush was equal to the wave period.

Bruun (1962) applied his empirical equation (Bruun 1954) for an equilibrium beach profile to estimate the amount of erosion occurring along the Florida coast as a result of long-term sea-level rise.

Bagnold (1963, 1966) developed formulas for calculating sediment transport rates, including cross-shore transport, based on a wave energy approach, and distinguishing between bed load and suspended load. This work has been refined and widely applied by others (Bailard and Inman 1981, Bailard 1982, Stive 1987). Bed load transport occurs through the contact between individual grains whereas in suspended load transport the grains are supported by the diffusion of upward eddy momentum. A superimposed steady current moves the grains along the bed. Inman and Bagnold (1963) derived an expression for the local

30

equilibrium slope of a beach based on wave energy considerations. The equilibrium slope was a function of the angle of repose and the ratio between energy losses at the bed during offshore- and onshore-directed flow.

Eagleson, Glenne, and Dracup (1963) studied equilibrium profiles in the region seaward of the influence of breaking waves. They pointed out the importance of bed load for determining equilibrium conditions and used equations for particle stability to establish a classification of beach profile shapes.

Iwagaki and Noda (1963) derived a graphically presented criterion for predicting the appearance of bars based on two nondimensional parameters, deepwater wave steepness, and ratio between deepwater wave height and median grain size. The change in character of breaking waves due to profile evolution in time was discussed. The importance of suspended load was believed to be indicated through the grain size, this quantity emerging as a significant factor in beach profile change.

Zenkovich (1967) presented a summary of a number of theories suggested by various authors for the formation of bars.

Wells (1967) proposed an expression for the location of a nodal line of the net cross-shore sand transport based on the horizontal velocity skewness being zero, neglecting gravity, and derived for the offshore, outside the limit of breaking waves. Seaward of the nodal line material could erode and shoreward-moving sand could accumulate, depending on the sign of the velocity skewness.

Berg and Duane (1968) studied the behavior of beach fills during field conditions and suggested the use of coarse, well-sorted sediment for the borrow material to achieve a more stable fill. The mean diameter of the grains in the profile roughly decreased with depth with the coarsest material appearing at the water line (Bascom 1951, Scott 1954).

Mothersill (1970) found evidence through grain size analysis that longshore bars are formed by plunging waves and a seaward-

31

directed undertow (Dally 1987). Sediment samples taken in
troughs were coarser, having the properties of winnowed residue,
whereas samples taken from bars were finer grained, having the
characteristics of sediments that had been winnowed out and then
re-deposited.

Sonu (1969) distinguished six major types of profiles and
described beach changes in terms of transitions between these
types.

Edelman (1969, 1973) studied dune erosion and developed a
quantitative predictive procedure by assuming that all sand
eroded from the dune was deposited within the breaker zone. On
the basis of a number of simplifying assumptions, such as the
shape of the after-storm profile being known together with the
highest storm surge level, dune recession caused by a storm was
estimated.

Sonu (1970) discussed beach change caused by the 1969
hurricane Camille, documenting the rapid profile recovery that
took place during the end of the storm itself and shortly
afterward (Kriebel 1987).

Nayak (1970, 1971) performed small-scale laboratory experi-
ments to investigate the shape of equilibrium beach profiles and
their reflection characteristics. He developed a criterion for
the generation of longshore bars that is similar to that of
Iwagaki and Noda (1963), but included the specific gravity of the
material. The slope at the still-water level for the equilibrium
profile was controlled more by specific gravity than by grain
size. Furthermore, the slope decreased as the wave steepness at
the beach toe or the dimensionless fall velocity (wave height
divided by fall velocity and period) increased. The dimension-
less fall velocity was also found to be a significant parameter
for determining the reflection coefficient of the beach.

Allen (1970) quantified the process of avalanching on dune
slopes for determining the steepest stable slope a profile can
attain. He introduced the concepts of angle of initial yield and

32

residual angle after shearing to denote the slopes immediately before and after the occurrence of avalanching.

Dyhr-Nielsen and Sørensen (1971) proposed that longshore bars were formed from breaking waves which generated secondary currents directed towards the breaker line. On a tidal beach with a continuously moving break point, a distinct bar would not form unless severe wave conditions prevailed.

Saylor and Hands (1971) studied characteristics of longshore bars in the Great Lakes. The distance between bars increased at greater than linear rate with distance from the shoreline, whereas the depth to crest increased linearly. A rise in water level produced onshore movement of the bars (cf. Evans 1940).

Davis and Fox (1972) and Fox and Davis (1973) developed a conceptual model of beach change by relating changes to barometric pressure. They reproduced complex nearshore features by schematizing the beach shape and using empirical relationships formed with geometric parameters describing the profile. Davis et al. (1972) compared development of ridge and runnel systems (King and Williams 1949) in Lake Michigan and off the coast of northern Massachusetts where large tidal variations prevailed. The tides only affected the rate at which onshore migration of ridges occurred and not the sediment sequence that accumulated as ridges.

Dean (1973) assumed suspended load to be the dominant mode of transport in most surf zones and derived on physical grounds the dimensionless fall velocity. Sand grains suspended by the breaking waves would be transported onshore or offshore depending on the relation between the fall velocity of the grains and the wave period. A criterion for cross-shore transport direction based on the nondimensional quantities of deepwater wave steepness and fall velocity divided by wave period and acceleration of gravity (fall velocity parameter) was proposed. The criterion of transport direction was also used for predicting profile response (normal or storm profile).

33

Carter, Liu, and Mei (1973) suggested that longshore bars could be generated by standing waves and associated reversal of the mass transport in the boundary layer, causing sand to accumulate at either nodes or antinodes of the wave. In order for flow reversal to occur, significant reflection had to be present. Lau and Travis (1973), and Short (1975a, b) discussed the same mechanism for longshore bar formation.

Hayden et al. (1975) analyzed beach profiles from the United States Atlantic and Gulf coasts to quantify profile shapes. Eigenvector analysis was used as a powerful tool to obtain characteristic shapes in time and space. The first three eigenvectors explained a major part of the variance and was given the physical interpretation of being related to bar and trough morphology. The number of bars present on a profile showed no dependence on profile slope, but an inverse relationship between slopes in the inshore and offshore was noted.

Winant, Inman, and Nordstrom (1975) also used eigenvector analysis to determine characteristic beach shapes and related the first eigenvector to mean beach profile, the second to the bar/berm morphology, and the third to the terrace feature. The data set consisted of two years of profile surveys at Torrey Pines, California performed at monthly intervals.

Davidson-Arnott (1975) and Greenwood and Davidson-Arnott (1975) performed field studies of a bar system in Kouchibouguac Bay, Canada and identified conditions for bar development namely, gentle offshore slope, small tidal range, availability of material, and absence of long-period swell. They distinguished between the inner and outer bar system and described in detail the characteristics of these features. The break point of the waves was observed to be located on the seaward side of the bar in most cases and not on the crest. Greenwood and Davidson-Arnott (1972) did textural analysis of sand from the same area, revealing distinct zones with different statistical properties of the grain size distribution across the profile (Mothersill 1970).

34

Exon (1975) investigated bar fields in the western Baltic
Sea which were extremely regular due to evenly distributed wave
energy alongshore. He noticed the sensitivity of bars to
engineering structures, reducing the size of the bar field.

Kamphuis and Bridgeman (1975) performed wave tank experi-
ments to evaluate the performance of artificial beach nourish-
ment. They concluded that the inshore equilibrium profile was
independent of the initial slope and a function only of beach
material and wave climate. However, the time elapsed before
equilibrium was attained as well as the bar height depended upon
the initial slope.

Sunamura and Horikawa (1975) classified beach profile shapes
into three categories distinguished by the parameters of wave
steepness, beach slope, and grain size divided by wavelength.
The criterion was applied to both laboratory and field data, only
requiring a different value of the empirical coefficient to
obtain division between the shapes. The same parameters were
used by Sunamura (1975) in a study of stable berm formations. He
also found that berm height (datum not given) was approximately
equal to breaking wave height.

Swart (1975, 1977) studied cross-shore transport properties
and characteristic shapes of beach profiles. A cross-shore
sediment transport equation was proposed where the rate was
proportional to a geometrically-defined deviation from the
equilibrium profile shape. A numerical model was presented based
on the empirical relationships derived and applied to a beach
fill case.

Wang, Dalrymple, and Shiau (1975) developed a computer-
intensive three-dimensional numerical model of beach change
assuming that cross-shore transport occurred largely in suspen-
sion. The transport rate was related to the energy dissipation
across-shore.

van Hijum (1975, 1977) and van Hijum and Pilarczyk (1982)
investigated equilibrium beach profiles of gravel beaches in

35

laboratory tests and derived empirical relationships for geometric properties of profiles. The net cross-shore sand transport rate was calculated from the mass conservation equation, and a criterion for the formation of bar/step profiles was proposed for incident waves approaching at an angle to the shoreline.

Hands (1976) observed in field studies at Lake Michigan that plunging breakers were not essential for bar formation. He also noted a slower response of the foreshore to a rising lake level than for the longshore bars. A number of geometric bar properties were characterized in time and space for the field data.

Dean (1976) discussed equilibrium profiles in the context of energy dissipation from wave breaking. Different causes of beach profile erosion were identified and analyzed from the point of view of the equilibrium concept. Dean (1977a) analyzed beach profiles from the United States Atlantic and Gulf coasts and arrived at a 2/3 power law as the optimal function to describe the profile shape, as previously suggested by Bruun (1954). Dean (1977a, 1977b) proposed a physically-based explanation for the power shape assuming that the profile was in equilibrium if the energy dissipation per unit water volume from wave breaking was uniform across-shore. Dean (1977b) developed a schematized model of beach recession produced by storm activity based on the equilibrium profile shape (Edelman 1969, 1973).

Owens (1977) studied beach and nearshore morphology in the Gulf of St. Lawrence, Canada, describing the cycles of erosion and accretion resulting from storms and post-storm recovery.

Chiu (1977) mapped the effect of the 1975 hurricane Eloise on the beach profiles along the Gulf of Mexico (Sonu 1970). Profiles with a gentle slope and a wide beach experienced less erosion compared with steep slopes, whereas profiles in the vicinity of structures experienced greater amounts of erosion.

Dalrymple and Thompson (1977) related the foreshore slope to the dimensionless fall velocity using laboratory data and

presented an extensive summary of scaling laws for movable-bed modeling.

Felder (1978) and Felder and Fisher (1980) divided the beach profile into different regions with specific transport relationships and developed a numerical model to simulate bar response to wave action. In the surf zone, the transport rate depended on the velocity of a solitary wave.

Aubrey (1978) and Aubrey, Inman, and Winant (1980) used the technique of eigenvector analysis (Hayden et al. 1975) in beach profile characterization to predict beach profile change. Both profile evolution on a daily and weekly basis were predicted from incident wave conditions, where the weekly mean wave energy was found to be the best predictor for weekly changes. Aubrey (1979) used measurements of beach profiles in southern California spanning five years to investigate its temporal properties. He discovered two pivotal (fixed) points, one located at 2-3-m depth and one at 6-m depth. Sediment exchange across the former point was estimated at 85 m^3/m and across the latter at 15 m^3/m per year.

Hunter, Clifton, and Phillips (1979) studied nearshore bars on the Oregon coast which attached to the shoreline and migrated alongshore. A seaward net flow (undertow) along the bottom was occasionally observed shoreward of the bar during the field investigations (Mothersill 1970).

Greenwood and Mittler (1979) found support in the studies of sedimentary structures of the bar system being in dynamic equilibrium from sediment movement in two opposite directions. An asymmetric wave field moved the sand landward and rip-type currents moved the material seaward.

Greenwood and Davidson-Arnott (1979) presented a classification of wave-formed bars and a review of proposed mechanisms for bar formation (Zenkovich 1967).

Hallermeier (1979, 1984) studied the limit depth for intense bed agitation and derived an expression based on linear wave

shoaling. He also proposed an equation for the yearly limit depth for significant profile change involving wave parameters exceeded twelve hours per year (see also, Birkemeier 1985b).

Hattori and Kawamata (1979) investigated the behavior of beach profiles in front of a seawall by means of laboratory experiments. Their conclusion was that material eroded during a storm returned to the seawall during low wave conditions to form a new beach (cf. reviews of Kraus 1987, 1988).

Chappell and Eliot (1979) performed statistical analysis of morphological patterns from data obtained along the southern coast of Australia. Seven inshore states were identified which could be related to the current, the antecedent wave climate, and the general morphology (Sonu 1969).

Nilsson (1979) assumed bars to be formed by partially reflected Stokes wave groups and developed a numerical model based on this mechanism. Sediment transport rates were calculated from the bottom stress distribution, and an offshore directed mean current was superimposed on the velocity field generated by the standing waves.

Short (1979) conducted field studies along the southeast Australian coast which formed the basis for proposing a conceptual three-dimensional beach-stage model. The model comprised ten different stages ranging from pure erosive to pure accretive conditions. Transitions between stages were related to the breaking wave height and breaker power. Wright et al. (1979) discussed the characteristics of reflective and dissipative beaches as elucidated from Australian field data. The surf scaling parameter (Guza and Bowen 1977) was considered an important quantity for determining the degree of reflectivity of a specific profile. Long-period waves (infragravity waves, edge waves) were believed to play a major role in the creation of three-dimensional beach morphology.

Bowen (1980) investigated bar formation by standing waves and presented analytical solutions for standing waves on plane

sloping beaches. He also derived equilibrium slopes for beach profiles based on Bagnold's (1963) transport equations and assuming simple flow variations.

Dally (1980) and Dally and Dean (1984) developed a numerical model of profile change based on the assumption that suspended transport is dominant in the surf zone. The broken wave height distribution across-shore determined by the numerical model supplied the driving mechanism for profile change. An exponential-shaped profile was assumed for the sediment concentration through the water column.

Davidson-Arnott and Pember (1980) compared bar systems at two locations in southern Georgian Bay, the Great Lakes, and found them to be very similar despite the large differences in fetch length. The similarity was attributed to the same type of breaking conditions prevailing, with spilling breakers occurring at multiple break points giving rise to multiple bar formations (Hands 1976).

Hashimoto and Uda (1980) related beach profile eigenvectors for a specific beach to shoreline position. Once the shoreline movement could be predicted, the eigenvectors were given from empirical equations and the three-dimensional response obtained.

Shibayama and Horikawa (1980a, 1980b) proposed sediment transport equations for bed load and suspended load based on the Shield's parameter (Madsen and Grant 1977). A numerical beach profile model was applied using these equations which worked well in the offshore region but failed to describe profile change in the surf zone.

Davidson-Arnott (1981) developed a numerical model to simulate multiple longshore bar formation. The model was based on the mechanism proposed by Greenwood and Mittler (1979) for bar genesis, and the model qualitatively produced offshore bar movement, but no comparison with any measurements was made.

Bailard and Inman (1981) and Bailard (1982) used Bagnold's (1963) sediment transport relationships to develop a model for

transport over a plane sloping beach. They determined the influence in the model of the longshore current on the equilibrium profile slope. The beach profile was flattened in the area of the maximum longshore current and the slope increased with sand fall velocity and wave period.

Hughes and Chiu (1981) studied dune recession by means of small-scale movable-bed model experiments. The amount of dune erosion was found from shifting the barred profile horizontally until eroded volume agreed with deposited volume (Vellinga 1983). Geometric properties of the equilibrium bar profile were expressed in terms of dimensionless fall velocity.

Sawaragi and Deguchi (1981) studied cross-shore transport and beach profile change in a small wave tank and distinguished three transport rate distributions. They developed an expression for the time variation of the maximum transport rate and discussed the relation between bed and suspended load.

Gourlay (1981) emphasized the significance of the dimensionless fall velocity (Gourlay 1968) in affecting equilibrium profile shape, relative surf zone width, and relative uprush time.

Hattori and Kawamata (1981) developed a criterion for predicting the direction of cross-shore sediment transport similar to Dean (1973), but including beach slope. The criterion was derived from the balance between gravitational and turbulent forces keeping the grains in suspension.

Watanabe, Riho, and Horikawa (1981) calculated net cross-shore transport rates from the mass conservation equation (van Hijum 1975, 1977) and measured profiles in the laboratory, and arrived at a transport relationship of Madsen and Grant (1977) type. They introduced a critical Shield's stress below which no transport occurred and assumed a linear dependence on the Shields parameter.

Moore (1982) presented a numerical model to predict beach profile change produced by breaking waves. He assumed the

40

transport rate to be proportional to the energy dissipation from breaking waves per unit water volume above an equilibrium value (Dean 1977a). An equation was given which related this equilibrium energy dissipation to grain size. The beach profile approached an equilibrium shape in accordance with the observations of Bruun (1954) if exposed to the same wave conditions for a considerable time.

Kriebel (1982, 1986) and Kriebel and Dean (1984, 1985a) developed a numerical model to predict beach and dune erosion using the same transport relationship as Moore (1982). The amount of erosion was determined primarily by water-level variation, and breaking wave height entered only to determine the width of the surf zone. The model was verified both against large wave tank data (Saville 1957) and data from natural beaches taken before and after 1975 hurricane Eloise (Chiu 1977). The model was applied to predict erosion rates at Ocean City, Maryland, caused by storm activity and sea level rise (Kriebel and Dean 1985b).

Holman and Bowen (1982) derived three-dimensional morphologic patterns by interactions between edge waves and reflected waves, assuming the drift velocities associated with these waves to cause bar formation.

Watanabe (1982, 1985) used a cross-shore transport rate which was a function of the Shield parameter to the 3/2 power in a three-dimensional model of beach change. The model simulated both the effects of waves and nearshore currents on the beach profile. The transport direction was obtained from an empirical criterion (Sunamura and Horikawa 1975).

Vellinga (1982, 1986) presented results from large wave tank studies of dune erosion and discussed scaling laws for movable-bed experiments (Hughes and Chiu 1981). The dimensionless fall velocity proved to provide a reasonable scaling parameter in movable-bed studies, and the dependence of the sediment concentration on wave breaking was stressed.

41

Dolan (1983) and Dolan and Dean (1984) investigated the origin of the longshore bar system in the Chesapeake Bay and concluded that multiple breaking was the most likely cause (Hands 1976). Other possible mechanisms discussed were standing waves, edge waves, secondary waves, and tidal currents, but none of these could satisfactorily explain the formations.

Kajima et al. (1983a, 1983b) discussed beach profile evolution using data obtained in a large wave tank with waves of prototype-size. Beach profile shapes and distributions of the net cross-shore transport rates were classified according to the criterion developed by Sunamura and Horikawa (1975). A model of beach profile change was proposed based on a schematized transport rate distribution which decayed exponentially with time. The data set given by Kajima et al. (1983b) is used in the present work.

Sasaki (1983) developed a conceptual three-dimensional beach stage model based on extensive field measurement from two beaches in Japan (see also Sonu 1969, Short 1979). Transition between the different stages was determined as a function of the average deepwater wave steepness and the average breaker height divided by the median grain size. A larger breaker height and deepwater wave steepness caused greater shoreline recession during storms, whereas a coarser grain size gave reduced shoreline retreat.

Sunamura (1983) developed a simple numerical model of shoreline change caused by short-term cross-shore events and described both erosional and accretional phases of a field beach. Exponential-type response functions were used to calculate the magnitude of shoreline change, and direction was given by the criterion proposed by Sunamura and Horikawa (1975).

Vellinga (1983, 1986) presented a numerical model for calculating dune erosion during high surge-short duration storm events. The amount of dune recession was determined from the significant wave height, storm surge level, and beach profile shape during storm conditions. van de Graaff (1983) discussed a

42

probabilistic approach for estimating dune erosion. Distribution functions for a number of important parameters regarding dune erosion were suggested such as maximum storm surge level, significant wave height, median grain size, and profile shape. Visser (1983) applied a probability-based design scheme to the dunes in the Delta area of the Netherlands (Verhagen 1985).

Seelig (1983a, b) analyzed large wave tank data from Saville (1957) and developed a simple prediction method to estimate beach volume change above the still-water level.

Balsillie (1984) related longshore bar formation to breaking waves from field data, and developed a numerical model to predict profile recession due to storm and hurricane activity.

Davidson-Arnott and Randall (1984) performed field measurements of the spatial and temporal characteristics of the surface elevation and cross-shore current spectra on a barred profile at St. Georgian Bay, Lake Ontario. The greatest portion of the energy was found in the frequencies of the incident short-period waves.

Sunamura (1984a) derived a formula to determine the cross-shore transport rate in the swash zone taken as an average over one hour. The transport rate was related to the near-bottom orbital velocity, and the transport equation predicted the net direction of sand movement.

Takeda (1984) studied the behavior of beaches during accretionary conditions based on field investigations from Naka Beach, Japan. He derived predictive relationships for determining if onshore movement of bars occurs, average speed of onshore bar migration, and berm height. He pointed out the rapid formation of berms in the field, where the build-up may be completed in one or two days (cf. Kriebel, Dally, and Dean 1986).

Greenwood and Mittler (1984) inferred the volume flux of sediment over a bar by means of rods driven into the bed on which a freely moving fitting was mounted to indicate changes in bed elevation. Their study indicated an energetics approach in

43

accordance with Bagnold (1963) to be reasonable for predicting equilibrium slopes seaward of the break point.

Sunamura (1984b) obtained empirical expressions for the beach-face slope involving the breaking wave height, wave period, and grain size. Different equations were developed and applied for laboratory and field conditions.

Shibayama (1984) investigated the role of vortices in sediment transport and derived transport formulas for bed and suspended load based on Shield's parameter. The generation of vortices was not confined to plunging breakers but could occur under spilling breakers as well.

Sunamura and Takeda (1984) quantified onshore migration of bars from a two-year series of profile data from a beach in Japan. They derived a criterion to determine if onshore bar movement would occur and a predictive equation to estimate the migration speed (Takeda 1984). Onshore transport typically took place in the form of bed load carried shoreward in a hydraulic bore.

Wright and Short (1984) used the dimensionless fall velocity, based on the breaking wave height, in a classification process of three-dimensional beach stages.

Mei (1985) mathematically analyzed resonant reflection from nearshore bars that can enhance the possibility for standing waves to generate bars.

Shimizu et al. (1985) analyzed data obtained with a large wave tank to investigate the characteristics of the cross-shore transport rate. Transport rate distributions were classified in three categories, and the criterion of Sunamura and Horikawa (1975) was used to delineate between different types. The transport rate distribution was modeled by superimposing three separate curves representing the transport rate on the foreshore, in the surf zone, and in the offshore zone (cf. Kajima et al. 1983a).

Aubrey and Ross (1985) used eigenvector and rotary component analysis to identify different stages in the beach profile and the corresponding frequency of change. A frequency of one year related to exchange of sediment between bar and berm was the most dominant mode found in the analysis.

Deguchi and Sawaragi (1985) measured the sediment concentration at different locations across the beach profile in a wave tank. Both the bed load and suspended load were determined, and the sediment concentration was found to decay exponentially with distance above the bed (Kraus and Dean 1987).

Mason et al. (1985) summarized a field experiment conducted at Duck, North Carolina where a nearshore bar system was closely monitored during a storm. Bar dynamics showed a clear dependence on wave height, the bar becoming better developed and migrating offshore as the wave height increased. Birkemeier (1985a) analyzed the time scale of beach profile change from a data set comprising 3 1/2 years of profile surveying at Duck, North Carolina. Large bar movement occurred with little change in the depth to crest. If low-wave conditions prevailed for a considerable time, a barless profile developed.

Jaffe, Sternberg, and Sallenger (1985) measured suspended sediment concentration in a field surf zone with an optical back-scattering device. The concentration decreased with elevation above the bed, and an increase in concentration was found over the nearshore bar.

Birkemeier (1985b) modified parameter values in an equation proposed by Hallermeier (1979) to describe the seaward limit of profile change at Duck, North Carolina.

Gourlay (1985) identified four different kinds of profile response related to dominant breaker type. The dimensionless fall velocity (sediment mobility parameter) was a decisive quantity both regarding profile response and profile geometry (Hughes and Chiu 1981). The effect of beach permeability was discussed with respect to wave set-up and berm height.

Sallenger, Holman, and Birkemeier (1985) observed the rapid response of a natural beach profile at Duck, North Carolina, to changing wave conditions. Both offshore and onshore bar movement occurred at much higher speeds than expected, and the ratio between trough and crest depth was approximately constant during offshore bar movement but varied during onshore movement.

In a numerical model developed by Stive and Battjes (1985), offshore sand transport was assumed to occur through the undertow and as bed load only. They verified the model against laboratory measurements of profile evolution produced by random waves. Stive (1987) extended the model to include effects of asymmetry in the velocity field from the waves in accordance with Bailard (1982).

Verhagen (1985) developed a probabilistic technique for estimating the risk of break-through of dunes during storm surge and wave action. A main part of this technique was the use of a model to calculate expected dune erosion during a storm (Vellinga 1983) modified by statistical distributions of the factors influencing dune erosion (van de Graaff 1983, Visser 1983).

Kriebel, Dally, and Dean (1986) studied beach recovery after storm events both during laboratory and field conditions, noting the rapid process of berm formation. They could not find evidence for breakpoint bars moving onshore and welding onto the beach face during the recovery process, but the berm was built from material originating further inshore. Beach recovery following the 1985 hurricane Elena was also discussed by Kriebel (1987) who concluded that the presence of a seawall did not significantly affect the process of beach recovery at the site.

Wright et al. (1986) concluded from field measurements that bar-trough morphology was favored by moderate breaker heights combined with small tidal ranges. Short-period waves were the main cause of sediment suspension in the surf zone, although long-periodic waves were believed to be important for the overall net drift pattern.

46

Rushu and Liang (1986) proposed a criterion for distinguishing between beach erosion and accretion involving a number of dimensionless quantities. A new parameter consisting of the friction coefficient, critical velocity for incipient motion of the grains, and the fall velocity of the grains was introduced.

Thomas and Baba (1986) studied berm development produced by onshore migration of bars for a field beach at Valiathura, at the south-west coast of India, and related the conditions for onshore movement to wave steepness.

Dette (1986), Uliczka and Dette (1987), and Dette and Uliczka (1987a, b) investigated beach profile evolution generated in a large wave tank under prototype-scale conditions. The tests were carried out with both monochromatic and irregular waves for a dune-like foreshore with and without a significant surf zone. For one case starting from a beach without "foreshore", mono-chromatic waves produced a bar, whereas irregular waves of significant height and peak spectral period of the monochromatic waves did not. Sediment concentration and cross-shore velocity were measured through the water column at selected points across the profile.

Wright et al. (1987) investigated the influence of tidal variations and wave groupiness on profile configuration. Higher values of the wave groupiness factor tended to correlate with beach states of more dissipative character.

Howd and Birkemeier (1987) presented four years of profile data obtained at four different shore-normal survey lines at Duck, North Carolina. Corresponding wave and water level data were also published, making this data set one of the most complete descriptions available of beach profile response to wave action.

Seymour (1987) summarized results from the Nearshore Sediment Transport Study (NSTS) six-year program in which nearshore sediment transport conditions were investigated. He pointed out the importance of bar formation for protecting the

47

foreshore against wave action and the resulting rapid offshore movement of the bar on a beach exposed to storm waves.

Takeda and Sunamura (1987) found from field studies in Japan the great influence of the bar formation on the subaerial response on beaches with fine sand.

Dally (1987) tested the possibility of generating bars by long-periodic waves (surf beat) in a small wave tank, but found little evidence for this mechanism. Instead, breaking waves in combination with undertow proved to be the cause of bar formation in the studied cases, whether spilling or plunging breakers prevailed.

Hallermeier (1987) stressed the importance of large wave tank experiments for providing valuable information of the beach response to storm conditions. He compared results from a large wave tank experiment (Case 401, see Kraus and Larson 1988) with a natural erosion episode at Bethany Beach, Delawere, and found similar erosive geometry.

Sunamura and Maruyama (1987) estimated migration speeds for seaward moving bars as given by large wave tank data. The studied bars were generated by breaking waves and located somewhat shoreward of the break point (Greenwood and Davidson-Arnott 1975). Bars generated by plunging breakers reached an equilibrium state faster than if spilling breakers were the forming mechanism.

Kobayashi (1987) presented analytical solutions to idealized cases of dune erosion simplifying the governing equations to result in the heat diffusion equation (cf. Edelman 1969, 1973, Dean 1977b).

Hughes and Cowell (1987) studied the behavior of reflective beaches in southern Australia, in particular, changes in the foreshore step. The height of the beach step was correlated to the breaking wave height and the grain size, where a larger wave height and a coarser grain size both produced a higher step.

Kriebel, Dally, and Dean (1987) performed laboratory experiments using a small wave tank and beach shapes designed with the dimensionless fall velocity as the scaling parameter. They found marked differences in profile response depending on the initial shape being planar or equilibrium profile type (Bruun 1954, Dean 1977a). An initially plane beach produced a more pronounced bar and steeper offshore slopes. The fall velocity parameter (Dean 1973) and the deepwater wave steepness were used to distinguish erosional and accretionary profiles using large wave tank data.

Mimura, Otsuka, and Watanabe (1987) performed a laboratory experiment with a small wave tank to investigate the effect of irregular waves on the beach profile and the representative wave height to describe profile response. The mean wave height represented macroscopic beach changes such as bar and berm development most satisfactorily, whereas microscopic phenomena such as threshold of transport and ripple formation were better described by use of significant wave height.

Nishimura and Sunamura (1987) applied a numerical model to simulate a number of test cases from the large wave tank experiments by Kajima et al. (1983a). The cross-shore transport rate expression employed the Ursell number and a mobility parameter proposed by Hallermeier (1982). The numerical model had the capability of generating bars but failed to predict bar location.

Boczar-Karakiewicz and Davidson-Arnott (1987) proposed non-linear interaction between shallow water waves as a possible cause of bar formation. A mathematical model was developed to predict the generation of bars and model results were compared with field data.

Sunamura (1988) gave a comprehensive summary of beach profile morphology presenting quantitative relationships for many of the geometric parameters of the beach profile. Laboratory data was mainly used to derive the predictive equations. Furthermore, a descriptive model of three-dimensional beach change was proposed consisting of eight topographic stages

49

delineated by a dimensionless quantity (breaking wave height squared to the product of gravitational acceleration, median grain size, and wave period squared).

Kraus and Larson (1988) described the large wave tank experiments on beach profile change performed by Saville (1957), giving a listing of all the data.

Synthesis of Previous Work

This section summarizes findings from previous work of particular relevance to this study. The role of breaking waves in bar formation was pointed out in pioneering studies by Lehmann (1884), Hartnack (1924), Evans (1940), King and Williams (1949), and Shepard (1950) based on field observations. Also, numerous early laboratory investigations showed that breaking waves were a main cause of bar genesis, e.g., Waters (1939), Keulegan (1948), Rector (1954), and Saville (1957). Wave breaking generates turbulent motion and provides the necessary mechanism for suspending and keeping sediment in suspension, thus mobilizing the grains for transport by mean currents. The importance of transport as suspended load in the surf zone was emphasized by Dean (1973) and verified through measurements under prototype-scale laboratory conditions by Dette (1986) and under field conditions by Kraus and Dean (1987) among others.

Although profile change is highly stochastic on a micros-cale, involving turbulence, movement of individual and collective grains, and various types of organized flows, if viewed on a macroscale, changes in the profile are surprisingly regular and consistent with respect to large features such as bars and berms. Several landmark studies, such as Keulegan (1945), Shepard (1950), Hands (1976), and Sunamura (1988) have characterized the geometry of geomorphologic features of beach profiles in the field. The possibility of semi-empirically describe geomor-

phologic features under complex wave and water level conditions encountered in the field, as indicated by the above studies, formed much of the early foundation of the present study in the development of a numerical model of beach profile change.

It was shown by Sonu (1969), Short (1979), Sasaki (1983), Wright and Short (1984), and Sunamura (1988) that even very complex three-dimensional beach changes may be described by a small number of schematized beach states characterized by different values of one or two nondimensional parameters. Consequently, if the main processes of beach profile change are identified, the response of the profile to wave and water level variations may be predicted based on semi-empirical relationships developed from relevant data.

Several criteria for delineating bar and berm profile response expressed in terms of wave and sediment properties have been proposed. The first criterion involved only wave steepness (Waters 1939, Scott 1954), whereas later-developed criteria included nondimensional quantities characterizing the beach sediment (Kemp 1961, Iwagaki and Noda 1963, Nayak 1970, Dean 1973, Sunamura and Horikawa 1975, and Rushu and Liang 1986, Kriebel, Dally, and Dean 1987). The formation of bar and berm profiles is closely related to the direction of the cross-shore transport. Criteria similar to those used to distinguish between bar and berm formation have been applied to determine transport direction (Rector 1954, Hattori and Kawamata 1979).

The existence of an equilibrium profile, a profile of constant shape which is approached if exposed to fixed wave and water level conditions, was proved to be a valid concept under laboratory conditions by Waters (1939), Rector (1954), and Swart (1977). Bruun (1954) proposed a power law to relate water depth to offshore distance, which was supported by Dean (1977a) on theoretical grounds. The empirical shape parameter in this simple power equation was related to the grain size by Moore (1982).

51

Characteristics of cross-shore sand transport were studied first by Keulegan (1948) and King and Williams (1949) through trap measurements in laboratory wave tanks. By integrating the mass conservation equation between consecutive profiles in time, the net cross-shore transport rate distribution can be obtained, as discussed by van Hijum (1975, 1977), Watanabe, Riho, and Horikawa (1981), Kajima et al. (1983a, 1983b), and Shimizu et al. (1985). Classification of the cross-shore transport rate distributions has been performed by Sawaragi and Deguchi (1981), Kajima et al. (1983a), and Shimizu et al. (1985).

Various formulas for predicting the cross-shore sand transport rate have been expressed in terms of local fluid velocity (Bagnold 1963, 1966, Bailard and Inman 1981); local shear stress (Madsen and Grant 1977, Shibayama and Horikawa 1980a, Watanabe 1982); and local energy dissipation per unit volume (Moore 1982, Kriebel 1982, Kriebel and Dean 1985a). A cross-shore transport equation based on energy dissipation per unit volume under breaking and broken waves was successfully applied in engineering numerical models for predicting beach profile change (Moore 1982, Kriebel 1982, Kriebel and Dean 1985a).

A variety of numerical models for predicting beach profile change has been developed, although few have been used for engineering predictions. Many of the earlier models included mechanisms for bar generation that did not explicitly assume breaking waves as the primary factor (Felder 1978, Nilsson 1979). Numerical models of profile change based on breaking waves as the cause of bar formation were developed by Dally (1980), Dally and Dean (1984), Moore (1982), Kriebel (1982), and Kriebel and Dean (1985a). Currently, the most successful and widely used numerical model is that developed by Kriebel (1982) and Kriebel and Dean (1985a), which has been applied to a number of sites along the U.S. coast (Kriebel and Dean 1985b, Kraus et al. 1986).

52

However, this model does not incorporate bar formation and bar movement and does not simulate beach accretion.

In the present work, an empirically-based model of beach profile change is developed for engineering use with the express aim of replicating the dynamics of macroscale features of bars and berms.

PART III: DATA EMPLOYED IN THIS STUDY

Introduction

Three approaches can be used to obtain data for studying
beach profile change and the underlying physical processes;
laboratory experiments using small wave tanks, field measure-
ments, and experiments employing large wave tanks. For refer-
ence, a small wave tank is considered to generate wave heights on
the order of 0.1 m, whereas wave heights on the order of 1 m can
be generated in large wave tanks.

Small-scale laboratory approach

Numerous laboratory studies of beach profile change have
been performed with small wave tanks (for example, Waters 1939,
Bagnold 1940, Keulegan 1945, 1948, Nayak 1970, Rector 1954, Scott
1954, Watts 1954, Watts and Dearduff 1954, McKee and Sterrett
1961, Iwagaki and Noda 1963, Sunamura 1975, Sunamura and Horikawa
1975, Hughes and Chiu 1981, van Hijum and Pilarczyk 1982,
Shibayama 1984). Such experiments have proven valuable for
identifying potential parameters controlling beach change and for
qualitatively describing profile features. However, as demon-
strated in a landmark paper by Saville (1957), in which profile
change generated in small and large wave tanks was compared, a
large scale effect is introduced through the magnitude of the
wave height. Other independent variables may also produce a
scaling distortion, and generally applicable scaling laws for
interpreting results of small-scale movable bed models of beach
change have yet to be determined (Hughes 1983, 1984, Sayao 1984,
Vellinga 1984). Thus, data sets from laboratory experiments
performed with small-scale facilities are of limited value for

54

establishing quantitative understanding of profile change in nature.

Field approach

Field data sets useful for quantitative study of beach profile change are extremely rare because of the required high resolution in time and space of morphology and associated wave climate and water level. Due to the great spatial and temporal variability of waves and the three-dimensional character of nearshore bathymetry in the field, it is difficult to extract firm cause and effect relationships between waves and profile change resulting solely from wave-induced, cross-shore component of sediment transport. Recently, Birkemeier (1985a), Sallenger, Holman, and Birkemeier (1985), and Howd and Birkemeier (1987) have reported results from repetitive concurrent field measurements of the beach profile, waves, and water level. However, horizontal spacing between measurements along the profile was typically tens of meters, and the time interval between surveys was on the order of a half day to a week, during which wave conditions and water level varied substantially. Hands (1976) quantified several geometric properties of a longshore bar system in Lake Michigan, but could not make direct correlations with the waves and water level due to a lack of measurements. Wright, Short, and Green (1985) made daily observations over 6-1/2 years of Narrabeen Beach, Australia, and related gross change in nearshore morphology to a single parameter, the dimensionless fall velocity, discussed further below.

Several descriptive models of beach profile change have been developed based on field observations and measurements, but these are primarily either statistical or conceptual and are not capable of quantitative prediction (e.g., Evans 1940, King and Williams 1949, Shepard 1950, Bascom 1951, Sonu 1969, Davis and Fox 1972, Davidson-Arnott 1975, Aubrey, Inman, and Nordstrom

1977, Owens 1977, Short 1979, Sasaki 1983, Takeda 1984, Wright and Short 1984, Wright, Short, and Green 1985, Wright et al. 1986, Sunamura 1988).

Prototype-scale laboratory approach

The third approach available for quantitative investigation of beach profile change is use of large wave tanks (abbreviated as LWT hereafter). Such facilities enable controlled reproduction of near-prototype conditions of beach slope, wave height and period, turbulence induced by wave breaking, and resultant sediment transport and beach change. The problem of scaling is eliminated, and the required high resolution measurement of the profile can also be attained. Disadvantages associated with wave tanks include contamination by reflection from the beach and wave generator and formation of wave harmonics (Buhr Hansen and Svendsen 1975). Experience indicates that these factors are negligibly small under reasonable experiment design.

Experiments using LWT have been performed with monochromatic waves (Saville 1957, Caldwell 1959, Kajima et al. 1983a, 1983b, Dette and Uliczka 1987a, Kraus and Larson 1988) and irregular waves with random heights and periods (Vellinga 1986, Dette and Uliczka 1987b, Uliczka and Dette 1987). Irregular waves will most closely reproduce naturally occurring profile change. Mimura, Otsuka, and Watanabe (1987) compared beach change produced in a small laboratory wave tank by irregular waves and corresponding representative monochromatic waves. They found that macroscale patterns of profile change, such as bar and berm development, were similar if representative monochromatic waves were chosen as the mean wave height and period of the irregular wave train. On the other hand, microscale features, such as initiation of sand motion and ripple size, were best described by the significant wave. Properties compared included profile

56

morphology, cross-shore sand transport rate, and critical depth for sediment motion.

Irregular waves introduce additional independent parameters associated with the wave spectrum, whereas in monochromatic wave tests the effects produced by the basic parameters of wave height and period can be isolated and systematically investigated. Hughes and Chiu (1981) discuss theoretical and practical problems associated with use of irregular waves in movable bed modeling. At this first stage of quantification of prototype beach change, it is probably most fruitful to examine the response of the profile to elemental, monochromatic waves.

Recently, two independent data sets on beach profile change have become available from experiments performed using LWT and monochromatic waves (Kajima et al. 1983a, 1983b, Kraus and Larson 1988). These experiments involved combinations of waves, water levels, beach slopes, and sands of the scale that exist in the field, but with the advantages of true two-dimensionality, control of the external (wave) force, and an optimized measure-ment schedule. These data sets formed the core data for this study and are described next.

Data Employed in This Study

Data base

Two data sets on beach profile change generated in LWT were employed. These independent data sets allowed systematic examination of profile evolution through time for a wide range of realistic incident wave heights and periods, water levels, initial beach slopes, and sand grain sizes.

One data set was obtained in experiments performed by the U.S. Army Corps of Engineers (abbreviated CE) in the years 1956-1957 and 1962 (Saville 1957, Caldwell 1959, Kraus and Larson

57

1988) at Dalecarlia Reservation, Washington D.C. The second data set pertains to experiments performed at the Central Research Institute of Electric Power Industry (abbreviated CRIEPI) in Chiba, Japan (Kajima et al., 1983a, 1983b).

CE experiments

The CE experiments were performed using American Customary Units. Conversion is made here to metric units to achieve generality, but customary units are retained for equipment specifications. The concrete tank used in the CE experiments was 193.5 m long, 4.6 m wide, and 6.1 m deep (635 x 15 x 20 ft). The standard operating depth of the tank was 4.6 m (15 ft) which required a water volume of approximately 3800 m^3. A mobile instrument carriage mounted on rails on top of the tank carried equipment and personnel for making measurements. A picture of the CE tank is displayed in Figure 2, in which the wave generator and instrument carriage are seen at the far end of the tank.

The wave generator consisted of a vertical bulkhead 4.6 m (15 ft) wide and 7.0 m (23 ft) high mounted on a carriage which moved back and forth on rails to create the wave motion. The carriage was given oscillatory movement by arms 13 m in length (42 ft 9 in.), connected to two driving discs. Each disc was 5.8 m (19 ft) in diameter, weighed 12.7 tons, and was driven through a train of gears by an 800-hp variable speed electric motor. Wave periods between 2.6 and 24.8 sec could be generated by a gearing mechanism, and the maximum usable wave height at the standard operating depth was approximately 1.8 m (6 ft). Figure 3 gives a view of the wave generator where the bulkhead is seen in the front of picture and the two rotating discs are distinguished in the back. The experimental facility is further described by Raynor and Simmons (1964) and Kraus and Larson (1988).
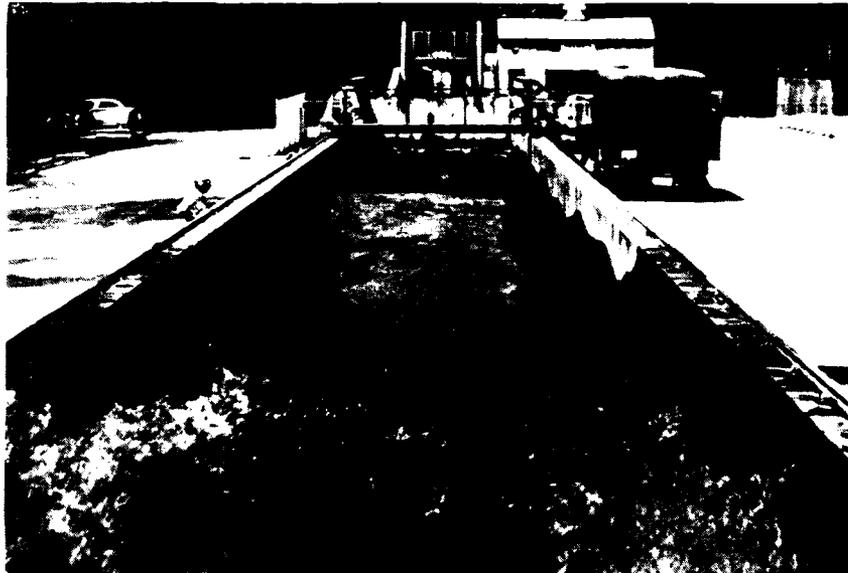
Figure 2. Tank for large waves at Dalecarlia Reservation, Washington DC, where the CE experiments were conducted in 1956-57 and 1962
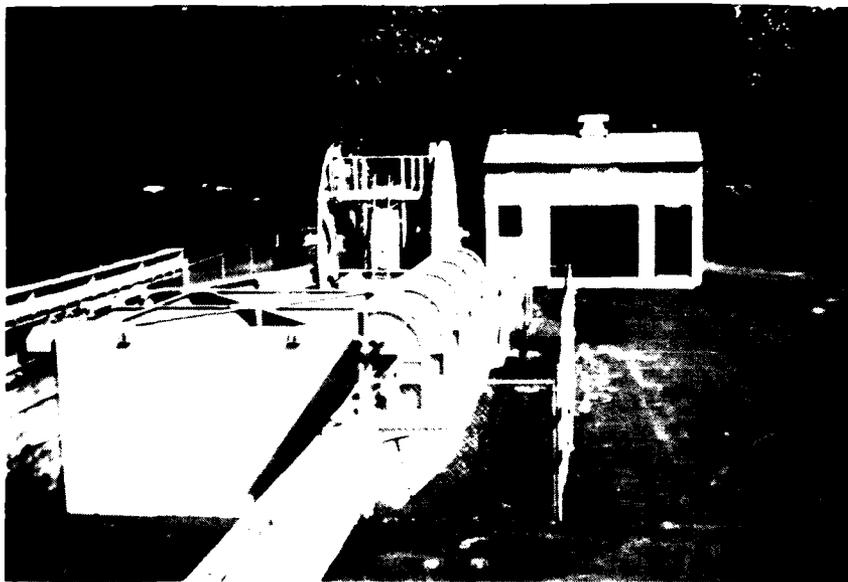
Figure 3. View of the wave generator in the tank for large waves

Eighteen distinct cases have been documented (see Kraus and Larson 1988) of which all but two were started from a plane slope of 1/15. Approximately 1500 m^3 of sand were needed to grade the plane initial slope, which was done with a small bulldozer. The wave parameters ranged from periods between 3.75 and 16.0 sec and generated wave heights between 0.55 and 1.68 m in the horizontal part of the tank. The wave height and period were held constant during a run, except in one case for which the water depth was varied in order to simulate a tide. The water depth ranged from 3.5-4.6 m in the different cases and two grain sizes were used with median diameters of 0.22 and 0.40 mm. The 0.22-mm grain size was employed in the 1956-57 experiments and the 0.40-mm grain size was used in the 1962 experiments. The specific gravity of the sand grains was 2.65 (Saville 1957). Cases were run until a stable beach profile had developed and no significant changes were detected, which normally occurred after 40-60 hr. A "case" is defined as a collection of profile surveys for a unique combination of incident waves, beach slope, and grain size. A "run" is more loosely used to refer to either a case or an interval of wave action between two profile surveys.

Profile surveys were made intermittently during a run with shorter time increments in the beginning when large profile changes where expected. On the order of 10-15 profile surveys were made during a typical case and the survey interval was 1.2 m (4 ft). For the initial cases with the 0.22-mm sand (Simmons, personal communication, 1986) and all cases with the 0.40-mm sand, profiles were surveyed along three different lines in the tank. Corresponding differences in depth between the three lines were small, and for the 0.22-mm sand only the survey along the center line was retained. However, for the 0.40-mm sand, although the cross-tank depth difference was small, surveys along three lines were made through the entire experiment series and the profile depths used in this report are an average of the three lines.

60

The numbering of the CE cases is discussed by Kraus and Larson (1988) and essentially agrees with the system used by Hallermeier (1987). Table 1 summarizes the CE cases which started from a plane slope of 1/15 giving the wave and water level conditions. The deepwater wave steepness is also listed and was calculated using linear wave theory. Two cases not given in Table 1 were conducted from an initial profile that was irregular (Case 510 and Case 610). Also, a repetition run was performed for Case 100 (Case 110) and satisfactory agreement was achieved between the two cases (Saville 1957). In Case 911 the water level varied stepwise in a sinusoidal manner, but the wave and sand parameters were identical to Case 901. The period of the water level variation was approximately 12 hr, the amplitude 0.45 m, and the mean water level 3.96 m.

The wave height was measured with a step resistance gage placed in a fixed position at the toe of the beach during the experiments. The incident wave was measured before any reflection occurred against the wave paddle. The accuracy of the wave measurements was about 3 cm (0.1 ft) and the wave period was quite accurately set due to the large stroke length of the wavemaker and fixed gear ratio. For most of the cases the breaking wave height and breaker location were estimated visually at specific times during a run.

CRIEPI experiments
X X

The CRIEPI LWT is similar in size to the CE LWT, except that it is somewhat narrower (205 x 3.4 x 6 m). The experiment program consisted of 24 cases with wave periods ranging between 3.0 and 12.0 sec and generated wave heights between 0.3 and 1.8 m. All CRIEPI-cases were performed with monochromatic waves and fixed water level. Many of the cases started from a plane beach slope (17 of the 24), but the initial slope was varied, ranging from 1/50 to 1/10 in individual cases.

Table 1

CE Experiments: Wave Height, Wave Period, and Water Depth
in the Horizontal Section of the Tank, and Deepwater
Wave Steepness

Case No.	Wave Height m	Wave Period sec	Water Depth m	Deepwater Wave Steepness
0.22-mm Sand				
100	1.28	11.33	4.57	0.0054
200	0.55	11.33	4.57	0.0023
300	1.68	11.33	4.27	0.0070
400	1.62	5.60	4.42	0.0351
500	1.52	3.75	4.57	0.0750
600	0.61	16.00	4.57	0.0011
700	1.62	16.00	4.11 (3.81)[*]	0.0028
0.40-mm Sand				
101	1.28	11.33	4.57	0.0054
201	0.55	11.33	4.57	0.0023
301	1.68	11.33	4.27	0.0070
401	1.62	5.60	4.42	0.0351
501	1.52	3.75	4.57	0.0750
701	1.62	16.00	3.81	0.0028
801	0.76	3.75	4.57	0.0377
901	1.34	7.87	3.96	0.0129
911	1.34	7.87	3.96**	0.0129

* Water level decreased after 10 hr.
** Mean of variable water level.

As in the CE experiments, two different grain sizes were
used, 0.27 mm and 0.47 mm. For the present study the CRIEPI
profile survey was digitized from charts enlarged from those
given by Kajima et al. (1983b) with a length increment of 0.5 or
1.0 m depending on the resolution necessary to distinguish
principal morphologic features. The accuracy of the digitization

is judged to be compatible with the profile surveys of the CE data, which is of the order of +/- 1.5 cm in the vertical coordinate. No attempt was made to distinguish small-scale profile features such as ripples.

In the CRIEPI experiments the wave height along the profile was measured from a vehicle mounted on rails on top of the tank. To confirm the two-dimensionality of the experiment, the profiles were surveyed along three lines in the tank during the first few runs. Because the depth difference was small between the three survey lines, only the center line was surveyed in later cases (Kajima et al. 1983a). Wave measurements were usually carried out between profile surveys and wave set-up was also determined. Plunging, spilling, and surging breaking waves were observed, although plunging breakers occurred in the majority of cases. A summary of the CRIEPI cases is given in Table 2, in which the numbering is identical to that used by Kajima et al. (1983b). Cases started from nonplanar bottom (in most cases the beach profile that remained from the previous test case) are not included in Table 2, namely Cases 1-2, 1-4, 1-5, 1-6, 1-7, 4-4, and 6-3.

Field data

At the Field Research Facility (FRF) of the Coastal Engineering Research Center (CERC) located at Duck, North Carolina, profile surveys are taken regularly together with measurements of the wave and water level climate. During the time period 1981-1984, four shore-normal profile lines (Lines 58, 62, 188, and 190) were surveyed approximately every two weeks with a typical spacing between survey points of 10 m (Howd and Birkemeier 1987).

Wave data are tabulated at 6-hr intervals based on a 20-min record at a wave gage (Gage 620) located at the end of the research pier, and data are simultaneously collected by a Waverider buoy off the end of the pier in 18 m of water (Gage

63

625). Water level is sampled from a tide station located at the end of the pier at 6-min intervals and consists of the total change including both tide and storm surge. Water level measurements were available to the author at 1-hr intervals.

Table 2

CRIEPI Experiments: Wave Height, Wave Period, and Water
Depth in the Horizontal Section of the Tank, Initial Beach
Slope, and Deepwater Wave Steepness

Case No.	Wave Height m	Wave Period sec	Depth m	Beach slope	Deepwater wave steepness
0.47-mm Sand					
1-1	0.44	6.0	4.5	1/20	0.0082
1-3	1.05	9.0	4.5	1/20	0.0075
1-8	0.81	3.0	4.5	1/20	0.0607
2-1	1.80	6.0	3.5	3/100	0.0313
2-2	0.86	9.0	3.5	3/100	0.0058
2-3	0.66	3.1	3.5	3/100	0.0473
0.27-mm Sand					
3-1	1.07	9.1	4.5	1/20	0.0074
3-2	1.05	6.0	4.5	1/20	0.0196
3-3	0.81	12.0	4.5	1/20	0.0029
3-4	1.54	3.1	4.5	1/20	0.108
4-1	0.31	3.5	3.5	3/100	0.0178
4-2	0.97	4.5	4.0	3/100	0.0335
4-3	1.51	3.1	4.0	3/100	0.107
5-1	0.29	5.8	3.5	1/50	0.0057
5-2	0.74	3.1	3.5	1/50	0.0533
6-1	1.66	5.0	4.0	1/10	0.0456
6-2	1.12	7.ɔ	4.5	1/10	0.0125

The data set from the FRF is the most detailed known on profile change, encompassing profile surveys, water level, and

64

wave data, and showing both seasonal and short-term changes in the beach profile. The FRF data set was primarily used for verifying the numerical model of beach profile change.

Summary

Use of two independent data sets from LWT studies is expected to increase reliability of relationships derived between waves and morphologic features. Also, by using only data from LWT experiments it is believed that scaling effects are minimal and that the process occurring during bar and berm formation in the field are closely reproduced in the wave tanks. Relationships developed from the LWT experiments can then be tested for their applicability to the real system by use of the quality FRF data set.

PART IV: QUANTIFICATION OF MORPHOLOGIC FEATURES

Data Analysis Procedure

Profile morphologic features of interest are formations
created by wave action, directly or indirectly, during time
scales orders of magnitude greater than the wave period. To
numerically evaluate geometric properties of morphologic fea-
tures, the profile data were approximated by a set of cubic
spline polynomials (on the order of 75-250 polynomials per
profile). This allowed geometric properties such as volumes,
distances, slopes, and curvatures to be determined analytically
once the spline coefficients were calculated. Also, by using
accurate interpolation polynomials, a continuous description of
the profile depth was obtained from the discrete depth values at
survey points.

A main problem immediately encountered in the analysis of
morphologic features is specification of an unambiguous defini-
tion of the feature that will preserve the characteristics
intuitively associated with it. For example, a bar is normally
considered to be a subaqueous accretionary feature where sand is
deposited from material redistributed along the profile. From
observation of a natural barred beach profile it is quite easy to
determine the crest of the bar and the approximate location of
the bar, but it is much more difficult to define or agree upon
the exact extent of the bar, which is needed if a volume calcula-
tion is to be done. Keulegan (1945) used the concept of a
barless beach profile to which he referenced bar properties. The
barless profile is constructed by drawing a curve joining maximum
trough depths along the profile and the point of zero depth.
Apart from the arbitrary nature of this definition, it is
sometimes difficult to determine the seaward limit of the bar.

66

Using points where the second derivative is zero (radius of curvature is zero) to define a bar is found to be convenient on the shoreward side of the bar where the curvature of the profile changes sign going from trough to crest. However, in many cases no such point exists on the seaward side of a bar since an immediate trough may not be present.

In the present study it was found most natural and productive to define morphologic features with respect to the initial profile, since a time sequence of profiles was available. Areas where material accretes constitute bar- or berm-like features, whereas areas where material erodes are trough-like in appearance. Figure 4a shows a definition sketch for a beach profile with representative bar and trough features, and Figure 4b illustrates the corresponding berm case. Nomenclature describing the geometric properties is given in the figures, and a typical wave height envelope is outlined in Figure 4a.

The main purpose of the analysis of the morphologic features is to establish the most important parameters governing beach profile evolution expressed in terms of wave and sediment characteristics. This procedure is expected to provide valuable information of the fundamental response of beach profiles and facilitate a more physically-based approach for development of the numerical model. By relating bar properties to the initial profile, some of these properties will depend on the initial profile slope such as bar volume. For example, two erosional profiles with the same grain size and exposed to the same wave climate will show different equilibrium bar properties if the initial slopes differ. However, the inshore slope of the equilibrium profile will still be similar (Kamphuis and Bridgeman 1975), but different amounts of material must be redistributed within the profile. In this respect, bar volume is a function of initial profile slope, which makes such a bar definition less useful in field data analysis for some bar properties.

67
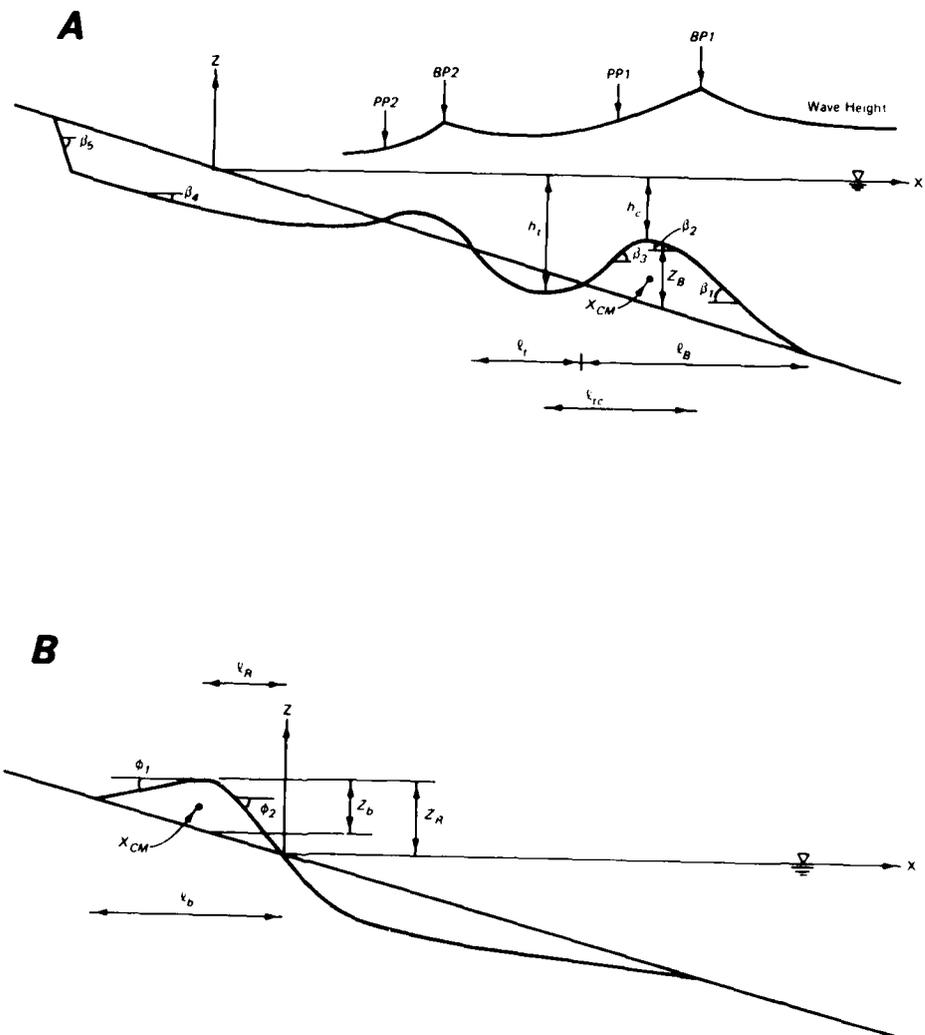
Figure 4.   Notation sketch for beach profile morphology: (a)
bar profile, and (b) berm profile

68

Definition of morphologic features with respect to the
initial profile does not affect net sand transport rate distribu-
tions, which only depend upon two consecutively surveyed profiles
in time, as will be shown. Furthermore, the main objective of
the data analysis is to identify the dominant factors of beach
profile change, supporting the development of the numerical
model. These factors can be distinguished with any reasonable if
arbitrary definition of the features if it is consistently
applied through time. For example, a bar definition according to
Keulegan (1945) would give different values of the evolution of
bar volume with time, but the trend of bar development towards
equilibrium and the factors controlling this growth would be
similar to the present definition.

Only profiles with an initially plane slope where used in
calculation of morphologic features to more easily allow com-
parison between different cases and to more clearly identify
relationships between wave parameters and beach profile evolu-
tion. Defining morphologic features with respect to the initial
profile involves no limitations in characterizing the behavior of
the features or understanding the fundamentals of profile
response to wave action. Instead, a clear definition provides a
strict interpretation of where the bar, berm, or trough is
located at a specific instant in time. Definition of a mor-
phologic feature related to a specific profile has no meaning if
a single beach profile is studied. However, the object here is
not necessarily to present a general definition of a bar or other
feature applicable to an arbicrary beach profile, but to employ a
useful definition as a means to understand the process of beach
profile change and to enable a quantitative description of the
dynamic response of morphologic features.

An extensive correlation and regression analysis was carried
out to investigate relations between geometric properties of the
different profile morphologic features and wave and sand charac-
teristics. The primary parameters used were: wave period (T) or

69

deepwater wavelength (L_o), deepwater wave height (H_o), breaking wave height (H_b), water depth (h), median grain size (D), sand fall velocity (w), and beach slope ($\tan\beta$). Also, various non-dimensional quantities were formed, both for deepwater and breaking conditions, such as H/L, H/wT, $\tan\beta/\sqrt{H/L}$, D/H, and D/L. These quantities were related to geometric properties normalized by different wave and sand parameters.

Concept of Equilibrium Beach Profile

A fundamental assumption in the study of beach profile change is the existence of an equilibrium profile which a beach will attain if exposed to constant wave conditions for a sufficiently long time. The basic idea is that the beach profile in its equilibrium state dissipates incident wave energy without significant net change in shape. If an equilibrium profile did not exist the beach would continue to erode (or accrete) indefinitely if exposed to the same wave conditions and with no restrictions in the sand supply.

The concept of equilibrium profile is an idealization that cannot be fully achieved in practice, since wave, water temperature, water level, and other conditions cannot be held perfectly fixed. Also, wave breaking and sediment motion introduce randomness on the microscale, and resulting small continuous adjustments of the profile. Nevertheless, it has been demonstrated that an equilibrium profile can be approached, in which no significant systematic net sand transport occurs, although small perturbations still remain.

Numerous laboratory studies (e.g., Rector 1954, Nayak 1970, Swart 1975) as well as the data used in this study support the equilibrium beach profile concept, since profile changes diminish with time and the beach profile approaches a stable shape on the macroscale level.

70

From a theoretical point of view, it is of minor importance if an equilibrium profile ever occurs in the field, because of variable wave conditions and complex three-dimensional processes, as long as the concept is verified by experiment. Of course, from a practical point of view, it is of great significance if a natural beach of representative grain size has a preferred shape under a given representative wave climate.

As an indicator of beach profile approach to equilibrium, the cumulative change along the profile was calculated, defined as the sum of the absolute differences in bottom elevation between initial profile and profile at a specific time (see also Shimizu et al. 1985). This quantity is plotted in Figure 5 for selected CE and CRIEPI cases.

The cumulative profile change will ideally approach a constant value under constant applied waves as the beach profile
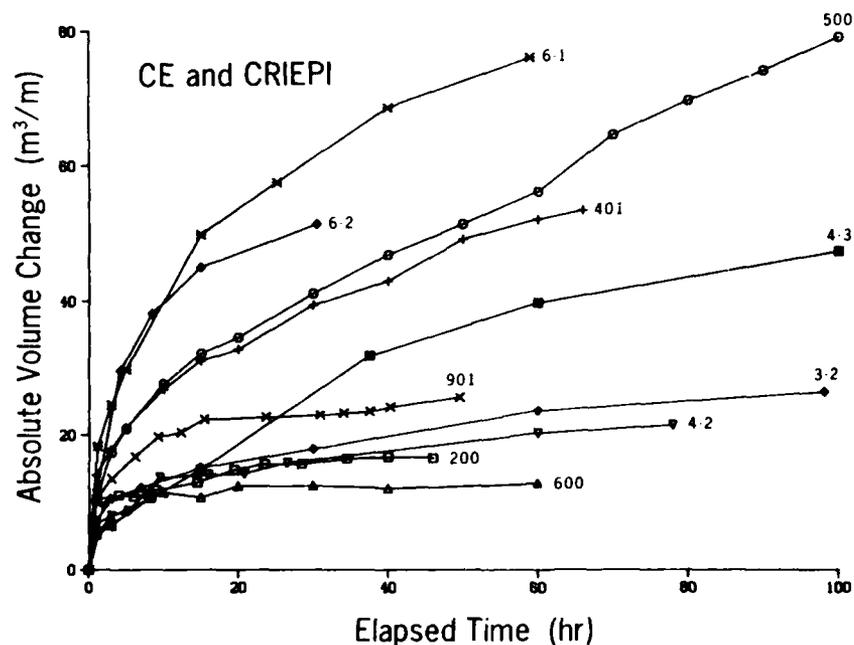
Figure 5. Absolute sum of profile change as a function of time for selected CE and CRIEPI cases

71

attains the equilibrium shape. The decrease in the slope of the resultant curve is a measure of the rate at which equilibrium is approached. However, there will always appear some transport activity because of unsteadiness in experiment conditions, turbulent fluid, and random character of sediment motion, and thus profile change will fluctuate about the average equilibrium shape. Some cases showed curves which had not completely leveled off, but the rate of change was still an order of magnitude smaller than the initial change. Decreasing rates of accumulated profile change indicate an increasingly stable shape since less material was redistributed along the profile.

A greater difference between initial profile and equilibrium profile for a specific wave climate and grain size implies that a larger amount of sand must be redistributed in the process of reaching equilibrium. Dean (1977a) derived an analytical expression for the beach profile shape based on the concept of a constant dissipation of wave energy per unit water volume. This expression agrees well with the relationship established by Bruun (1954) on purely empirical grounds from field data. The beach profile shape may be written

$$h = A \ x^{2/3} \tag{1}$$

where

      h = water depth

      A = shape parameter

      x = cross-shore coordinate (positive in seaward direction)

The shape parameter is mainly a function of grain size, in which a coarser grain size implies a larger value of A and thus a steeper beach (Dean 1977a, Moore 1982).

For an equilibrium profile developed during a storm, where a bar normally is formed close to the breakpoint, Equation 1 is expected to apply only to the portion of the surf zone shoreward

72

of the bar, where strong turbulence is present and energy dissipation mainly volume-related. If wave reformation occurs, several areas along the profile may arise in which profile change is controlled by energy dissipation per unit volume and should be well approximated by Equation 1.

Criterion for Distinguishing Profile Response

Bar and berm

If a beach profile is not in equilibrium with the wave climate, sand will be redistributed as the beach adjusts toward equilibrium shape. De₍ ʾnding on the wave conditions, beach profile shape, and sediment properties, the cross-shore sand transport rate will be predominantly directed either offshore or onshore in most cases. Offshore transport results in erosion on the upper part of the profile and formation of a notable bar at the break point(s), whereas onshore transport leads to accretion of sand on the foreshore and berm build-up. These two types of profile response forming two distinctly different beach shapes are commonly known as bar/berm profiles (other expressions are: winter/summer profile, storm/normal profile, erosional/accretion-ary profile, bar/step profile, bar/non-barred profile, dis-sipative/reflective profile).

Different criteria to distinguish these two types of profiles have been developed by various authors. From his laboratory experiments, Waters (1939) found deepwater wave steepnesses (H_o/L_o) greater than 0.025 produced a bar profile and values less than 0.025 produced a berm profile (Waters used the terminology storm/ordinary profile). Rector (1954) suggested the same criterion but recognized the occurrence of a transition zone between bar and berm profile defined by a range of steepness values of 0.016-0.025. This convenient rule of thumb is still

73

commonly applied today to the field situation, but it is known not to be correct, at first pointed out by Saville (1957). Rector (1954) also developed an empirical equation for predicting the cross-shore transport direction based on the deepwater wave steepness and the ratio median grain size to deepwater wavelength (D/L_o).

Kemp (1961) defined a "phase difference" parameter in terms of the uprush time (time for the wave to travel from the break point to the limit of uprush) and the wave period. The transition from a berm to a bar profile was considered to occur if the uprush time equalled the wave period (Kemp used the terminology bar/step profile).

Iwagaki and Noda (1963) used a combination of two non-dimensional parameters, namely the deepwater wave steepness and the ratio between deepwater wave height and median grain diameter (H_o/D). Nayak (1970) approached the problem in a fashion similar to Iwagaki and Noda but incorporated the specific gravity in the denominator of the second dimensionless quantity.

Dean (1973), assuming most of the transport in the surf zone occurred as suspended load, pointed out the significance of the fall velocity. The bar/berm criterion used by Dean is expressed in terms of deep water wave steepness and the parameter $\pi w/gT$ in which g is the acceleration of gravity (cf. Kriebel, Dally, and Dean 1986). Sunamura and Horikawa (1975) used three different quantities in their criterion namely, deepwater wave steepness, median grain size divided by deepwater wavelength, and beach slope $(\tan\beta)$. Different values of the empirical coefficient in the equation delineating bar/berm profiles were obtained for laboratory and field conditions, but it is of interest that the same functional form of the equation proved valid for both the laboratory and field situation.

Hattori and Kawamata (1981) developed a criteria for on/offshore transport (berm/bar profile response) based on parameters essentially identical to the ones chosen by Dean

74

(1973) except that the initial beach profile slope was incor-
porated in the wave steepness parameter. Table 3 gives a summary
of several criteria developed for distinguishing bar/berm profile
response. Note that the criterion from Rector (1954) refers to
the cross-shore transport direction, but it is closely related to
the profile response as discussed later.

By comparing prototype-size wave tank data of beach profile
change with small-scale laboratory data, Saville (1957) recog-
nized that deepwater wave steepness criterion of 0.025 was not
accurate to distinguish bar/berm profiles in the prototype. For
his LWT experiments bar profiles occurred at much smaller wave
steepnesses (as small as 0.0028 in the CE experiments), whereas
corresponding cases scaled down to 1:10 experienced marked berm
build-up. As mentioned previously, suspended sediment transport
appears to dominate in the field surf zone, making the fall
velocity an important parameter for characterizing beach pro-
files. Dean (1973) introduced the dimensionless fall velocity
(H/wT) on physical grounds (previously used by Gourlay (1968) and
by Nayak (1970)) from purely dimensional considerations, and
developed it as an indicator of cross-shore transport direction.

In study of criteria for the occurrence of bar/berm profiles
performed as part of the present work, the deepwater wave
steepness and the dimensionless fall velocity were found to be
the most reliable parameters. Figure 6 is a plot of the proto-
type-scale data together with the developed empirical criteria to
distinguish bar/berm profiles. The criterion is given by the
equation

$$\frac{H_o}{L_o} = 0.00070 \; (\frac{H_o}{wT})^3 \tag{2}$$

75

Table 3

Selected Criteria for Classifying Bar and Berm Profiles

Author	Parameters	Comments
Waters (1939) (Johnson, 1949)	H_o/L_o	$H_o/L_o > 0.025$, bar $H_o/L_o < 0.025$, berm
Rector (1954)	H_o/L_o, D/L_o	$D/L_o < 0.0146(H_o/L_o)^{1.25}$, bar $D/L_o > 0.0146(H_o/L_o)^{1.25}$, berm
Iwagaki and Noda (1963)	H_o/L_o, H_o/D	Graphically determined
Nayak (1970)	H_o/L_o, H_o/SD	Graphically determined
Dean (1973) Kriebel, Dally, and Dean (1986)	H_o/L_o, $\pi w/gT$	$H_o/L_o > A\pi w/gT$, bar $H_o/L_o < A\pi w/gT$, berm $A = 1.7$, mainly lab scale $A = 4\text{-}5$, prototype scale
Sunamura and Horikawa (1975)	H_o/L_o, D/L_o, $\tan\beta$	$H_o/L_o > C(\tan\beta)^{-0.27}(D/L_o)^{0.67}$ (bar) $H_o/L_o < C(\tan\beta)^{-0.27}(D/L_o)^{0.67}$ (berm) $C = 4$, small-scale lab. $C = 18$, field conditions
Hattori and Kawamata (1981)	$(H_o/L_o)\tan\beta$, w/gT	$(H_o/L_o)\tan\beta > 0.5$ w/gT, bar $(H_o/L_o)\tan\beta < 0.5$ w/gT, berm
Wright and Short (1984)	H_b/wT	> 6, bar $H_b/wT = 1\text{-}6$, mixed bar and berm < 1, berm
Present Work	H_o/L_o, H_o/wT	$H_o/L_o < 0.00070(H_o/wT)^3$, bar $H_o/L_o > 0.00070(H_o/wT)^3$, berm

Notation: H_o, deepwater wave height; L_o, deepwater wavelength; D, median grain size; S, specific gravity of sand; w, sand fall velocity; g, acceleration of gravity; T, wave period; $\tan\beta$, beach slope; H_b, breaking wave height.

76

In the classification of the different cases, the prominent macromorphology of the profile was considered. For example, a small berm formed on the foreshore was ignored if a large bar formed offshore, since the main transport direction during the run was offshore. In such a case the profile was considered to be a bar profile. Similarly, a small bar may have formed close to the breakpoint in a case where the main trend of transport was onshore and a large berm build-up occurred. The classification of the beach profile responses coincides with that used by Kriebel, Dally, and Dean (1987) except for two cases which were designated as mixed response by these authors, but in this study as berm type. Similarity in classification indicates the results were not strongly influenced by subjective judgement.
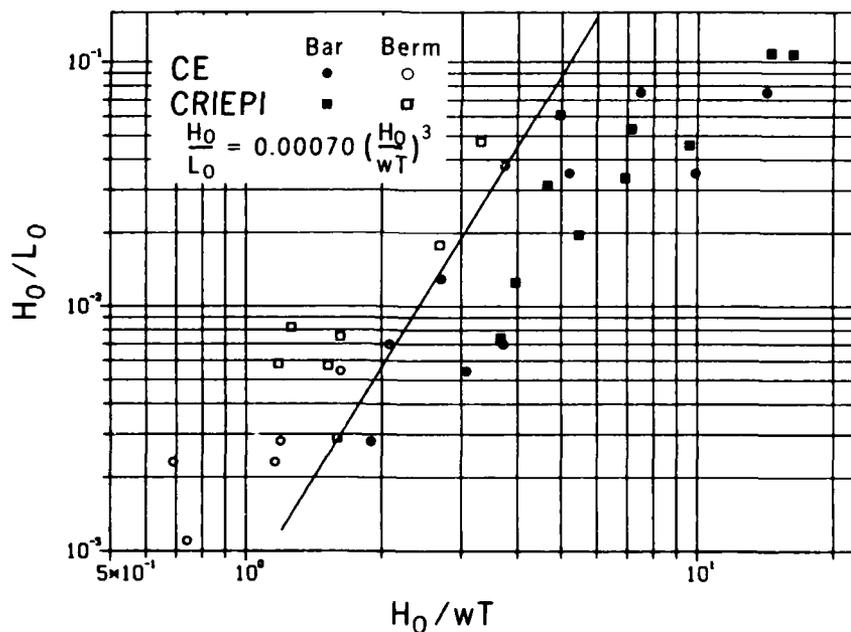
Figure 6. Criterion for distinguishing bar and berm profiles by use of wave steepness and dimensionless fall velocity

As an alternative to use of the dimensionless fall velocity, the parameter suggested by Iwagaki and Noda (1963), H_o/D, was combined with the deepwater wave steepness to yield a criterion for bar/berm profiles for the prototype-scale data. Figure 7 shows a clear distinction results between bar and berm profiles. The line of delineation between bar and berm is given by

$$\frac{H_o}{L_o} = 4.8 \ 10^8 \ (\frac{H_o}{D})^{-3} \tag{3}$$
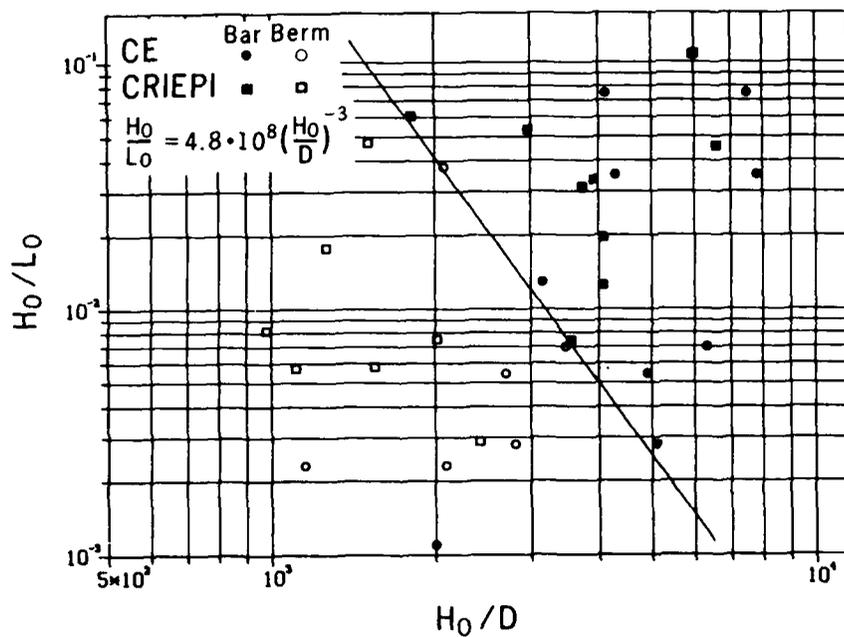
Figure 7. Criterion for distinguishing bar and berm profiles by use of wave steepness and ratio of wave height to grain size

78

Dean (1973) identified the dimensionless fall velocity as an important quantity for determining the type of profile response. Starting from this quantity he derived a criterion based on the deepwater wave steepness and the parameter $\pi w/gT$, called the "fall velocity parameter." Figure 8 shows the CE and CRIEPI data classified according to these parameters.
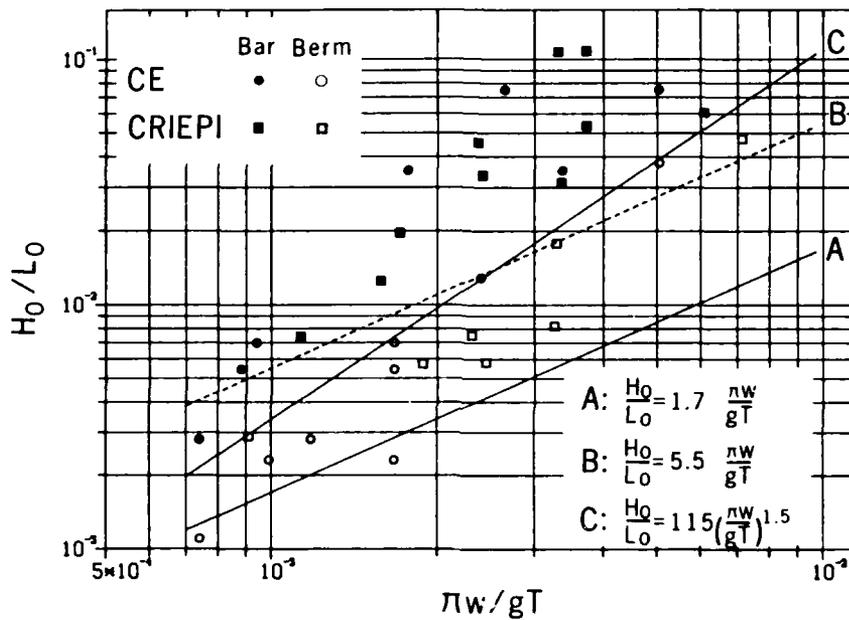
Figure 8. Criterion for distinguishing bar and berm profiles by use of wave steepness and fall velocity parameter

The equation of the separation line (Line B) is

$$\frac{H_o}{L_o} = 5.5 \frac{\pi w}{gT} \tag{4}$$

The value of the empirical coefficient is 5.5 (Line B) which is different from the value 1.7 (Line A) originally given by Dean (1973) and determined from mainly small-scale laboratory data. Kriebel, Dally, and Dean (1987) reevaluated this coefficient and obtained a band of values in the range of 4-5 using a part of the CE and CRIEPI data set. It is, however, possible to achieve even a better delineation between bar/berm profiles if the fall velocity parameter is raised to an exponent (Line C) according to

$$\frac{H_o}{L_o} = 115 \left(\frac{\pi w}{gT}\right)^{1.5} \tag{5}$$

Sunamura (1988) proposed two somewhat different dimension-less quantities for classifying beach profile response involving breaking wave properties instead of deepwater wave conditions, namely D/H_b and H_b/gT^2. The second parameter is basically the inverse of the Ursell parameter $U = HL^2/h^3$ evaluated at breaking if linear wave theory is used. With these two parameters it is possible to obtain a good profile classification (Figure 9) although one point is located in the wrong area.

The equation of the line separating bar/berm profiles is

$$\frac{D}{H_b} = 0.014 \left(\frac{H_b}{gT^2}\right)^{0.68} \tag{6}$$

In summary, it is possible to obtain a clear distinction between bar/berm profiles if the dimensionless quantities chosen for the criterion are composed of parameters characterizing both sand and wave properties.
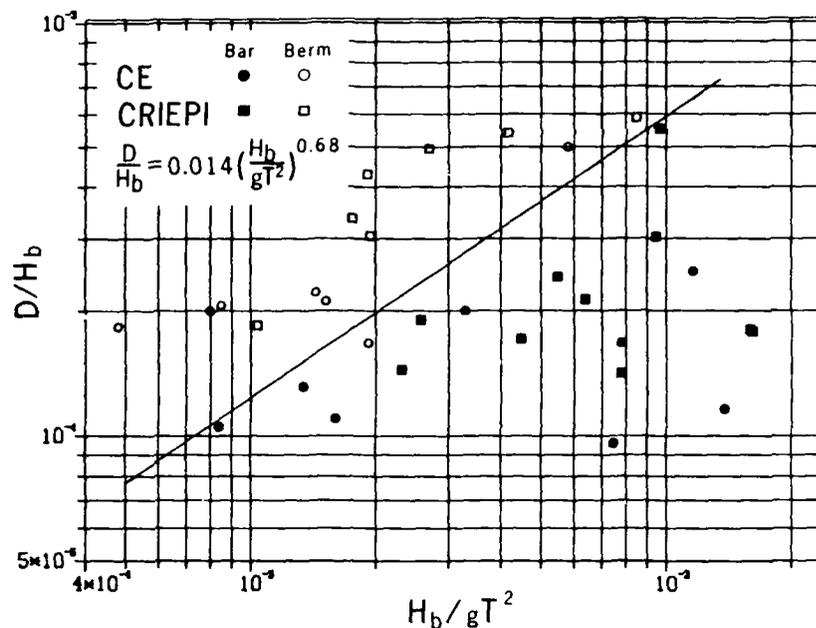
Figure 9. Criterion for distinguishing bar and berm
profiles by use of ratio of breaking wave height
and grain size, and Ursell number at breaking

Significant differences occur, however, in the values of the
empirical coefficients in the criteria depending on whether
small-scale or prototype-scale data are used. Deepwater wave
steepness appears in most criteria together with a parameter
involving a quantity for describing the sediment, such as fall
velocity or grain size. Using the dimensionless fall velocity as
the second parameter gives a good delineation between bar/berm
profiles and this parameter has a sound physical basis as
explained by Gourlay (1968) and Dean (1973). Furthermore, as
will be shown later in this report, in quantifying morphologic
features the dimensionless fall velocity appears naturally in
many of the developed relationships. In most cases, the value of
the dimensionless fall velocity varies over the same order of

magnitude for a wide range of sand and wave conditions making it more appealing to use than, for instance, H_o/D.

Examination of transport rate distributions inferred from successive profile change (Part V) shows that there is a close relationship between development of bar/berm profiles and the direction of net cross-shore transport (offshore/onshore). Thus a criterion for predicting bar/berm development can also be applied to predict the main net transport direction. Typically, if a bar is formed, the main direction of transport is offshore even if the bar receives a net contribution from onshore transport of material originating from areas seaward of the bar in the situation of a relatively mild wave climate. A criterion which refers to onshore/offshore movement will, in most cases, predict offshore-directed sand movement if a bar is present, and onshore-directed movement if a berm is present. However, profiles in between bar and berm type may have a complex transport distributions where a clear trend for onshore or offshore transport is not apparent.

Shoreline movement

An investigation was made to incorporate initial beach slope in the criterion for bar/berm profile classification. Addition of this parameter did not increase predictability. Also, it added the complication of determining a representative slope. Slope is implicitly contained in the use of fall velocity (or grain size), as the equilibrium beach profile depends on this quantity.

If, instead of bar/berm profile type, shoreline retreat/advance is studied a less clear distinction is obtained by use of only dimensionless fall velocity and deepwater wave steepness for a criterion. In this case incorporation of the initial beach slope increases predictability of the criterion because the initial slope is closely related to the amount of material that

82

moves before equilibrium is attained. Also, a gentle slope dissipates more incident wave energy because the waves have to travel a longer distance in the surf zone before they reach the shoreline. Some CRIEPI cases showed that shoreline advance occurred for situations with a gentle initial slope even if considerable erosion took place in the surf zone, to produce a distinct barred profile.

Figure 10 plots shoreline retreat/advance that occurred in the CE and CRIEPI experiments together with a line distinguishing between the two types of response. The initial profile slope was added to the non-dimensional quantities to increase the predictability of the criterion.
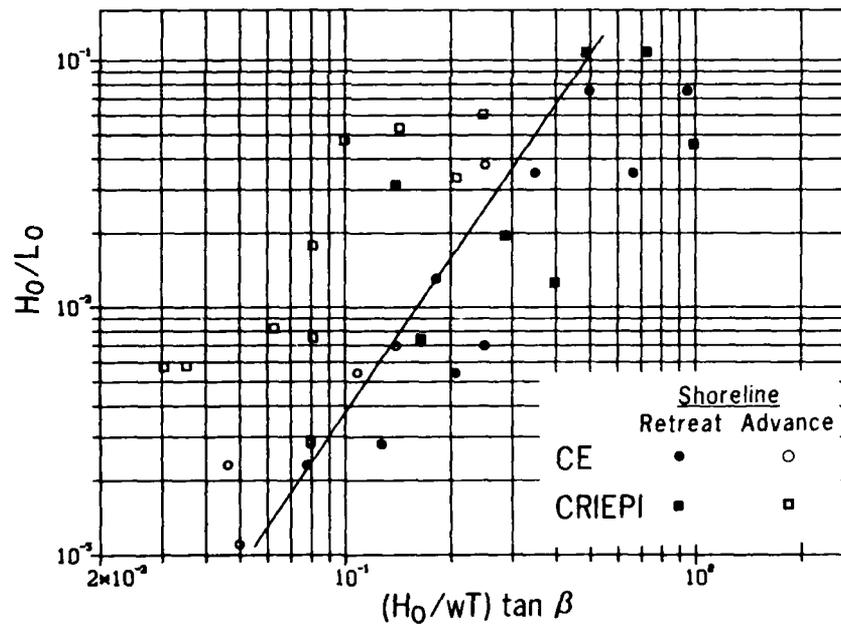
Figure 10. Criterion for distinguishing shoreline retreat and advance by use of wave steepness, dimensionless fall velocity, and initial beach slope

83

Application to small-scale data

The dimensionless fall velocity and the deepwater wave steepness were also used to classify the data pertaining to small-scale laboratory profile change found by Rector (1954), Iwagaki and Noda (1963), and Nayak (1970). As seen from Figure 11a, the criterion derived from the large-scale tests is not applicable to the small-scale data using the coefficients given in Equation 2. By modifying these coefficients it would be possible to obtain a crude delineation with the quantities in Equation 2. However, the dimensionless fall velocity seems to be of less significance in distinguishing between bar/berm profile response in small-scale laboratory experiments. This is attributed in great part to the mode of transport, the main transport mode probably being bed load during these types of experiments and not suspended load as under higher waves in the field.

Therefore, use of the parameter H_o/D instead of H_o/wT should provide a better basis for profile classification since it expresses a relationship between the force exerted by the waves and the resistance offered by the grains (Nayak, 1970). This interpretation is closely connected with the physics of bed load transport, where the main driving force is the horizontal water particle velocity. In suspended transport, the upward transport of eddy momentum keeps the grains in suspension and make them available for transport. Figure 11b illustrates the improvement of using H_o/D for classifying beach profiles. Although the points denoting bar and berm profile response still are somewhat mixed, it is possible to obtain a better delineation than in Figure 11a.

The importance of wave period in scaling is also stressed through the significant difference between small-scale and prototype-size experiments if classifying the beach response using the dimensionless fall velocity.

84
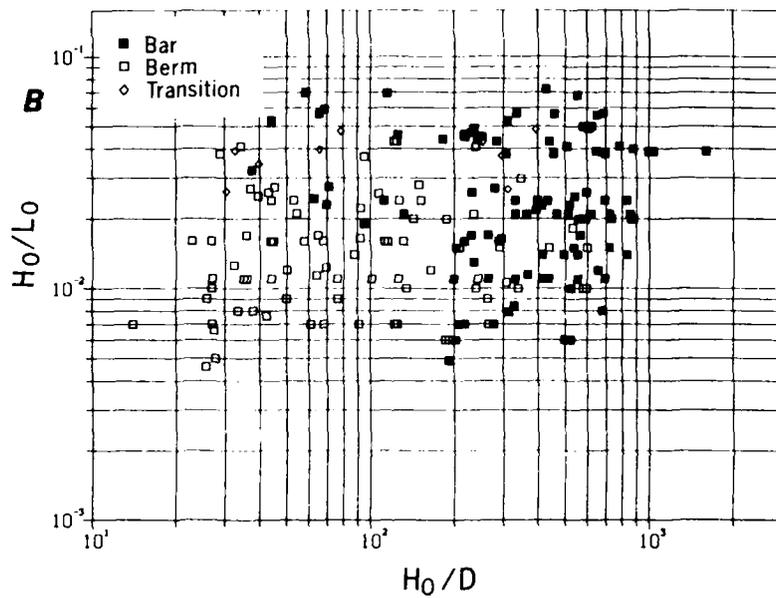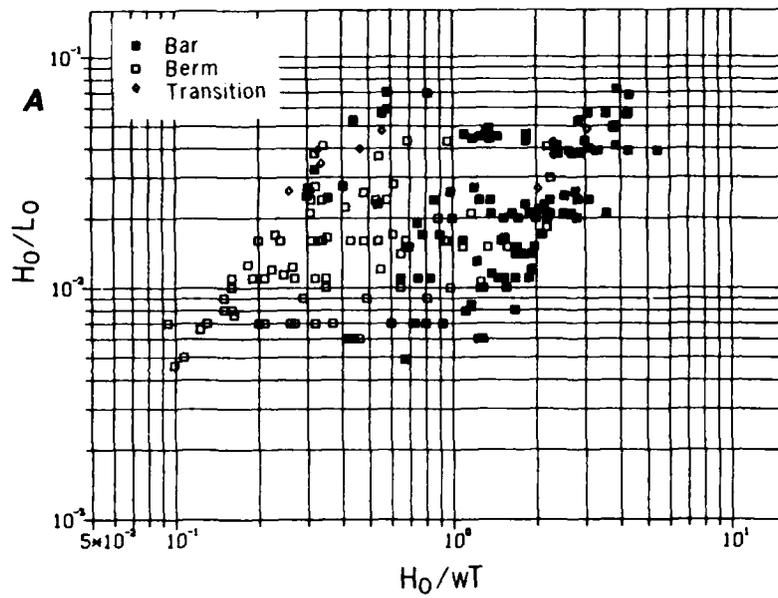
Figure 11   Criterion for distinguishing bar and berm
             profiles applied to small-scale laboratory data
             by use of wave steepness and (a) dimensionless
             fall velocity, and (b) ratio of wave height to
             grain size

85

Form and Movement of Bars

Bar genesis

Several theories have been suggested to explain the forma-
tion of longshore bars. Since a wide variety of bed forms has
been classified as a bar-like feature by different authors,
different mechanisms presumably prevail in the formation process.
This investigation considers morphologic features resulting from
depth-limited breaking waves and does not attempt to describe
beach change produced by other causes. As waves break near
shore, energy is dissipated providing a turbulent fluid environ-
ment where grains may be entrained and maintained in suspension.
Depending on the vertical profile of both the cross-shore
velocity field and sediment concentration, the sediment will
experience a net onshore or offshore movement resulting in a
berm- or bar-type profile. Sediment transported in the offshore
direction will be deposited where the turbulence starts decreas-
ing, somewhat seaward of the plunge point, where the breaking
wave has its maximum energy dissipation (Miller 1976, Skjelbreia
1987). A berm is formed as material is transported onshore and
deposition on the foreshore occurs, for which the force of
gravity and properties of the uprush bore determine the berm
height (Bagnold 1940, Sunamura 1975).

The type of bars investigated in this study are those formed
by breaking waves occurring on beaches exposed to moderate or
high wave-energy conditions with a moderate tidal variation (for
a bar classification, see Greenwood and Davidson-Arnott 1979).
Waves approaching shore on a sloping beach increase in height due
to shoaling, until depth-limited breaking occurs. The condition
for incipient breaking is a function of the local beach slope and
the wave steepness (e.g., Weggel 1972, Singamsetti and Wind
1980). As breaking occurs, energy dissipation of the waves
increases sharply producing the necessary work to intensively

entrain and transport sediment in the surf zone. The maximum in the cross-shore transport rate appears to be located in the vicinity of the plunge point, where the maximum energy dissipation occurs. Seaward of the point of maximum energy dissipation, the transport drops off, leading to accretion of sand in this region and bar formation. As the bar grows, the waves break further offshore and the break point and plunge point translate seaward, causing the location of the maximum transport rate and the bar to move offshore. This process continues until a stable beach profile is achieved which dissipates wave energy without significant changes in shape.

A wave that has broken may after further travel reach a stable wave height and reform. Dissipation of energy decreases in the reformed waves, implying a corresponding decrease in transport rate. Eventually the reformed waves shoal and break again closer to shore, forming a second bar in the same manner as the more seaward main breakpoint bar was formed. The described mechanism is valid for both plunging and spilling breakers, both producing a trough in the profile shoreward of the break point (Sunamura 1988), although the time scale of bar development will be longer under spilling breakers (Sunamura and Maruyama 1987). Figure 12 displays consecutive profiles in time for one of the CE cases (Case 500), showing a typical example of beach profile evolution with a main breakpoint bar and another smaller bar further inshore. Average breaker locations are indicated in the figure for the profiles where such information was available.

Another mechanism for bar formation is long-periodic waves generated, for example, by reflection from the beach (Bowen 1980). Standing waves as a possible mechanism for bar formation have been investigated by Carter, Liu, and Mei (1973), Lau and Travis (1973), Short (1975a, 1975b) and Mei (1985). An oscillating velocity field induces a steady mean current in the boundary layer close to the bed. If the oscillations are produced by purely progressive waves, the mean drift in the boundary layer

87
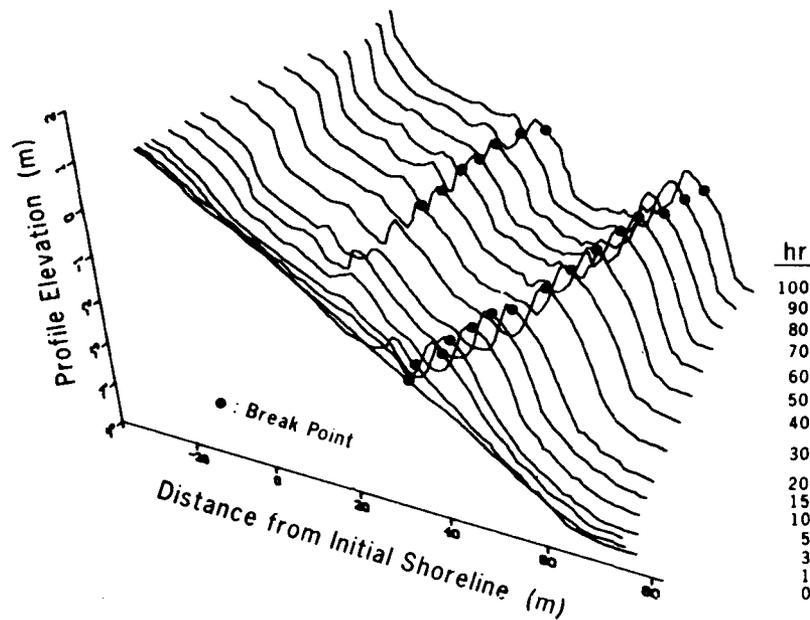
Figure 12. Growth and movement of breakpoint bar with elapsed time and location of break point

will always be in the direction of the propagating waves. Partial reflection of the incoming wave may cause the direction of mass transport in the lower part of the boundary layer to reverse if the reflection is large enough. (Theoretically, the reflection coefficient should exceed 0.414 according to Carter, Liu, and Mei 1973.) A complete standing wave induces mass transport towards the nodes in the lower part of the boundary layer and mass transport towards the antinodes in the upper part of the boundary layer. Depending on which height the grains are lifted to in the water column when transported, the grains will experience a net drift and accumulate under the nodes or antinodes. However, this should depend on grain size to some extent (De Best and Bijker 1971). 'Iolman and Bowen (1982) assumed that suspended sediment transport was dominant and used the average mass transport in the upper part of the boundary

88

layer to determine equilibrium shapes of beaches based on a
Bagnold-type transport formula. Complex three-dimensional
geometries were derived by superimposing progressive waves to
obtain standing wave patterns alongshore and cross-shore.

In some of the CRIEPI cases started from the steep plane
slope of 1/10, considerable reflection was present (a reflected
wave height of 0.4 m superimposed on the wave height distribu-
tion) but the effect of the reflected wave on the profile shape
appeared to be very small (see Figure 13). Actually, as the bar
grew in size and the seaward slope became steeper, the bar
promoted reflection but it is surmised that the main effect was
to alter the breaking wave process somewhat.
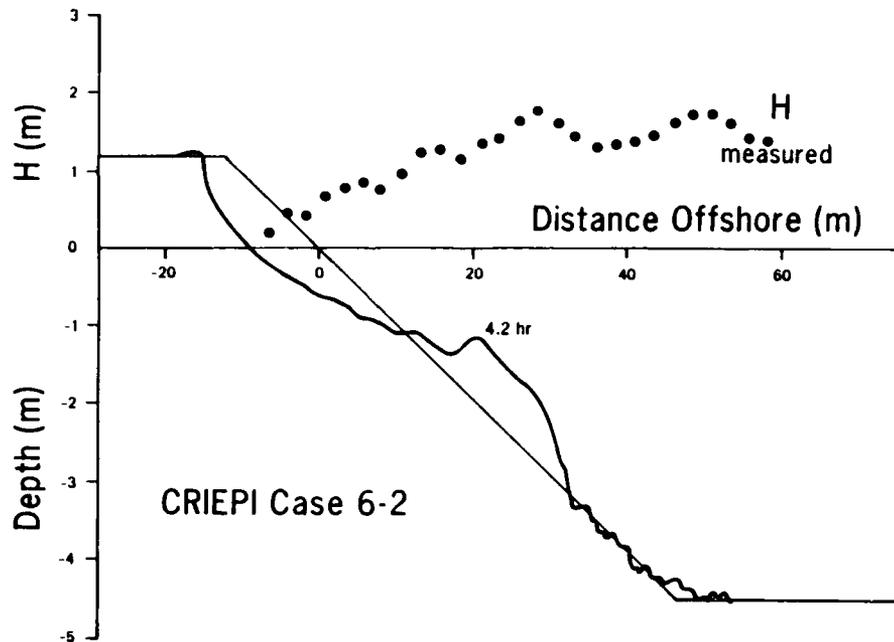
Figure 13. Beach profile from CRIEPI Case 6-2 measured
            after 4.2 hr of wave action together with the
            initial profile and the wave height distribution
            across-shore

89

Equilibrium bar volume

As the bar moves offshore it simultaneously increases in
volume to approach an equilibrium value. Figures 14a and 14b
show bar volume for the main breakpoint bar as a function of time
for the CE and CRIEPI experiments, respectively. Some of the
cases were not run sufficiently long to reach the equilibrium
volume. The approach to equilibrium is typically smooth. If a
breakpoint bar formed on a profile where onshore transport
(accretion) dominated, equilibrium volume was reached very fast
and was relatively small. Examples are Cases 101, 301, and 801
from the CE data and Case 2-3 from the CRIEPI data. Bar volume
changed abruptly if a secondary breakpoint bar grew together with
the main breakpoint bar. Often, further growth of the main
breakpoint bar was hindered by this coalescence of bars, as shown
in Case 300 (occurs at 15.0 hr). Profiles having only one bar
showed a more regular development in time toward an apparent
equilibrium volume.

Since equilibrium bar volume in some cases was not entirely
reached, and in order to obtain the least subjective method for
determining equilibrium bar volume, a simple expression of an
exponential type was least-square fitted to the data for each
case. The expression chosen is often encountered in growth
problems where an equilibrium state exists. The same expression
was used by Kriebel and Dean (1985a) to characterize dune
erosion. The bar volume V is assumed to grow toward the
equilibrium volume V_{eq} according to

$$V = V_{eq} (1 - e^{-\alpha t}) \qquad (7)$$

where t is time and α is an empirical temporal rate coeffi-
cient. Correlation analysis (25 cases evaluated) involving
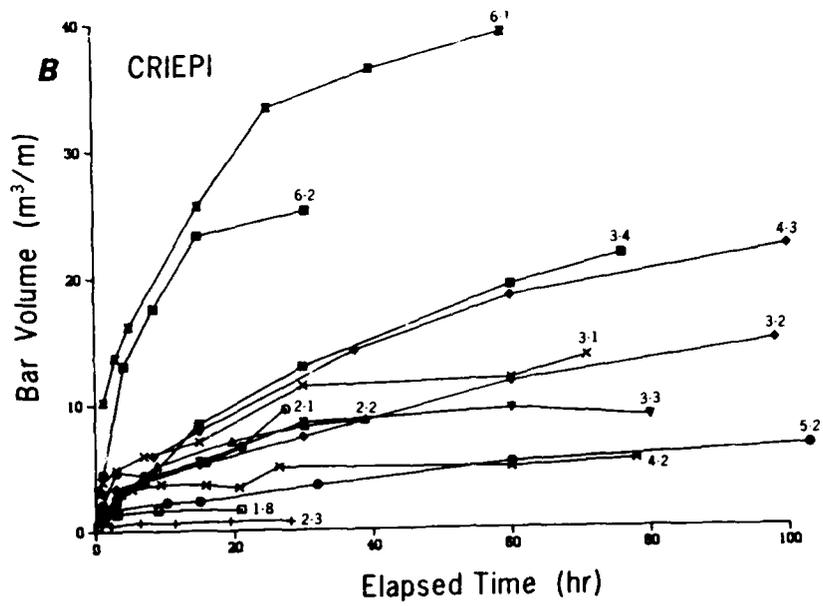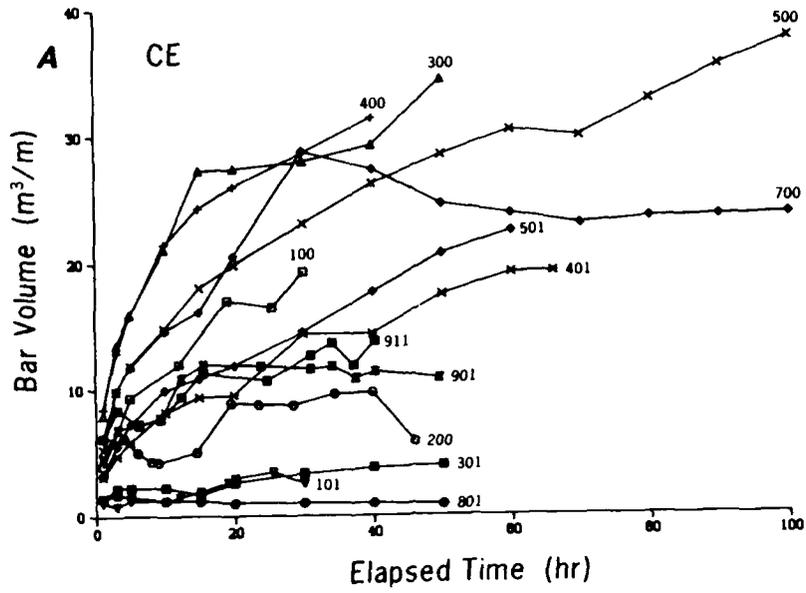
Figure 14. Growth of bar volume with elapsed time: (a) CE data, and (b) CRIEPI data

91

pertinent wave and beach profile parameters showed that equi-
librium bar volume was most closely related to deepwater wave
height, fall velocity (or grain size), and initial beach slope,
although the correlation coefficients were not high (0.6-0.7). A
larger wave height implied a larger bar volume, a larger fall
velocity (or larger grain size) implied a smaller bar volume, and
an initially steeper slope also produced a larger bar volume for
a given grain size. Fall velocities were calculated from an
expression given by Hallermeier (1981) for the CRIEPI data, and
in the CE cases fall velocities determined by Seelig (1983a) were
used. Fall velocities depended on water temperature in the wave
tank (Kajima et al. 1983b and Kraus and Larson 1988).

In the range of interest the fall velocity is almost
linearly dependent on grain size, resulting in similar correla-
tion values for grain size and fall velocity. A stepwise
regression analysis incorporating these factors explained 70 % of
the variation in the data; wave height was most important,
accounting for 35 %; followed by the fall velocity which ex-
plained 30 %. Wave period and initial beach slope accounted
together for only 5 %. If only bars formed on a profile which
mainly experienced erosion (transport directed offshore), the
coefficient of determination increased to 80 %, with the afore-
mentioned parameters being most important. The dimensional
regression relationship involving equilibrium bar volume (V_{eq}),
deepwater wave height, sand fall velocity, and wave period for
bars formed on erosional profiles is

$$V_{eq} = 0.088 \ H_o^{2.26} \ w^{-1.36} \ T^{0.55} \tag{8}$$

It is desirable to use non-dimensional quantities to obtain
general relationships relating morphologic features to wave and
sand parameters. From the regression equation describing

92

equilibrium bar volumes on erosional profiles, Equation 8, it was possible to identify dimensionless parameters by dividing by the wave period raised to a properly chosen exponent. Equilibrium bar volume was normalized by the deepwater wavelength squared, and the independent parameters emerged as dimensionless fall velocity and deepwater wave steepness. The coefficient of determination (r^2, see Ostle and Mensing 1975), defined as the percentage of the sum of squares explained by the regression equation, will increase by incorporating the wave period in the parameters (from 75% (without beach slope incorporated) to 90%). The resultant regression equation determined is

$$\frac{V_{eq}}{L_o^{\,2}} = 0.028 \; (\frac{H_o}{wT})^{1.32} \; (\frac{H_o}{L_o})^{1.05} \tag{9}$$

Actually, Equation 9 is an inferior predictor of equilibrium bar volume than the original regression equation (r^2 drops from 75% to 70%) formed by dimensional variables, since the least-square estimate will be more influenced by wave period, which is less important for determining equilibrium bar volume than wave height and sand fall velocity. Thus, use of non-dimensional quantities is somewhat at the expense of predictability, but will give a more general and physically-based relationship. Figure 15 displays a comparison between the predicted equilibrium volume according to Equation 9 and equilibrium volumes extrapolated from the measurements with Equation 7.

The temporal rate coefficient, α , appearing in Equation 7 controls the speed at which equilibrium bar volume is attained. Correlation between the rate coefficient and wave and beach profile properties was in general very low (correlation coefficients less than 0.5). Qualitatively, α appears to increase with fall velocity (or grain size) and decrease with wave height

7 93
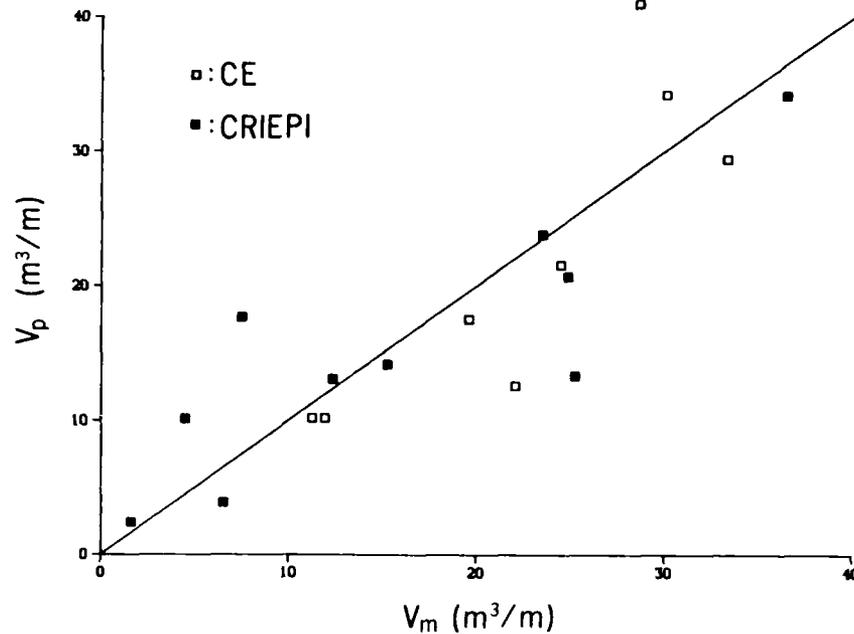
Figure 15. Comparison of measured equilibrium bar volume V_m
and empirical prediction V_p

and wave period. A large α-value gives a rapid response towards
equilibrium. If the wave height is large more wave energy has to
be dissipated along the beach profile, that is, the bar becomes
larger and forms further offshore, causing more material to be
moved before the equilibrium shape is reached (lower α-values).
Furthermore, larger (heavier) grain sizes require higher wave
energy in order to be moved, implying more rapid attainment of
equilibrium (higher α-values).

Depth to bar crest

As a bar moved offshore, its height increased so that the
depth to the crest (h_c) was roughly constant during a run (except
perhaps, at the very first surveys) (cf. Birkemeier 1985a, Dette
and Uliczka 1987). In Figures 16a and 16b the minimum depth on

the bar, called the crest depth, is plotted as a function of time for the CE and CRIEPI data. For some cases for which the bar formed on an accretionary profile, it remained stationary, or even moved slightly onshore, causing the crest depth to decrease. Also, if two bars joined together the crest depth changed abruptly, since the inner bar crest was located in more shallow water.

A comparison between Cases 901 and 911 shows that even though the equilibrium bar volume was almost the same (11.3 and 12.0 m^3/m respectively), Case 911 experienced a considerably larger fluctuation in depth at the bar crest. Wave parameters and beach properties were identical for these two cases, the only difference being a stepwise sinusoidal water level change imposed in Case 911 to simulate a tide. Consequently, during cycles of increased water level in Case 911, the depth at the bar crest increased and the bar grew closer to the initial still-water level. During cycles of lower water level, the depth at the crest decreased and a portion of the bar eroded, causing the bar crest to move away from the reference initial still water level. There was no significant time lag between water level change and corresponding change in depth at the bar crest (cf. Shepard 1950).

The average depth at the bar crest was calculated for all profiles comprising an individual case. This average was closely related to the breaking wave height and showed little dependence on wave period and grain size. If an inshore bar grew together with the main breakpoint bar, the most seaward bar crest was used in determining the depth at the bar crest. The following relationship with the breaking wave height was obtained

$$h_c = 0.66 \ H_b \qquad\qquad (10)$$
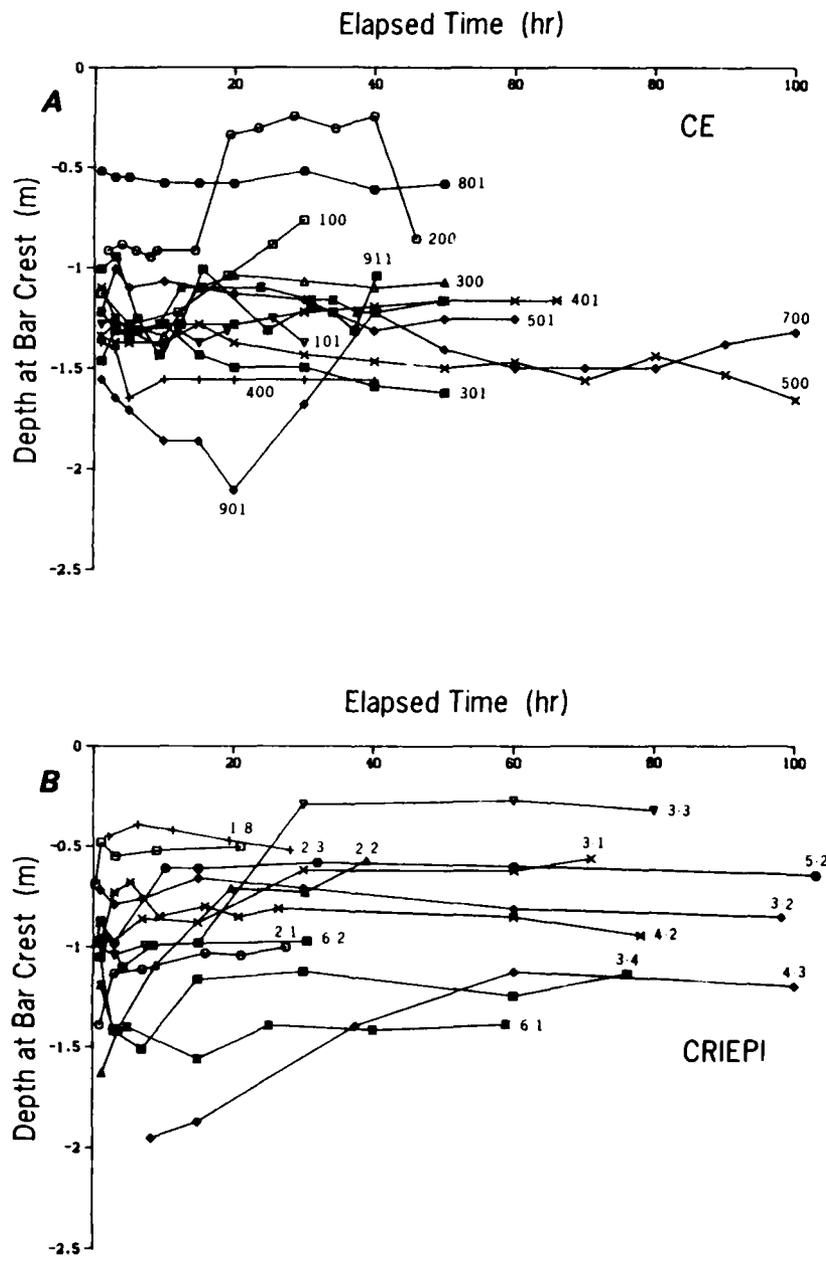
Figure 16. Depth to bar crest as a function of elapsed
time: (a) CE data, and (b) CRIEPI

Equation 10 is plotted together with the CE and CRIEPI data in Figure 17. The coefficient of determination of the regression line was 70%.
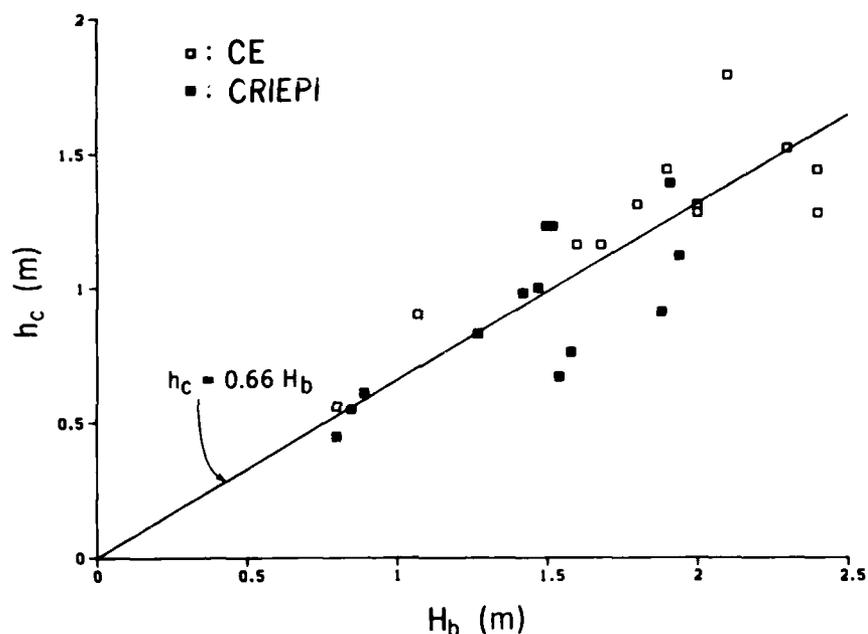
Figure 17. Relationship between depth to bar crest h_c and breaking wave height H_b

For the cases where a small bar formed on an accretionary profile, the crest depth had a tendency to decrease slightly with time if onshore bar movement occurred, which contributed to the scatter in the data. Sunamura (1988) found a coefficient of 0.59 as opposed to 0.66 in Equation 10, based on small-scale labora-tory wave tank data and some CRIEPI data.

Ratio of trough depth to crest depth

The minimum occurring immediately shoreward of the bar was taken as the trough bottom in the analysis. This was considered as a natural and objective definition of trough location even

though a trough was sometimes located in an area where material
was accreting with respect to the initial profile. Keulegan
(1945) studied the relation between the trough depth (h_t) and bar
crest depth (h_c). He found an average value of 1.69 for labora-
tory beaches and 1.65 for field beaches. Shepard (1950) observed
much lower ratios at the Scripps pier with a mean value of 1.16
(referenced to mean sea water level).

In the present study, this ratio was calculated for 26 CE
and CRIEPI cases and ranged between 1.26 to 2.16, with an average
of 1.74 and standard deviation of 0.26. The ratio was calculated
as an average for all profiles surveys during a case and showed
little change in time for most cases. However for some cases the
very first profile survey showed a markedly different ratio,
typically much lower than the average, and these spurious values
were excluded from the calculation of the average.

The ratio of trough depth to crest depth showed a marked
inverse dependence on the wave period, as illustrated in Figure
18. The wave period accounted for 60 % of the variation in the
data using a regression relationship between the ratio and the
wave period. Expressed as an empirical power law in terms of
wave steepness, regression analysis gave:

$$\frac{h_t}{h_c} = 2.50 \left(\frac{H_o}{L_o}\right)^{0.092} \tag{11}$$

Equation 11 had a coefficient of determination of 55%,
slightly lower than using only the wave period, but from a
general point of view it is more attractive to use in a predic-
tive relationship. Note that Keulegan (1948) did not distinguish
any dependence on wave steepness in his analysis.

Qualitative examination of the scattered data indicated that
the ratio seemed to increase with grain size for bars formed on
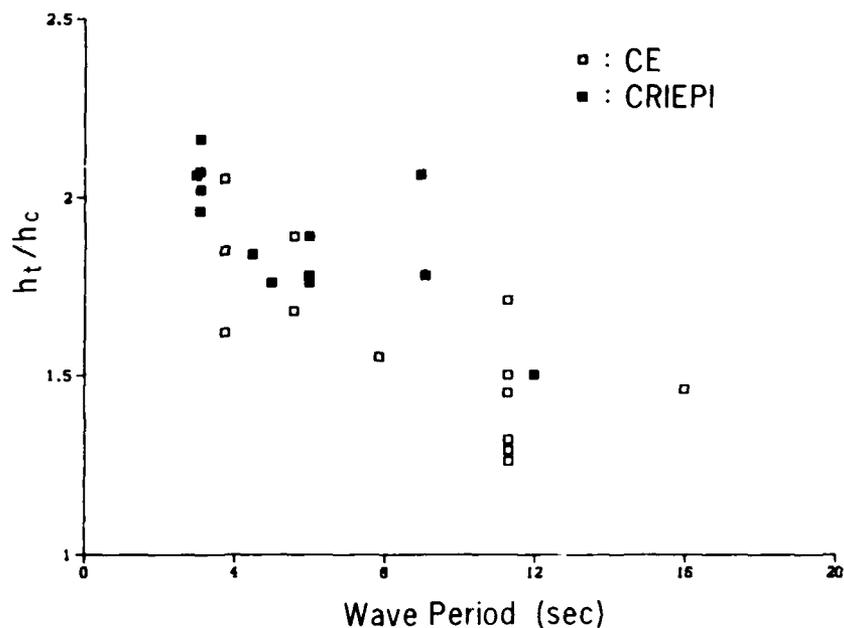
Figure 18. Ratio of depth to trough bottom and depth to bar
crest h_t/h_c as a function of wave period.

erosional profiles but decreased with grain size for bars formed
on accretionary profiles. In erosional cases, the profile for
coarser grain sizes in general showed a steeper shoreward slope
of the bar, allowing for a larger vertical distance between bar
crest and trough bottom. The breakpoint bar formed on an
accretionary profile was normally small and its size decreased
with increasing grain size, making the bar flatter with a lower
ratio between trough depth and crest depth.

Maximum bar height

As a bar moved offshore its maximum height defined with
respect to the initial profile increased to approach an equi-
librium value. Figures 19a and 19b show maximum bar height (Z_B)
as a function of time for the CE and CRIEPI experiments, respec-
tively. Bars formed on an accretionary profile achieved equi-

99

librium height very rapidly, often during the first hour of the run (see Cases 101, 801, 2-3, 3-3). A coarser grain size produced a smaller equilibrium bar height for the same wave parameters, and a larger wave height produced a larger equilibrium bar height for fixed wave period and initial profile properties. The curves displayed in Figures 19a and 19b are readily approximated by an expression similar in form to Equation 7. (Some cases where the bar formed on an accretionary profile showed an almost constant bar height in time and thus were not used in the analysis.) Maximum equilibrium bar height for all cases was estimated by least-square fitting the data to an expression similar to Equation 7. Correlation analysis of the 24 values showed that the equilibrium bar height was most closely related to deepwater wave height and sand fall velocity. If the wave height increased, the bar height increased, whereas a higher fall velocity implied a smaller bar height. Equilibrium bar height was only weakly related to wave period, where a longer period seemed to produce a smaller bar height.

Regression analysis between the maximum equilibrium bar height and basic wave and beach parameters, maintaining dimensions, accounted for 65 % of the variation in the data. The deepwater wave height and the sand fall velocity together accounted for 60 %. If only bars formed on erosional profiles were considered (19 values), the coefficient of determination increased considerably, to 80 %, for which deepwater wave height and sand fall velocity accounted for 75 %. The dimensional regression equation involving deepwater wave height and sand fall velocity, for the erosional cases, is

$$Z_B = 0.128 \ H_o^{1.36} \ w^{-0.58} \tag{12}$$
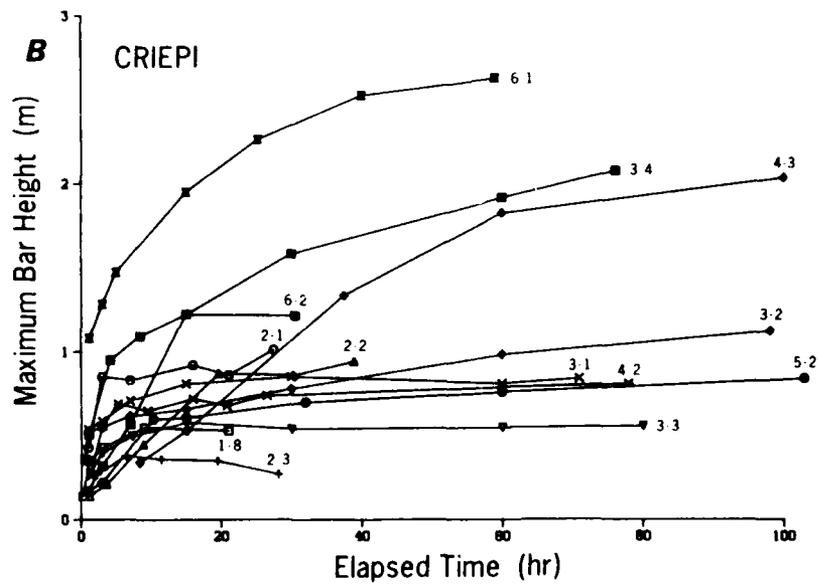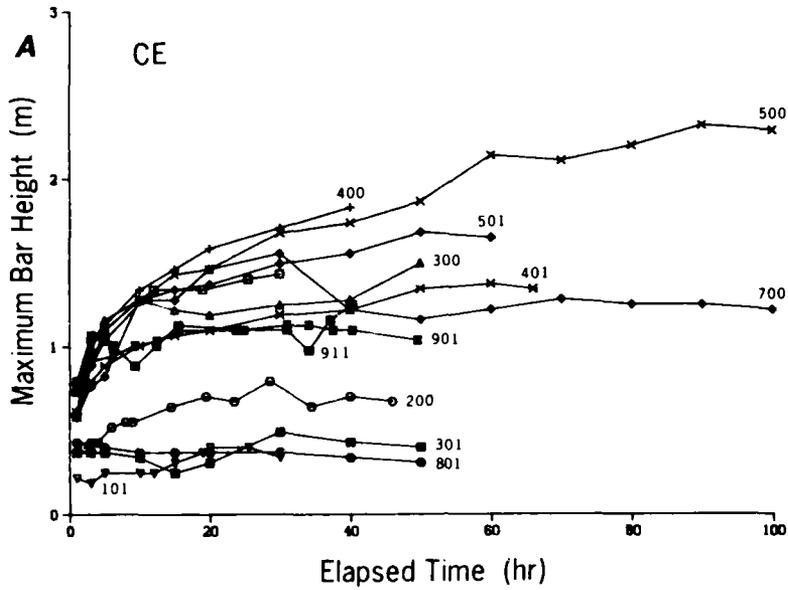
Figure 19.   Maximum bar height as a function of time
             elapsed: (a) CE data, and (b) CRIEPI data

From the regression relationship derived with dimensional quantities, Equation 12, it was possible to form nondimensional parameters by division with the wave period raised to a properly chosen exponent. The maximum equilibrium bar height divided by the wavelength is a function of dimensionless fall velocity and deepwater wave steepness. Although wave period had little effect on bar height, as mentioned previously, inclusion of the wave period may increase the coefficient of determination but not the predictability of the maximum equilibrium bar height. The regression equation is written

$$\frac{Z_B}{L_o} = 0.122 \ (\frac{H_o}{wT})^{0.59} \ (\frac{H_o}{L_o})^{0.73} \tag{13}$$

Use of nondimensional quantities in this case did not lower the coefficient of determination notably (from 80% to 75%) for predicting the maximum equilibrium bar height. Figure 20 shows a comparison between predicted equilibrium bar height by the regression model (Equation 13) and the measurements.

The temporal rate coefficients governing growth toward the maximum equilibrium bar height for bars formed on erosional profiles had highest correlation with sand fall velocity. Similar to the situation for the rate coefficient governing bar volume growth, correlation coefficients were quite low (less than 0.5). However, a regression relationship between the rate coefficient and wave period, deepwater wave height, and sand fall velocity gave a relatively high coefficient of determination of 70%. This was considerably larger than any regression relationship obtained for the rate coefficient pertaining to bar volume growth. The sand fall velocity and the deepwater wave height accounted for 60 % of the variation in the data giving the relationship
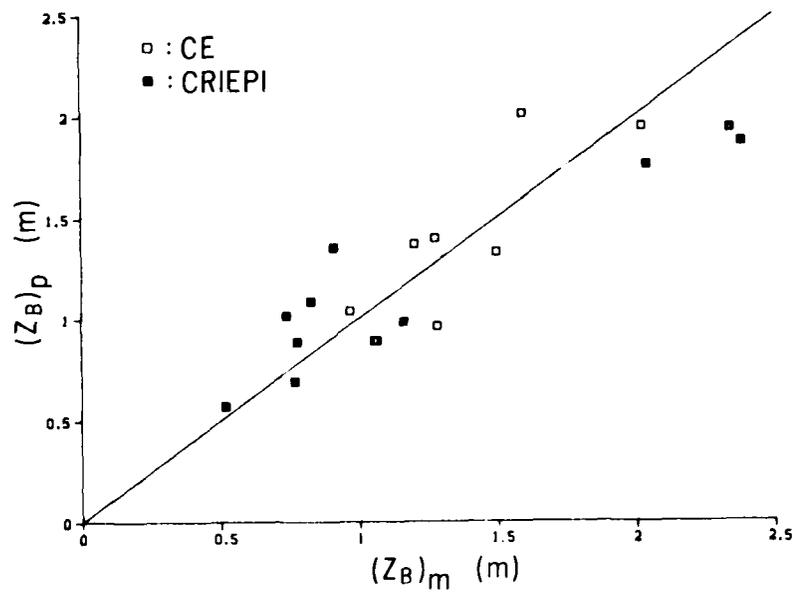
Figure 20.   Comparison of measured equilibrium bar height
(Z_B)_m and empirical prediction (Z_B)_p

$$\alpha = 34.1 \ H_o^{-1.43} \ w^{1.98} \ T^{1.23} \tag{14}$$

From the dimensional regression equation, Equation 14, the
dimensionless fall velocity was identified as an important
quantity. By normalizing with wave period, the dimensionless
quantity thus obtained was related to the dimensionless fall
velocity according to

$$\alpha T = 117 \ (\frac{H_o}{wT})^{-2.30} \tag{15}$$

The coefficient of determination was only 55%, but Case 700 contributed to more than half of the sum of the residuals. The reason is probably due to a decrease in wave height that occurred between 20-30 hr during the run, strongly affecting build-up of the bar (Kraus and Larson 1988).

Bar location and speed of movement

Movement of a bar during wave action is perhaps most accurately characterized by its center of mass (x_{CM}). The bar crest, which is the most convenient measure of bar location in the field, is not as accurate a measure since the shape of the bar changes during the course of its growth, influencing the location of the crest more than the center of mass. In general, the mass center of the bar moved offshore on an erosional profile unless a more shoreward bar grew together with the main break-point bar. Actually, if a secondary bar merged with the main bar, further clear movement of the bar conglomerate was absent. On an accretionary profile the bar moved somewhat onshore or was stationary.

In Figures 21a and 21b the horizontal location of the mass center is shown as a function of time for the CE and CRIEPI experiments. Distance was measured from the intersection of the initial profile and the still-water level. Bars formed on a beach composed of coarser grains in general moved less than those on beaches composed of finer grains under the same wave condi- tions (compare Cases 400-401 and 500-501). Case 911, which involved a sinusoidally varying water level, showed back and forth movement of the bar in response to the change in water level, an effect not observed in control Case 901 with a fixed water level.

It was difficult to detect trends in the movement of the vertical position of the bar center of mass. For bars formed on accretionary profiles, vertical position of the mass center was
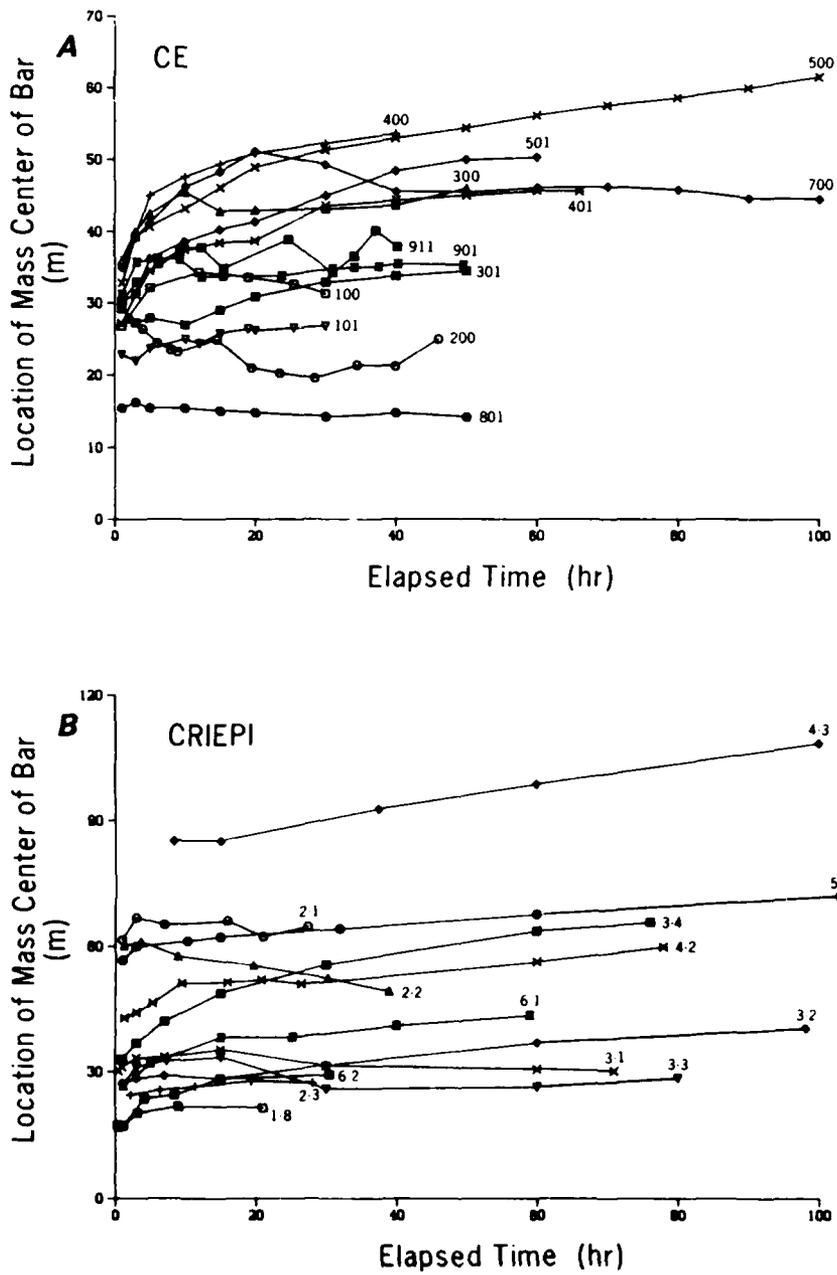
Figure 21. Horizontal movement of bar center of mass with
elapsed time: (a) CE data and (b) CRIEPI data

relatively constant since the equilibrium bar volume was attained
rapidly, and horizontal movement of the bar was limited.
However, the overall trend for bars formed on erosional beach
profiles was for the vertical distance to the bar mass center to
increase with time.

Bars appeared to be initiated at the same location along the
profile for the same wave parameters and initial beach slope,
irrespective of beach grain size. However, the bar center of
mass at later times was usually located further offshore and in
deeper water for finer grain-sized beaches.

Both the location of the bar crest and the bar center of
mass were used as reference points to determine the speed of bar
migration. Evolution of bar speed had the same characteristic
features for both quantities. Only bars formed on erosional
profiles were included in analysis of migration speed, since bars
formed on accretionary profiles were almost stationary (see
Figures 21a and 21b). Furthermore, if an inner bar grew together
with the main breakpoint bar, only the seaward portion of the bar
conglomerate was considered in order to eliminate spurious
instantaneous shoreward displacements of the center of mass
resulting from coalescence of the bars. Figures 22a-d display
speed of bar migration. Positive speeds of bar migration
indicate movement directed offshore. The main trend was similar
for all cases and defined quantities, exhibiting a high initial
speed of bar migration which slowed as the profile approached the
equilibrium shape.

Case 911 from the CE experiment, which had a variation in
water level, showed intermittent onshore movement and consequent-
ly negative bar speeds as the water level dropped. A negative
speed of bar migration also occurred if bar shape changed
considerably during a run, particularly if the location of the
crest was used as the reference point. For example, Case 100
showed a negative bar speed after about 20 hr as the beach eroded

back to the end of the tank and marked reflection started to
occur, influencing bar shape.

Initial speeds of bar migration in the LWT were close to a
value found in field measurements by Sallenger, Holman, and
Birkemeier (1985) during a storm at Duck, North Carolina. In
general, morphologic features of the beach profile showed rapid
response to changing wave conditions, in qualitative agreement
with that generated in the LWT. The bar crest at Duck had an
average offshore speed of 2.2 m/hr during the initial phase of
one storm (6-hr average) and a speed of 1.4 m/hr for another
storm with smaller waves. Migration speeds measured by Sal-
lenger, Holman, and Birkemeier (1985) were close to those
obtained in the CE and CRIEPI studies for the cases showing
strong erosion (Figures 22b and 22d).

The distance between the location of the maximum trough
depth and the bar crest was approximately constant during cases
with a well-developed trough. Coarser grain-sized beaches seemed
to have greater distances between trough bottom and bar crest.
Larger waves also caused the distance from the bar crest to the
trough bottom to increase for a specific grain size. For a
typical uni-barred profile, the vertical distance between maximum
trough bottom, and bar crest appeared to increase slightly with
time up to the equilibrium value.

Distance from break point to trough bottom

According to the small-scale wave tank results of Miller
(1976), the trough located shoreward of a breakpoint bar is
initiated where the breaking waves completely disintegrate.
Sunamura (1988) made the observation that this process is valid
not only for plunging breakers, but also for spilling breakers
even though the trough is not so marked and takes longer to form
in the latter case. Distance between break point and "plunge
point" may thus be generalized to include both plunging
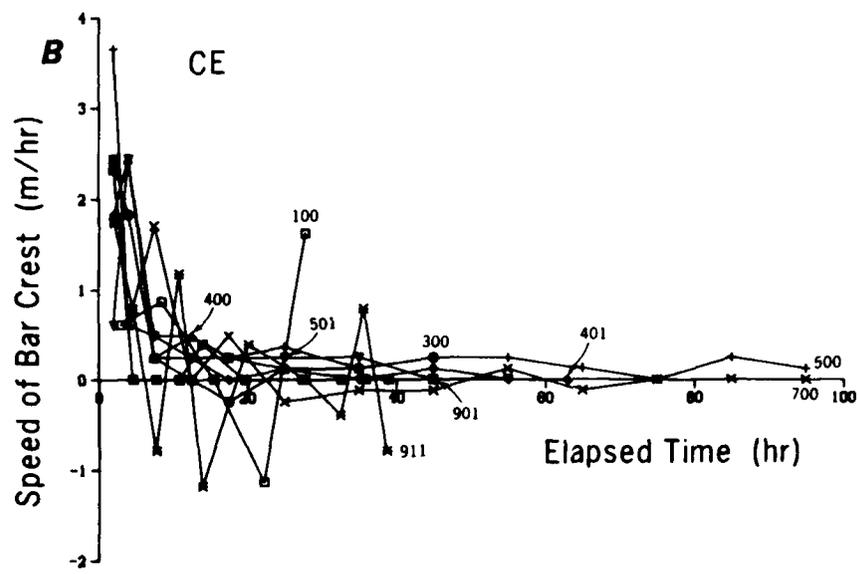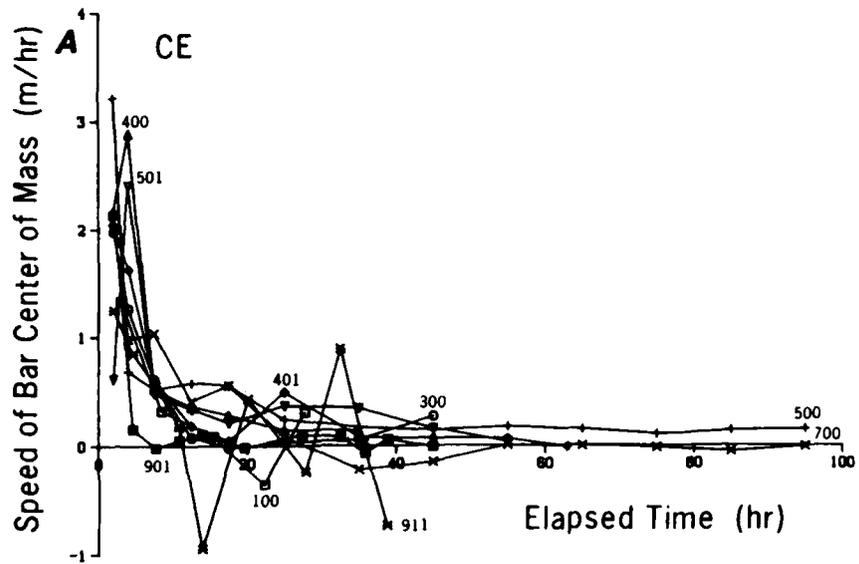
Figure 22. Speed of bar movement with elapsed time: (a) CE data, bar center of mass; (b) CE data, bar crest; (c) CRIEPI data, bar center of mass; and (d) CRIEPI data, bar crest

108
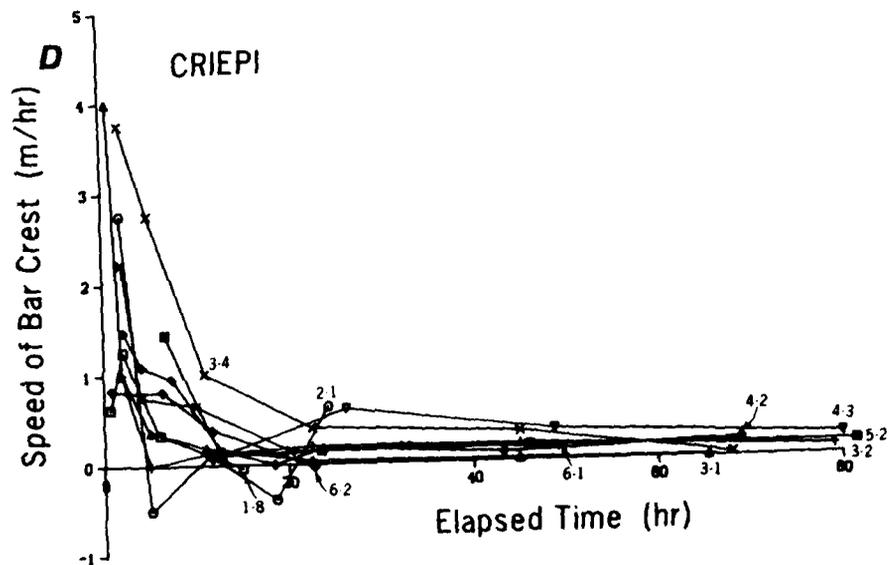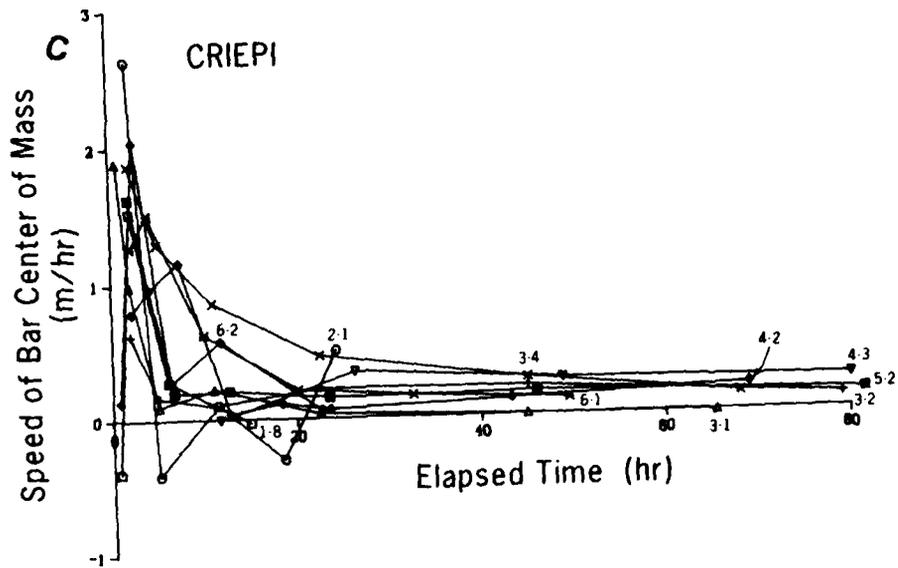
Figure 22. Speed of bar movement with elapsed time: (a) CE data, bar center of mass; (b) CE data, bar crest; (c) CRIEPI data, bar center of mass; and (d) CRIEPI data, bar crest

and spilling breakers to yield a "plunge distance." Galvin
(1969) noted through small-scale and prototype-scale experiments
that this distance was equal to about $4H_b$. Sunamura (1988) used
the CRIEPI data to relate distance between trough bottom and
break point to bottom slope and wave steepness at breaking using
the deepwater wavelength. In the relationship, the distance was
normalized by the deepwater wavelength, which gives the impres-
sion of a stronger correlation between parameters than is
actually the case.

In the present study, the CRIEPI data set, which contains
comprehensive wave information, was used to determine the
distance (l_{tc}) between the break point and the maximum trough
depth normalized by the deepwater wavelength. This quantity was
best correlated with the breaking wave height to the deepwater
wave height and the local slope ($\tan\beta$) just prior to breaking.
Evaluation of the slope was somewhat subjective, and it was
defined as the average for the region of approximately half a
local wavelength seaward of the breakpoint. Consideration was
also taken to characteristics of the cross-shore distribution of
wave height to determine the region of considerable shoaling and
thus where wave properties were greatly influenced by the profile
shape. The regression relationship derived is

$$\frac{l_{tc}}{L_o} = 0.12 \ (\tan\beta)^{-0.44} \ (\frac{H_b}{H_o})^{-2.36} \tag{16}$$

The coefficient of determination for Equation 16 is 65% for
the 110 values. Only profiles having a distinct trough were used
in the analysis. Figure 23 displays predicted normalized plunge
point distances (subscript p) and measurements (subscripts m).
The location of the maximum trough depth was inferred to be
closely related to the location of the maximum cross-shore

transport rate. A bar typically formed immediately seaward of
the trough as an accretionary feature resulting from the seaward
decrease in cross-shore transport rate.
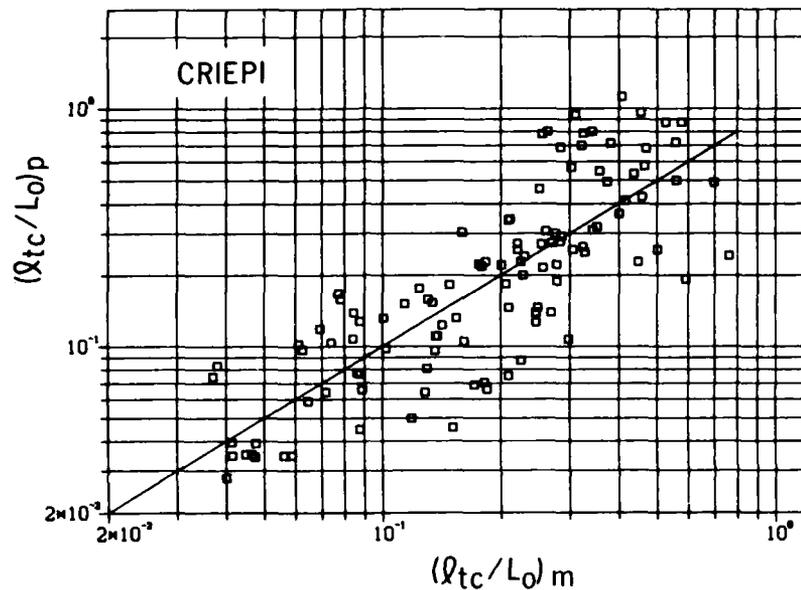
Figure 23. Comparison of measured and predicted nondimen-
sional horizontal distance between break point
and trough bottom

Bar slopes

The growth of a bar is ultimately restricted by the maximum
slope sand grains can maintain without moving under the action of
gravity. If this limiting slope is exceeded, avalanching will
occur and the sand will be redistributed to attain a gentler
slope which is stable. Allen (1970) recognized these two
different slopes and called them the angle of initial yield and
residual angle after shearing, respectively. From his experi-
ments with natural sand (diameters ranging from 0.27 to 3.17 mm
used in the experiments), he obtained an angle of about 48 deg to
cause avalanching and an angle of about 33 deg as the stable
slope after avalanching had ceased.

In the LWT experiments, as a bar approached equilibrium, its
shoreward face appeared to approach the angle of initial yield
followed at later survey times by intermediate lower values.
This alternating behavior in bar angle supports the concept of a
continuous steepening of the shoreward slope to a limiting angle
followed by avalanching which adjusts the slope to a lower value.
Figure 24 shows how the average shoreward slope of a bar (β_3)
varied with time for Cases 401 and 501, increasing at first and
then having lower values after a certain initial maximum slope
was reached. However, the number of profile surveys is too small
to obtain reliable information about the avalanching process
apart from circumstantial evidence that it appeared to occur.

In general, the average shoreward face slope of bars
increased with time and it could happen that the angle of initial
yield was not achieved during a run (see Cases 400 and 500 in
Figure 24). In particular, for the finer grain sizes, steepening
of the shoreward face slope appeared to be slower even though the
angle of initial yield should be approximately independent of
grain size for the range of material studied.

If a second bar formed immediately shoreward of a main
breakpoint bar, steepening of the shoreward slope of the main bar
was usually hindered, and the slope sometimes decreased. The
maximum bar face slope encountered on the shoreward side of a bar
was 35 deg (Case 4-3), which is considerably less than Allen's
(1970) limiting value. A smaller maximum slope is logical
because of the turbulent fluid environment existing in the surf
zone, which is considerably different than the laminar flow
conditions under which Allen (1970) performed his experiments.
The expected result of turbulent flow would be increased des-
tabilization of the sand grains, thus lowering the maximum stable
slope, which is in agreement with the trend of the observations.
Evaluation of the 14 cases where the angle of initial yield
appeared to have been attained indicated that the maximum slope
on the shoreward bar face was in the range of 20-35 deg, with an

112
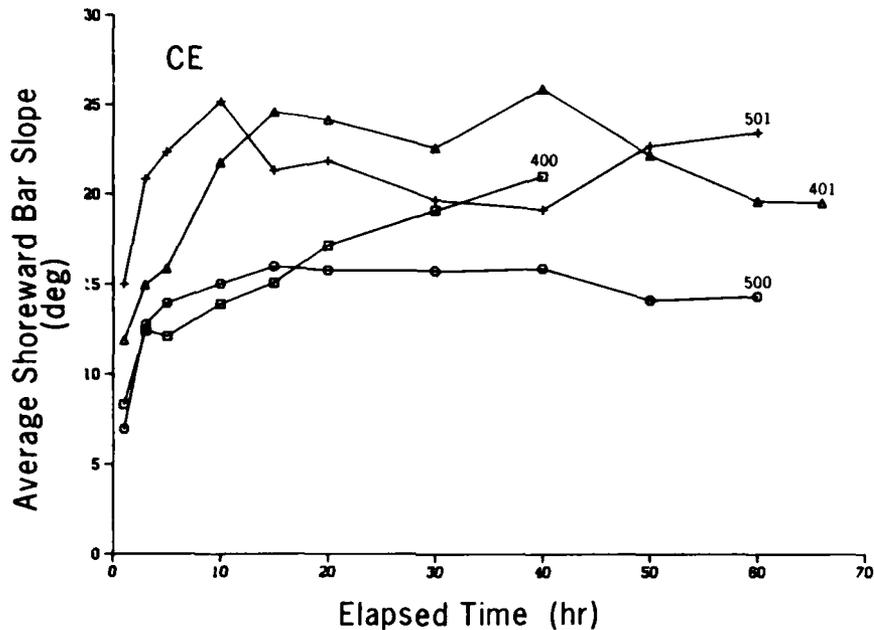
Figure 24.   Shoreward slope of main breakpoint bars as a
function of elapsed time

average of 28 deg. In each of the cases the angle of initial
yield should be somewhat larger than the value determined as the
maximum slope. An estimate of bar face slope after avalanching
occurred may be obtained by examining the minimum shoreward bar
face slope after the angle of initial yield apparently been
exceeded. The slope thus calculated (10 cases showing clear
minima) ranged from 20-25 deg, with an average of 22 deg. These
values should be somewhat higher than the actual residual angle
after shearing since some steepening of the slope probably
occurred between the times of avalanching and the profile survey.

The average seaward bar face slope was fairly constant
through time, sometimes exhibiting a slight increase during the
first hours of the run. Figure 25 shows the seaward bar face
slope as a function of time for representative cases. The
average slope was typically in the range of 8-12 deg. although

113

local slopes reached as high as 20 deg. The variation in average
seaward bar face slope was small and appeared to be independent
of grain size but weakly related to wave period, for which longer
periods gave a more gentle slope.
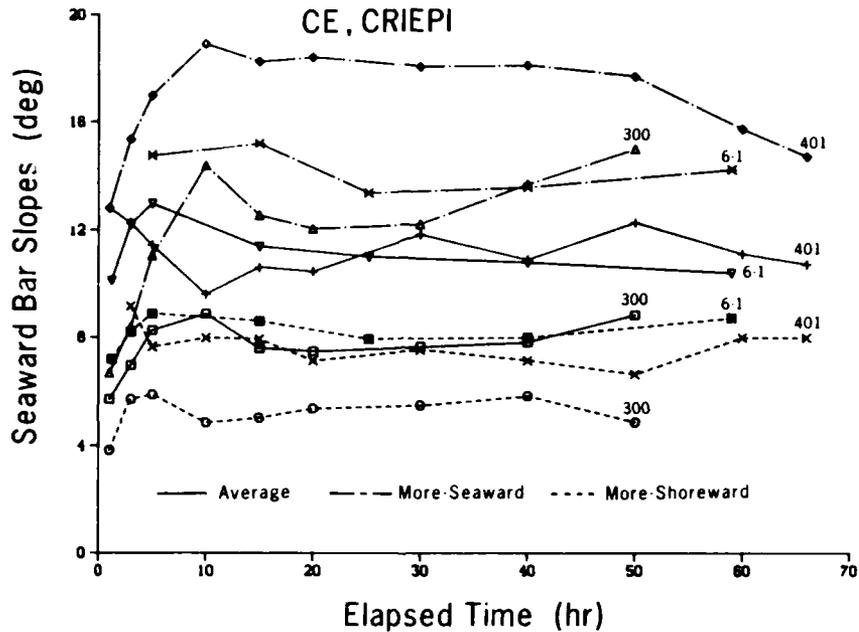
Figure 25.   Seaward slopes of main breakpoint bars as a
             function of elapsed time

The seaward face of the bar was in many cases well ap-
proximated by two or three planes having distinctly different
slopes. The upper part of the bar face seaward from the crest
had a slope β_2 ranging from 4-8 deg, whereas the slope of the
lower part of the bar β_1 was in the range of 8-18 deg. In some
cases the very end of the bar could be approximated by a third
line of constant slope, often with a magnitude smaller than the
two shoreward slopes. The location of the intersection between
the upper and lower seaward face slopes approximately coincided
with the location of the break point in many cases (see Figure
13).

Since the average shoreward and seaward bar face slopes were considerably different, the bars were asymmetric in shape. The average shoreward bar slope was always steeper than the corresponding average seaward slope, making the bar positively skewed.

Slopes encountered in the field are in general milder than slopes in the CE, CRIEPI, and most other wave tank studies. One possible reason is that monochromatic waves and constant water levels were employed in most laboratory studies, and this situation lacks the smoothing effect on the profile of random waves and varying water level which normally exist in nature (e.g., Keulegan 1948). For example, Hands (1976) stated that maximum bottom slope was always less than 10 deg for numerous measurements of Lake Michigan bars. On the basis of frequent and repetitive high-accuracy surveys on an Atlantic Ocean beach over five years, Birkemeier (personal communication, 1987) found that steepest shoreward bar slopes of approximately 10 deg occurred when bars moved onshore during the profile recover' process after a high wave event, not when bars moved offshore. Seaward bar faces rarely exceeded 10 deg.

The difference between present and field results can be attributed to the action of random waves and varying water level, which would widen the breaker zone and smooth profile features in the field. Another factor is that steady wave conditions usually are not of sufficient duration in the field for bars to reach equilibrium form.

Step and terrace slope

In the LWT experiments, if erosion occurred the beach profile retreated to produce a characteristic scarp or step immediately landward of the still-water level and a gentle terrace slope having a value less than that of the initial profile. The slope of the step increased with time and sometimes

reached the angle of initial yield, exhibiting the same tendency
of alternate slope maxima and minima, similar to the behavior of
the shoreward slope of breakpoint bars as discussed above. If
the initial slope was mild, the retreat of the shoreline was in
general small, and the shoreline sometimes advanced somewhat even
if a breakpoint bar formed offshore. In this latter case most of
the material in the bar was taken from the surf zone and not from
the foreshore. If the wave climate was not too severe in these
cases, the bar may have also received a net contribution of
material by onshore transport from the area located seaward of
it. However, if the wave climate was severe, a step formed even
if the slope was relatively gentle since the surf zone was not
wide enough to dissipate all the incident wave energy, resulting
in strong wave attack and erosion of the foreshore.

Figure 26 illustrates the average slope of the step β_5 as
a function of time for selected cases in which considerable
erosion of the foreshore took place. Also, time development of
the average terrace slope β_4 immediately seaward of the step is
presented. For a coarser grain size, steepening of the step
slope was slower (Case 401) and may have achieved an equilibrium
value before the angle of initial yield was reached. The slower
response of the coarser grains is probably due to their greater
stability against dislodgement and transport by the bore. The
terrace slope was more gentle than the initial slope and appeared
to be almost independent of grain size, but with finer grain
sizes showing a tendency to form gentler slopes.

Form and Movement of Berms

Berm genesis

As wave steepness becomes smaller, for example, as a storm
wanes (Sonu 1970, Kriebel 1987), the transport direction changes

116
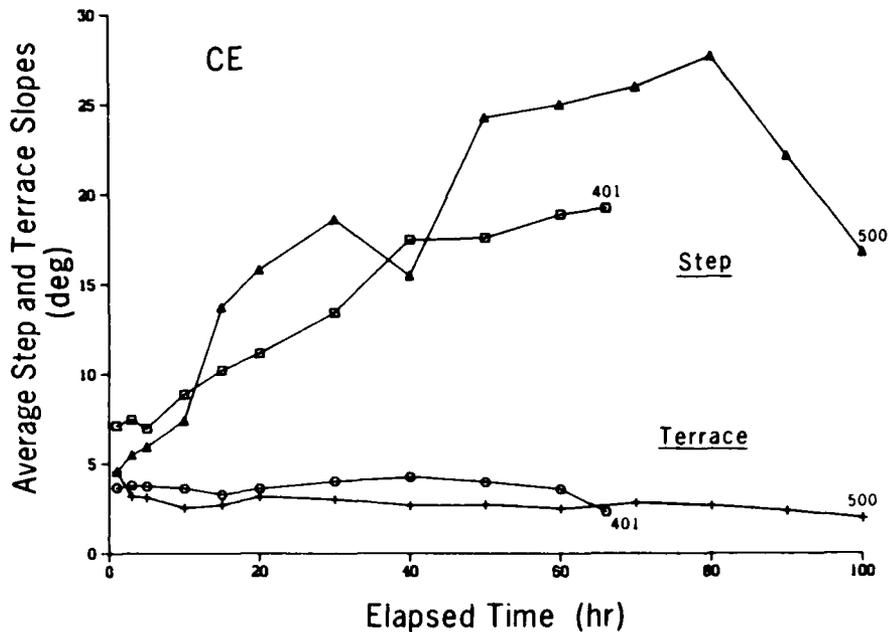
Figure 26. Time evolution of representative step and
terrace slopes

from offshore to onshore and material builds up on the foreshore.
A berm forms which is a function of local wave characteristics at
the shoreline and sediment properties. In this study, the berm
was defined as the volume of material which is accreted on the
foreshore with reference to the initial plane slope (Figure 4b).
This is a natural definition since a berm is intuitively thought
of as an accretionary feature. The berm typically forms above
the still-water level, but may extend below the water surface and
move the shoreline position slightly seaward as it grows with
time. The vertical extent of the berm is closely related to the
runup limit, whereas its shoreward extent in the equilibrium
state is mainly determined by how the grains move under gravita-
tional force. The point on the foreshore where berm formation is
initiated mainly depends on the runup limit, where a larger runup

117

implies berm initiation further shoreward. Runup is essentially
a function of local beach slope, wave period, and breaking wave
height (Hunt 1959, Savage 1959).

No information about runup was available from the CRIEPI
experiments and only little information from the CE experiments.
In the CE experiments, runup was measured for most cases,
typically during the first 10-20 waves (Larson and Kraus 1988).
Only five cases from the CE experiments exist which had berm
build-up and measurement of runup. However, an indication of the
relationship between berm formation and runup may be obtained by
viewing Figure 27, where the distance to the mass center of the
berm is plotted as a function of the runup length (l_r), all
quantities referenced to the initial still-water level. The
runup length is the average of all runup measurements, and the
first profile survey (typically performed after about 1 hr of
wave action) was used to calculate the distance to the berm
center of mass. The distance to the center of mass was roughly
half the runup length which, if the berm is considered to be
approximately symmetrical, indicates that the runup length was
close to the shoreward end of the berm as would be expected. All
berms in the previously-mentioned five cases were formed on
profiles showing a strong tendency for onshore transport during
the full duration of the run, although a small breakpoint bar may
have been present.

In cases where a berm was present but the transport rate was
more variable in direction both along the profile and in time,
the berm was often small and sometimes formed with its center of
mass below the still-water level. Equilibrium properties of the
berm on such profiles (berm volume, maximum berm height) were
reached very rapidly, typically by the time of the first profile
survey.

For most berms, the horizontal movement of the center of
mass was small, indicating that the berm grew uniformly in time
over its length. If the berm showed a net movement of its center

of mass, it was always in the shoreward direction. The length of
the berm at equilibrium appeared to depend mainly on breaking
wave height, and little on wave period (Bagnold 1940, Sunamura
1975, Takeda 1984).
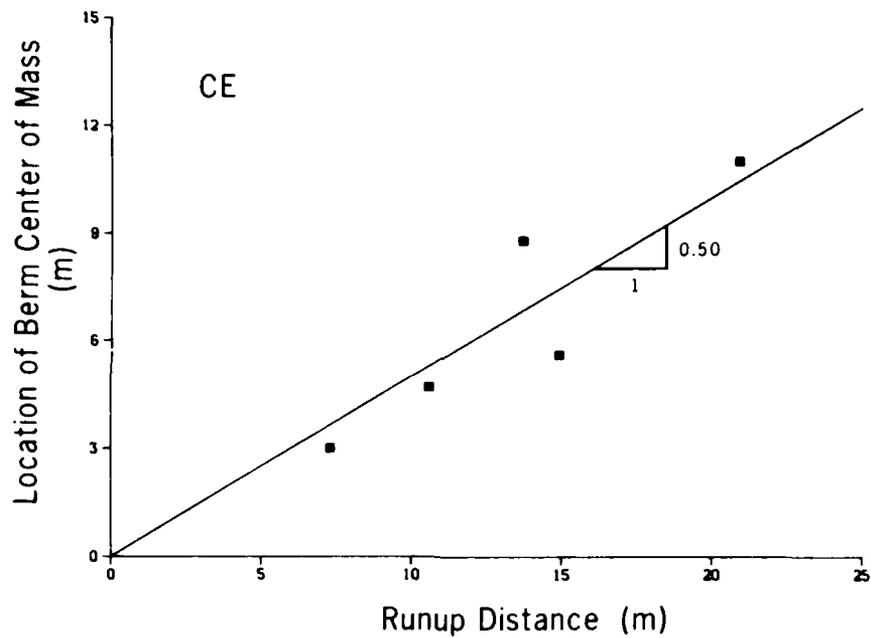
Figure 27.   Relation between berm center of mass and wave
            runup

Active profile height

A quantity Z_R was defined as the maximum subaerial
elevation of the active profile above still-water level for
either bar or berm profiles (Figure 4b). An empirical equation
was obtained from the LWT data by relating this quantity to the
surf similarity parameter $(\tan\beta/\sqrt{H_o/L_o})$ (Battjes 1975). The surf
similarity parameter was expressed in terms of the initial beach
slope resulting in the empirical equation

119

$$\frac{Z_R}{H_o} = 1.47 \ (\frac{\tan\beta}{\sqrt{H_o/L_o}})^{0.79} \tag{17}$$

The coefficient of determination was 75% for 32 cases where the height of the active profile could be distinguished.

Equilibrium berm volume

In the LWT experiments, the volume of the berm increased with time to approach an equilibrium value attained when the profile was in balance with the incident waves, dissipating wave energy without significant changes in shape. Seventeen cases exhibiting any kind of foreshore build-up were identified from the CE and CRIEPI data sets. However, only eight of these cases showed strong berm build-up with onshore transport occurring during most of the run. In some CRIEPI cases, accretion on the foreshore started to occur only at the very last few profile surveys, and equilibrium was reached almost immediately (for example, Cases 4-2 and 5-2). Profiles of this type were of erosional character, but had a moderate wave climate and a gentler initial slope, allowing for a small amount of onshore transport on the foreshore as the breakpoint bar system approached equilibrium. In Figures 28a and 28b, the berm volume as a function of time is displayed for the CE and CRIEPI experiments, respectively.

To estimate the equilibrium volume, an expression similar to Equation 7 was least-squares fitted to the data for the previously mentioned eight cases. The number of cases was too small to derive reliable empirical relationships between berm volume and wave characteristics and beach profile properties. Some tendencies noted may be of interest to indicate which factors appear to
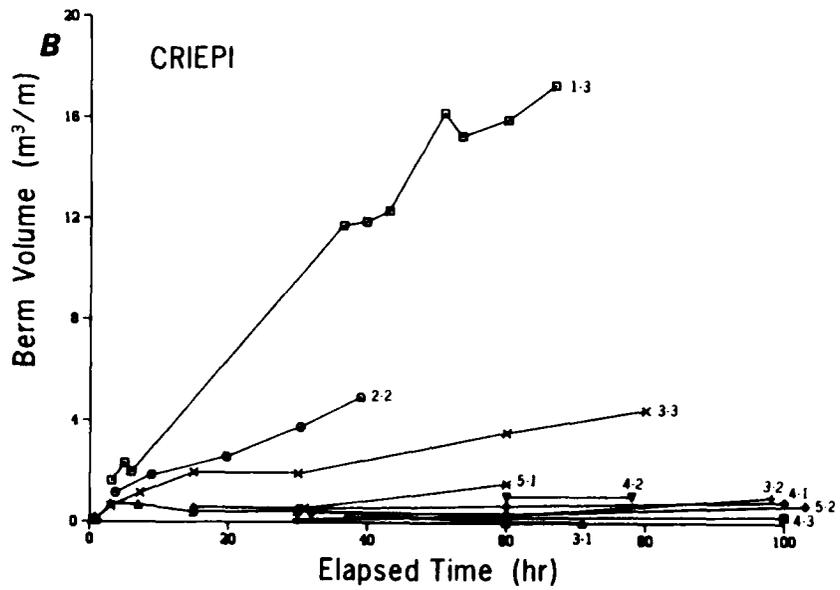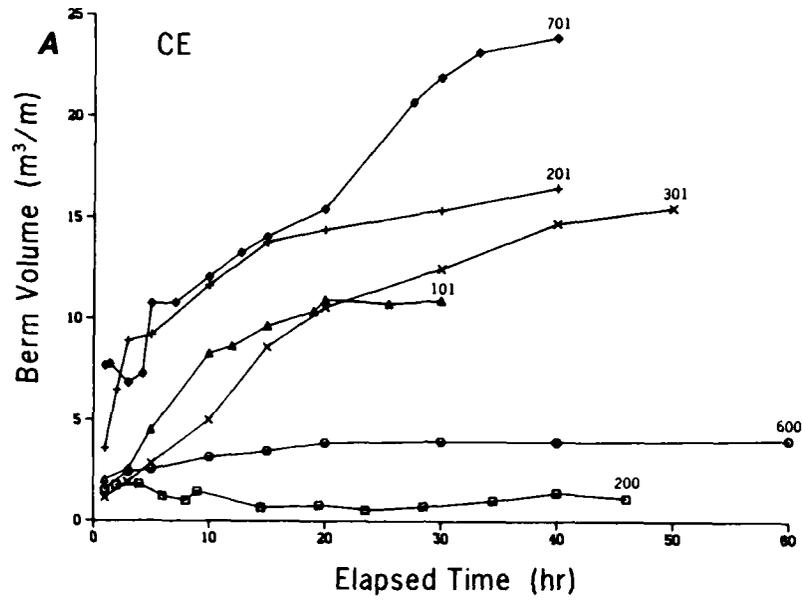
Figure 28. Growth of berm volume with elapsed time: (a) CE
data, and (b) CRIEPI data

121

control equilibrium berm volume. Berm volume showed the greatest dependence on sand fall velocity, where a higher fall velocity implied a larger berm volume. This seems reasonable because the tendency for onshore transport increases with higher fall velocity for the same deepwater wave steepness (Figure 6). Within the range of grain sizes tested in the experiments, coarser material often experienced more marked onshore transport. In contrast, the finer material, for the cases where berm build-up occurred, had a less dominant transport direction, thus resulting in smaller equilibrium berm volumes. An increase in wave height produced a larger berm volume, whereas wave period seemed to be a negligible factor. However, wave period influenced the rate at which equilibrium berm volume was reached, with a longer period producing faster berm build-up.

Maximum berm height

Maximum berm height (Z_b), defined with respect to the initial profile, showed development with time similar to berm volume. Figures 29a and 29b show growth of maximum berm height as a function of time. If accretion on the foreshore occurred in cases with predominant offshore transport, equilibrium berm height was attained quickly, as seen in Cases 200, 3-1, and 4-2. Equilibrium maximum berm height was estimated from a least-squares fit of the data from each case (eight cases used in total), with an expression of the form of Equation 7. Grain size emerged as an important variable for the same reasons as discussed for equilibrium berm volume. Breaking wave height appeared as a considerably more decisive factor than deepwater wave height, probably because runup is more closely related to breaking wave height. The ratio between maximum equilibrium berm height and breaking wave height had a relatively small range. The average value of the ratio was 0.5, ranging from 0.3 to 0.8 for the eight cases analyzed. The standard deviation was 0.16.
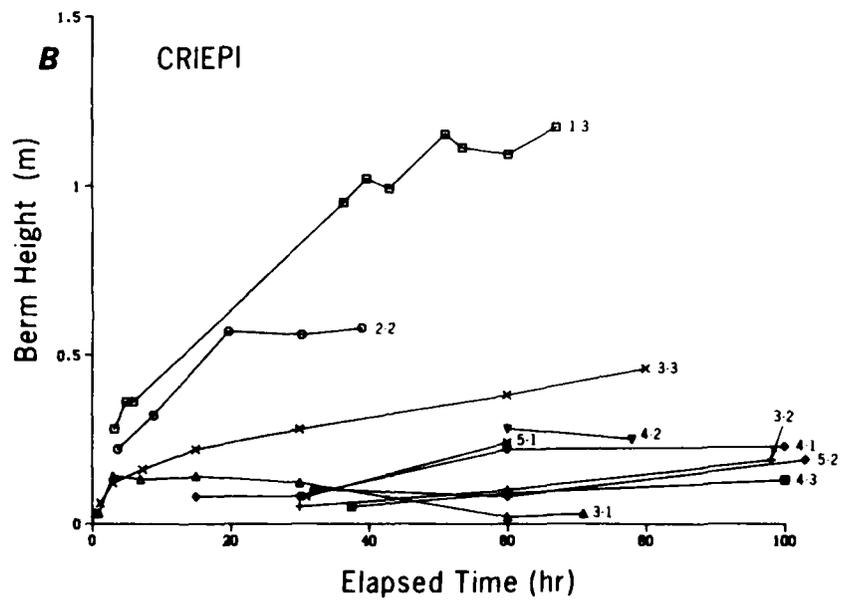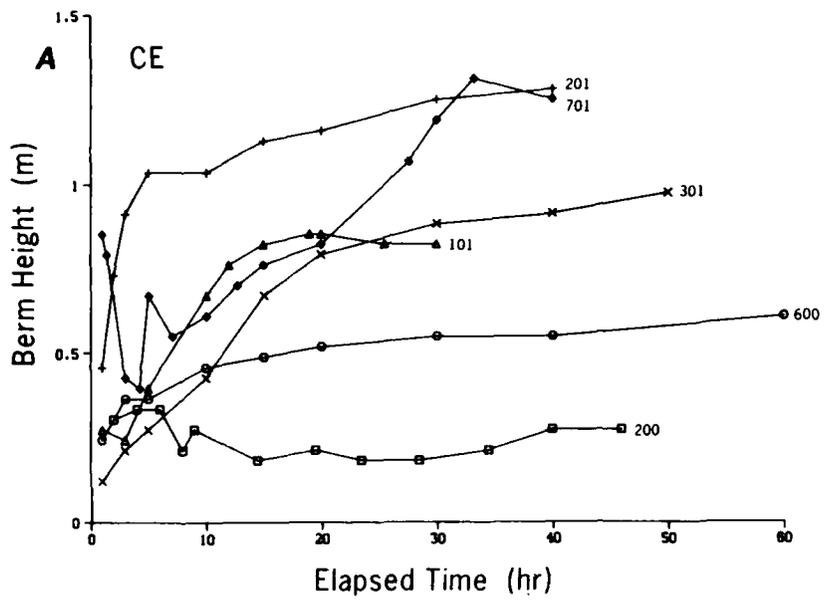
Figure 29. Growth of maximum berm height with elapsed time:
(a) CE data, and (b) CRIEPI data

123

Berm height, normalized by some appropriate length scale
(wave height or wavelength) showed no correlation with dimension-
less fall velocity, not surprising since this quantity is
generally believed to characterize suspended transport, which is
not the dominant transport mode on the foreshore. For a specific
grain size, berm height divided by breaking wave height was found
to be weakly dependent on the surf similarity parameter, but a
clear overall relationship could not be obtained. Runup height
is usually expressed in terms of the surf similarity parameter
(compare Hunt 1959) so this dependence is expected; however, the
present data sets on berm growth are too limited to verify such a
relationship.

Berm slopes

If a berm formed on the foreshore, its seaward face slope
steepened and a positive slope developed on its shoreward face.
Average seaward berm face slope was relatively constant, with a
slight tendency to increase with time. Figure 30 shows how the
shoreward (ϕ_1) and seaward (ϕ_2) average berm face slope changed
with time during two typical cases (Cases 300 and 1-3) with berm
build-up. The seaward berm slope was approximately independent
of grain size and ranged between 6-8 deg.

If a well-developed shoreward berm face slope was present,
it was considerably more gentle than the seaward face slope.
Typical values of the average shoreward berm face slope were 2-4
deg, although steeper slopes occurred. The average shoreward
berm face slope also appeared to be independent of grain size and
constant in time, except for one case which showed a strong
increase with time (Case 201) toward an equilibrium value of
about 15 deg. In this case the grain size was coarse, and the
wave height and wave steepness were relatively small. The waves
were probably breaking very close to the shoreline, one of
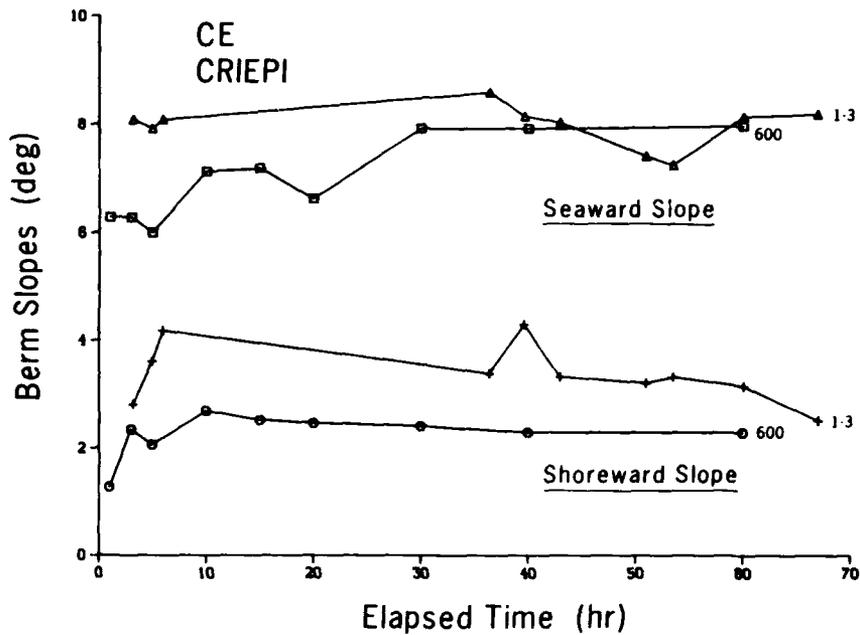
Figure 30. Growth of representative berm slopes with elapsed time

the few cases where no breakpoint bar appeared along the profile, strongly affecting the shape of the berm.

Summary and Discussion of Morphologic Features

Numerous morphologic features of beach profiles generated under breaking waves in large wave tanks were quantitatively described in this chapter. Selected results are presented in Tables 4 and 5 together with the breaking wave height. Under steady monochromatic waves and constant or slowly varying water level, the evolution of bars and berms was found to be regular, exhibiting clear growth and equilibrium properties that were readily described by simple regression expressions. The dimensionless fall velocity, H_o/wT, emerged as an important parameter in predicting both profile response and geometric properties of

9   125

various major morphologic features. The strong relationship between wave and sand characteristics and morphologic features suggests the possibility of quantitatively predicting the evolution of macro-scale features of the profile.

The effect of scale was made apparent through the different values of empirical coefficients in the criteria for bar/berm formation for small-scale and prototype-scale wave and beach conditions. Criteria applied to natural beaches should preferably be developed using data from experiments replicating prototype conditions. In general, profile response in the LWT experiments, apart from effects related to use of monochromatic waves, were much in agreement with what is observed to happen on a natural beach. Random waves encountered in the field are expected to give a smoother character and slower rate of change of morphologic features.

Table 4

CE Experiments: Values of Selected Quantities.

Case No.	Bar				Berm		
	V_{eq} m^3/m	h_c m	$(h_t/h_c)_{avg}$	H_b m	V_{eq} m^3/m	z_b m	z_R m
100	18.5	1.16	1.45	1.68	- - - -	- - - -	- - - -
200	8.2	0.90	1.50	1.07	- - - -	- - - -	0.89
300	30.1	1.31	1.71	2.00	- - - -	- - - -	1.56
400	28.6	1.52	1.68	2.30	- - - -	- - - -	1.50
500	33.3	1.44	1.84	1.90	- - - -	- - - -	1.05
600	- - - -	- - - -	- - - -	1.15	3.8	0.53	0.88
700	24.5	1.79	1.46	2.10	- - - -	- - - -	1.81
101	3.7	1.31	1.26	1.80	11.7	0.88	1.29
201	- - - -	1.18	1.32	1.90	14.9	1.17	1.45
301	2.9	1.44	1.29	2.40	18.3	1.01	1.36
401	19.6	1.28	1.89	2.40	- - - -	- - - -	1.48
501	22.1	1.16	2.05	1.60	- - - -	- - - -	0.72
701	- - - -	- - - -	- - - -	1.95	23.1	1.14	2.56
801	- - - -	0.56	1.62	0.76	- - - -	- - - -	0.47
901	11.3	1.28	1.55	2.00	- - - -	- - - -	0.97
911	12.0	- - - -	- - - -	- - - -	- - - -	- - - -	1.26

Table 5

CRIEPI Experiments: Values of Selected Quantities.

Case No.	Bar				Berm		
	V_{eq} m^3/m	h_c m	$(h_t/h_c)_{avg}$	H_b m	V_{eq} m^3/m	Z_b m	Z_R m
1-1	----	0.47	1.89	0.95	----	----	0.37
1-3	----	----	----	1.40	27.7	1.12	1.31
1-8	1.6	0.55	2.06	0.85	----	----	0.24
2-1	7.5	1.12	1.78	1.94	----	----	0.23
2-2	8.7	0.67	2.06	1.54	7.3	0.60	0.52
2-3	0.7	0.45	1.96	0.80	----	----	0.14
3-1	12.4	0.91	1.78	1.88	----	----	0.75
3-2	15.3	0.76	1.76	1.58	----	----	0.55
3-3	9.1	1.00	1.50	1.47	5.0	0.43	0.98
3-4	24.9	1.23	2.16	1.50	----	----	0.48
4-1	----	----	----	0.50	----	----	0.21
4-2	4.5	0.83	1.84	1.27	----	----	0.37
4-3	23.5	1.23	2.07	1.52	----	----	0.34
5-1	----	----	----	0.63	----	----	0.36
5-2	6.5	0.61	2.02	0.89	----	----	0.43
6-1	36.5	1.39	1.76	1.91	----	----	1.66
6-2	25.3	0.98	----	1.42	----	----	1.19

PART V: CROSS-SHORE TRANSPORT RATE

Introduction

If a beach profile is not in equilibrium with the existing
wave climate, sediment will be redistributed along it to approach
an equilibrium shape, in which state the incident wave energy
will be dissipated without causing further significant net
sediment movement. It has been established that as sediment is
transported across the shore, certain characteristic net trans-
port rate distributions occur, and these distributions have
specific properties in time and space. Regularity in transport
rate distributions is to be anticipated since the previous
chapter showed that beach profile morphology itself behaved
regularly through time.

The objective of this section is to describe properties of
the cross-shore sand transport rate and relate them to wave
parameters, sand characteristics, and beach profile shape.
Quantitative knowledge of the cross-shore transport provides the
necessary foundation for the numerical modeling component of this
investigation.

Keulegan (1948) appears to have been the first to measure
cross-shore sand transport along the profile. He used traps
mounted in a small wave tank and found that the maximum transport
rate was located at the point of impending wave breaking, where
the front of the wave was almost vertical near the crest.
Furthermore, he pointed out a correlation between sand transport
rate and total displacement of the water surface, and recognized
the existence of a critical wave height for sand transport to
occur.

Several early papers concerned development of criteria for
predicting the predominant direction of the transport (onshore or
offshore). Rector (1954) used deepwater wave steepness and ratio

between median grain size and deepwater wavelength. Ippen and Eagleson (1955) studied the movement of individual particles on a plane sloping beach under shoaling waves and found net sediment motion to result from inequality of hydrodynamic drag and particle weight. Their criterion for distinguishing between onshore and offshore motion contained three non-dimensional parameters: wave steepness, ratio of wave height and water depth, and ratio of sediment fall velocity and wave celerity.

van Hijum (1975, 1977) determined the distribution of the cross-shore transport rate on a beach of coarse material by comparing consecutive beach profiles in time. The equation of mass conservation was integrated from frequent beach profile surveys, and thus an average over the studied time interval was obtained for the net transport rate. The technique of determining the distribution of the net cross-shore transport rate from consecutive profile surveys has been employed in other studies (for example Hattori and Kawamata 1981, Watanabe, Riho, and Horikawa 1981, Shimizu et al. 1985). A classification of transport rate distributions for LWT results was proposed by Kajima et al. (1983a), based on a beach profile classification by Sunamura and Horikawa (1975), who used data from tests with a small tank.

By determining the transport rate from profile change, an average net distribution of the cross-shore transport rate is obtained for the elapsed time between two surveys. An alternative method of acquiring information about the cross-shore transport rate is by measurement of the sediment concentration and velocity field at a point. Sawaragi and Deguchi (1981) and Deguchi and Sawaragi (1985) measured sediment concentrations in small-scale laboratory experiments and obtained concentration profiles at selected locations across the beach profile. Vellinga (1986) and Dette and Uliczka (1987b) made similar measurements of concentration profiles in experiments performed with large tanks and waves of prototype scale.

130

The average net cross-shore transport rate may be obtained
by integrating the equation of mass conservation between two
beach profiles in time. The transport rate q(x) across the
profile is thus calculated from the mass conservation equation
written in difference form with respect to time as

$$q(x) = \frac{1}{t_2 - t_1} \int_{x_o}^{x} (h_2 - h_1) \, dx \qquad (18)$$

where

x_o = shoreward location of no profile change $(q(x_o)=0)$

h_1, h_2 = profile depths at survey times 1 and 2

t_1, t_2 = times of profile surveys

In order to conveniently evaluate the transport rate
numerically, measured profiles used in this study where ap-
proximated by a set of cubic spline polynomials (see Part IV).
Subsequent calculations used in the analysis were carried out
from a point on the shoreward end of the profile where no change
occurred during the run to a seaward point where there was no
movement of material (typically in the horizontal part of the
tank beyond the toe of the beach).

In Equation 18, sand porosity has been incorporated in q,
the cross-shore transport rate, implying that the porosity is
independent of time and space. Qualitatively, it was noted
during the CE experiments that the foreshore sand tended to
compact, whereas sand at the flanks of the breakpoint bar tended
to be looser. The error introduced by assuming constant porosity
is judged to be negligible.

Errors may be introduced through limitations in accuracy of
the profile surveys or an insufficiently small spatial survey
interval. A small systematic error in profile depth may give a
finite contribution if summed over the profile length and could

131

give rise to an apparent transport at the seaward boundary of the
profile, where no transport actually occurred. In particular,
the CE surveys, having a 1.2-m (4 ft) spatial interval, were in
some cases not taken frequently enough to indicate negligible
transport at the seaward boundary. Therefore, in these cases, in
order to proceed with the analysis, one of the profiles was
slightly displaced vertically to achieve the condition of zero
transport at the boundary. The vertical displacement was in
general small (less than 1 cm) and below the accuracy of the
profile survey itself (+/-1.5 cm). Displacement of one of the
profiles somewhat influences the magnitude of maximum and minimum
transport rates along the profile, but only slightly changes the
shape of the transport rate distribution.

General Features of Cross-Shore Transport

Distributions of the net cross-shore transport rate were
determined for both the CE experiment (18 cases) and the CRIEPI
experiment (24 cases). However, in most of the analysis a subset
comprising 33 cases was used which encompassed those cases
starting from an initial plane slope. Profile behavior was
thereby more readily isolated, and the added complexity of an
arbitrary initial profile shape avoided. Between 5-10 transport
rate distributions were calculated for each case, depending on
the number of profiles surveyed. Information about the specific
cases, such as wave conditions, sand grain size, and initial
profile slope are summarized in Tables 1 and 2.

Figure 31 shows the beach profile at consecutive times for
CE Case 300, which is an example of a bar profile with transport
mainly directed offshore. A double-bar feature occurred, and the
shoreline receded considerably with a pronounced scarp or step
formation. Seaward of the step, the foreshore eroded with a
slope more gentle than the initial slope (1/15). In Figure 32
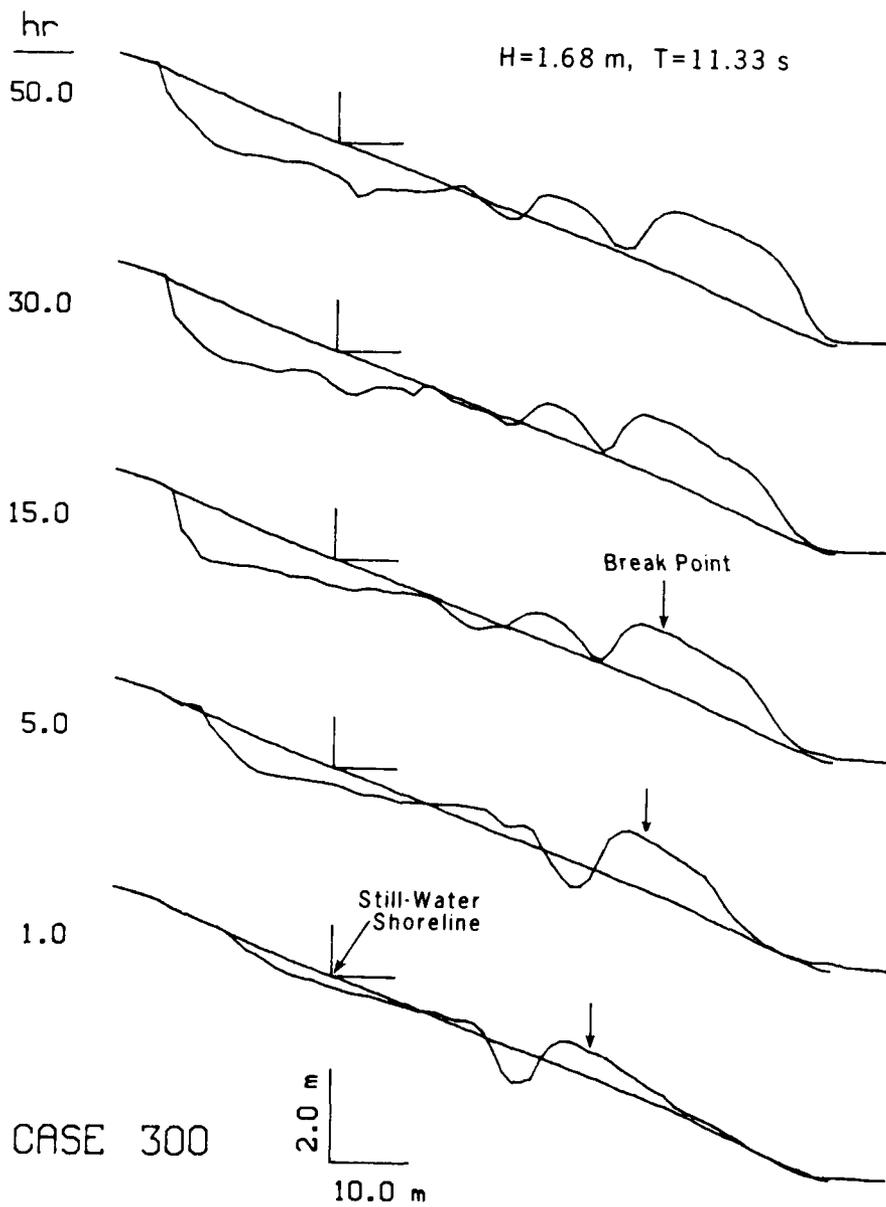
Figure 31. Evolution of beach profile under constant incident wave conditions for an erosional case (Case 300)

133

are shown the calculated distributions of the cross-shore sand
transport rate associated with Case 300. Transport directed
offshore has positive sign, and the coordinate system originates
from the position of the initial still-water shoreline. Decay of
the transport rate with time is clear from Figure 32, and it is
noted that the maximum transport rate calculated from the final
two surveys is more than one order of magnitude smaller than the
maximum from the first two surveys.
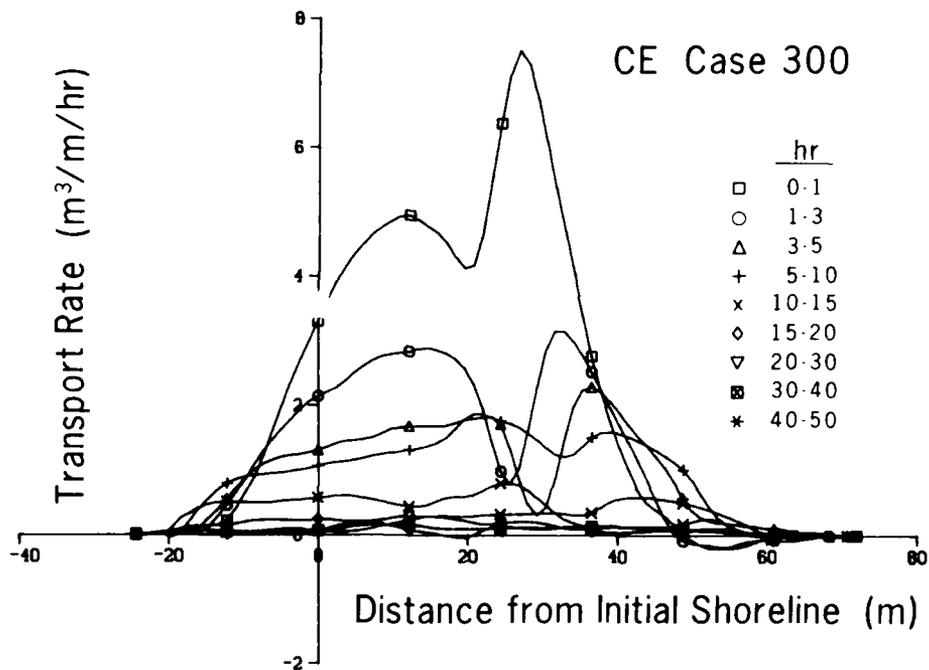
Figure 32. Calculated distributions of net cross-shore sand
transport rate for an erosional case (Case 300)

The peak in the transport rate distribution translated
seaward with the break point, and thus the bar moved seaward.
The first maximum in the transport rate occurred shoreward of the
first breakpoint, close to the plunge point and slightly seaward
of the location of the trough bottom. Another, smaller maximum
in the transport rate was present further inshore, and this

134

maximum also moved slightly seaward with time. For the transport rate distributions at later times, the shape was flatter and no maxima were prominent, indicating that material was mainly conveyed from the inner to the outer part of the profile. Seaward of the first maximum the transport rate decreased rapidly with an approximate exponential shape.

CE Case 101 is an example of a case of mainly onshore transport, resulting in deposition on the foreshore and creation of a berm. Figure 33 shows the profiles surveyed at consecutive times, in which the initial slope was 1/15. Although a large berm formed on the foreshore, a small bar was also present just shoreward of the break point. The bar was created mainly during the first hours of the run, and it rapidly reached an equilibrium volume. The trough shoreward of the bar, however, became less pronounced with time as the berm grew.

In Figure 34, distributions of the transport rate pertaining to Case 101 are shown, where a negative transport rate implies onshore transport. The transport rate decreased with time as the profile approached equilibrium shape. Initially, the transport rate distribution showed a clear negative peak, but the shape of the distribution became more attenuated as the breakpoint bar approached equilibrium volume. Material was thus transported shoreward over the bar and deposited on the foreshore. The breakpoint bar was formed mainly by onshore transport and is seen as the minimum occurring in the first transport rate distribution. Similar to Case 300, the seaward part of the transport rate distribution may be well approximated with an exponential function decaying with distance in the offshore direction.

Classification of Transport Rate Distributions

Depending on wave conditions and sand size, the distribution of the cross-shore transport rate took a specific shape. Since
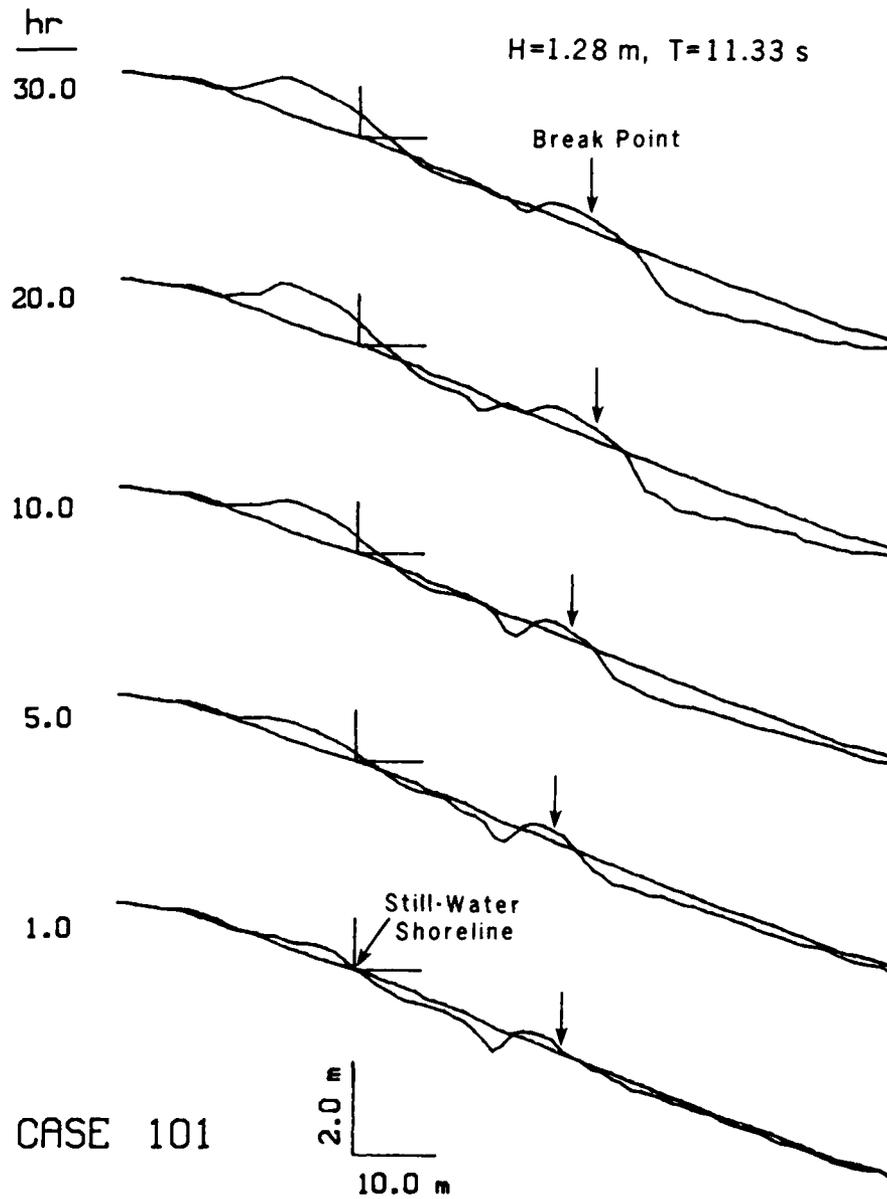
Figure 33.   Evolution of beach profile under constant
             incident wave conditions for an accretionary
             case (Case 101)

136

CE Case 101

hr

- □   0-1
- ○   1-3
- △   3-5
- +   5-10
- x   10-12
- ◇   12-15
- ▽   15-20
- ▣   20-25.5
- ✳ 25.5-30

Distance from Initial Shoreline (m)
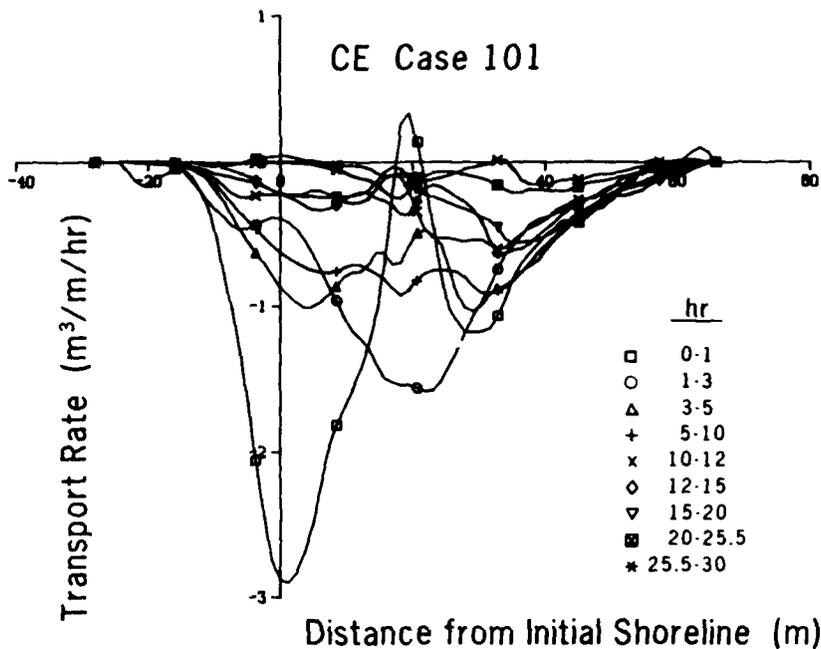
Figure 34.   Calculated distributions of net cross-shore sand transport rate for an accretionary case (Case 101)

the transport rate in this study is determined from consecutive profile surveys, calculated distributions represent an average net response of the profile and not the instantaneous transport rate.   If the initial and final profiles from a specific case are used to calculate the distribution of the transport rate, an overall picture of the profile response is obtained.   The distribution determined from the initial and final profile surveys will be termed the "equilibrium distribution," although it is recognized that the final profile survey only approximates the actual equilibrium configuration and the time weightings are not equal between cases.

Based on this so-defined equilibrium distribution, a classification of net transport rate distribution shapes is more easily performed than if consecutive profiles in time are used.

137

This description also indicates where the sand originated which supplied the bar and berm. For example, depending on the wave and sand properties, a bar may be formed from sand supplied from either its shoreward side or its seaward side, or from both sides.

From the equilibrium transport rate distributions, three main shapes were identified, although general trends in the distributions often exhibited small perturbations. Figure 35a-c illustrates the three principal distribution shapes calculated for three cases, CE Cases 300 and 101, and CRIEPI Case 3-2. Note that the cases shown from the CE data are identical to those presented in Figures 32 and 34, where the distribution of the net transport rates were given corresponding to consecutive survey times and not as equilibrium forms. The classification of the transport rate distributions is closely related to criteria for bar/berm formation. A barred profile is generally associated with erosive conditions, implying offshore transport, whereas a profile with berm build-up mainly experiences onshore transport. However, in some cases where a bar was formed, even though much of the material composing the bar was eroded from the foreshore, onshore transport from the region seaward of the bar also contributed.

The equilibrium transport rate distribution illustrated by Case 300, is called Type E (Erosional), and is characterized by transport in the offshore direction along the full extent of the active profile. A positive derivative in the transport rate with respect to the cross-shore coordinate indicates local erosion of the profile, whereas a negative derivative indicates local deposition. Where the derivative is zero, the profile depth was constant and material was simply conveyed through the point. A minimum or maximum in the equilibrium distribution of the transport rate pertains to a morphologic feature along the beach profile. Cases where the transport was directed offshore along the entire profile are by definition subject to strong erosion,

138
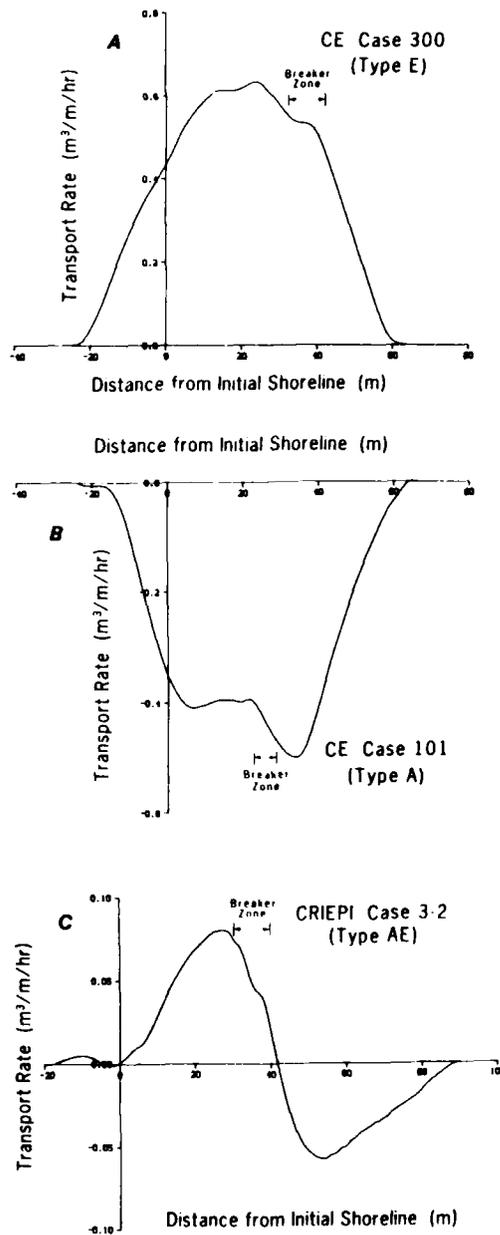
Figure 35. Classification of net cross-shore sand transport
rate distributions: (a) Type E, Erosional; (b)
Type A, Accretionary; and (c) Type AE, Mixed
Accretionary and Erosional

139

giving rise to one or more breakpoint bars. For larger grain sizes, the width of the peak of the equilibrium transport rate distribution decreased, for the same wave conditions, indicating that the major part of the sand movement was concentrated in a narrow portion of the profile. This is caused by the requirement of a greater energy dissipation to achieve the equivalent transport condition for the larger grains.

For the second main type of equilibrium transport rate distribution, exemplified by Case 101 and called Type A (Accretionary), transport is directed onshore along the full extent of the active profile. The distribution is in essence the mirror image, through the cross-shore coordinate axis, of the Type-E distribution. In general, however, any secondary minimum in the transport rate distribution is more pronounced than for Type E, related to the small bar frequently present slightly shoreward of the break point on accretionary profiles. The onshore-directed transport gives rise to a berm formation on the foreshore.

The third main type of equilibrium transport rate distribution, Type AE, and typified by Case 3-2, is characterized by one peak with offshore-directed transport occurring on the foreshore and another peak with onshore-directed transport located seaward of the break point. Thus, the bar receives contributions of material from both offshore- and onshore-directed transport. The Type-AE equilibrium transport rate distribution is characteristic of bar profiles which were closer to the dividing line between bar/berm profiles than profiles associated with Type-E distributions. Figure 36 illustrates profile evolution for CRIEPI Case 3-2, which is a typical example of a Type-AE equilibrium transport distribution.

Of the 33 cases examined, 29 were easily classified as having Type A, E, or AE equilibrium transport rate distributions (15 E-type, 10 A-type, and 5 AE-type). In some cases, particularly if the change in beach profile was small, that is, the beach profile was almost stable under the incident waves, the
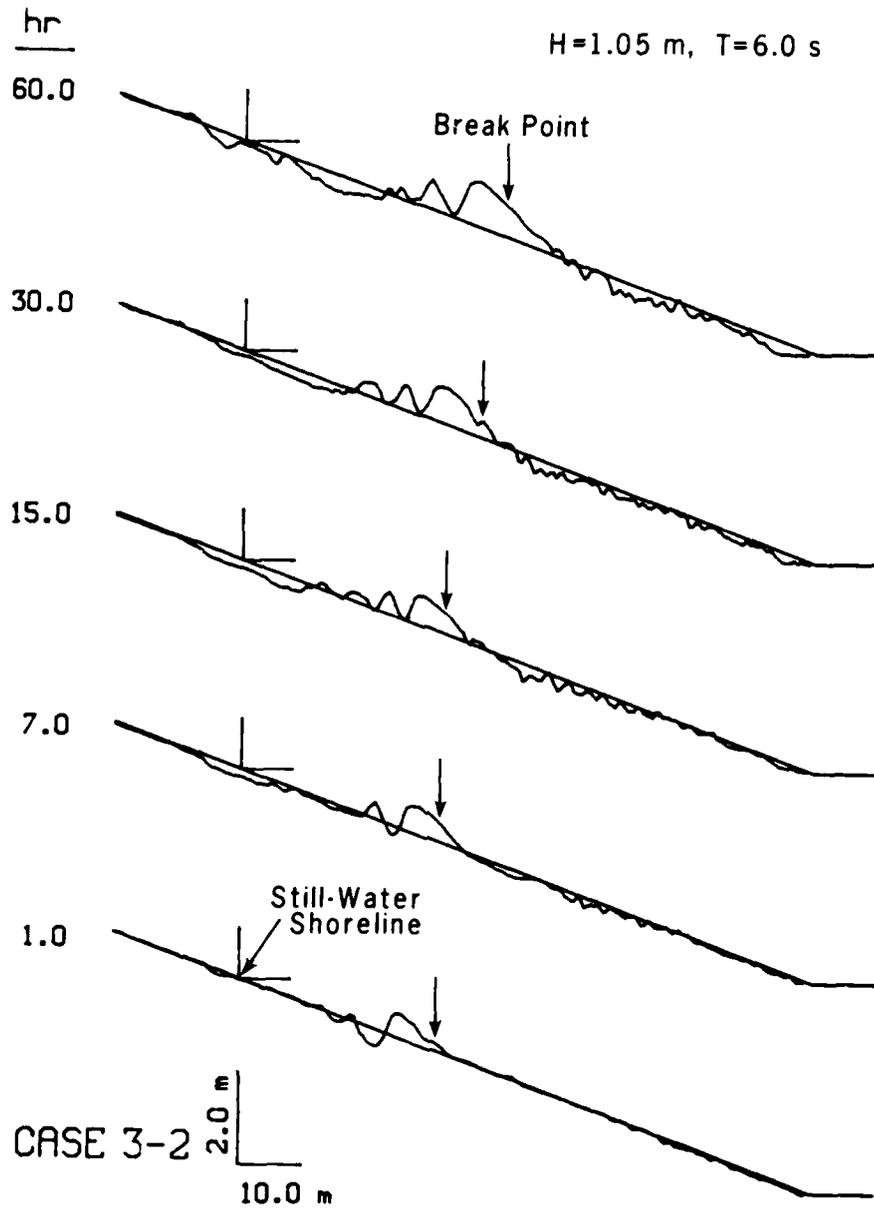
Figure 36. Evolution of beach profile under constant
incident wave conditions tor a mixed accretion-
ary and erosional case (Case 3-2)

distributions take on a more complex form with multiple peaks for onshore- and offshore-directed transport appearing along the profile. If the beach profile is close to its equilibrium shape it is expected that the transport rate distribution will not show such a strong net overall trend as compared to a profile that is far from equilibrium. Distributions having a peak for onshore-directed transport on the foreshore and a peak for offshore-directed transport located more seaward rarely occurred, and then only if minor changes in the profile occurred.

Kajima et al. (1983a) proposed a classification similar to that developed in this study, in which three basic distribution types and two subdivisions were defined. One of their main distributions differs from that presented here; their distribution corresponding to Type AE has a peak with onshore-directed transport located shoreward of the peak with offshore-directed transport, opposite to the classification presented here. The two subdivisions each contain three peaks, varying in direction onshore and offshore. Sawaragi and Deguchi (1981) derived distribution shapes from schematic profile shapes identified by Sunamura and Horikawa (1975). Their classification is also similar to the two mentioned above.

A factor that may influence profile development and net transport rate distribution is the limited depth in the horizontal section of the tanks in the CE and CRIEPI experiments. The effect is judged to be relatively minor since the depth in the horizontal section was at least 2-3 times the wave height in that part of the tank. Nevertheless, it is probable that some amount of onshore transport would have occurred if the depth and movable bottom had not been limited for those cases having transport distribution Type E. In any case, such a contribution would probably be small compared to the amount of material eroded from the foreshore.

Aubrey (1979) studied long-term exchange of material across the profile in the field. He applied empirical eigenfunction

142

analysis to determine characteristic bar and berm profiles
(prevalent during the winter and summer, respectively) and
discovered two pivotal points where the profile depth was
effectively constant. One pivotal point occurred for the studied
beach at 2-3 m depth and the second one at a depth of 6 m below
mean sea level. The seasonal volume exchange over the two
pivotal points had a relation of 1 to 5, with the largest
exchange taking place over the pivotal point closest to shore.
This indicates, that in a long-term perspective during which weak
onshore movement of sand may give a finite contribution, material
exchange in deeper water is much smaller than in the nearshore.
For a single storm event giving rise to bar formation simulated
in the LWT experiments, the ratio between the sand transport rate
from the seaward and shoreward sides of the bar should be small.

Approach to Equilibrium

As a beach profile approaches an equilibrium shape dictated
by the incident waves, the net cross-shore transport rate
decreases towards zero at all points along the profile. By
studying a relevant quantity related to the transport rate
distribution at consecutive times, a picture of the approach to
equilibrium can be attained. The peak onshore or offshore
transport rate along the profile is a candidate quantity which
might be considered for examining the decay of the transport rate
distribution with time. However, since the shape of the trans-
port rate distribution also varies with time, a peak transport
rate may not be the best overall indicator. Instead, the average
absolute transport rate Q_A along the profile was used since it
provided a better measure of all transport activity along the
profile. The average absolute transport rate was calculated as

$$Q_A = \frac{1}{x_1 - x_o} \int_{x_o}^{x_1} |q| \, dx \qquad (19)$$

where x_1 is the seaward limit of profile change.

Figures 37a and 37b illustrate the decay of Q_A with time for the CE and CRIEPI experiments. The general trend was for rapid decay during the first 10 hr, followed by a slower decrease toward zero with elapsed time. The approach to zero transport was slow at longer elapsed time since small adjustments in the profile occurred even if the profile had attained a near-equilibrium shape.

In many of the CRIEPI cases, Q_A was quite small from the beginning of the run, since the initial beach profile was close to the equilibrium shape. The maximum occurring for one of the CE cases (Case 700) just before 20 hr approximately coincided with a decrease in wave height that took place during the experiment (Kraus and Larson 1988), forcing the profile toward another equilibrium condition. The general conclusion made based on Figures 37a and 37b is that the equilibrium concept is valid and that a numerical model of beach profile change should include this property.

Peak offshore transport

In order to quantify time decay of the transport rate distribution as a function of wave parameters and sand size, the peak onshore or offshore transport rate is a good target quantity, since the peak rate has a clear physical meaning. Figure 38 plots the peak transport rate as a function of time for 16 of the CE cases. For cases with strong erosion, decay with time of the peak offshore transport rate was much more pronounced than
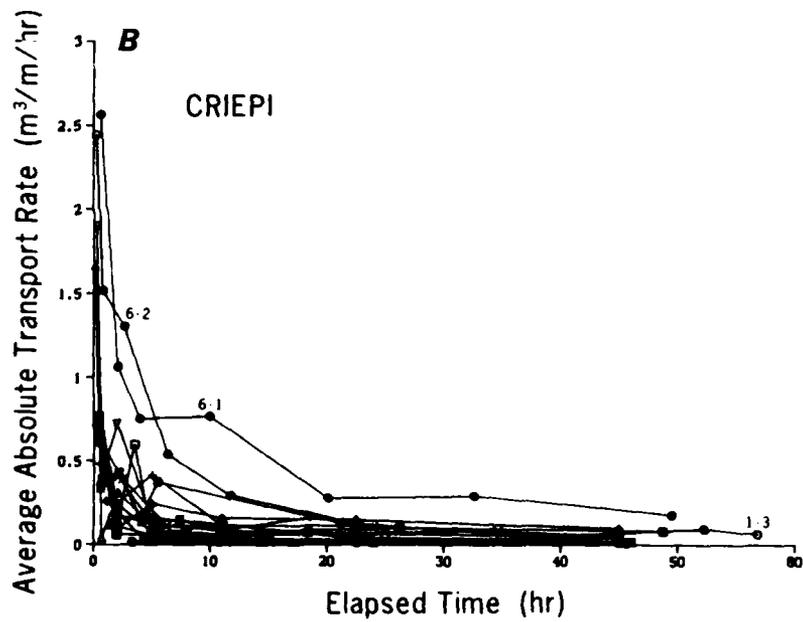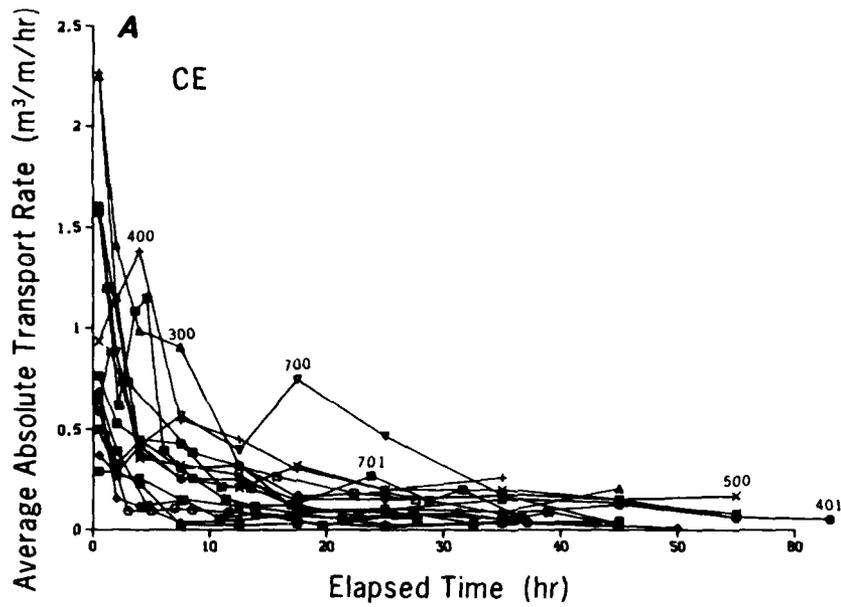
Figure 37. Decay of average absolute net cross-shore sand transport rate: (a) CE data, 16 cases; and (b) CRIEPI data, 17 cases

145

for cases with mainly accretion on the foreshore. If onshore transport prevailed, the peak offshore transport rate was usually small or sometimes even zero through most of the run (see Figure 34).
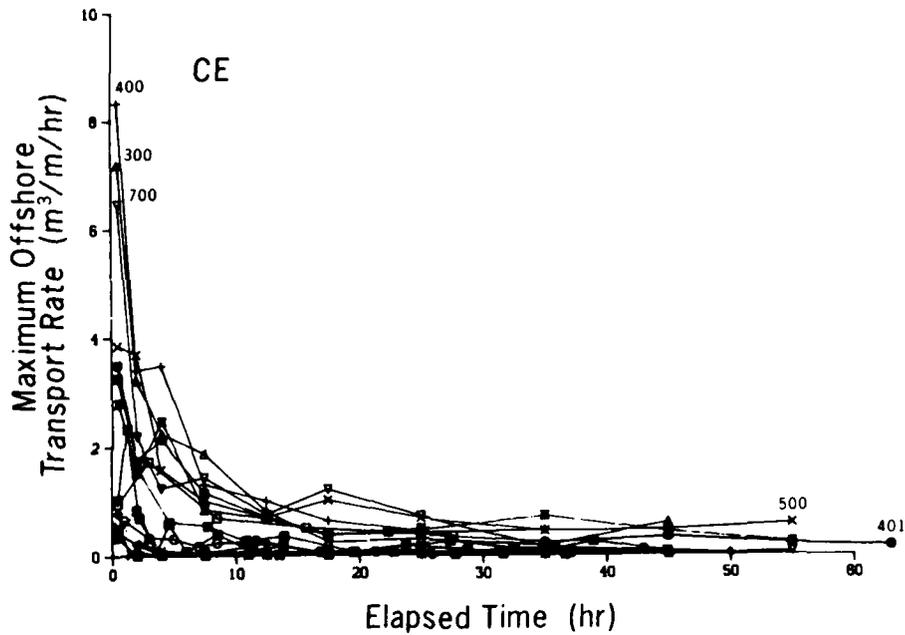
Figure 38. Evolution of peak offshore net sand transport
rate with time for 16 CE cases

Various trial empirical expressions to describe time decay of the peak offshore transport rate were least-squares fitted for cases having strong offshore transport in the combined CE and CRIEPI data set (12 cases). The best general agreement was obtained with an inverse dependence of the maximum transport rate on time according to

$$q_m = \frac{q_{mo}}{1 + \alpha t} \tag{20}$$

146

where

q_m = peak transport rate

q_{mo} = peak transport rate at time $t=0$

α = rate coefficient of decay of peak transport rate

t = time

The rate coefficient α controls the time rate of decay of the peak offshore transport rate.

Figure 39 displays the peak offshore transport rates from Case 300 and the least-squares fitted line according to Equation 20 (solid line). The agreement is very good and the regression equation explained over 90 % of the total variation.
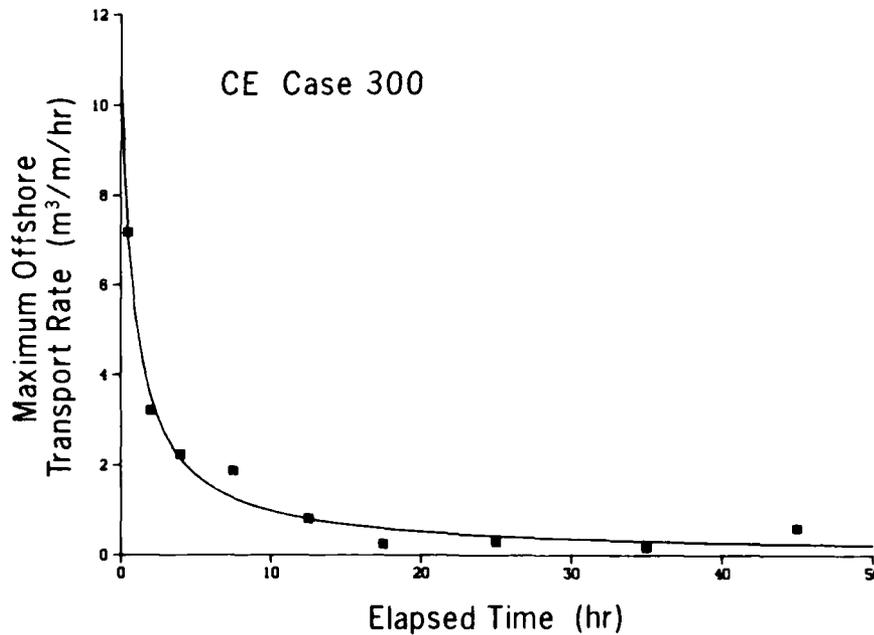
Figure 39. Decay of peak offshore sand transport rate with time for Case 300, and a best-fit empirical predictive expression

The average value of α was 0.91 hr^{-1}, and the standard deviation was 0.48 hr^{-1} for the 12 cases. In order to relate the decay coefficient to wave and sand properties, a correlation analysis was carried out, although the available data set was

small. The decay coefficient showed the strongest correlation to wave period (r=0.60) and the initial maximum transport rate (r=0.65). That is, a longer wave period or a larger initial peak offshore transport rate (profile far from equilibrium shape) resulted in faster decay in the peak offshore transport rate. Correlation with grain size (or fall velocity) was very weak, and no dependence on wave height could be found. Furthermore, it was not possible to arrive at a regression equation with an acceptable coefficient of determination by using any wave or sand parameters.

Among the trial functions examined was also an exponential decay with time, but this expression gave an inferior fit compared to Equation 20, especially at longer elapsed times, as there was a tendency for the peak offshore transport rate to have a small but still significant value at the end of a case. The exponential decay function approached zero too fast to accurately reproduce this feature. Kajima et al. (1983a, 1983b) developed a conceptual model of beach profile change assuming that the peaks in the transport rate distribution decayed exponentially with time. Sawaragi and Deguchi (1981) also used an exponential decay to derive a time-dependent transport relationship.

An exponential decay is expected on general theoretical grounds, since the response of the profile should be proportional to the "distance" away from equilibrium. However, microscale processes and, possible, non-constant forcing conditions evidently alter the time decay to a more gradual approach to equilibrium, causing a departure of the profile response from the expected exponential idealization based on linear concepts.

Peak onshore transport

The same analysis as for the peak offshore transport rate was carried out for the peak onshore rate, which encompassed 13 cases with strong onshore transport conditions. Figure 40 shows

time decay of the peak onshore transport rate for the CE experi-
ments. Similar to the behavior of the peak offshore rate, the
peak onshore transport rate decayed very rapidly initially, when
the profile was far from its equilibrium shape, and then more
slowly at the end of the run. Equation 20 was used to obtain an
empirical expression to describe the decay with time by least-
squares fitting. Figure 41 shows the agreement for a typical
case (Case 101) between the peak onshore transport rate calcu-
lated from the profile surveys and Equation 20 (solid line). In
this case also, the regression equation explained over 90 % of
the total variation.
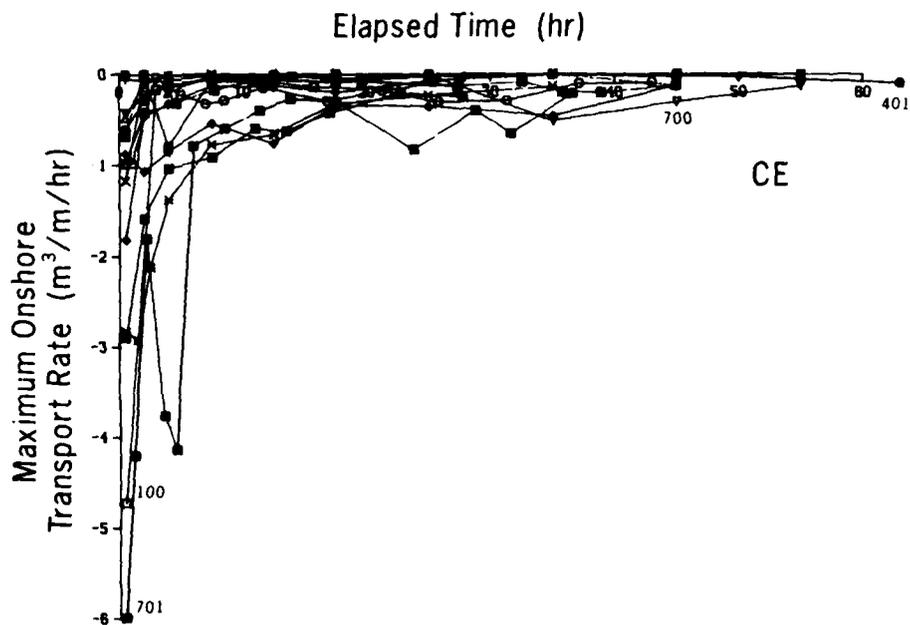
Figure 40. Evolution of peak onshore net sand transport
rate with time for 16 CE cases

The average temporal rate coefficient in Equation 20 was $\alpha =$
1.42 hr^{-1} for the studied cases, with standard deviation of 2.50
hr^{-1}. Thus, decay in the peak onshore transport rate was more
rapid than for the peak offshore rate. This is in agreement with

149

Elapsed Time (hr)
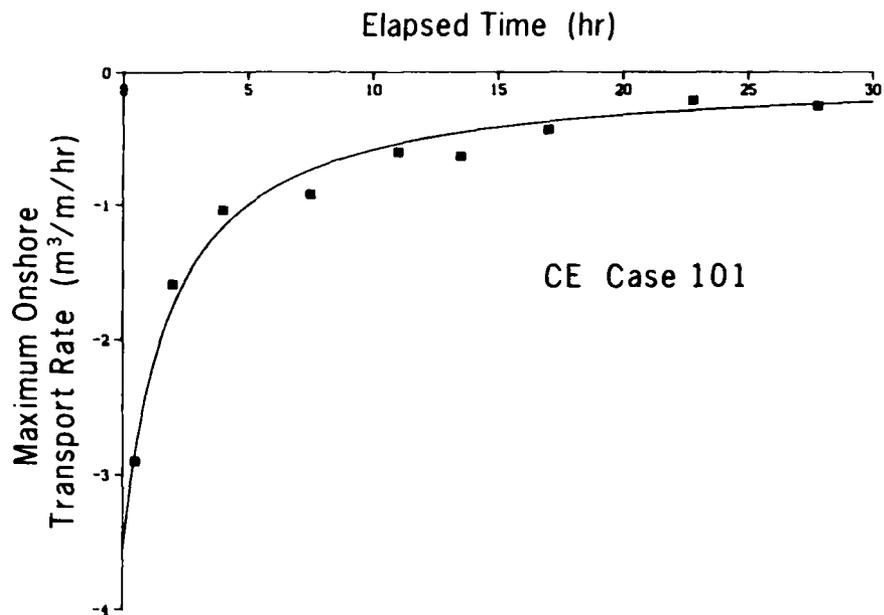
Figure 41. Decay of peak onshore sand transport rate with time for Case 101, and a best-fit empirical predictive equation

observations made by Sawaragi and Deguchi (1981) from laboratory experiments, where they noted that the onshore transport decayed faster with time than the offshore transport. It is hypothesized here that the peak onshore transport rate decays more rapidly than the peak offshore rate because of the retarding force of gravity on onshore sand motion on a sloping beach.

Also, in the present case, there was a wider range in values of the rate coefficient for the peak onshore transport rate compared to the peak offshore rate, illustrated by the larger standard deviation. The rate coefficient showed a lower correlation with wave period (r=0.50) than did that for offshore transport, but still a rather high correlation with the initial peak onshore transport rate (r=0.75). No significant correlation of peak onshore rate with wave or sand parameters was found.

Magnitude of Net Cross-Shore Transport Rate

In the LWT experiments, breaking waves caused sand movement
that changed the shape of the beach profile. Depending on the
wave properties, the net cross-shore sand transport is expected
to have different characteristics in different regions along the
profile, at least in a morphological sense (Keulegan 1948). In
regions of breaking waves the energy dissipation is large,
maintaining grains in suspension, and more material is trans-
ported than in regions of non-breaking waves. Also, the swash
zone is governed by quite different dynamics than the surf zone,
even if breaking waves prevail in both zones. Keulegan (1948)
identified three regions where "the laws of transportation of
sand" were expected to be different; from the point of impending
wave break to the point where wave reformation occurs, from the
point of impending wave break and seaward, and from the point of
wave reformation to the shoreline.

A similar division was developed in this study in order to
more closely relate transport rate properties to local wave
characteristics. Figure 42 is a definition sketch illustrating
division of the profile into four zones. Wave breaking in the
surf zone (excluding the swash zone) can be separated into two
hydrodynamic regions according to the scale and intensity of the
induced vortices, as described by Miller (1976), Svendsen,
Madsen, and Buhr Hansen (1979), Basco (1985), Jansen (1986), and
others. Svendsen, Madsen, and Buhr Hansen (1979) called the
region extending shoreward of the wave breaking point for a
distance of several breaker depths the "outer or transition
region." The more seaward region of the surf zone was called the
"inner or quasi-steady state region." The outer region is
characterized by large vortices and splash-jet motions, whereas
the inner region is characterized by bore-like movement and more
gradual change in internal fluid motion. The aforementioned
studies showed this classification to be valid for both spilling

151
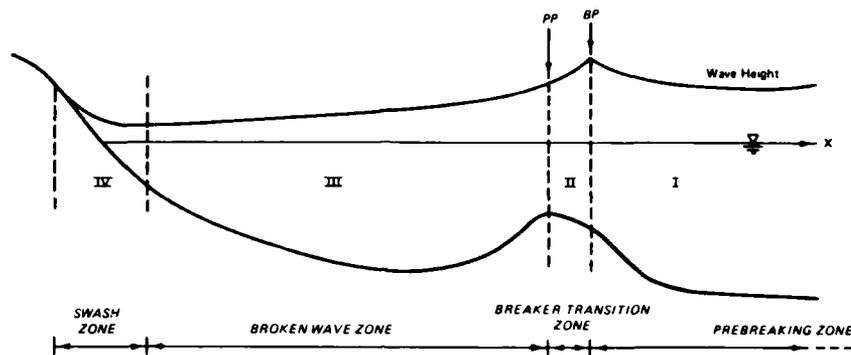
Figure 42.   Definition sketch for four principal zones of
cross-shore sand transport

and plunging breakers, with the intensity of the process being
less for spilling breakers.   Thus, when waves break, either by
spilling or plunging, there is a certain distance between the
incipient break point and the location where the waves are fully
broken (where the energy dissipation achieves a maximum or near-
maximum).   Sunamura (1988) similarly hypothesized a plunge point
for spilling breakers in analogy to that for plunging breakers.
Skjelbreia (1987) conducted a detailed laboratory study of
reproducible breaking solitary waves.   He reviewed the literature
of the wave breaking process and defined four zones of shoaling
wave transformation as gradual shoaling, rapid shoaling, rapid
decay, and gradual decay.   These zones are similar to those
developed in the present work based on considerations of cross-
shore sand transport, discussed next.

152

Transport Regions

Different regions with specific sand transport relationships
were defined based on generally accepted concepts of nearshore
wave dynamics, in accordance with Figure 42. One region extends
from the seaward limit of significant profile change to the break
point, called the pre-breaking region, denoted as Zone I. In
this region the transport rate is influenced by transport in the
zone of wave breaking through the sediment flux at its shoreward
boundary, but the governing transport processes on either side of
the boundary are quite different. Zone II corresponds to the
breaker transition region and is located between the break point
and the plunge point. From the location of the plunge point to
the point of wave reformation one specific region, Zone III, is
defined where the waves are fully broken and gradually decay
(inner region in hydrodynamic terms). In this region the energy
dissipation of the waves due to breaking becomes fully developed.
If several break points occur with intermediate wave reformation,
several zones of type II and III will be present along the
profile.

Transport conditions in the swash zone differ from those
prevalent in the surf zone, making it logical to define a fourth
transport region, Zone IV. Cross-shore sand transport in the
swash zone is expected to depend mainly on properties of the
runup bore, local slope, and sediment characteristics. The runup
limit approximately constitutes the shoreward boundary for cross-
shore transport by waves. In regions between zones of breaking
and fully broken waves, where wave reformation occurs, the
transport conditions are regarded as similar to what prevails in
the region seaward of the main breakpoint.

In summary, the four transport zones are located as follows
(Figure 42):

Zone I: From the seaward depth of effective sand transport
          to the break point (pre-breaking zone).

Zone II: From the break point to the plunge point (breaker
          transition zone).

Zone III: From the plunge point to the point of wave
          reformation or to the swash zone (broken wave
          zone).

Zone IV: From the shoreward boundary of the surf zone to
          the shoreward limit of runup (swash zone).

The division of the profile into different transport regions
is not immediately recognized viewing the net transport rate
distributions (see, for example, Figure 32) since the transport
regions interact, and the long-term average represented by the
calculated distributions has a smoothing effect. Nevertheless,
from a physical point of view it is attractive and productive to
divide the beach profile into regions with different governing
transport relationships. In the following, net transport rate
conditions are investigated in the different transport zones and
in three zones related to wave and sand characteristics.
Empirically-based relationships for the net transport rate are
formulated for the different regions based on physical considera-
tions and observations from the data.

Zone I: Net transport rate seaward of the break point

The net cross-shore transport rate seaward of the break
point has probably been the most intensively studied of all
regions on the profile, both in the field and in the laboratory.
Transport in the pre-breaking zone is in many cases governed by
ripple dynamics (e.g., Inman 1957, Dingler and Inman 1977,
Nielsen 1979, Sunamura 1981a). Sophisticated transport rate
formulas have been developed based on laboratory experiments
(e.g., Madsen and Grant 1977, Sato and Horikawa 1987), but these

empirically-based formulas must also be supplemented by other information for their application. Such formulas describe sand transport on spatial and temporal microscales which are not compatible with the present approach of quantifying large-scale profile features over intervals of tens of minutes.

As a wave approaches the point of breaking, its velocity field becomes more asymmetric with high, narrow peaks of onshore-directed flow and broad troughs of flow directed offshore. This motion could cause material to move either onshore or offshore depending on the elevation in the water column at which a grain is suspended in relation to the duration of the on/offshore flow. Sorting of material is thus expected along the profile, with coarser material migrating closer to shore (Ippen and Eagleson 1955).

Erosional cases. For erosional profiles, in the vicinity of the break point it is expected that diffusion of sand in the seaward direction that was set in suspension by the breaking waves dominates over the material placed in motion along the bottom by oscillatory wave forces. As seen from Figure 32, the shape of the net transport rate distribution is well approximated by an exponential decay with distance from a point somewhat seaward of the location of the maximum transport rate. This point is located in the vicinity of the break point and the transport rate q in Zone I may accordingly be written

$$q = q_b \, e^{-\lambda x} \tag{21}$$

where

    x = cross-shore coordinate originating at the break point

    q_b = transport rate at the break point

    λ = spatial decay coefficient

155

In analysis of distributions of the net transport rate
seaward of the break point, cases involving mainly onshore
transport and offshore transport were studied separately.
Equation 21 was least-squares fitted through the data for 12
cases showing mainly erosion and for 13 cases showing mainly
accretion. Each case typically comprised between 5-10 transport
rate distributions for which a spatial decay coefficient was
obtained. For a specific transport rate distribution a high
coefficient of determination was always obtained (above 90 %).
The estimated decay coefficient λ was quite stable and showed
only a slight tendency to decrease with time. Figure 43 il-
lustrates the spatial decay coefficient as a function of time for
four of the erosional CE cases.
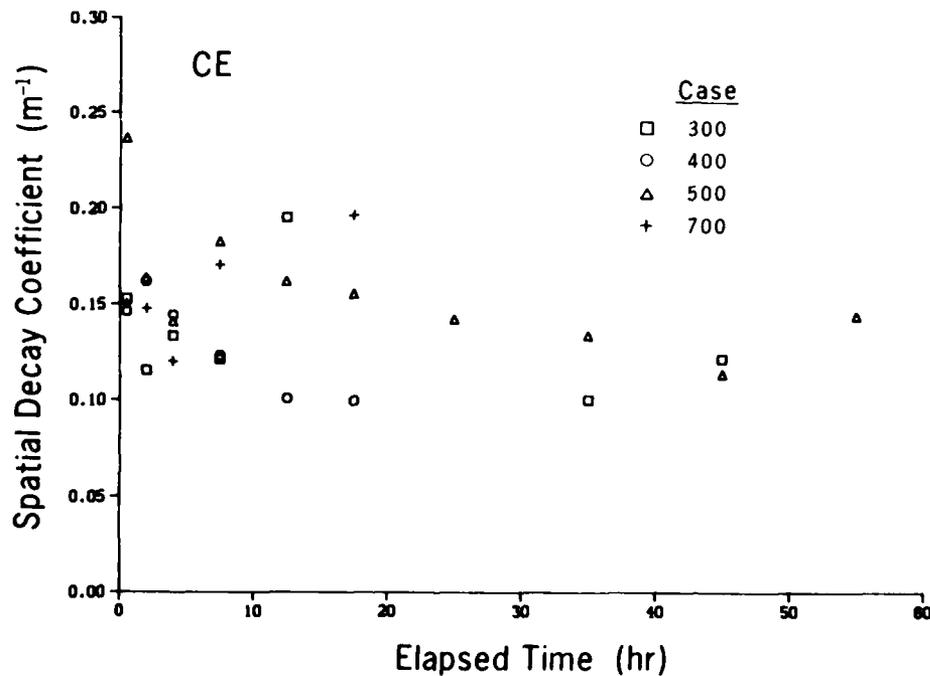
Figure 43. Time-behavior of spatial decay rate coefficient
for the zone seaward of the break point

To obtain an overall estimate of the spatial decay coeffi-
cient for a specific erosional case, the transport rate for each
distribution during a run was normalized with the q_b-parameter as
given by the least-squares fit for the individual distribution.
Figure 44 illustrates, for CE Case 500, the decay of the normal-
ized transport rate from the break point and seawards for
consecutive transport rate distributions (indicated by different
symbols) through time, together with a solid line showing the
least-squares estimate of the exponential decay. The coefficient
of determination in this case was 92 %. The difference between
averaging the individual estimates of the spatial decay coeffi-
cient and obtaining an overall estimate by using the normalized
transport rates was small.
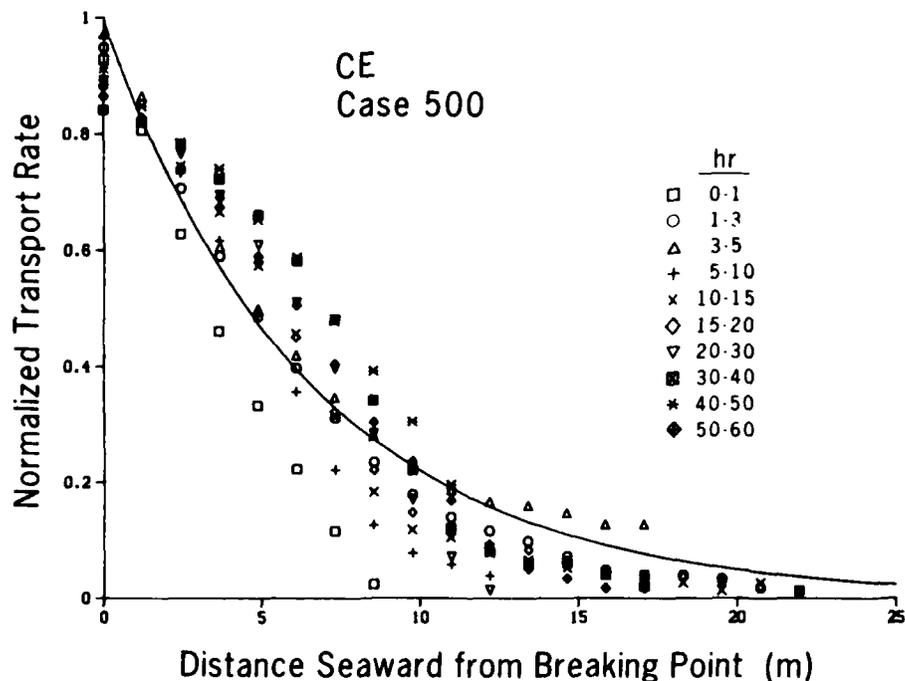
Figure 44. Comparison of net offshore sand transport rates
at different times seaward of the break point
and an empirical predictive expression

The average spatial decay coefficient for the erosional cases was calculated for each case and related to wave properties and sand characteristics. The overall average value of the decay coefficient was 0.18 m^{-1} with a standard deviation of 0.06 m^{-1}. Values ranged from a minimum of 0.12 m^{-1} to a maximum of 0.34 m^{-1}.

Correlation analysis showed an inverse dependence of the spatial decay coefficient on the breaking wave height and a direct dependence on the grain size (correlation coefficients of -0.70 and 0.75, respectively). In principal, a larger breaking wave height, for a specific grain size, would stir up more sand and thus allow more of the entrained grains to disperse seaward from the break point implying a more gradual decay in the transport rate. For constant breaking wave height, larger sand grains are less likely to be put into suspension and the transport rate distribution decays more rapidly seaward of the break point. This intuitive picture is supported by the correlation analysis.

The spatial decay coefficient showed only a weak inverse dependence on the wave period, giving a small correlation coefficient. Regression between the decay coefficient and the breaking wave height and the grain size explained 70 % of the variation in the data. The regression equation is

$$\lambda = 0.40 \ (\frac{D}{H_b})^{0.47} \tag{22}$$

Note that in Equation 22 the units of median grain size D are mm and the units of H_b are m.

Figure 45 illustrates the decay coefficients calculated from the data compared with values predicted by Equation 22. Note in Figure 45 that one of the points influences the regression and correlation analysis considerably. The regression relationship
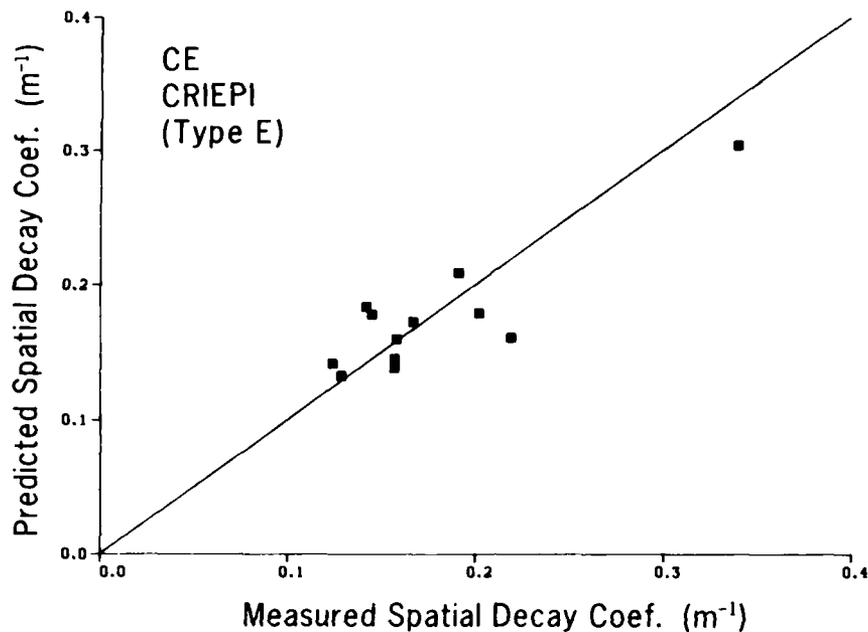
Figure 45. Comparison of spatial decay rate coefficients
and an empirical predictive expression

given by Equation 22 contains a coefficient which is dimensional.
Effort was made to form a non-dimensional quantity involving the
decay coefficient and a relevant wave or sand property, but no
significant dependence was achieved.

Accretionary cases. A similar analysis of the decay of the
transport rate for the zone seaward of the break point was
carried out for cases which showed mainly onshore transport. The
coefficients of determination obtained by least-squares fitting
of an exponential decay function were in almost all cases greater
than 90 % for the individual transport rate distributions.
Figure 46 illustrates, in analogy with Figure 44, the decay in
the transport rate seaward of the break point and the correspond-
ing calculated result from the regression equation (coefficient
of determination 95 %) for a typical case (Case 101). Transport
was directed onshore at all times.

159

Distance Seaward from Breaking Point (m)
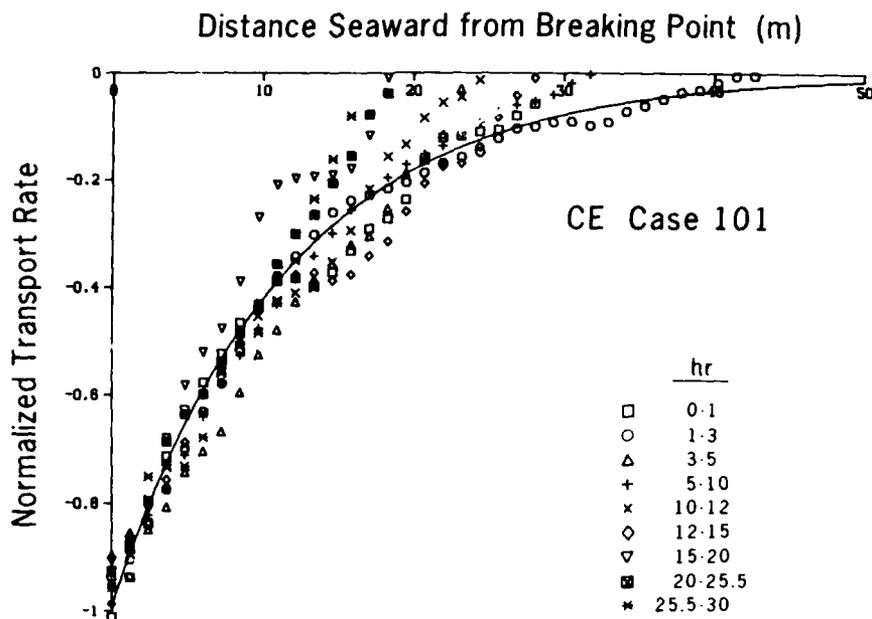
Figure 46.   Comparison of net onshore sand transport rates
at different times seaward of the break point
and an empirical predictive equation

Spatial decay coefficients for accretionary cases were in
general smaller than for erosional cases, indicating that a
larger portion of the profile seaward of the hreak point was
affected by the waves for the accretionary cases. The average
spatial decay coefficient for all accretionary cases studied (13
cases exhibiting mainly onshore transport) was 0.11 m^{-1}, with
standard deviation of 0.02 m^{-1}. There was significantly less
spread in the values of λ for the accretionary cases, indicated
by the smaller standard deviation and the more narrow range
between minimum and maximum values (0.08-0.16 m^{-1}). Contrary to
the erosional cases, the spatial decay coefficient could not be
related with any significance to wave and sand properties.
Secondary Zone I transport. The above analysis concerned Zone I,
the region from the break point and seaward, in the absence of

160

multiple break points. If wave reformation occurred and waves broke again closer to shore, the region seaward of the second breaker appeared to show transport rate characteristics similar to those in the region immediately seaward of the first breaker line. Only a few of the cases had a second breaker, and often the second breakpoint bar formed during the initial part of the run, rapidly reaching an equilibrium volume. However, the main breakpoint bar had to develop to a certain size before the trough shoreward of the bar was sufficiently deep to allow the waves to reform. Formation of a second bar was manifested in the transport rate distribution as a local minimum, indicating that material was deposited shoreward of this point. implying a negative derivative of the transport rate. A local minimum in the transport rate was typically found only in the first few transport rate distributions of a run, since the second breakpoint bar soon attained equilibrium.

The present data sets do not provide sufficient information to determine any reliable quantitative empirical relationships for the net transport rate in areas of wave reformation. Some qualitative observations may be made from the data with regard to the shape of the transport rate. The transport rate decayed in the seaward direction from a point located somewhat shoreward of the second break point, and the spatial decay in the net transport rate appeared to be more gradual than seaward of the main breakpoint bar. It is speculated that even though breaking ceases, more turbulence is generated or convected in areas of reformation than in the area seaward of the main breakpoint, thus making the decay of the transport rate in wave reformation zones more gradual.

Zone II: Net transport rate between break point and plunge point

Waves must propagate shoreward a certain distance from the break point before breaking fully develops and energy dissipation

reaches a maximum (Miller 1976, Svendsen, Madsen, and Buhr
Hansen, 1979, Basco 1985, Jansen 1986, Basco and Yamashita 1987,
Svendsen 1987). This distance appears to be approximately equal
to the plunge distance for plunging breakers and provides the
basis for a definition of an equivalent plunge distance for a
spilling breaker. The shape of the main breakpoint bar was in
many cases well approximated by two linear slopes on the seaward
side of the bar (see Part IV). The break in slope was located in
the vicinity of the break point, indicating that the properties
of the net transport rate were presumably different in the areas
seaward and shoreward of the break point.

It proved too difficult to determine quantitative charac-
teristics of the net transport rate in the region between the
break point and the plunge point. This region is of small
spatial extent. Furthermore, the breaker transition zone moves
together with the bar over the course of wave action, which makes
analysis problematic as the transport rate calculations are based
on average profile changes that occurred over a considerable
time. However, from a conceptual point of view it is important
to recognize this region as being different from neighboring
areas.

Some transport rate distributions provided insight into the
nature of the net transport rate distribution in Zone II,
particularly during later times of a run, when changes in the
beach profile shape were more gradual. Figure 47 illustrates the
transport rate distribution in the region between the break point
and the location of the maximum transport rate for selected cases
and times The transport rate decreased in the offshore direc-
tion at a lower rate than in the region seaward of the break
point. Analysis of a small data subset where Zone II transport
could be distinguished as in Figure 47 indicated that an exponen-
tial decay was a reasonable approximation, with the spatial decay
coefficient approximately 0.20-0.25 of the value of the spatial
decay coefficient governing transport seaward of the break point.
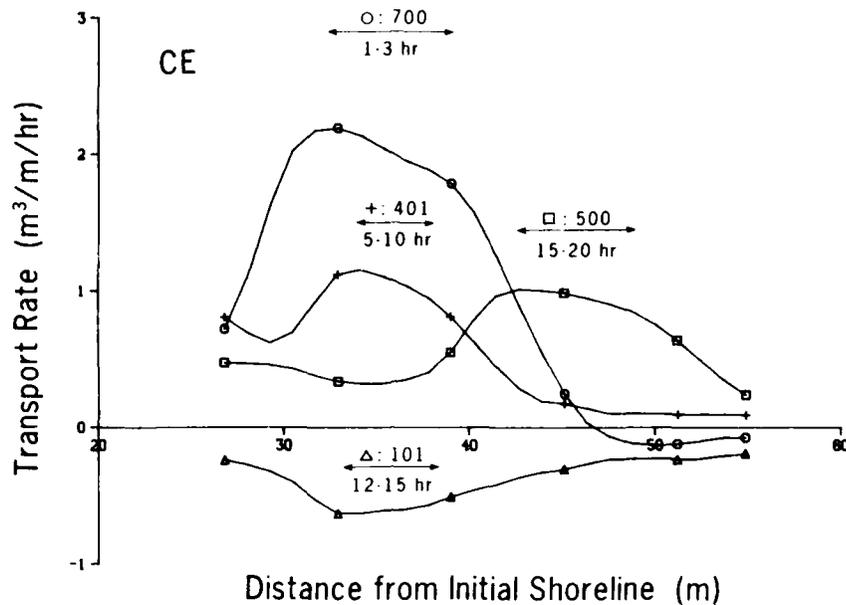
Figure 47. Net cross-shore sand transport rate distribu-
tions between break point and plunge point

Zone III: Net transport rate in broken waves

Estimation of energy dissipation. Breaking and broken waves
produce turbulent conditions that put grains into suspension and
make them available for transport across the profile (Watts 1953,
Fairchild 1973, Kana 1977, Kraus and Dean 1987). Thus, it is
plausible to assume that the magnitude of the transport rate is
closely related to energy dissipation of the waves (Dean 1977a).
Different models of wave height decay in the surf zone due to
energy dissipation have been developed (e.g., Dally 1980,
Mizuguchi 1981, Svendsen 1984, and Dally, Dean, and Dalrymple
1985a, b).

The CE data set did not include detailed measurements of the
wave height distribution across the profile, whereas the CRIEPI

data set provided wave height data for most of the cases with a
resolution of 2.5 m. The wave height distribution was usually
measured in between profile surveys, making the exact beach
profile shape unknown for the time of the measurement. To obtain
a picture of the relationship between the cross-shore transport
rate and local wave parameters in broken wave zones, the CRIEPI
data set was used, although the number of cases that contained
significant profile change and corresponding measurements of wave
height across-shore was limited. Only four cases allowed
thorough analysis of the correlation between local wave proper-
ties and transport rate at consecutive times during a run.

Energy dissipation is related to the change in wave energy
flux along the profile. The energy flux F may be written using
shallow water wave theory

$$F = \frac{1}{8} \rho g H^2 \sqrt{gh} \qquad\qquad (23)$$

where

ρ = water density

g = acceleration of gravity

H = wave height

h = water depth

The energy dissipation may thus be expressed as dF/dx.

Due to the relatively wide resolution in measurement of wave
height, the evaluation of the derivative and transport proved
sensitive to individual measurement values. To obtain a better
estimate, the wave decay model of Dally (1980) was least-squares
fitted through discrete values of each measured wave height
distribution from the point of breaking to shoreward, until wave
reformation occurred or the water depth became small (ap-
proximately 20 cm). The wave model is presented in Part VI,
where the analytic solution which was used in the least-square
fit is given (Equation 29). It is noted that a change in broken

wave height is not completely indicative of wave energy dissipa-
tion; energy reordering may also occur, as discussed by Svendsen,
Madsen, and Buhr Hansen (1979).

The empirical coefficient relating stable wave height to the
water depth employed in the Dally model (still-water depth
without set-up) was determined from the wave height measurements
by examining the ratio between wave height and water depth in the
proximity of areas of wave reformation. An average stable wave
height coefficient was calculated for each case and values ranged
from 0.3-0.5, showing a marked dependence on the beach slope
(compare with Dally, Dean, and Dalrymple 1985b). Steeper beach
slopes yielded larger values of the stable wave height coeffi-
cient. The wave decay coefficient was then least-squares
estimated, giving values in the range of 0.15-0.3. In most
cases, there was a tendency for the wave decay coefficient to
decrease with time as the inshore slope became more gentle.

At first, both empirical parameters in the wave decay model
(stable wave height and wave decay coefficient) were least-
squares estimated (cf. Part VI). However, the minima of the sum
of squares were located in a very flat region, causing differen-
ces between optimum parameter combinations and neighboring values
to be small. To achieve a certain increase in the energy
dissipation, the wave decay coefficient might be increased or the
stable wave height coefficient decreased. Thus, in the optimiza-
tion process, since the region surrounding the minimum was very
flat, almost the same agreement could be obtained with a small
value of the stable wave height coefficient and a large value of
the wave decay coefficient, or the reversed situation. In some
cases the optimum parameter values gave unrealistically low
coefficients of stable wave height, such as 0.2. This was the
reason for employing the former method and only a least-squares
estimate of the wave decay coefficient, giving a sum of squares
deviating only slightly from the optimum value.

165

Dissipation in wave energy flux was determined from the wave decay model, calculated starting at the location of the maximum transport rate, somewhat shoreward of the break point, and ending where the wave decay model calculation was arbitrarily stopped. For each case, different quantities connected with the energy flux dissipation were correlated with the cross-shore sand transport rate in Zone III for all distributions obtained during a run. The net cross-shore transport rate showed good correlation with energy flux dissipation per unit water volume for all cases studied (correlation coefficients of 0.7-0.8), which was higher than the correlation resulting from tests using only the energy flux dissipation per unit area of beach. Figure 48 shows the transport rate plotted against the energy flux dissipation per unit volume as evaluated for Case 6-1.
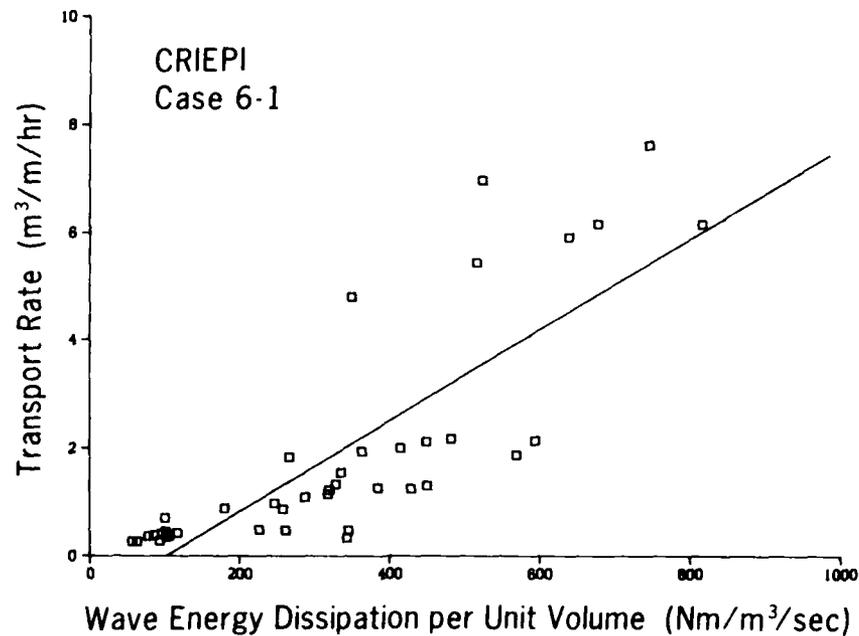
Figure 48. Net cross-shore sand transport rate versus calculated wave energy dissipation per unit volume in broken wave region

Correlation was in general higher for individual transport rate distributions than if all values from a specific case were used. Other parameters pertaining to the geometry of the beach profile, such as beach slope, and wave characteristics, were also correlated with the transport rate. To determine geometric parameters of the beach profile, the average profile calculated from surveys taken before and after the measurement of the wave height distribution was used. No significant correlation was found that was consistent for all cases between any other parameters studied and the transport rate. For some cases there was a positive correlation between transport rate and beach slope, but it did not encompass all cases.

A linear regression equation relating the transport rate to energy dissipation per unit volume and local beach slope was least-squares fitted to the data. The regression relationship explained about 50-70 % of the total variation in the data for the different cases studied, in which local beach slope accounted at most for 10 % of the total variation.

Kriebel and Dean (1985a) assumed that the cross-shore sand transport rate was proportional to the excess energy dissipation per unit volume over a certain equilibrium value of energy dissipation, which was defined by the amount of energy dissipation per unit volume a beach with a specific grain size could withstand (cf. Part VI). From the regression analysis between wave energy dissipation per unit volume and transport rate, it was possible to obtain an estimate of the transport rate coefficient corresponding to the proportionality constant used by Kriebel and Dean (1985a).

For the four cases intensively studied, the average value of the transport rate coefficient was determined from regression analysis to be $1.1 \ 10^{-6} \ m^4/N$, which is approximately half the value originally obtained by Moore (1982). Moore (1982) developed a numerical model of beach profile change using a transport equation for the cross-shore sand movement, in which the trans-

167

port rate was proportional to wave energy dissipation per unit volume. He arrived at a transport coefficient of $2.2 \ 10^{-6} \ m^4/N$ by calibration using profile change measured in one CE case and field measurements from Santa Barbara, California.

Two major causes are believed responsible for the difference in values obtained. First, Moore (1982) inferred the transport coefficient by comparison of simulated profile change and measurement, not directly between wave energy dissipation per unit volume and measured transport rate, as done here. Second, considerable smoothing of the calculated transport rate was used in Moore's model. By smoothing the energy dissipation along the profile, a higher transport rate coefficient is needed to achieve the same beach profile response as compared to no smoothing. A more thorough discussion of values of the transport rate coefficient is given in Part VII describing application of the numerical model.

It was not possible to relate the transport rate coefficient to wave or beach properties. In a numerical model the transport rate coefficient functions largely as a calibration parameter to give the proper time scale of profile change.

In the regression analysis between transport rate and energy dissipation per unit volume other beach and wave parameters were added to quantify their influence. For the cases where the local beach slope showed some influence on the transport rate, the coefficient in the regression equation was typically small, on the order of $0.0006 \ m^2/sec$. The equilibrium energy dissipation was determined from the constant term in the regression equation and varied considerably between the runs evaluated, although the grain size was the same for the studied cases. This was probably due to the scatter in the data relating transport rate to energy dissipation, which made the least-squares estimate of the constant in the regression equation less reliable. However, two of the studied cases resulted in equilibrium energy dissipations that were somewhat smaller than the values given by Moore (1982),

168

who used natural beach profiles to determine this parameter (108 and 134 Nm/m^3sec from the present data compared to Moore's value of 170 Nm/m^3sec).

The purpose of the previous analysis was to emphasize the close relationship between wave energy dissipation per unit volume and magnitude of the transport rate in zones of broken waves. Although the number of satisfactory cases for obtaining quantitative information about wave height and associated sand transport rate distribution was small, the relationship between the two quantities was clearly evident. All of the studied cases encompassed beach profiles which experienced erosion of the foreshore and bar formation in the vicinity of the break point. It is expected that profiles with accretion on the foreshore will also show transport rates that are related to the energy dissipation per unit volume, although it was not possible to directly confirm this assumption by means of the present data.

Zone IV: Net transport rate on the foreshore

The net transport rate in the swash zone is expected to be a function of the local beach slope, sediment characteristics, and properties of the bore propagating upon the beach. No wave or bore information was available for this study, except for some runup measurements from the CE data. Consequently, it was not possible to derive a relationship connecting the net transport rate on the foreshore to local wave properties and other factors. However, some qualitative observations were made of the shape of the net transport rate distribution on the foreshore. The region discussed in this section extends approximately from the runup limit seaward to some specific depth corresponding to the point of maximum retreat of the waves in the swash. This depth is a function of the incident waves, which cause set-up at the shoreline roughly proportional to the breaking wave height. Swash oscillates about the mean shoreline elevation with a range

169

dependent mainly on wave height and surf similarity parameter
(Guza and Thornton 1982, Holman 1986).

For some cases, the net transport rate showed a fairly
complex spatial dependence on the foreshore, in particular at the
early stages of the experiments. However, the net rate had an
almost linear decay with distance for a majority of the cases,
both for onshore and offshore transport conditions. Figure 49
gives a representative example of the transport rate distribution
over the foreshore for CE Case 300, in which different consecu-
tive distributions in time are plotted. The slope of the
transport rate decreased with time as the profile approached
equilibrium, but the shape of the distribution roughly maintained
linear form. Observe in the figure that the profile retreated
shoreward as the foreshore eroded during the run. (The location
of the still-water shoreline is indicated by vertical lines for
the different distributions in time.) A linear decay in the
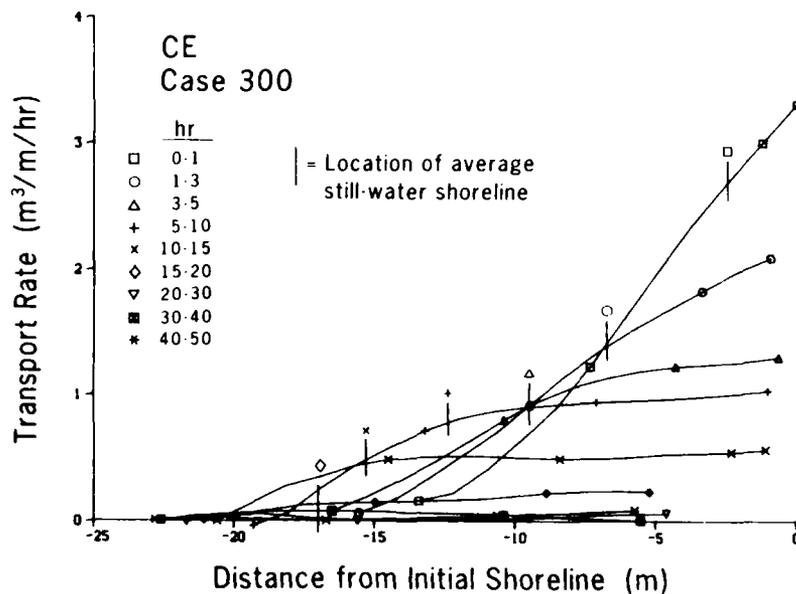
Figure 49. Time behavior of net cross-shore sand transport
rate distribution on the foreshore

170

transport rate implies that an equal amount of material is eroded
at all points along the foreshore up to the runup limit (compare
field observations of Seymour 1987).

As the foreshore eroded, a step formed extending approxima-
tely from the still-water shoreline to the runup limit. The
slope of the step may have increased until the angle of initial
yield was exceeded (Allen 1970) and avalanching occurred, which
adjusted the slope to a lower value (residual angle after
shearing). This type of slope-failure sediment transport is
expected to occur very rapidly and would produce a transport rate
distribution of a quadratic shape, since the step rotate at a
fixed angle around some point along its face. Averaging of the
net transport rate smooths over the process of avalanching.
Also, avalanching is probably not ideal with a pure and constant
steepening of the step face but, rather, transport occurs at the
base of the step, undermining it.

Summary and Discussion of Net Transport Rate

Calculated distributions of the net cross-shore transport
rate from measured profile change over intervals on the order of
hours displayed very regular and smooth properties, despite the
random character of the grain-by-grain movement that actually
took place. Consequently, it appears possible to estimate the
net cross-shore sand transport rate with sufficient reliability
to predict the development of main morphologic features of the
beach profile. Available equilibrium distributions of the net
transport rate could be classified almost exclusively into three
main types, where two types corresponded to either onshore or
offshore transport along the profile. Transport distributions
with one onshore and one offshore peak were not common and
occurred mainly for cases which fell close to a derived line
delineating between bar/berm profiles. Consequently, assumption

171

of a unidirectional transport rate along the profile appears to
be a reasonable first approximation in most cases for describing
the overall profile response to incident short-period waves.

Division of the profile into four transport zones with
different properties, based in part on general observations of
nearshore wave dynamics, proved to be fruitful both from concep-
tual and predictive points of view. The net transport rate in
zones of broken waves, where the most active transport is
expected to occur, showed good correlation with the wave energy
dissipation per unit water volume. The net transport rate in the
pre-breaking zone decayed exponentially with distance offshore.
On the foreshore the net transport rate showed an approximately
linear behavior decreasing in the shoreward direction from the
end of the surf zone.

Quantitative information on the net cross-shore transport
rate is difficult to obtain in the field due to the limited
resolution in time and space of profile surveys, number of
instruments that can be deployed, contaminating effects of
longshore sand transport, and changing wave conditions. In this
respect, data from large wave tanks provided valuable insight
into the behavior of the net cross-shore transport rate and
enhanced the possibility of modeling beach profile change.
Although monochromatic waves were used in the large wave tank
experiments, it is expected that the main features of the
transport rate are representative of processes associated with
random waves in the field. This hypothesis is tested in Part
VII, where model predictions are compared with field data.

PART VI: NUMERICAL MODEL OF BEACH PROFILE CHANGE

Introduction

It is of great engineering importance to predict changes in the beach profile caused by wave action and changes in water level. Accurate simulation of dune erosion, the effect of catastrophic storm events, and the initial adjustment and long-term evolution of a beach fill would be of great economic benefit for project planning and design. In this regard, a numerical model can be an efficient tool, providing the capability to evaluate different design alternatives while easily incorporating detailed process data, such as wave and water level time series.

Many attempts have been made to develop numerical models of beach profile change, but presently no model exists which can be applied to an arbitrary beach profile exposed to variable wave and water level conditions which will give reliable results and reproduce bar formation and movement. It is a major goal of the present investigation to model the growth and movement of bars since these features constitutes natural protection for a beach exposed to severe erosional conditions. Furthermore, any kind of long-term modeling must necessarily incorporate events producing onshore transport and berm build-up, which no known general numerical model can simulate.

This chapter describes a numerical model developed for simulating beach profile change, focusing on the main morphologic features of the profile, in particular, bars and berms. Many of the assumptions and relationships used in development of the numerical model were founded on observations made in previous chapters of this report. The numerical model is aimed at reproducing macro-changes of the beach profile in a deterministic fashion, neglecting small-scale features such as ripples and

avoiding problems associated with detailed specification of the fluid flow and sediment concentration.

In Part IV a strong connection was shown between different macro-features of the beach profile and wave and sand characteristics, thereby indicating the possibility of deterministically modeling profile change. Furthermore, predictability of the distribution of the net cross-shore sand transport rate distribution on a macro-scale was demonstrated in Part V. Thus, all preparatory work performed here supported the feasibility of numerically modeling beach profile change.

Methodology

At the present state of knowledge, it is clear that any kind of numerical model of beach profile change to be used in engineering practice must be based on semi-empirical relationships derived from measurements. The model presented here was developed using data from experiments carried out in large wave tanks (LWT) involving waves of prototype size.

Dally (1980) and Birkemeier et al. (1987) suggested a number of criteria to judge the suitability of a numerical model of beach profile change. In the present work, the following properties were considered to be fundamental:

a. Accurately simulate time evolution of a profile of arbitrary shape subjected to changes in water level and incident wave parameters.

b. Attain an equilibrium configuration if all model parameters and input values are held constant.

c. Simulate formation and movement of main morphologic profile features, such as bars and berms.

d. Reproduce erosional and accretionary beach change.

e. Be verified for a wide range of realistic conditions.

174

A short description of the capabilities of existing numeri-
cal models is contained in the literature review in Part II. Of
the various numerical models proposed to date, that of Kriebel
(1982) (see also Kriebel and Dean 1985a, Kriebel 1986) comes
closest to satisfying the five criteria listed above. The
Kriebel model was critically evaluated and determined to be the
best available tool for estimating erosion on U.S. coasts
(Birkemeier et al. 1987). The Kriebel model satisfies criteria
a. and b., and, in part e., but not criteria c. and d. The model
was originally developed and verified using several cases from
the CE data set, as well as an erosional event associated with
the 1985 hurricane Elena, and it has subsequently been used in
engineering studies (Kriebel and Dean 1985b, Kraus et al. 1986).
Development of the model presented in this chapter was stimulated
by the success of the Kriebel model.

In the following, a short overview of the structure of the
numerical model is given as an introduction before the various
components of the model are discussed in detail. Changes in the
beach profile are assumed to be produced by breaking waves;
therefore, the cross-shore transport rate is determined from the
local wave, water level, and beach profile properties, and the
equation describing conservation of beach material is solved to
compute profile change as a function of time.

The wave height distribution is calculated across-shore
applying small-amplitude wave theory up to the point of breaking,
and then the breaker decay model of Dally (1980) is used to
provide the wave height in regions of breaking waves. The
profile is divided into specific regions according to the wave
characteristics at the given time step for specification of
transport properties. The distribution of the cross-shore
transport rate is then calculated from semi-empirical relation-
ships valid in different regions of transport. At the shoreward
end of the profile the runup limit constitutes a boundary with no
material being transported across it, whereas the seaward

boundary is determined by the depth at which no significant sediment motion occurs. Once the distribution of the transport rate is known, profile change is calculated from the mass conservation equation. The described procedure is carried out at every time step using the current incident wave conditions and water level, and updating the beach profile shape.

First, the wave model is described and calculations compared with measurements from the CRIEPI data set. Then the various transport relations are developed for use in the profile change model. The next section gives a description of the numerical solution scheme and the associated boundary conditions. Finally, calibration and verification of the profile change model with the LWT data set is made. Applications of the model, including sensitivity analyses and tests of predictions with field data, are given in Part VII.

Wave Model

As waves approach shore over a gently sloping bottom, they increase in height and decrease in length due to shoaling. It will be assumed that the waves are ...cident normal to the coast, i.e., that refraction can be neglected. The increase in wave height continues until some critical ratio is reached between wave height and water depth, at which point the waves break. Here, calculation of the wave height distribution across-shore is done with linear wave theory. In initial model development. the nonlinear shoaling laws proposed by Shuto (1974) were used in an effort to provide an improved description of the increasing non-linearity of waves as they approach breaking. However, in comparison of predictions of the nonlinear wave model against wave height measurements from the CRIEPI data set, the height increased too steeply before breaking for longer-period waves. In simulations involving development of a prominent breakpoint

176

bar through time, a significant overestimation of wave shoaling was found just prior to breaking using Shuto's (1974) shoaling laws. Thus it was decided to use linear wave theory over all regions of the shoaling calculation.

Breaking criterion and breaker height

The ratio of wave height to water depth at breaking was evaluated using the CRIEPI data set. Only those cases with an initially plane slope were used and, if no profile survey was taken at the time of the wave height measurement, the depth at breaking was determined by interpolation from the two bracketing profiles in time. In total, 121 values were obtained from 17 cases having different wave conditions and initial beach slope. The average breaker ratio (wave height to water depth at breaking) was 1.00, with a standard deviation of 0.25. As shown in Figure 50, the distribution of the breaker ratios were somewhat positively skewed and values ranged from 0.58 to 1.79. The steep slope that developed on the seaward side of the growing bar caused the breaker ratio to increase with time, allowing the wave to break in more shallow water.

To evaluate this effect, a comparison was made with small-scale laboratory data tabulated by Smith and Kraus (1988) for experiments made with fixed plane bottom slopes typically more gentle than the seaward bar faces in the CRIEPI cases. Figure 51 shows the distribution of the breaker ratio for the small-scale experiment data, in analogy with Figure 50. Because of the more gentle slopes, the average breaker ratio for the small-scale data was only 0.82 (135 values), with a standard deviation of 0.18. If the beach slope grows steep seaward of the break point, the breaker ratio should accordingly be increased to account for the bottom slope effect on wave breaking.

177
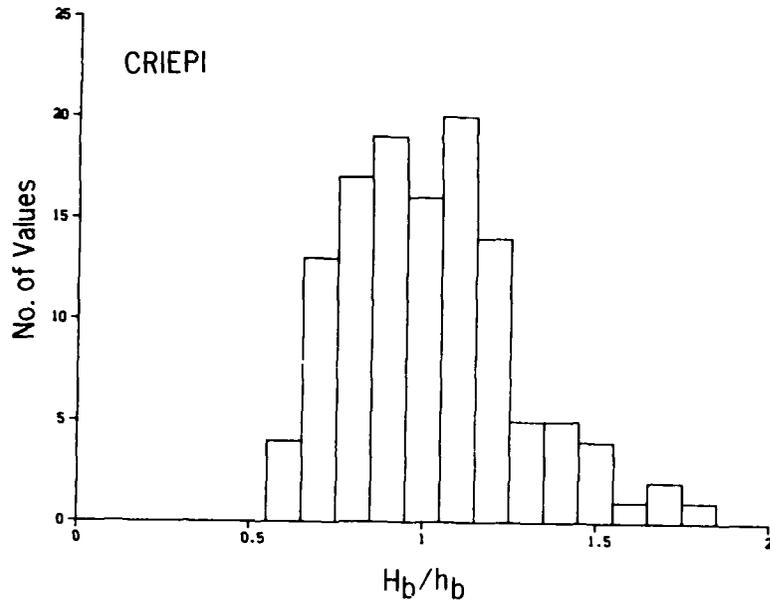
Figure 50. Distribution of breaker ratio for the CRIEPI
data
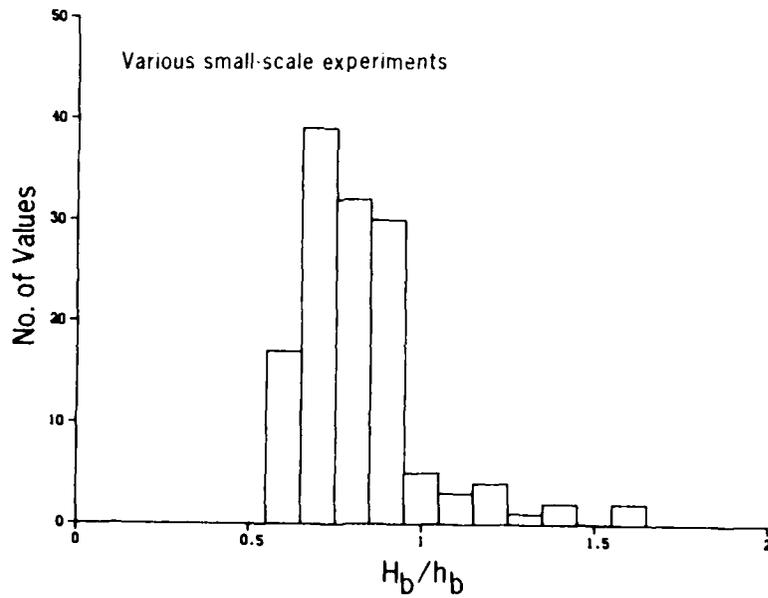
Figure 51. Distribution of breaker ratio for small-scale
laboratory data

178

Correlation analysis showed that the breaker ratio depended mainly on the slope before breaking and the deepwater wave steepness (see Galvin 1969, Weggel 1972, Singamsetti and Wind 1980, Sunamura 1981b). The slope was evaluated as an average over that part of the beach profile seaward of the break point where the waves showed a marked increase in height due to shoaling (typically between 10-20 m). The breaker ratio increased with an increase in bottom slope and decreased with an increase in wave steepness. For the profiles exhibiting bar development during a run, the average seaward slope in general showed an increase with time (Part IV), causing an increase in breaker ratio. Regression analysis between the aforementioned variables explained 55 % of the variation and also indicated that the beach slope and deepwater wave steepness could be combined to form the surf similarity parameter $(\tan\beta/\sqrt{H_o/L_o})$ (Battjes 1975) without loss of predictability. The regression equation is

$$\frac{H_b}{h_b} = 1.14 \ (\frac{\tan\beta}{\sqrt{H_o/L_o}})^{0.21} \tag{24}$$

where $\tan\beta$ is the local beach slope seaward of the breakpoint.

Values of the empirical multiplicative coefficient and exponent in the regression equation are very similar to those obtained by Battjes as reported by Singamsetti and Wind (1980) and Sunamura (1981b) based on small-scale laboratory data. In Figure 52 the data from the CRIEPI experiments are plotted together with Equation 24. The wave model uses Equation 24 to predict the breaking condition, for which the bottom slope is evaluated over one third of the local wavelength seaward of the break point.
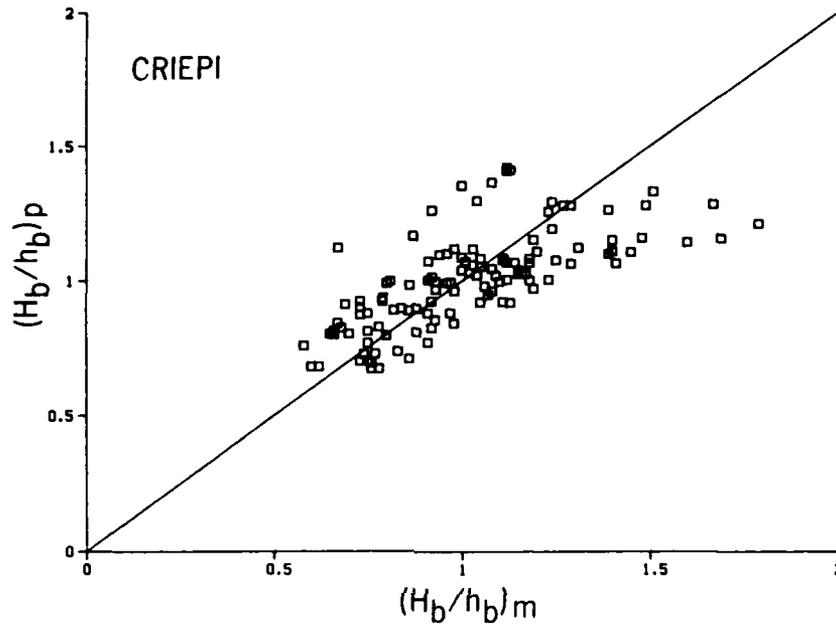
Figure 52.   Comparison between measured breaker ratio and
             predicted breaker ratio from an empirical
             relationship based on beach slope seaward of the
             break point and deepwater wave steepness

The breaking wave height on the movable bed bottoms of the
CE and CRIEPI experiments normalized by the deepwater wave height
was related to the deepwater wave steepness.   An average breaking
wave height was used for each case, making up a total of 32 cases
for the analysis.   Regression analysis with the deepwater wave
steepness explained 80 % of the variation in the data, leading to
the equation

$$\frac{H_b}{H_o} = 0.53 \; (\frac{H_o}{L_o})^{-0.24} \qquad\qquad (25)$$

Addition of initial beach slope to the regression equation did not improve predictability, probably due to the significant change in slope that occurred seaward of the break point during the course of wave action. Figure 53 illustrates the prediction from Equation 25 and the data points from the studied cases. The data points associated with different initial slopes have been plotted with different symbols. Note that the empirically determined exponent in Equation 25 is close in value to that which is obtained with linear wave theory for shoaling of normally incident waves from deep water to breaking (-0.20; cf. Komar and Gaughan 1973).
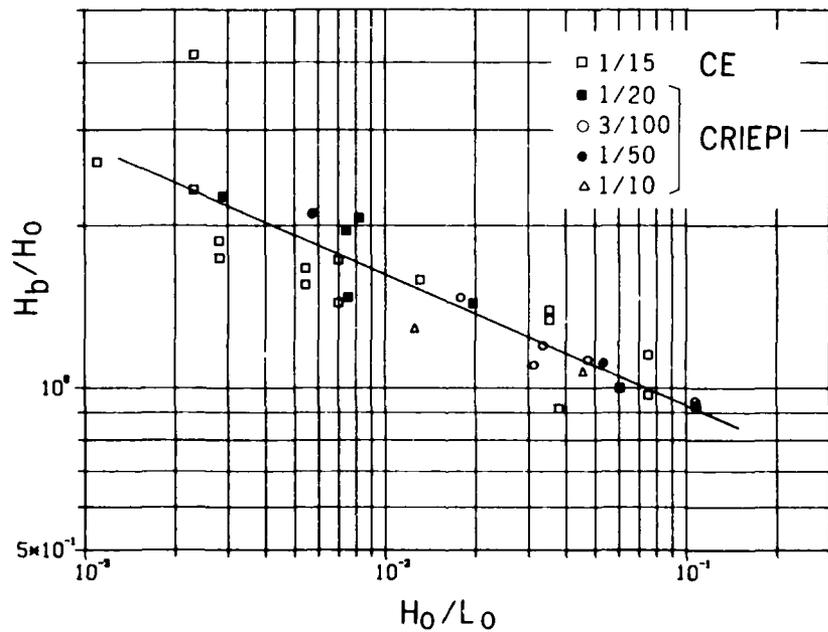
Figure 53. Ratio between breaking and deepwater wave height as a function of deepwater wave steepness

Breaker decay model

A number of numerical models have been developed for describing wave height decay in the surf zone (e.g., Battjes and Janssen 1979, Dally 1980, Mizuguchi 1981, Svendsen 1984). All of these models contain empirical parameters whose values have to be established by calibration against measurements. The wave model proposed by Dally (1980) and further discussed by Dally, Dean, and Dalrymple (1985a, 1985b) was chosen for use here since it has been extensively verified with both laboratory data (Dally 1980) and field data (Ebersole 1987). Furthermore, the breaker decay model allows for wave reformation to occur, which is an essential feature for modeling profiles with multiple bars. The governing equation for the breaker decay model is written in its general form as

$$\frac{dF}{dx} = -\frac{\kappa}{h}(F - F_s) \tag{26}$$

where

$F = E\,C_g =$ wave energy flux

$F_s =$ stable wave energy flux

$E =$ wave energy

$C_g =$ wave group velocity ($= \sqrt{gh}$ in shallow water)

$\kappa =$ empirical wave decay coefficient

$h =$ water depth

$x =$ cross-shore coordinate originating from the break point

The assumption behind Equation 26 is that the energy dissipation per unit plan beach area is proportional to the difference between the energy flux and a stable energy flux below which a wave will not decay. By using linear wave theory, the energy flux may be written for shallow water

$$F = \frac{1}{8} \rho g H^2 \sqrt{gh} \tag{27}$$

The stable energy flux is generally considered to be a function of the water depth (Horikawa and Kuo 1967), and a coefficient Γ is used to express the ratio between the local wave height and water depth at stable conditions according to

$$H_s = \Gamma h \tag{28}$$

Measurements of the wave height distribution from the CRIEPI experiments were used to evaluate performance of the breaker decay model and to estimate values of the two empirical parameters in the model. As described in Part V, the breaker decay model was least-squares fitted to the wave height data from the breakpoint and shoreward to the end of the surf zone. The solution of Equation 26 for a beach with an arbitrary shape, applying linear wave theory, is given by

$$H = \left[\frac{1}{\sqrt{h}} \left(H_b^2 \sqrt{h_b}\ e^{-\kappa_o \int^x \frac{dx}{h}} + e^{-\kappa_o \int^x \frac{dx}{h}}\ \kappa \Gamma^2 \int_o^x h \sqrt{h}\ e^{\kappa_o \int^x \frac{dx}{h}}\ dx \right) \right]^{\frac{1}{2}} \tag{29}$$

where, as previously mentioned, case the cross-shore coordinate axis originates from the break point. This equation was used to estimate the energy dissipation by a least-squares fit, as discussed in Part V. Figure 54 shows a typical fit between results of the breaker decay model and measured wave heights in the surf zone. The symbols connected by straight lines denote the model result for different times, whereas the corresponding

183

single points are the measured wave heights. The breaker decay
model was in this case least-squares fitted against all wave
height distribution measurements made during one run. In order
to evaluate parameters of the breaker decay model simultaneously
for different distributions, wave height was normalized with the
incipient breaking wave height, and cross-shore distance and
water depth were normalized with depth at incipient breaking.
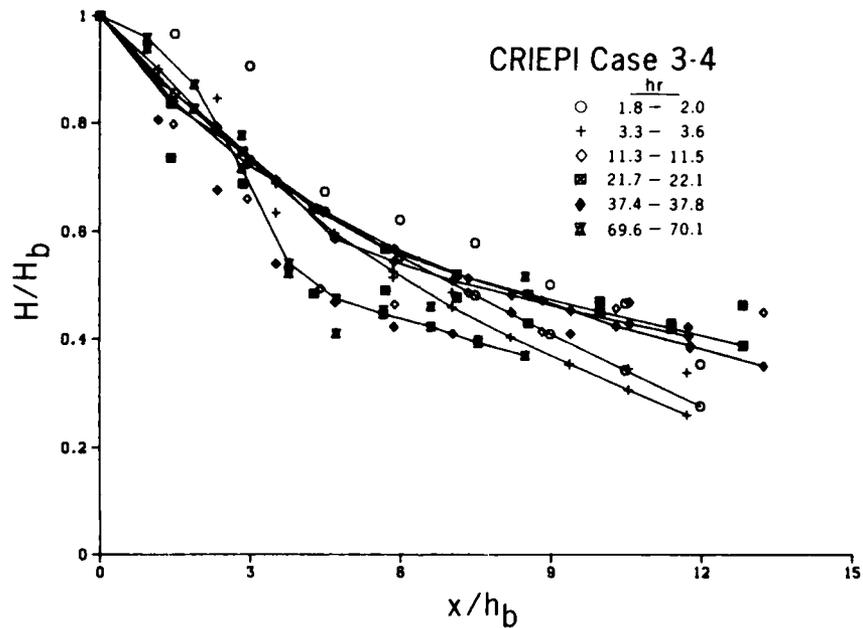
Figure 54. Measured wave height distributions across the
surf zone for Case 3-4 and corresponding wave
heights calculated with a breaker decay model

Wave set-up and set-down are incorporated in calculation of
the wave height distribution across-shore and determined by
solving the following differential equation together with
Equation 26 (Longuet-Higgins and Stewart 1963)

184

$$\frac{dS_{xx}}{dx} = -\rho g \ (h + \eta) \ \frac{d\eta}{dx} \tag{30}$$

where

η = wave set-up

S_{xx} = radiation stress component directed onshore

The radiation stress is written, using shallow-water approximations,

$$S_{xx} = \frac{3}{16} \ \rho g H^2 \tag{31}$$

Set-down in the first calculation cell is determined from the analytical solution to Equation 30 seaward of the break point, assuming no energy losses

$$\eta = \frac{\pi H^2}{4 L \ \sinh(\frac{4\pi h}{L})} \tag{32}$$

By calculating the wave height distribution across-shore at every time step in the model, a quasi-stationary approach is used assuming that the input wave height is changing at a time scale significantly longer than the wave period.

Energy dissipation by bottom friction is calculated in the model as done by Dally (1980) using linear wave theory to determine the bottom wave orbital velocity and assuming a shear stress proportional to the velocity squared. After the waves break, energy dissipation greatly increases due to the generation of turbulent motion. The energy dissipation caused by breaking

is considerably larger than the dissipation due to bottom friction.

Transport Rate Equations

The distribution of the transport rate was calculated using relationships developed for the four different zones of the profile described in Part V. In the surf zone, i.e., the region of breaking and broken waves, the distribution of the transport rate is mainly a function of the energy dissipation per unit volume. Seaward and shoreward of the surf zone, semi-empirical relationships derived from the LWT experiments are applied to calculate the transport rate distribution. The magnitude of the transport rate in all transport zones is governed by that calculated for the part of the surf zone where broken waves prevail (Figure 42, Zone III).

The direction of the net cross-shore transport is determined in the model by the criterion described in Part IV, which is based on the deepwater wave steepness and the dimensionless fall velocity (Equation 2). Although the criterion was developed to predict formation of bar and berm profiles, examination of associated cross-shore transport rate distributions showed that this relation was applicable to predict the direction of net transport as well. Onshore transport is predominant if a berm profile is formed, whereas offshore transport is predominant if a bar profile is formed. According to the criterion, material is transported offshore or onshore along the full length of the active profile at a specific instant in time. This is a good approximation if the profile is not too close to the equilibrium shape, in which case the transport rate would tend to be mixed, i.e., both onshore and offshore transport might occur along different regions of the profile at the same time.

186

Both Moore (1982) and Kriebel (1982) used transport formulas
for the surf zone in which the rate was proportional to the
excess energy dissipation per unit volume over an equilibrium
energy dissipation which the beach profile could withstand
without changing shape significantly. Dean (1977a) showed that
an equilibrium profile derived from the concept of a constant
energy dissipation per unit volume from the break point and
onshore corresponded to a shape governed by a power law with an
exponent of 2/3 (Equation 1). The relationship between excess
energy dissipation per unit volume and transport rate in zones of
broken waves was verified in Part V using wave and profile change
data from the CRIEPI experiments.

In the profile change model, a transport relationship
similar to that used by Moore (1982) and Kriebel (1982) is
applied in a region of fully broken waves (Zone III) with a term
added to account for the effect of local slope. A steeper slope
is expected to increase the transport rate down the slope. The
modified transport relationship is written

$$
q = \begin{cases} K\ (D\ -\ D_{eq}\ +\ \dfrac{\epsilon}{K}\ \dfrac{dh}{dx}) & D > D_{eq}\ -\ \dfrac{\epsilon}{K}\ \dfrac{dh}{dx} \\[2ex] 0 & D < D_{eq}\ -\ \dfrac{\epsilon}{K}\ \dfrac{dh}{dx} \end{cases}
\tag{33}
$$

where

    q = net cross-shore transport rate

    K = transport rate coefficient

    D = wave energy dissipation per unit volume

    D_{eq} = equilibrium energy dissipation per unit volume

    ϵ = transport rate coefficient for the slope-dependent term

The energy dissipation per unit volume is given from the change
in wave energy flux (Equati 1 27) as

$$D = \frac{1}{h} \frac{dF}{dx} \qquad (34)$$

Equation 33 indicates that no transport will occur if D becomes less than D_{eq}, corrected with a slope-dependent term, which may happen during variation in the water level. For example, if a well-developed bar forms, waves will break seaward of the bar crest, but a water level increase would make the depth inshore sufficiently large to decrease D below D_{eq} without wave reformation occurring. In this case, the transport rate should be set to zero.

As previously mentioned, the transport direction is deter-mined by an empirical criterion (Equation 2) and the magnitude by Equation 33. If D were allowed to become less than D_{eq}, Equation 33 would predict a reversal in sand transport, which might be in conflict with the imposed criterion specifying transport direction. Furthermore, in such a case, the magnitude of the sand transport would increase as D decreased to reach a maximum if no energy dissipation occurred. This is an incorrect description of what occurs since a cutoff energy dissipation exists under which no sand transport takes place (compare, for example, Kraus and Dean 1987). Consequently, the logical decision is to set q to zero if D falls below D_{eq}. Also, from Figure 48 it is seen that the transport rate is small in the vicinity of D_{eq} as compared to the values at break point.

Physically, the equilibrium energy dissipation represents a state in which the time-averaged net transport across any section of the beach profile is zero. The equilibrium energy dissipation may be expressed in terms of the beach profile shape parameter A in the equilibrium profile equation (Equation 1) according to

188

$$D_{eq} = \frac{5}{24} \rho g^{3/2} \gamma^2 A^{3/2} \tag{35}$$

where γ is the ratio between wave height and water depth at breaking (breaker index, H_b/h_b). In the derivation of Equation 35, Dean (1977a) assumed that the wave height was in a fixed ratio with the water depth in the surf zone.

From Equation 35 it may be deduced that D, itself, inherently contains a term proportional to the beach slope. The reason for incorporating the explicit slope-dependent term in the transport relationship (Equation 33) is that regression analysis showed a dependence on slope of the transport rate for some of the cases analyzed in Part V. Also, numerical stability of the model was improved by inclusion of this term, as will be discussed below. Dean (1984) also modified the equilibrium energy dissipation by reducing it depending on the ratio between the local beach slope and the limiting slope for the sand surface, thus including a further slope-dependence (cf. Watanabe 1985).

As discussed in Part V, the transport rate coefficient K determined by comparison of calculated energy dissipation per unit volume from measured wave heights and inferred or "measured" transport rates from the LWT data was about $1.1 \ 10^{-6} \ m^4/N$. In contrast, Moore (1982) and Kriebel (1982) obtained a value of $2.2 \ 10^{-6} \ m^4/N$ by making comparisons between calculated and measured profile change. This value was revised by Kriebel (1986) to become $8.7 \ 10^{-6} \ m^4/N$. The coefficient K is not entirely comparable between the models since their structures are different. The value of ϵ was found to be on the order of 0.0006 m^2/sec (in Part V).

The equilibrium energy dissipation was determined by Moore (1982) by fitting Equation 1 to 40 field and laboratory profiles. Beach material ranged from boulder (30 cm) to fine sand, and D_{eq}

was related to the mean sand diameter. Moore's (1982) analysis provided the best fit to profiles both with and without bars. These values were used in the numerical model and found to give reasonably accurate estimates of D_{eq} in regions of broken waves. However, in order to obtain optimal agreement between model simulations and measured profile change, values of D_{eq} as specified by Moore had to be reduced by 25% as discussed later.

By adding the slope term in Equation 33, the shape of the equilibrium profile will be somewhat gentler since a profile with a specific grain size will be able to withstand a lower energy dissipation per unit volume. The shape of the equilibrium profile, derived from Equation 33 in analogy to Dean (1977a), may be written

$$h \ (\sqrt{h} + \frac{\epsilon}{K} \frac{24}{5\rho g^{3/2} \gamma^2}) = A^{3/2} \ x \tag{36}$$

In Equation 36 the water depth is an implicit function of the cross-shore distance. The effect of incorporating beach slope is only noticeable close to the shoreline for the values of ϵ used in the model. Further seaward the profile agrees with Dean's (1977a) equilibrium profile.

In the numerical model, regions of fully broken waves are identified at each time step and the transport rates are determined from Equation 33. The waves are considered to be fully broken in the model from the plunge point to the end of the surf zone or to the point where wave reformation occurs. The location of the plunge point is determined from the location of the break point and the breaking wave height. Galvin (1969) estimated the plunge distance to be about four times the breaking wave height, showing a dependence upon beach slope ($\tan\beta$), where a steeper beach implied a shorter plunge length for the same breaking wave height. The equation given by Galvin (1969) is

190

$$\frac{1_p}{H_b} = 4.0 - 9.25 \tan\beta \tag{37}$$

In the numerical model an overall value of three times the breaking wave height is used to estimate the plunge distance (compare Singamsetti and Wind 1980, Svendsen 1987). Equation 37 was tested for predicting the plunge length, but gave unrealistically short distances for steep bar face slopes.

For the region seaward of the break point the transport rate distribution is well approximated by an exponential decay with distance (Equation 21). For offshore transport the spatial decay coefficient is a function of the breaking wave height and grain size (Equation 22), whereas for onshore transport the decay coefficient is effectively constant.

For the narrow region extending from the plunge point to the break point, an exponentially decaying transport rate is also used but with a smaller value of the spatial decay coefficient. Analysis of a limited number of cases available from the LWT experiments indicated the value of the spatial decay coefficient to be approximately 0.20-0.25 that of the spatial decay coefficient applicable seaward of the break point. A value of 0.20 is used in the numerical model to compute the spatial decay coefficient in the zone between the plunge point and the break point. Consequently, the magnitude of the transport rate at the plunge point is determined from Equation 33 and seaward from this point the transport rate is calculated from the exponential decay functions.

The transport rate distribution on the foreshore is approximated by linear decay with distance from the end of the surf zone (Part V). The slope of the transport rate distribution on the foreshore decreases with time as the profile approaches

191

equilibrium shape in the surf zone. Profiles generated in the LWT that underwent either erosion or accretion showed this linear behavior, implying a foreshore which receded or accreted uniformly along its full length. In the model, the transport rate is linearly extended from the end of the surf zone to the runup limit. (The surf zone is arbitrarily ended at a depth of 0.3-0.5 m.) However, as the foreshore erodes, the slope steepens and a pronounced scarp or step develops. Eventually, if erosive waves act long enough, the slope of the step will exceed the angle of initial yield as defined by Allen (1970). In Part IV the time evolution of profile slopes was analyzed and qualitative indications of avalanching were found to occur if profile slopes exceeded a limiting value of 28 deg on the average. This value is used in the numerical model to limit the growth of slopes along the profile.

Since the transport relationships fail to explicitly describe avalanching, a routine was incorporated in the model to simulate avalanching if the profile slope steepened excessively. If the angle of initial yield is exceeded, the profile slope decreases to a lower, stable value known as the residual angle after shearing (Allen 1970). From the LWT data a stable slope seemed to be reached at a value somewhat lower than 22 deg on the average. In the numerical model the residual angle after shearing was set to a value of 18 deg. The reason for this ambiguity was the difficulty of determining the residual angle after shearing from the profile data; instead, Allen's (1970) experimental results were used where the dilatation angle (difference between angle of initial yield and residual angle after shearing) was found to be in the range of 10-15 deg for sand. A dilatation angle of 10 deg was chosen, implying a residual angle after shearing of 18 deg.

If avalanching occurs in the numerical model, that is, the angle of initial yield is exceeded, sand is redistributed into neighboring cells so that the slope adjusts to the residual angle

192

after shearing. Once avalanching has started in one cell it
proceeds along the grid until a point is reached where the slope
is less than the residual angle after shearing. A definition
sketch is shown in Figure 55 illustrating a number of calculation
cells and one cell where the angle of initial yield is exceeded
(cell 1). Depths after avalanching, denoted with a prime in
Figure 55, can be determined once the change in depth in the cell
where avalanching is initiated is known. The change in depth in
the first cell is given by

$$\Delta h_1 = -(\frac{N-1}{N}) h_1 + \frac{1}{N} \sum_{i=2}^{N} h_i + \frac{1}{2} (N-1) \Delta h \qquad (38)$$

where

h_1 = depth in the first cell where angle of initial yield is
exceeded

N = number of cells where sand is to be redistributed

h_i = depth in cell i

Δh = difference in depth between two neighboring cells as
given by the residual angle after shearing.

After the depth change in the first cell has been determined
according to Equation 38, depth changes Δh_i in neighboring
cells are given by the following expression

$$\Delta h_i = h_1 + \Delta h_1 - h_i - (i-1) \Delta h \qquad (39)$$

where the index i refers to the cell number counting consecu-
tively from the starting point of the avalanching in the direc-
tion of avalanching. The number of cells N that the avalanch-
ing will effect is not known a priori and has to be determinated
iteratively as more cells are incorporated in the calculation

193

until the slope between cells N and N+1 is less than the
residual angle after shearing. The avalanching routine will
limit the growth of the step slope and also prevent the shoreward
slope of a bar from becoming too steep.
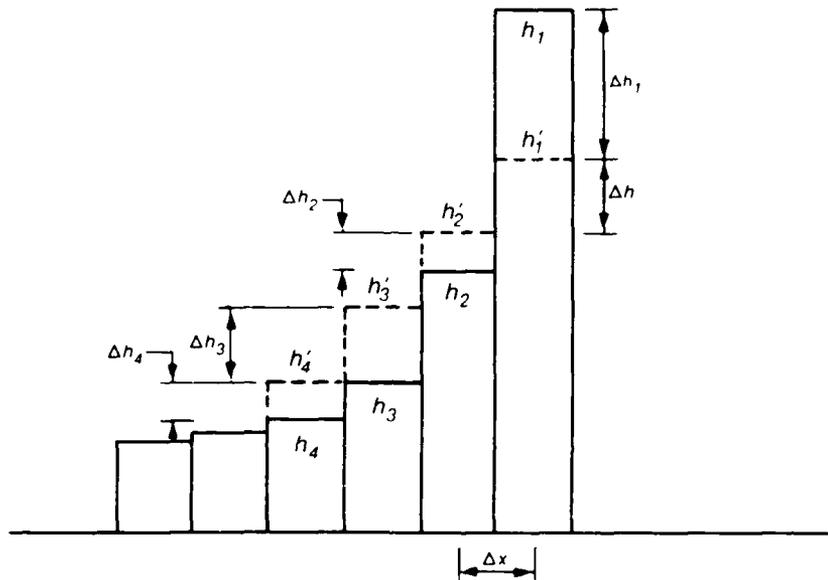
Figure 55. Definition sketch for describing avalanching
along the profile

Profile Change Model

Changes in the beach profile are calculated at each time
step from the distribution of the cross-shore transport rate and
the equation of mass conservation of sand. The equation of mass
conservation is written as

$$\frac{\partial q}{\partial x} = \frac{\partial h}{\partial t} \tag{40}$$

Standard boundary conditions in the model are no sand transport shoreward of the runup limit and seaward of the depth where significant sand movement occurs. The runup height is determined from an empirical expression, Equation 17, derived from the LWT experiment data relating the height of the active profile to the surf similarity parameter and the deepwater wave height. The depth of significant sand movement is determined through the exponential decay of the transport rate with distance seaward from the break point. If the transport rate decreases to a small predetermined value, the calculation stops, and the transport rate is set to zero at the next cell, making that cell the seaward boundary. An expression presented by Hallermeier (1984) for the seaward limit depth was investigated for use in the model. However, this equation failed to predict what were considered to be reasonable closure depths on a wave by wave basis, evidently because the formula was developed for extreme annual events. Also, apparently because of the limited range of values from which the equation was derived, the closure depth was found to be too shallow for profiles exposed to the very steep waves that were used in some of the LWT cases.

In calculation of the wave height distribution across-shore at a specific time step, the beach profile from the previous time step is used and the transport rates are calculated explicitly. The mass conservation is written in difference form as

$$\frac{h_i^{k+1} - h_i^k}{\Delta t} = \frac{1}{2} \left[\frac{q_{i+1}^{k+1} - q_i^{k+1}}{\Delta x} + \frac{q_{i+1}^k - q_i^k}{\Delta x} \right] \tag{41}$$

195

where k denotes the time level and i the cell number over which the discretization is carried out.

The equation of mass conservation is discretized over two time levels using transport rates evaluated at the present and previous time step. In order to obtain a realistic description of the wave height distribution across highly irregular profiles exhibiting bar formations, a moving average scheme is used to obtain representative depth values. Averaging of the profile depth is carried out over a distance of three breaking wave heights as determined from Equation 25 and was found to make the model numerically more stable. If the wave calculations are not based on a beach profile which has been filtered to some degree, the wave height will respond in an unrealistic manner to small changes in the profile. The beach profile generated with the moving average scheme is used only for calculation of the wave height distribution, and no actual changes in the profile itself are made.

Since the transport rate distribution is determined using different transport relationships in different regions of the profile, the derivative of the transport rate may be discontinuous at inter-region boundaries. In order to obtain a smoother transport rate, a three-point weighted filter is applied to the calculated transport rates. The wave height distribution is calculated explicitly in a manner similar to Dally (1980), proceeding from the most seaward cell and onshore until the end of the surf zone is detected. The advantage of using an explicit solution scheme in determination of the wave height distribution is that it easily allows description of initiation of breaking, switching to the breaker decay model, and reformation of broken waves. Use of an implicit solution scheme would considerably complicate the calculation and require an iterative procedure since the location of the break point and any point where wave reformation occurs are not known a priori.

196

By incorporating the slope term in Equation 33, the model became numerically more stable. Neglecting this term would in some cases initiate numerical oscillation in the solution at the shoreward bar face as the slope grew steep and the trough became more pronounced. The slope-term would tend to flatten the trough since the transport rate at the shoreward bar face would be reduced.

The numerical scheme proved to be very stable under a wide range of conditions in spite of the irregular bathymetry that occurs if bars are formed. Typical length and time steps used in the model are $\Delta x = 0.5\text{-}5.0$ m and $\Delta t = 5\text{-}20$ min. The length step has to be chosen so as to resolve the main morphologic features with a sufficient accuracy. A shorter length step requires a correspondingly shorter time step to maintain numerical stability. An effort was made to derive an explicit stability criterion, but was not successful. Therefore, at the present time trial and error must be used to determine appropriate values of Δx and Δt for the particular application.

For a beach profile exposed to constant wave and water level conditions, the profile shape predicted by the model approaches a steady-state to produce an equilibrium profile. The approach to equilibrium is controlled by the rate at which energy dissipation in the surf zone attains the equilibrium value D_{eq}. A bar, if formed, causes the break point to translate in the seaward direction as it grows, making the offshore boundary of the surf zone move accordingly. At equilibrium, the break point is stationary and the energy dissipation per unit volume is constant throughout the surf zone, being approximately equal to D_{eq}, corrected by the slope-dependent term in Equation 33.

197

Calibration and Verification of the Numerical Model

The numerical model was applied to simulate beach profile
evolution for a number of erosional cases from the LWT experi-
ments. As an objective criterion for judging agreement between
the simulated and measured beach profile, the sum of squares of
the difference of measured and calculated depths was formed
according to

$$R = \sum_i (h_{m,i} - h_{c,i})^2 \qquad\qquad (42)$$

where the subscripts m and c refer to measured and calculated
profile depths, respectively. The values of different model
parameters were varied in order to minimize the sum of the
squares. In the calibration process, equal weight was placed on
all measurement points along the profile without any bias towards
bar formations or eroded areas on the foreshore. Furthermore,
the model was restricted to generating one breakpoint bar to
limit the effort on reproducing the main breakpoint bar in the
calibration. However, the volume of the main breakpoint bar was
always at least one order of magnitude larger than any secondary
inshore bar, thus being significantly more important for deter-
mining the wave height distribution across-shore.

In simulation of beach and dune erosion, it is considered
most important to predict the evolution of the main breakpoint
bar, since this feature serves as a natural defensive response
for reducing incident wave energy that would otherwise arrive at
the beach face. Only a small amount of information was available
from the LWT data set to quantify the net cross-shore transport
rate in zones of wave reformation. Simulations to reproduce the
inshore bar are presented further below, however, for which it

198

was necessary to make assumptions on the net transport rate between zones of fully broken waves.

It is desirable to relate empirical parameters in the model directly to physical quantities or assign them a constant value to minimize the degrees of freedom in the calibration process. For instance, values recommended by Dally (1980) were used in the breaker decay model, i.e., a stable wave height coefficient of Γ = 0.40 and a wave decay coefficient of κ = 0.17. (The optimum value of the wave decay coefficient was modified slightly by Dally, Dean and Dalrymple (1985a) to 0.15.) Although the parameters in the breaker decay model showed a qualitative dependence on average beach slope in breaking wave data from the CRIEPI experiments, the above-mentioned constant values were used in the calibration. The number of parameters available for adjustment in the calibration process was thereby reduced with little loss of accuracy in determining an optimal calibration, since the minimum of the sum of squares in most cases was located in a rather flat region.

Based on preliminary calibration runs, the coefficient expressing the slope dependence of the transport rate (ϵ in Equation 33) was set to 0.001 m^2/sec. A smaller value of ϵ will allow the trough to be locally somewhat more pronounced, whereas a higher value will flatten the trough. The angle of initial yield was set to 28 deg according to slope behavior inferred from the LWT experiments, and the residual angle after shearing was set to 18 deg. A larger angle of initial yield will allow the profile slope to become steeper before avalanching occurs. During simulation of an erosional event with the LWT data, avalanching typically takes place on the foreshore step or on the shoreward side of the bar.

At the initial stage of model calibration, both K and D_{eq} in the transport equation (Equation 33) were used in the calibration procedure. The transport rate coefficient K was varied together with D_{eq} for ten erosional cases. Although it was

199

considered desirable to avoid using D_{eq} as a calibration parameter and instead determine its value from the design curve given by Moore (1982), it was found that in order to achieve best agreement between numerical model simulations and tank measurements, the value of D_{eq} had to be reduced. The equilibrium energy dissipation controls the amount of sand that is eroded before the equilibrium profile is attained. Moore's relationship was derived by a least-squares fit of a power-curve (Equation 1) to beach profiles in general, making this method not entirely compatible with the concept of regions with different transport rate relationships used in the present numerical model. In most cases, the parameter combination which gave the minimum sum of squares was located in the vicinity of an equilibrium energy dissipation value of about 75 % of that obtained by Moore's relationship. This fixed reduction (0.75) of the equilibrium energy dissipation was applied in all cases, and the optimal value of the transport rate coefficient K was determined by minimizing the sum of the squares of depths.

The transport rate coefficient for the 10 cases simulated giving the best agreement between measured and simulated profiles varied from 0.3 - 2.2 10^{-6} m^4/N, with an average of 1.4 10^{-6} m^4/N for 10 separate optimizations. Most of the cases, however, had a K-value ranging from 1.1 - 1.9 10^{-6} m^4/N. The sum of squares was minimized with respect to all profiles measured during the particular case, typically encompassing 5-10 profile surveys per case. Figure 56 shows a representative calibration run with the numerical model and a comparison with the measured beach profile from the last profile survey of the simulated case (Case 6-1). Beach profiles at selected time steps from the model calculations are shown together with the wave height distribution across-shore calculated at the last time step. The optimal K-value for this case was 1.9 10^{-6} m^4/N. As seen in Figure 56, bar formation (size and location) and the amount of erosion on the foreshore were well described by the numerical model. The small inshore

200

bar was purposefully neglected in the calibration simulation.
This feature appeared in the LWT experiment after 40 hr of run
time, just prior to the last profile survey. Measured wave
heights are shown across the profile indicating that the wave
height distribution was satisfactorily reproduced by the breaker
decay model.
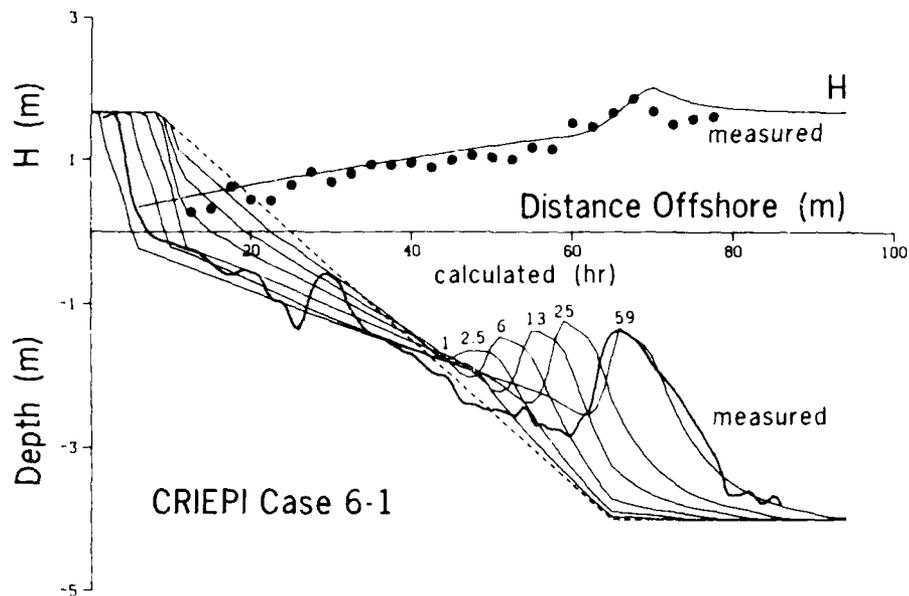
Figure 56. Calibration of numerical model against Case 6-1

Transport rate distributions calculated at selected times
are shown in Figure 57. The magnitude of the transport rate
decreased with time as the profile approached equilibrium shape
in accordance with the behavior of transport rate distributions
directly inferred from the profile survey in Part V. Occasional-
ly, the transport rate increased in the vicinity of the break
point compared with previous distributions, caused by movement of
the break point. As the break point moved offshore, energy
dissipation increased because of the decrease in depth occurring

201

at the plunge point, and the transport rate increased according-
ly.
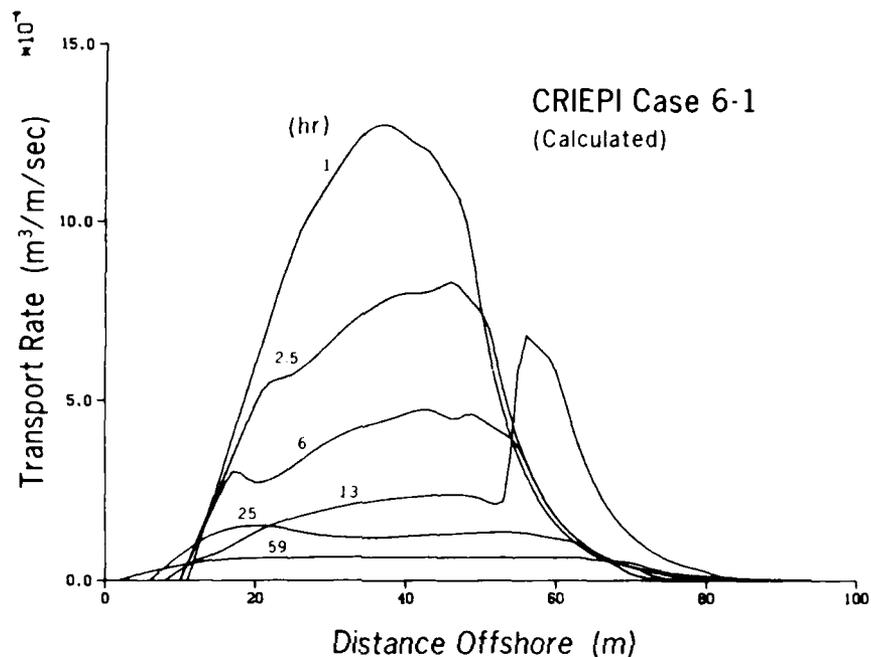
Figure 57.   Net cross-shore transport rates at selected
             times for Case 6-1

It was not possible to relate K obtained from individual
calibrations to wave or sand characteristics with any sig-
nificance for the number of cases available for study. Qualita-
tively, the transport rate coefficient seemed to decrease with
increasing grain size and increase with decreasing wave period.
A wave-period dependence of the profile time response was also
shown in the analysis in Part V of peak net cross-shore transport
rates calculated from LWT data.

Since it was not possible to relate the transport rate
coefficient to any physical properties, it was desirable to
achieve an optimal estimate of K for use in simulating all
cases. To obtain best overall agreement between simulated and
measured profiles with constant K, the model was calibrated for

202

seven of the cases with respect to the total sum of squares.
After the optimal value had been determined for K, the model was
verified through use of two independent cases. One case (Case
700 with $K = 0.3 \ 10^{-6} \ m^4/N$) was neglected in the overall calibra-
tion process since water was released from the tank during the
run (probably to reduce wave overtopping), and the water level
was lowered 0.3 m, thus contaminating the case for the purpose
here (see Kraus and Larson 1988). The sum of squares of the
difference in depth between measured and simulated beach profiles
was calculated for all profile surveys for all seven cases.
Figure 58 illustrates the total sum of squares for all cases as a
function of the transport rate coefficient. A minimum occurred
around the coefficient value $1.6 \ 10^{-6} \ m^4/N$.

Two cases, one from the CE data set (Case 400) and one from
the CRIEPI data set (Case 6-2), were used to verify the ap-
plicability of the numerical model with parameter values obtained
from the calibration. Figures 59a and 59b show the results of
the verification runs illustrating the development in time of the
beach profile together with a comparison with the measured
profile at the last time step. The wave height distribution
across-shore is also given at the last time step. The volume of
the main breakpoint bar and the amount of erosion on the fore-
shore are rather well predicted by the numerical model. However,
the crest of the bars is located somewhat too seaward, whereas
the trough is not deep enough for Case 400. In general, the
trough is not well reproduced in the numerical model, being less
pronounced than for the measurements, since the slope term in the
transport equation, Equation 33, counter-acts the seaward
transport of sand on the shoreward side of the bar. Elimination
of the slope term, however, seriously affects numerical stabil-
ity, resulting in a much shorter allowable time step in relation
to the length step.
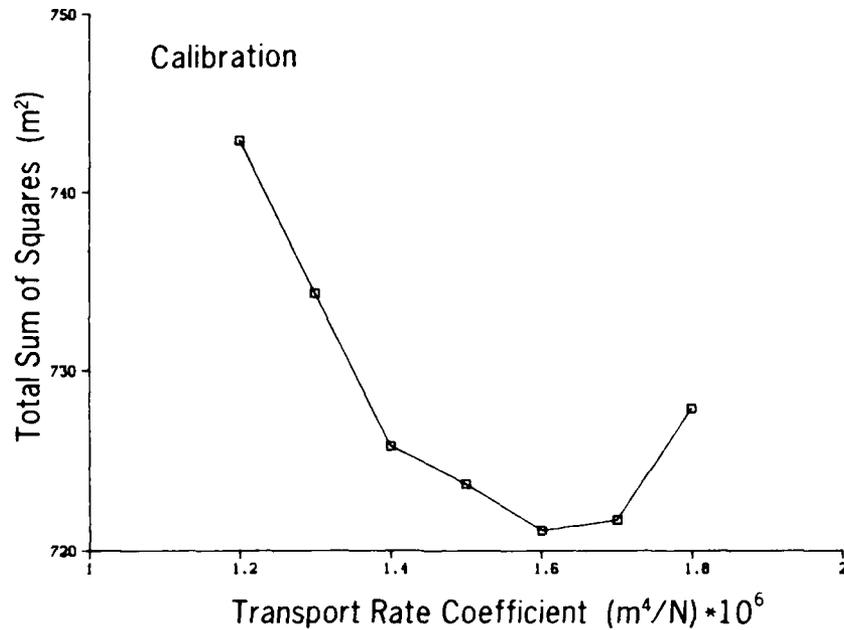
Figure 58. Total sum of squares of the difference between
measured profile and simulated profile with the
numerical model for all profile surveys and all
cases in the calibration

Summary and Discussion of Numerical Model

The numerical model was calibrated and verified to simulate
erosional (bar-type) profiles with relatively little ambiguity in
determining values of the required empirical coefficients. In
particular, both the time rate of growth, volume, and location of
the main breakpoint bar were well reproduced. The location of
the shoreline and the steep slope of the foreshore step were also
well simulated. Inclusion of avalanching was needed to restrict
bottom slopes to within measured angles, and an explicit slope-

204
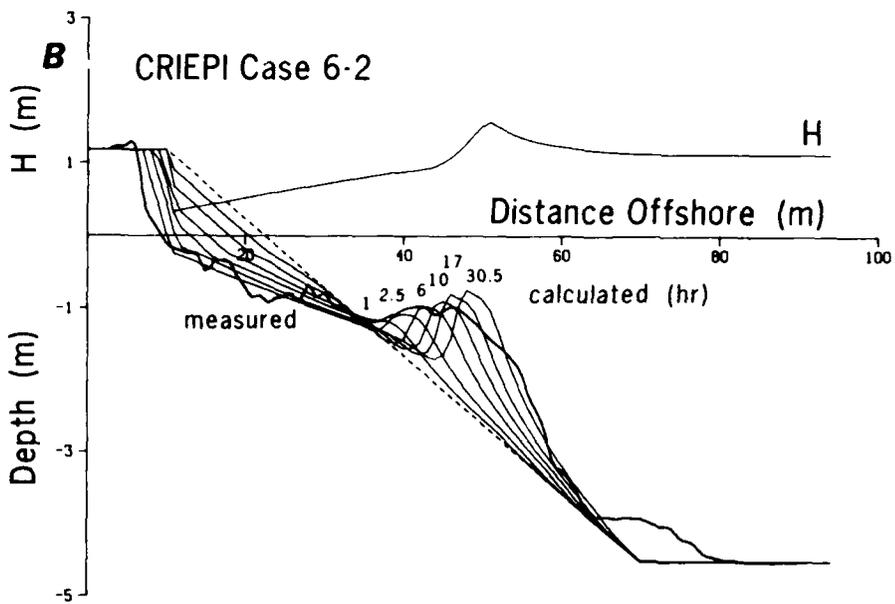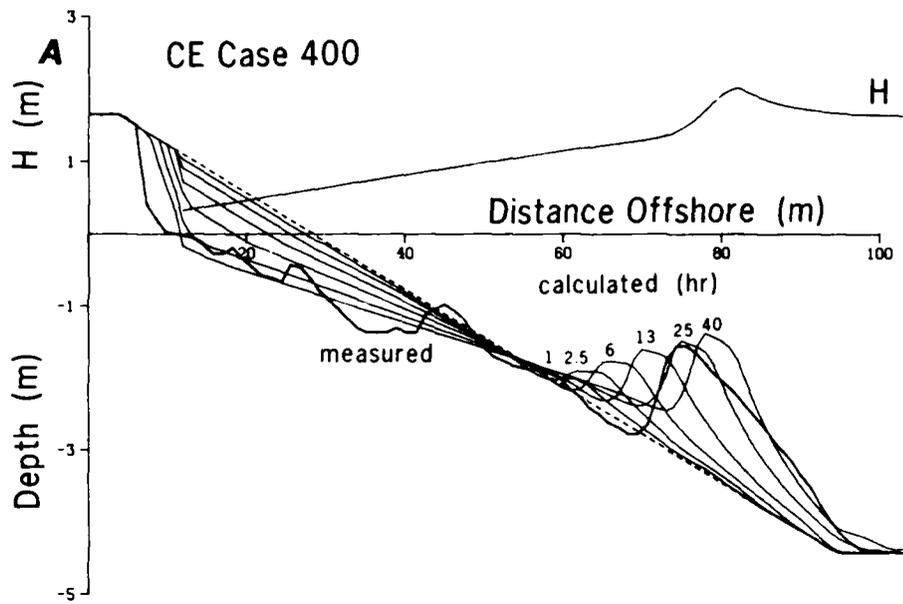
Figure 59. Verification of numerical model against: (a)
            Case 400, and (b) Case 6-2

dependent contribution to the transport rate was found to greatly improve stability of the model.

Most importantly, in all tests run with constant incident wave conditions and water level, the calculated profile approached an equilibrium form. This property is highly desirable to represent the proper time scale of profile change and to use the model in an arbitrary situation without the problem of numerical stability.

PART VII: APPLICATIONS OF THE NUMERICAL MODEL

Introduction

In the previous chapter the model was calibrated by means of
LWT measurements under the condition of constant wave and water
level.   In this chapter predictions of the model are examined for
a variety of hypothetical cases such as varying wave and water
level conditions.   Sensitivity analysis is carried out with
respect to a number of the model parameters to evaluate their
influence on simulation results.   Consideration is also given to
simulation of multiple bars.   The model is then put to the severe
test of reproducing beach profile change, in particular, bar
movement in the field.   Furthermore, example applications of the
model are made to investigate the effect of a vertical seawall on
beach profile development, as well as initial adjustment of beach
fill.   A comparison with an existing model, the Kriebel model
(Kriebel 1982), is performed for a number of hypothetical
conditions to evaluate the importance of bar formation on dune
retreat.   Finally, model simulations are carried out to qualita-
tively reproduce onshore sand transport and berm build-up.

Sensitivity Analysis of Model Parameters

In order to quantify the influence of various model parame-
ters or empirical coefficients on the simulation results, a
sensitivity analysis was performed.   Sensitivity analysis gives
valuable information about the physical implications of the model
parameters and their relative effect on the result.   In the
following, the influence of principal model parameters on beach
evolution is discussed with reference to bar properties.   To this
end, the change in shape and size of the bar was investigated for

a specific case (Case 401) under perturbations of optimal values of model parameters as determined by the calibration.

Influence of K

The empirical transport rate coefficient K (Equation 33) mainly governs the time response of the beach profile. A smaller value indicates a longer time elapsed before equilibrium is attained, whereas a larger value produces more rapid beach profile evolution However, K also affects equilibrium bar volume, as seen in Equation 36. Although Equation 36 was derived assuming uniform energy dissipation per unit volume everywhere along the profile and not just in zones of fully broken waves, it gives important qualitative information about the influence of the different coefficients. A smaller K-value implies a flatter equilibrium beach profile with correspondingly more sand to be moved from the inshore for a fixed initial profile slope before equilibrium is attained. Figure 60 illustrates the growth of bar volume with time for different values of the transport rate coefficient. For $K = 2.2 \ 10^{-6} \ m^4/N$, more than 90% of the equilibrium bar volume was achieved after 20 hr, whereas for $K = 0.4 \ 10^{-6} \ m^4/N$ only approximately 30% of the final bar volume was reached. The dependence of equilibrium bar volume on K is introduced through the slope term in the transport equation. Without this term the shape of the equilibrium beach profile would be independent of K and this coefficient would only influence the time response of the profile.

Calculated maximum bar height (defined with respect to the initial plane beach profile) as a function of time is shown in Figure 61 for different K-values. Equilibrium maximum bar height was found to be insensitive to the value of K. However, its time evolution is controlled, as expected, by K, showing a more rapid response for higher values. The location of the mass center of the bar was found to be only slightly influenced by the

208
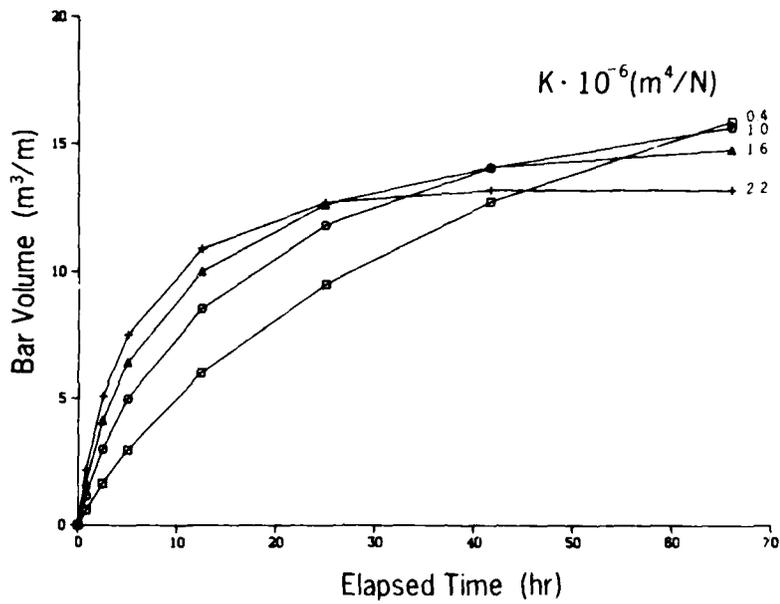
Figure 60. Evolution in time of bar volume for different
values of transport rate coefficient
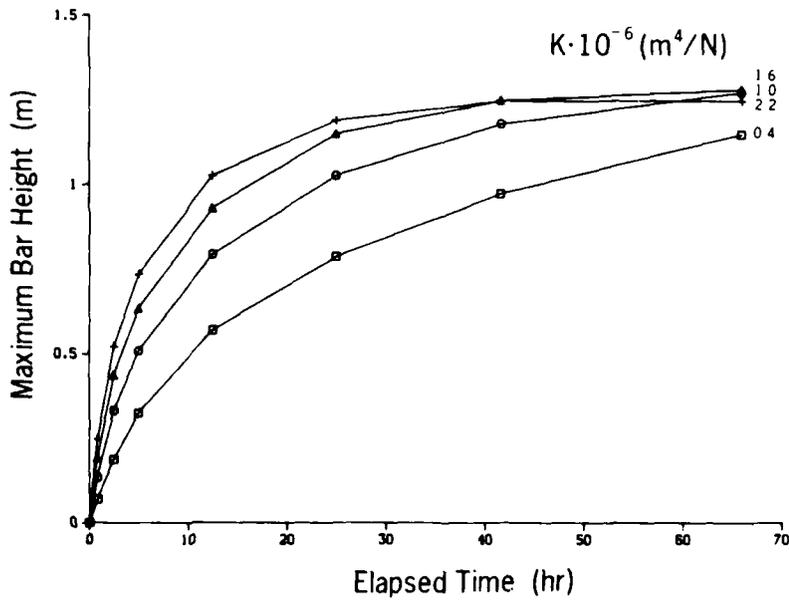
Figure 61. Evolution in time of maximum bar height for
different values of transport rate coefficient

209

value of K, with the mass center somewhat displaced shoreward if
the value of K was decreased.

Influence of ε

The empirical coefficient ε in the slope term in Equation
33 mainly influences equilibrium bar volume and thus the amount
of sand that is redistributed within the profile to reach
equilibrium. Profile response was similar for quite different
values of ε during the initial phase of the simulation and
differed only after longer elapsed times (see Figure 62).
Equation 36 indicates that a smaller ε-value implies a steeper
equilibrium beach profile and less sand to be moved before a
state of equilibrium occurs. The effect of the slope term on the
maximum bar height was weak, where a change in ε by a factor of
four gave a corresponding change in the equilibrium maximum bar
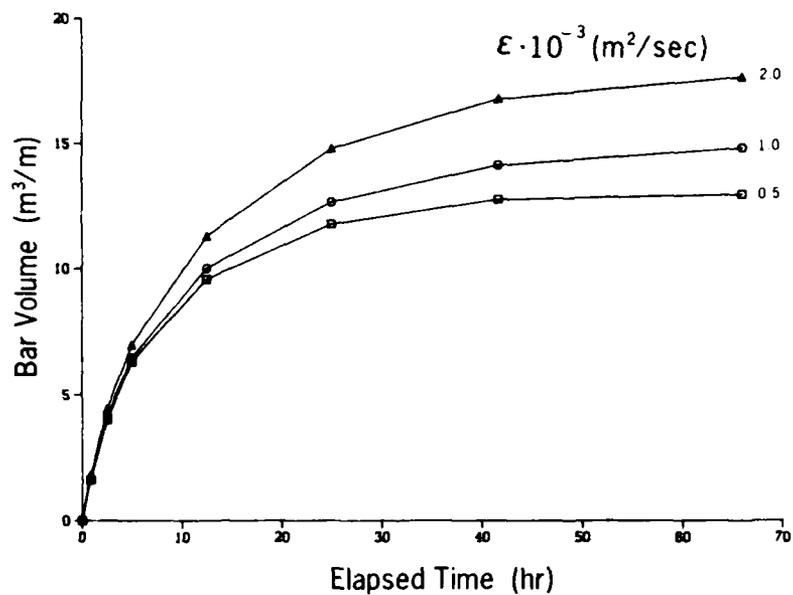
Figure 62. Evolution in time of bar volume for different
            values of slope coefficient in the transport
            equation

height of less than 10%. Similarly the location of the bar mass center was found to have a weak dependence on changes in ϵ.

Influence of wave model parameters

Parameter values in the breaker decay model were chosen in the calibration procedure as suggested by Dally (1980). To quantify the importance of variations in the wave height calculation, the wave decay coefficient κ in Equation 26 was varied. Figure 63 illustrates the growth of bar volume as a function of time for different values on κ. A smaller value of κ implied a larger equilibrium bar volume, although the time responses were similar at the very beginning of a simulation. As a theoretical background it proves valuable to digress and examine the shape of the equilibrium beach profile exposed to a wave height distribution which fulfills the breaker decay model developed by Dally (1980).
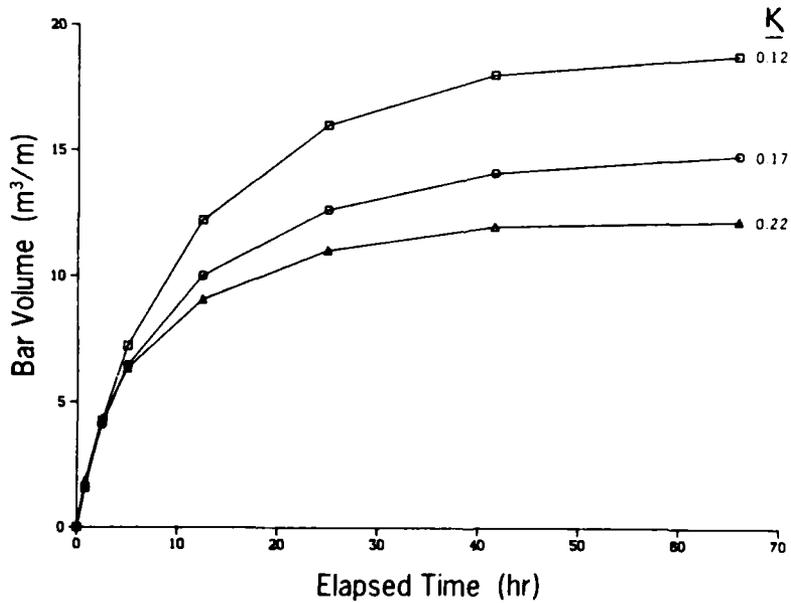
Figure 63. Evolution in time of bar volume for different values of wave decay coefficient

211

Dally, Dean, and Dalrymple (1985a, 1985b) presented analytical solutions for the cross-shore distribution of wave height for simple beach profile shapes. However, these solutions did not fulfill the Dean criterion of an equal energy dissipation per unit volume for equilibrium conditions to prevail on a beach. If the slope-dependent term in the transport equation (Equation 33) is dropped, it is possible to solve the coupled problem of requiring constant energy dissipation per unit volume subject to the Dally breaker decay model. The coupled system of equations consists of Equation 26 and Equation 33, for which the slope-term is neglected and D is equal to D_{eq} according to

$$\frac{1}{h} \frac{dF}{dx} = D_{eq} \tag{43}$$

$$\frac{dF}{dx} = \frac{\kappa}{h} (F - F_s) \tag{44}$$

Note that the x-axis is originating from the shoreline making Equation 44 differ in sign from Equation 26.

The depth of the beach profile in the solution is obtained as an implicit function of the location across-shore according to

$$(\frac{2}{\kappa} + \frac{5}{3} \frac{\Gamma^2 \rho g^{3/2}}{8D_{eq}} \sqrt{h}) \, h = x \tag{45}$$

The corresponding wave height distribution is given by

$$H = \left[\frac{8D_{eq}}{\kappa \rho g^{3/2}} h^{3/2} + \Gamma^2 h^2 \right]^{\frac{1}{2}} \tag{46}$$

212

As seen from Equation 45, a smaller value of the wave decay coefficient (κ) gives a flatter shape of the equilibrium beach profile and thus requires the redistribution of a greater amount of sand before equilibrium is attained. On the other hand, a smaller value of the stable wave height coefficient (Γ) gives a steeper equilibrium beach profile, resulting in a smaller equilibrium bar volume since less material has to be moved from the inshore to attain equilibrium.

Figure 64 shows the effect on bar volume of varying the stable wave height coefficient, supporting the qualitative result as predicted by Equation 45. The influence of changes in parameter values in the breaker decay model on the maximum bar height was less pronounced compared with the effect on the bar volume. The stable wave height coefficient affected the equilibrium maximum bar height only slightly, and the development in time was very similar in the initial phase of a simulation. The wave decay coefficient had a somewhat greater influence on the equilibrium maximum bar height, in which a smaller value implied a larger bar height.

Influence of equilibrium energy dissipation

Equation 45 also reveals the importance of the equilibrium energy dissipation, which was shown to be a function of grain size by Moore (1982). A change in grain size causes a marked change in the shape and size of the bar, which is more pronounced for finer material. A smaller value of D_{eq}, occurring for finer grain sizes, corresponds to a flatter equilibrium beach profile, thus requiring more sand to be moved before equilibrium is attained.

Sensitivity of model predictions on grain size was investigated. Since equilibrium energy dissipation decreases rapidly with grain size (Moore 1982), bar volume correspondingly increases, as illustrated in Figure 65. (Values of D_{eq} used to

213
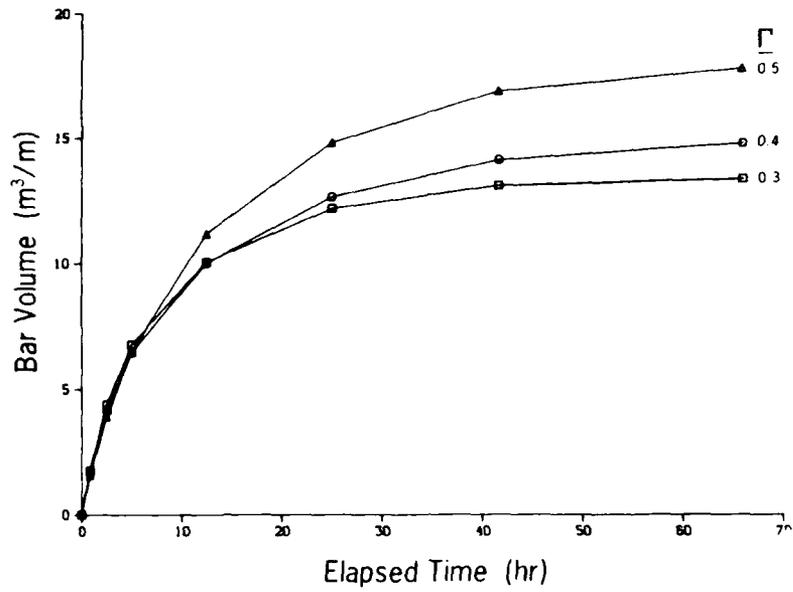
Figure 64. Evolution in time of bar volume for different
values of stable wave height coefficient
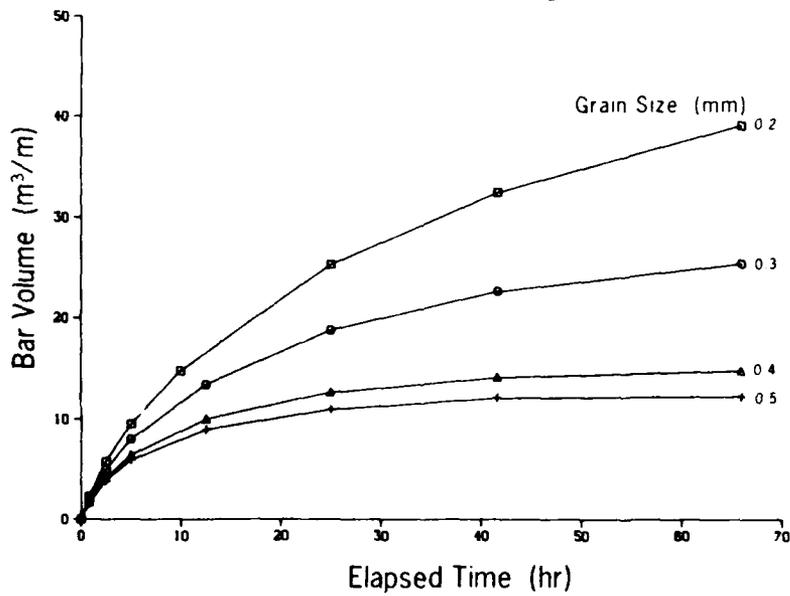
Figure 65. Evolution in time of bar volume for different
values of median grain size

214

obtain the curves in Figure 65 are 0.75 the value of those obtained by Moore (1982), according to the results of the model calibration in Part VI.)

Changing the median grain size from 0.50 mm to 0.40 mm increased the equilibrium bar volume by about 20%, whereas a decrease in median grain size from 0.40 mm to 0.30 mm gave an increase of about 90%. Corresponding changes in values of D_{eq} were 10% and 70%, respectively. Changes in maximum bar height were also significant as the grain size was decreased, although not as large as for bar volume. Equilibrium maximum bar height increased with about half the above-mentioned percentage values as for bar volume for the same changes in grain size. For changes in most parameters in the model, movement of the bar center of mass was only slightly affected. However, change in grain size did have a significant influence on the location of the center of mass, as seen in Figure 66. Initiation of bar formation occurred roughly at the same place independent of grain size, but movement of the bar was considerably greater for the finer grain size.

Grain size also influences the spatial decay coefficient for the transport rate seaward of the break point (see Equation 22) The decay coefficient increases with grain size, implying that the transport rate decreases more rapidly, moving sand less seaward.

Influence of wave period and height

So far in the sensitivity analysis only parameters which are expected to be effectively constant for a specific beach have been investigated. Since the driving force in the numerical model is wave breaking, it is of considerable interest to analyze the response of the beach profile to changes in wave input parameters. Therefore, wave height and period for Case 401 were

215
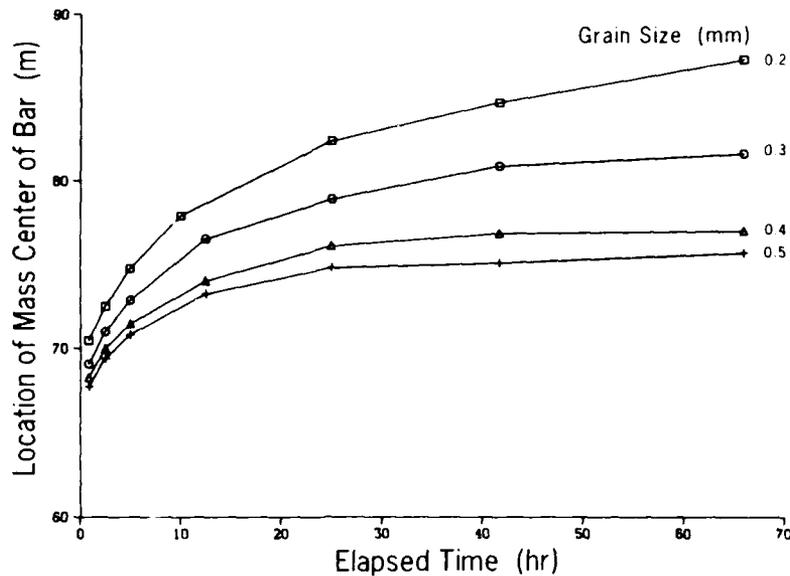
Figure 66. Movement of bar mass center as a function of
time for different values of median grain size

varied in order to investigate the sensitivity of the numerical
model to changes in wave input.

An increase in wave period resulted in an increase in bar
volume, as illustrated in Figure 67, which shows the evolution in
time of bar volume for different wave periods. Since small-
amplitude wave theory for shallow water conditions is applied in
the numerical model, wave period does not enter explicitly in the
shoaling calculation within the grid, but through shoaling from
deep water to the seaward boundary of the grid and through the
breaking wave criterion (Equation 24) (and, of course, in the
criterion determining direction of transport, Equation 2). A
longer wave period will allow a specific wave to shoal further
inshore before it breaks, thus inducing greater energy dissipa-
tion per unit volume and moving more sand before equilibrium is
attained. Maximum bar height was influenced by wave period in

216
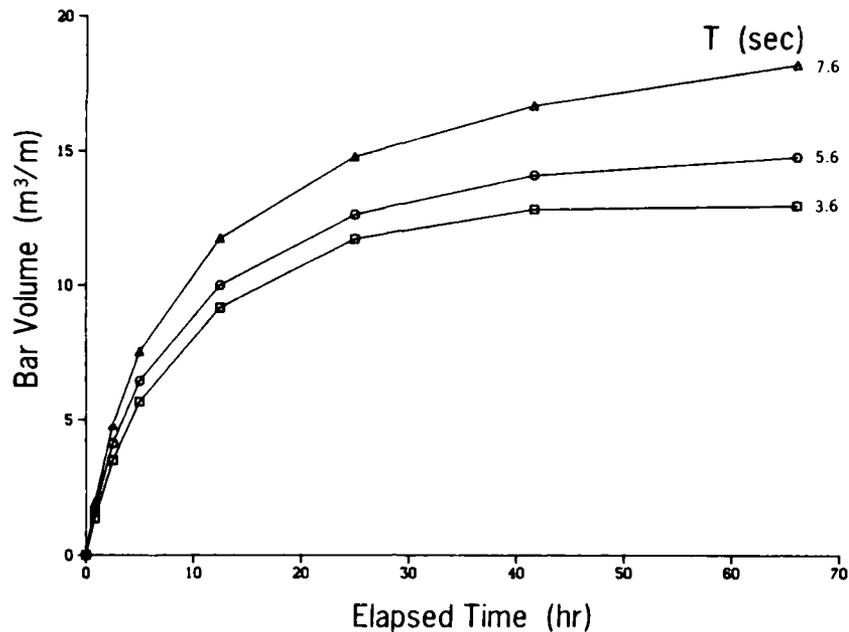
Figure 67. Evolution in time of bar volume for different
values of wave period

the same manner as bar volume, where an increase in period gave a
larger maximum bar height.

The effect of an increase in wave height on bar properties
is readily realized since a larger wave height involves a larger
amount of wave energy for the beach profile to dissipate in a
state of equilibrium. Both equilibrium bar volume and equi-
librium maximum bar height increased significantly if the wave
height increased.

Influence of runup height

The location of the shoreward boundary in the numerical
model is closely related to the runup height and can be predicted
by an empirical relationship (Equation 17). Since Equation 17

217

contains the slope of the beach, a difficult parameter to
quantify in a field application, it is of significance to
estimate the influence of runup height on the simulation result.
Figure 68 illustrates growth of bar volume with time for various
runup heights which were calculated through Equation 17.
Evolution of bar volume was only slightly affected by the
considerable variation in runup height. Consequently, even a
significant error in estimation of the runup height will not
notably degrade the description of the time evolution of the bar.
However, model prediction of the amount of erosion occurring on
the foreshore may be substantially in error.
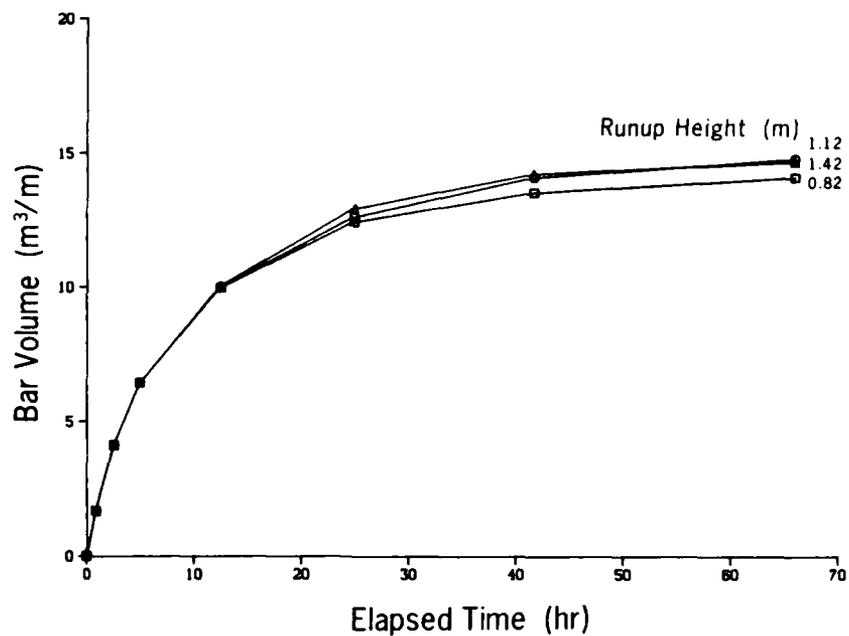
Figure 68.   Evolution in time of bar volume for different
             values of runup height

Effect of Time-Varying Water Level and Waves

In the calibration, verification, and sensitivity analysis all simulations were conducted with a fixed water level and with constant wave conditions during the run (except for Case 700 as pointed out previously). However, in one of the LWT experiments (Case 911), the water level was varied in a sinusoidal manner in order to simulate the influence of a tidal variation on evolution of the beach profile. This case provided the opportunity of evaluating performance of the numerical model in predicting profile change induced by constant incident waves but realistic varying water level. The water level variation had an amplitude of about 0.45 m and a period of approximately 12 hr. Optimal model parameters obtained in the overall calibration of the seven cases were used in the Case 911-simulation.

Figure 69 illustrates the result of the model run and a comparison with the measured beach profile at the end of the tank experiment. Development of the beach profile as predicted by the numerical model was as follows. The water-level increase portion of the tidal cycle at the beginning of the run resulted in an almost stationary emergent bar, as seen from the first few profiles. As the water level dropped, the break point rapidly moved seaward, and the bar correspondingly moved in the seaward direction. When the water level increased at later cycles and a well developed bar existed at the seaward end of the profile, waves passed over the bar and broke inshore creating a small second feature just shoreward of the main breakpoint bar.

As seen from the measured profile, a small berm built up on the foreshore during the latter part of the run which was not described by the numerical model. Otherwise, the numerical model reproduced the main shape of the beach profile, that is a main breakpoint bar with a smaller bar-like feature inshore, separated by a distinct trough-like formation. The location of the calculated bars was somewhat too seaward compared with the

219
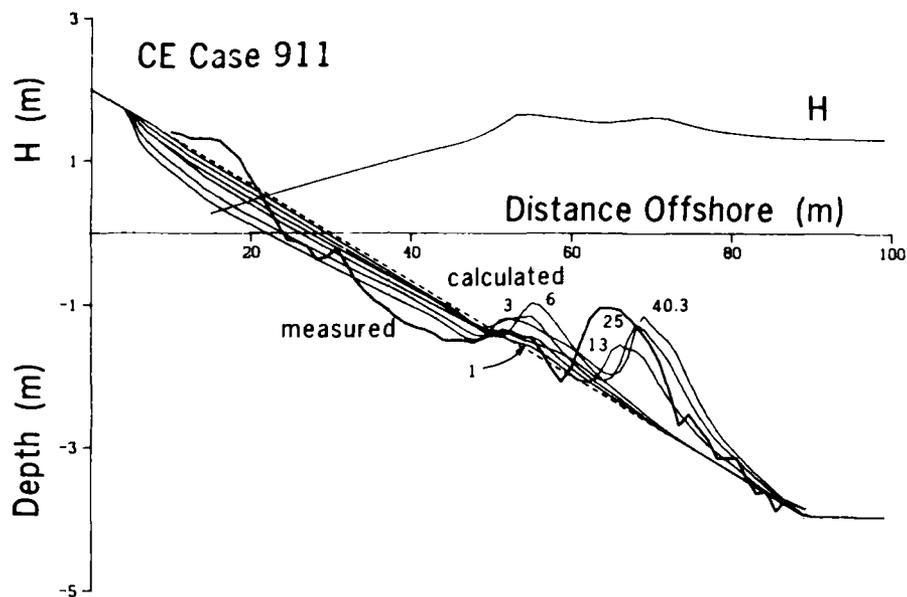
Figure 69. Verification of numerical model against Case 911
having a varying water level with time

measured beach profile, but the bar volume was reasonably well
predicted.

It was possible to obtain better agreement between model
simulation and measurements for Case 911 by changing model
calibration parameters, particularly with regard to the location
of the main bar and smaller feature inshore. However, it was not
possible to simulate berm build-up on the foreshore because the
empirical criterion for the transport direction (Equation 2)
predicts seaward-directed transport during the whole run. Wave
and sand parameters for Case 911 are such that intersection of
values of the non-dimensional quantities involved in the cri-
terion determining transport direction are very close to the line
separating bar and berm profiles. This fact may explain the
somewhat mixed response of the profile.

<u>Water level, wave height, and wave period</u>

In order to qualitatively evaluate model performance for varying water level, wave height, and wave period, a number of hypothetical cases were simulated. In all cases the initial beach profile consisted of a dune with a steep face having a plane slope (1/5) joined to a more gentle plane slope (1/15) at the still-water shoreline and running seaward. The cycle of the variation for wave period, wave height, and/or water level was set at 200 time steps (Δt = 5 min), and the simulation was carried out for 1000 time steps. First, the effect of a varying wave period was investigated, where the deepwater wave height was chosen as 2.0 m, and the water level was fixed. The wave period was varied sinusoidally between 6 and 10 sec with the previously-mentioned time cycle. Figure 70 shows the simulated beach profile at selected time steps and the wave height distribution at the last time step.
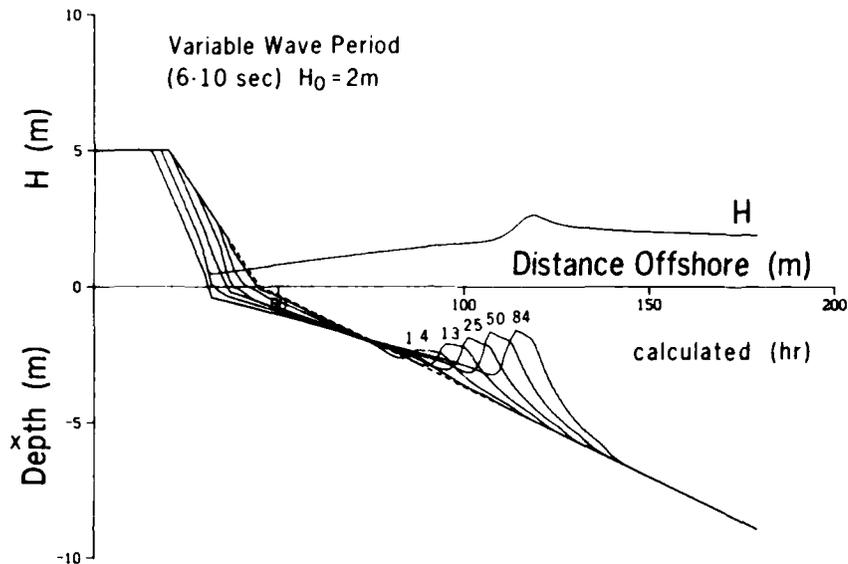
Figure 70. Numerical simulation of hypothetical case with sinusoidally varying wave period between 6 and 10 sec, and constant wave height and water level

The shape of the bar is somewhat more gentle than for a fixed wave period (compare Watts 1954), and changes in the profile decrease with time, approaching a near-equilibrium state, even though the wave period continues to change. The direction of bar movement was seaward during the entire simulation period.

Beach profile change produced by a sinusoidally varying water level showed features similar to the Case 911-simulation. The simulated example had a water-level amplitude of 1 m, a wave height of 2 m, and a wave period of 6 sec. Figure 71 illustrates the calculated beach profile at selected time steps and the wave height distribution across-shore at the last time step. As the water level increased the bar was stationary or even moved somewhat shoreward, whereas during the drop in water level the bar moved rapidly in the seaward direction. Once a noticeable bar had formed, a rise in water level allowed the waves to pass over the main bar and break inshore, causing deposition of sand shoreward of the bar.
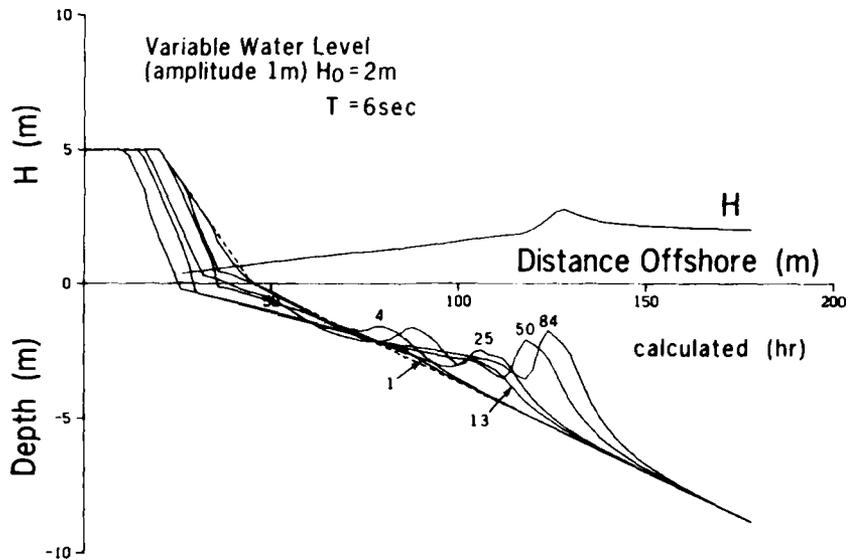
Figure 71. Numerical simulation of hypothetical case with sinusoidally varying water level between -1.0 and 1.0 m, and constant wave height and period

The flat portion of the bar was a result of waves breaking
shoreward of the bar crest because the water level increased so
waves could pass over the crest. The seaward peak of the bar was
created from waves breaking at the bar crest when the water level
was at its minimum.

Somewhat similar profile development occurred when the wave
height was changed sinusoidally with time. As an example, the
deepwater wave height was varied between 1 and 3 m while the wave
period was fixed at 10.0 sec, and the water level was held
constant. In Figure 72, selected profiles are displayed at
consecutive times as predicted by the numerical model, together
with the wave height distribution at the last time step. The bar
had a flat shape initially, but a pronounced peak formed after a
number of wave-height cycles had been completed, after the
largest waves had sufficient duration to produce build-up of a
distinct bar at the seaward end.
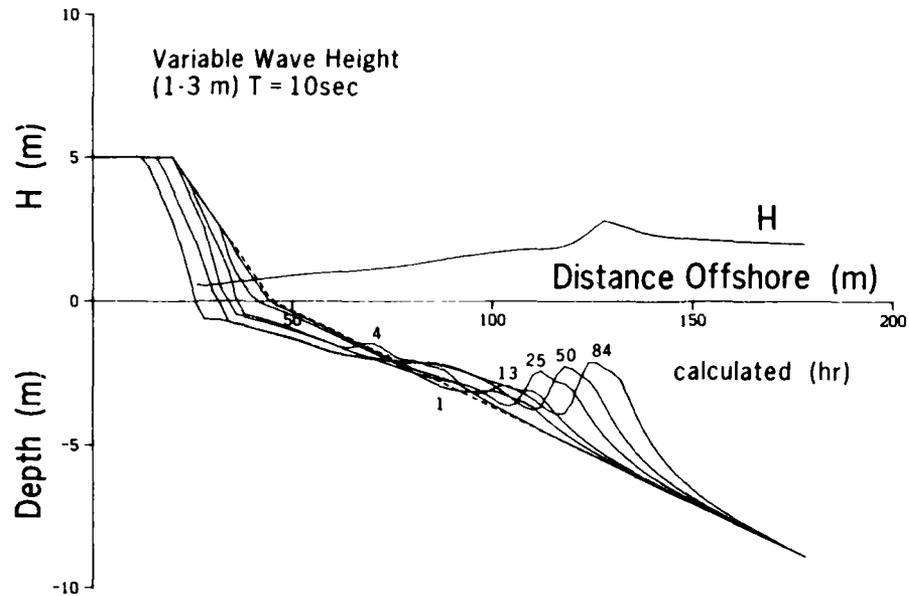
Figure 72. Numerical simulation of hypothetical case with
sinusoidally varying wave height between 1.0 and
3.0 m, and constant wave period and water level

223

The constant supply of sand from the dune as the wave height changed, together with the movement of the break point, prevented the inshore from developing the characteristic monotonic shape. However, if the wave height would be held constant, the beach profile would approach an equilibrium shape with a concave profile inshore.

As an example of the shape of the net cross-shore transport rate, distributions associated with Figure 72 were plotted in Figure 73. The peak of the transport rate distribution moved across-shore as the wave height varied with movement of the break point. At some time steps a small peak appeared at the foreshore (not shown in Figure 73 but in Figure 57), particularly if avalanching took place on the dune slope. In this case sand accumulated in the foreshore cells as the slope adjusted down to the angle after residual shearing.
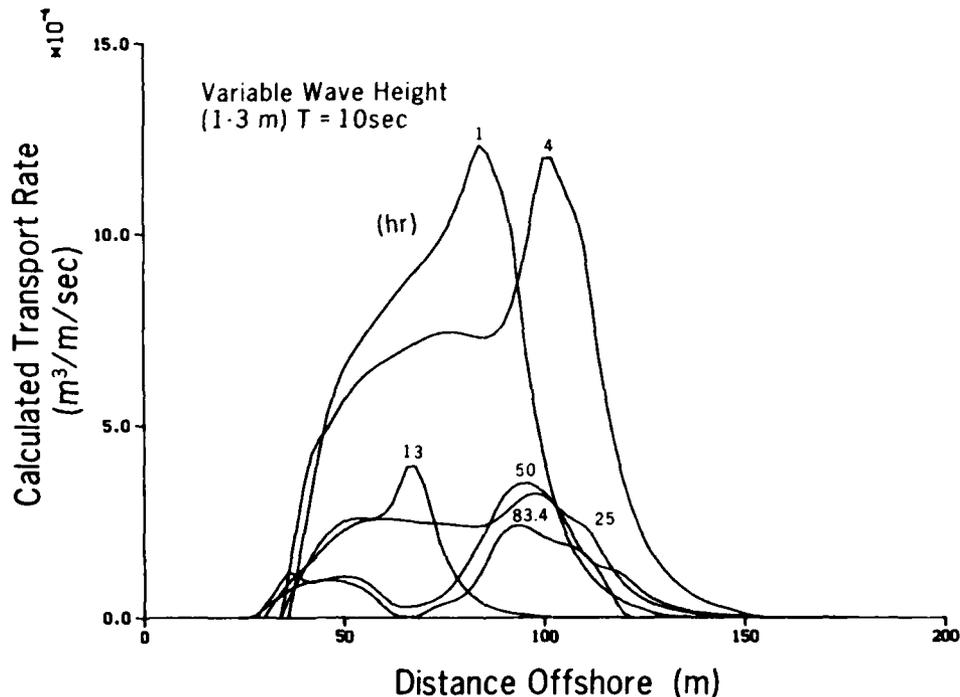
Figure 73. Transport rate distributions at selected times for case with sinusoidally varying wave height

224

The corresponding decrease in depth produced a larger energy dissipation per unit volume in the cells, resulting in a greater transport rate. Figure 73 also shows that the transport rate distribution had a more complex shape at later times, when the depth was not monotonically decreasing.

A hypothetical case was also simulated with the numerical model for simultaneous variation of water level (+/- 1 m) and wave height (2 m +/- 1 m) in a sinusoidal manner. The variation of the two parameters was in phase with a period of 200 time steps ($\Delta t = 5$ min) and the total simulation time was 1000 time steps. The wave period was set to 8 sec. As seen from Figure 74, the shape and width of the bar changed considerably as the wave height and water level varied.
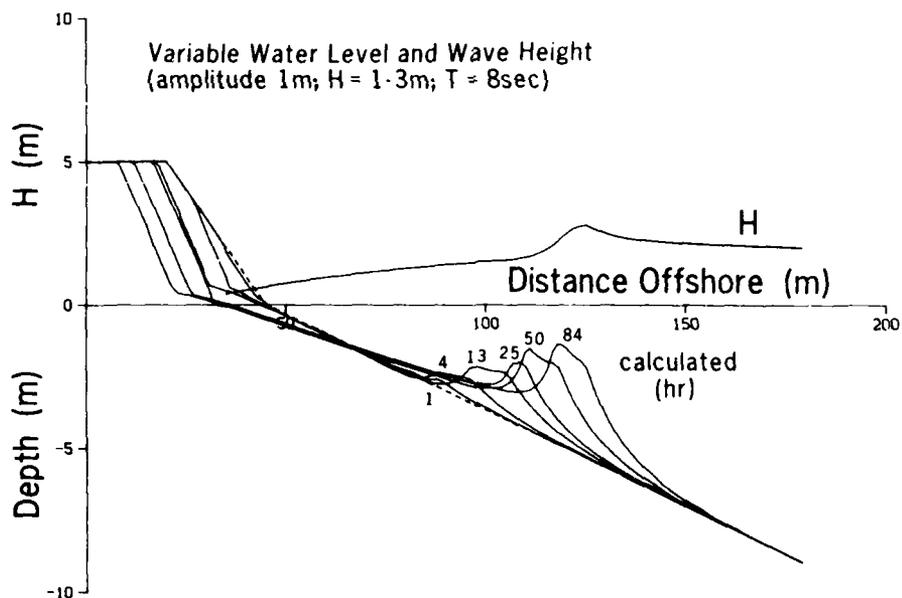
Figure 74. Numerical simulation of hypothetical case with sinusoidally varying wave height between 1.0 and 3.0 m, water level varying between -1.0 and 1.0 m, and constant wave period

225

Also, the dune face retreated more than for the case with just a wave height variation, since the waves could attack higher on the dune because of the water level variation.

Multiple Barred Profiles

If water level varies simultaneously with wave height, it may happen that waves reform as they pass over the trough after breaking on the bar. The reformed waves will break further inshore and create another bar, thus producing a multiple barred profile. The shape and properties of the net transport rate in zones of broken waves, seaward of the break point and on the foreshore, was investigated in Part V, whereas in zones of wave reformation less empirical information was available for analysis and deduction. However, some general conclusions of a qualitative nature can be made from observations of calculated transport rate distributions obtained from the LWT studies.

Formation of a second bar inshore is recognized in the transport rate distribution as a local minimum, with monotonically decreasing transport rates seaward and shoreward of this point. Since calculation of the net transport rate yielded an average between profile surveys which were separated in time, the inshore peak of the distribution was sometimes not clear. Furthermore, the number of cases studied in which wave reformation occurred was limited. This made information scarce about the net transport rate in zones of wave reformation, and choice of the shape of the transport rate distribution became somewhat arbitrary.

It is reasonable to suppose that the transport rate in zones of wave reformation is a function of the transport characteristics in the bordering zone of broken waves since mobilization and transport are expected to be most intense in the broken wave zone. It is therefore assumed that the magnitude of the trans-

226

port rate at the boundary of the broken wave zone determines the
magnitude of the transport rate in the wave reformation zone.
Then, only information about the functional form of the decay of
the transport rate to the point of minimum transport and the
location of this minimum are required to completely specify the
transport rate distribution in the wave reformation zone. The
magnitude of the minimum transport rate in the wave reformation
zone is given by the decay function once the location of the
minimum is specified. Various trial functions were investigated
in order to find a suitable description of the transport rate
distribution in the wave reformation zone, mainly exponential-
and power-type functions. A qualitatively acceptable picture of
beach profile evolution was obtained by an exponential decay from
the point of wave reformation and shoreward to the point of
minimum transport. From the second break point and seaward to
the point of minimum transport, a power law was applied to
describe the transport rate. By introduction of these empirical
functions, additional parameters are introduced in the model
whose values must be determined through calibration against
measurement. The two empirical transport relationships used to
describe the transport rate q in zones of wave reformation are

$$q = q_r \, e^{-\nu(x_r - x)} \qquad\qquad x_m \leq x < x_r \qquad (47)$$

$$q = q_b + (q_m - q_b) \left(\frac{x - x_b}{x_m - x_b}\right)^n \qquad x_b < x < x_m \qquad (48)$$

where

q_r = transport rate at wave reformation point

x_r = location of wave reformation point

ν = spatial decay coefficient

q_b = transport rate at second break point

227

q_m = minimum transport rate in wave reformation zone
 (determined from Equation 47)

x_b = location of break point

x_m = location of minimum transport rate

 n = exponent determining spatial decay in transport rate

In order to investigate the possibility of modeling wave reformation and multiple bar formation, one of the CE cases was used for which measurements of a second break point were made (Case 500). Since the wave height in the surf zone approaches the stable wave height (Γ) asymptotically as the waves progress onshore (Horikawa and Kuo 1967, Dally 1980), wave reformation will not occur in the model for a beach with monotonically decreasing depth in the surf zone that is exposed to constant wave conditions and water level. As a bar grows in size, the trough becomes more pronounced, but the slope-dependent term in the transport equation (Equation 33) will not allow the trough to become sufficiently deep to initiate wave reformation.

One method of forcing waves to reform is by turning off breaking at a predetermined level somewhat higher than the value of the stable wave height coefficient (see Dolan 1983, Dolan and Dean 1984). A physical argument for this may be that an asymptotic decay towards the stable wave height probably is unrealistic in nature and wave reformation is initiated through a delicate balance between competing processes close to stable conditions. Consequently, by forcing wave reformation to occur, the phenomena is included in the model although the details of the process are simplified. In this particular simulation, a stable wave height coefficient of $\Gamma = 0.4$ was used in all simulations, whereas breaking was turned off at a value of $\Gamma = 0.5$ to initiate wave reformation. In Figure 75 a typical simulation result is displayed for Case 500 for which breaking is turned off, causing a second break point to appear and thus another bar to form. Beach profiles at consecutive times from the model simulation are given together with the measured beach

228

profile at the last time step. The wave height distribution
across-shore for the last time step is also shown in the figure.
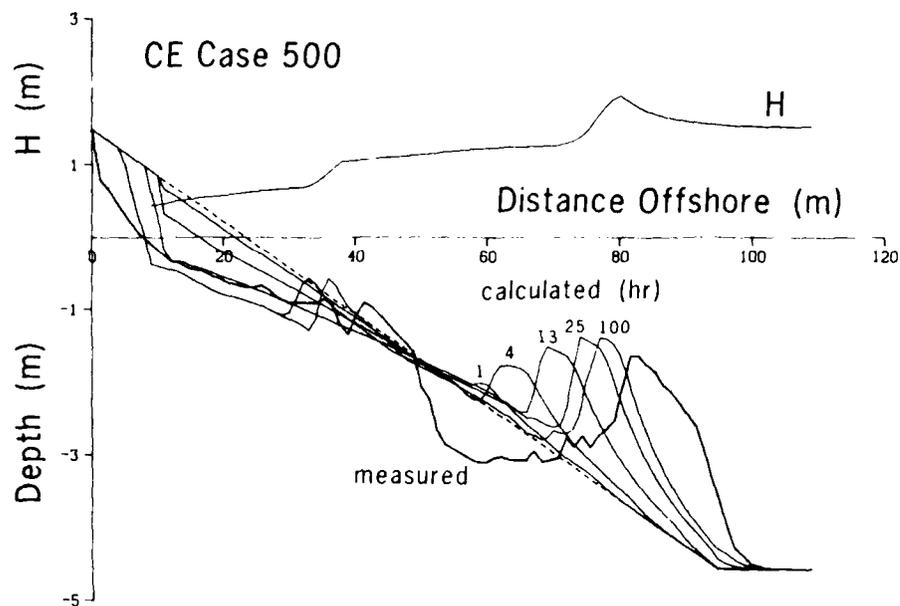
Figure 75.   Calibration of numerical model against Case 500,
             reproducing the second breakpoint bar

Viewing Figure 75, the location of the two bars and the
amount of erosion on the foreshore were well described by the
numerical model, whereas the very marked trough shoreward of the
main break point was not reproduced. When the second bar
appeared, sand transport to the main breakpoint bar was hindered
and growth of this bar decreased.

As previously mentioned, between the shoreward break point
(x_b) and the point where the transport rate attains a minimum in
the reformed wave zone (x_m), a power curve was used to describe
the decrease in transport rate. An exponent of 0.5 proved
adequate in the simulation, although the calculation was not
sensitive to changes in this value. Changes in the exponent did
not affect the shape or size of the outer bar, but did influence

229

somewhat the location of the inner bar. A larger value of the exponent made the inner bar move further seaward, whereas a smaller value decreased seaward movement of the bar. From the point of wave reformation (x_r) and shoreward, an exponential decay with distance was used, thus introducing another spatial decay coefficient ν. Typical coefficient values used were around 0.10 m^{-1}, which is in between values found for spatial decay coefficients for the main breakpoint bar from the plunge point to the break point and from the break point seaward (Part V).

The location of the minimum transport rate x_m in the wave reformation zone has to be specified to completely determine the transport rate distribution there. Once this point is known, the transport rate is calculated from the exponential decay from the wave reformation point and shoreward. The power curve then connects the minimum transport rate thus determined with the transport rate at the second break point. As waves reform, a certain amount of turbulence is still advected onshore with the waves, keeping grains in suspension and making them available for transport. However, because the generation of turbulent motion through wave energy dissipation decreases considerably, the transport rate decreases correspondingly. Closer to the second break point on the seaward side, the transport rate is expected to increase again, caused by the large energy dissipation shoreward of the break point. Since the sand transport capacity of a reformed wave probably is larger than for waves in the zone immediately seaward of a break point, the point of minimum transport should probably be located closer to the second break point than to the point of wave reformation. In the numerical model, the location of the minimum transport rate in zones of wave reformation was arbitrarily placed seaward of the second break point one third of the distance to the wave reformation point.

230

In initial simulations of multiple bar formation with the numerical model, the inshore bar formed in most cases too close to the main breakpoint bar, compared with measured beach profiles from the LWT experiments. This was caused by rapid shoaling in the model after wave reformation, making the second break point appear too seaward, since energy dissipation of the waves drastically changed as they reformed and shoaling became dominant. Since wave reformation is a gradual phenomena it was believed that a successive turn-off of energy dissipation would provide a more adequate representation of what actually happens in this zone. The turn-off is implemented in the numerical model by decreasing the wave decay coefficient κ exponentially with distance from the wave reformation point and shoreward. A decay coefficient of 0.025 m^{-1} in the exponential damping function proved sufficient to accurately describe the location of the second bar.

Simulation of Field Profile Change

The numerical model was used to simulate beach profile change measured at the Field Research Facility (FRF) located in Duck, North Carolina. The FRF is operated by the Coastal Engineering Research Center (CERC), U.S. Army Engineer Waterways Experiment Station. Beach profiles have been measured regularly for more than four years at the FRF along four different shore-normal lines, together with the associated wave climate and water level. Procedures for making the measurements and a listing of the data are given by Howd and Birkemeier (1987). Surveys are carried out at approximately two-week intervals, whereas statistical wave parameters are calculated every 6 hr, and the water level recorded every six minutes. The quality of this data set is probably the highest in the world in resolution in time and space of beach profiles measured in the field.

231

Five time periods were chosen for simulation, distinguished by two beach profile surveys between which erosional conditions prevailed (storm events). Erosional conditions were characterized by offshore movement of one or two bars, whereas shoreline position in most cases was very stable and no retreat was noted. Anomalous stability of shoreline position is characteristic of the FRF beach, and may be caused in part by coarser material present around the shoreline, producing an armoring effect and thus requiring a larger amount of wave energy to move material.

Figure 76 shows the sediment size distribution across the profile at one particular time (810317) as given by Howd and Birkemeier (1987). The median grain size was more than an order of magnitude larger on the foreshore compared to the seaward region. Due to the large grain size, the slope of the foreshore is often very steep, allowing for waves to break on the shoreface.
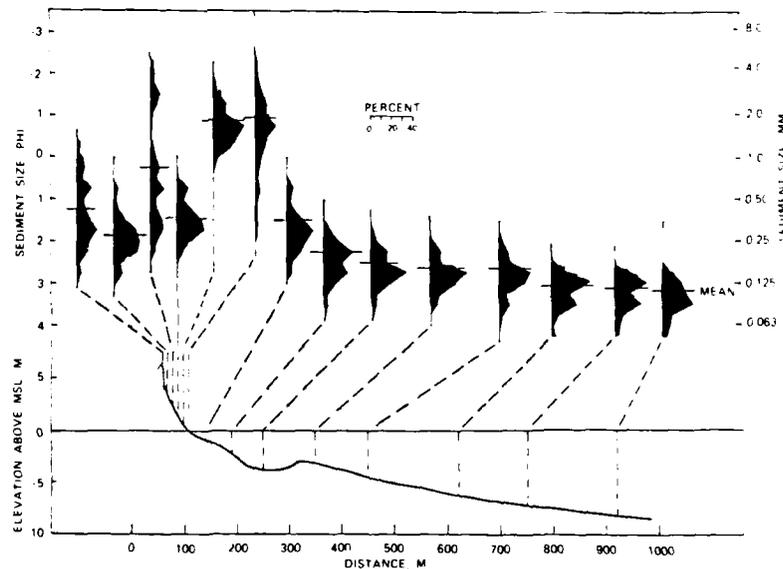
Figure 76. Distribution of sediment grain sizes across profile line 188 at Duck, North Carolina (after Howd and Birkemeier 1987)

232

Although the profile data from the FRF are thus unsuitable for evaluating shoreline change and the prediction of eroded subaerial volume, movement of the bar may still be simulated with reasonable confidence. Furthermore, beach changes may be highly three-dimensional in the field, making it essential to identify profile change in the record for use here that was likely minimally affected by longshore transport and rip currents. Howd and Birkemeier (1987) documented a wave event (821013 - 821015) during which closely located profiles in space showed very different response, with a bar moving both onshore respectively offshore on different survey lines, thus illustrating the importance of choosing events which show approximately similar profile response alongshore. Therefore, in the present study time intervals were selected during which neighboring profile lines displayed similar development.

Data set

Survey line 188 (Howd and Birkemeier 1987) located southeast of the FRF pier was selected for profile simulation. The survey line is beyond the influence of the pier and located in an area of offshore bathymetry with nearly straight and parallel bottom contours. In order to minimize the effect of longshore variability in profile change in selecting storm events for simulation, the response of survey line 188 was compared with survey line 190, located less than 100 m away. Five events were chosen for which profile evolution was similar for the two survey lines, making it reasonable to believe that beach changes were predominantly two-dimensional during the storm events. However, for most of the events used, mass was not rigorously conserved in comparison of consecutive surveys, indicating that longshore effects influenced profile response to some degree.

Measured wave height and period were available every 6 hr and water level every hour. Since a shorter time step (typical-

233

ly, $\Delta t = 20$ min; $\Delta x = 5.0$ m) was used in the numerical model than the wave and water level measurement intervals, cubic spline interpolation was used to provide input values for time steps between measurements. The energy-based wave height (H_{mo}) used was determined from the wave spectrum as four times the standard deviation, which corresponds to the significant wave height if a Rayleigh distribution is assumed. The wave period was given as the peak period of the spectrum. Data from gage 620, located in 18 m of water off the end of the pier, were used to obtain wave input information. Wave height was then transformed using linear wave theory to the beginning of the calculation grid, located at a depth of about 8 m below mean sea level.

The water level (tide) gage was located at the end of the pier and values given were the total water level variation with respect to the mean water level. Thus, the water level includes both storm surge and tidal variation, the latter of which was semidiurnal (two high and two low waters in a tidal day).

Profile surveys were made at an average interval of two weeks, with more frequent surveys at times when greater profile change took place. Although the profile data from the FRF probably represents the most detailed and accurate data set on profile change in existence, horizontal spacing between measurement points is typically tens of meters. Small features in the profile are not resolved, and the general shape has a more smoothed character than actually exists. However, the data set is highly suited to the present application.

Calibration of numerical model with field data

Initially, the parameter values given by calibration with the LWT data sets were used in simulation of the field profile change data. However, it became apparent that values of some empirical coefficients would have to be modified in order to achieve agreement between measured and calculated profiles. Four

234

storm events (811022 - 811103; 811110 - 811116; 840210 - 840216; 840403 - 840406) were chosen for calibration of the numerical model, and one event (821207 - 821215) was used for the verification. Calibration was performed for the four selected events by minimizing the total sum of squares of the difference between calculated and measured depths. The optimum transport rate coefficient K obtained for the four events was smaller than the value obtained by use of the LWT data. As previously described (Part VI), the optimum transport rate coefficient for the LWT calibration was determined to be $1.6 \ 10^{-6} \ m^4/N$. In contrast, for the field data a value of $0.7 \ 10^{-6} \ m^4/N$ proved to give the best agreement.

A smaller transport coefficient is not unexpected because the shoreline at the FRF acts as an effective seawall, and because the transport rate coefficient showed an inverse dependence on wave period for the LWT experiments. Calibration of K via the LWT data set is somewhat biased toward lower-period waves, whereas wave periods in the field data were somewhat longer than for the LWT data. Use of the K-value determined from the LWT data made the beach profile respond too quickly and the bar to become too pronounced, not having the smooth character observed in the field measurements. Transport induced by random waves that exist in the field, i.e., wave heights and periods varying above and below the representative monochromatic (but time-varying) waves used in the model is also expected to change the value of the transport coefficient, as both transport thresholds and mean rates will be different (Mimura, Otsuka, and Watanabe 1987). The amount of change in K between LWT and field calibrations is considered surprisingly small. Three cases gave the best fit for $0.9 \ 10^{-6} \ m^4/N$, whereas the remaining case gave $0.4 \ 10^{-6} \ m^4/N$.

Values of other empirical coefficients appearing in the various transport rate relationships were kept at the values given by the LWT calibrations, which appeared to give adequate

235

results. In the breaker decay model the stable wave height coefficient was set to $\Gamma = 0.4$ as for the LWT calibration, whereas a wave decay coefficient of $\kappa = 0.13$ gave better agreement between measured and simulated profile evolution. A smaller wave decay coefficient is expected for the FRF data compared to the LWT data since this coefficient depends slightly on beach slope (Part V), and the field profiles had more gentle slopes than the LWT experiments. The stable wave height coefficient was also varied, but the simulation was rather insensitive to changes in this parameter.

The breaking criterion developed from the LWT data caused the waves to break too far offshore, creating a bar farther seaward than found in the measurements. Instead, a constant value of the breaker ratio of 1.0 was applied, which provided a better description of the bar location. In the breaker criterion derived from the CRIEPI data set, the slope seaward of the break point was used. At the seaward side of the bar the slope was normally relatively steep, making the breaker ratio correspondingly high. Beach profiles from the FRF data set showed more gentle slopes than the CRIEPI experiment making the predicted breaker ratio lower, and thus the waves broke further offshore. Consequently, the relationship derived from the LWT data produced a slope dependence which appears not to apply to the more gently sloping bars found in the field.

The energy-based significant wave height was used in the numerical model to determine the wave height distribution across-shore. On a field beach the break point constantly moves back and forth due to random variation in wave parameters. A problem is to find a measure of the wave height that will on the average reproduce properties of the random breaking waves. As an alternative to the significant wave height the mean wave height (H_{avg}), determined by assuming a Rayleigh distribution, was used in some simulations. Since H_{avg} is smaller than H_{mo}, the waves broke further inshore, but moved less sand. However, better

236

agreement was not achieved using H_{avg} instead of H_{mo} as opposed
to what was reported by Mimura, Otsuka, and Watanabe (1987).

The non-linear shoaling law derived by Shuto (1974) was also
employed in some simulations with the field data, but seemed to
overestimate shoaling just before breaking, as was the case for
the LWT experiments. Longer period waves calculated by the non-
linear theory markedly increased in height in shallow water,
creating a bar too far offshore. Consequently, linear wave
theory was judged to be more satisfactory and was used through-
out.

Median grain size probably varied across the beach profile
(see Figure 76) with a noticeably larger grain size on the
foreshore. In order to represent this variation in the numerical
model, two different grain sizes were used along the profile. A
larger grain size (2.0 mm) was employed on the foreshore to a
distance approximately 130 m from the base line, whereas a finer
grain size (0.15 mm) was employed from this point and seaward.
The larger grain size implied a larger equilibrium energy
dissipation with correspondingly more wave energy needed to move
material. Furthermore, the equilibrium energy dissipation as
given by Moore (1982) was reduced according to the 0.75-factor
determined from the LWT experiments. Additional variation in
median grain size across-shore somewhat improved the fit of the
model in trial simulations, but was considered to be unrealistic
because of the added complexity and because the movement and
mixing of individual grains was not simulated in the model.

Results

Calibration. Figure 77a and 77b illustrates the result of a
typical calibration for one event (840403-840406), together with
the wave and water level data. The initial measured profile is
displayed together with the measured and calculated final
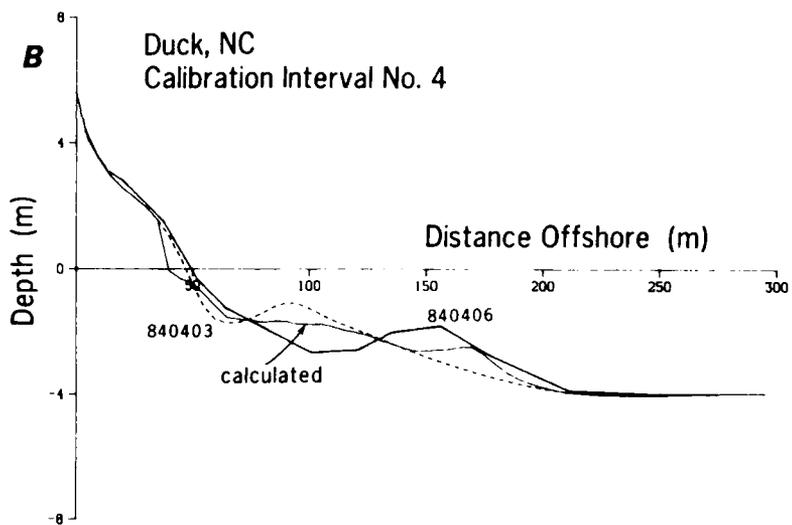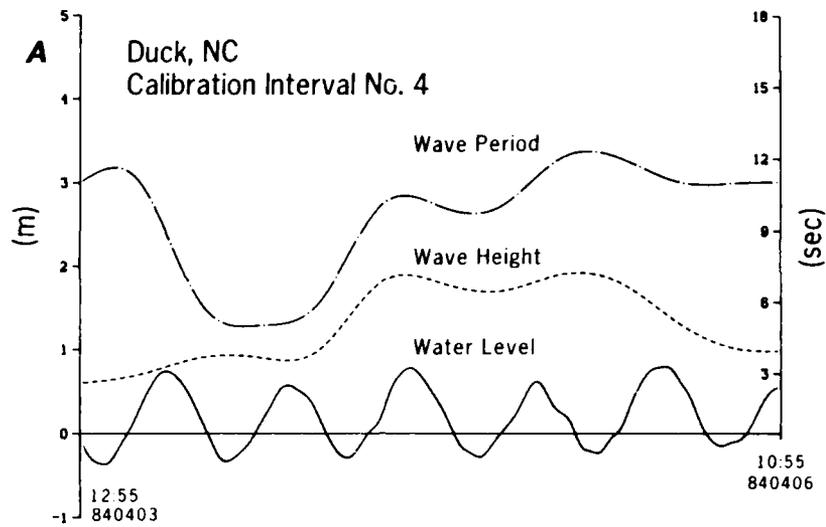
Figure 77. Calibration of numerical model against field
data from profile line 188 at Duck for event
(840403-840406). Variation with time of: (a)
wave height, wave period, and water level; and
(b) simulation result

238

profiles. Movement of the bar was rather well predicted by the model regarding location, but the amount of material moved was underestimated and the trough was not sufficiently pronounced. Also, even though a larger equilibrium energy dissipation was used on the foreshore corresponding to the measured 2-mm grain size, the shoreline still receded somewhat in the numerical model, whereas this did not occur in the field. One reason for this retreat was transport produced by small waves that passed over the bar and broke immediately on the shoreface. Indeed, wave breaking at the step is commonly observed at the FRF; nevertheless, little shoreline movement takes place. Application of the concept of cross-shore transport being proportional to energy dissipation may be questionable if a surf zone is absent and waves break directly on the shoreface. At any rate, lack ⌐f shoreline movement at the FRF is anomalous, and model results cannot be fully interpreted.

The numerical model proved very stable despite the considerable time variation in wave parameters and water level in the field simulation. Longer time and length steps were employed in the calculation in order to reduce the computational effort, namely a time step of 20 min and a length step of 5 m.

Verification. Optimum parameter values determined from the calibration were used to simulate an independent storm event (821207-821215) and thus evaluate the applicability of these values for an arbitrary erosional case. In Figures 78a and 78b the result of the model verification is shown together with input wave height, wave period, and water level. The initial beach profile possessed two bars, with the long outer bar having a very smooth shape. The model simulation reproduced the main changes of the beach profile in that both bars moved offshore. However, the amount of material moved was underpredicted as in the calibration, and the calculated shoreline receded further than what occurred. Movement of the inner bar was overestimated by the model, whereas the outer bar was located correctly but with

239
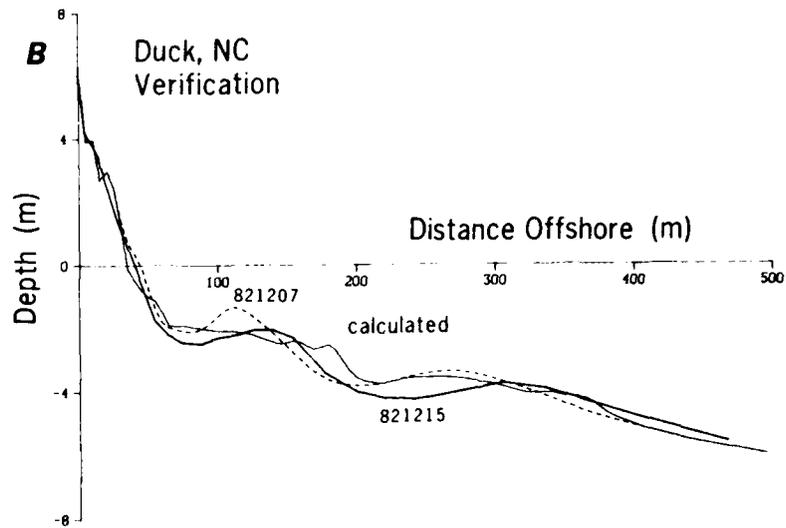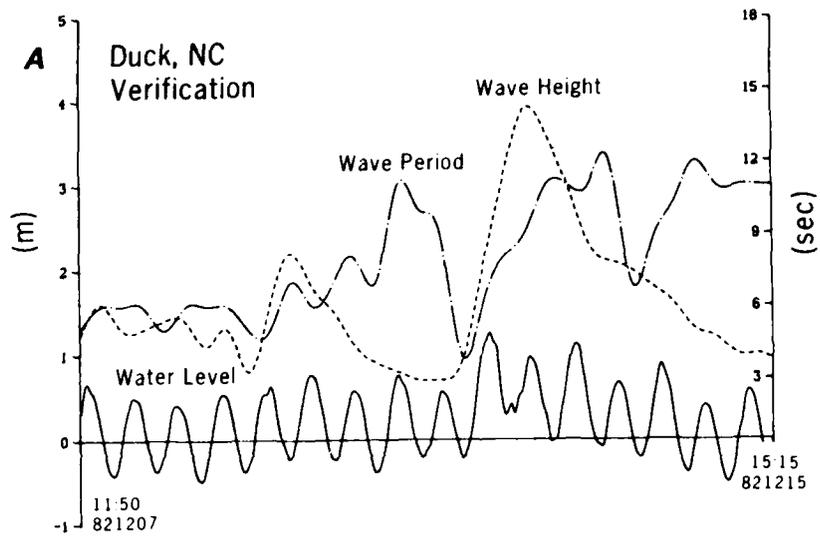
Figure 78. Verification of numerical model against field data from profile line 188 at Duck for event (821207-821215). Variation with time of: (a) wave height, wave period, and water level; and, (b) simulation result

240

less volume than measured. Also, the long smooth trough located shoreward of the outer bar did not appear in the model simulation, and only a small amount of material was eroded from this region.

Sensitivity tests

In order to determine the influence of input wave and water level conditions and to put the results in perspective, variant simulations using the verification case (821207-821215) were performed. Since calibration was not carried out for this case, changes in wave parameters and water level better reflect model sensitivity to these input data. Parameter values given from calibration were used in these simulations. First, the extent to which the rapidly changing water level improves or degrades the model results was investigated.

First, the water level variation was neglected completely, and neither the storm surge nor the tidal variation were represented. Figure 79 illustrates the measured profile and simulated profile obtained by omitting water level changes. A constant water level implied that only wave height and period would determine the location of the surf zone and the amount of energy dissipation. Comparison with Figure 78b shows that the bar closest to the shore developed a double-peaked shape because no water level change occurred. Furthermore, the most seaward bar was smaller in size and not as smooth as the corresponding bar formed under a varying water level. The sum of squares of the difference between measured and calculated profile was smaller for the case including the water level variation, thus giving a better objective measure of agreement with the actual profile change. However, the constant water level simulation showed less shoreline retreat, which is artificial since the waves did not attack the beach as high as for the variable water level case.

In another simulation, the wave height and period were kept

241
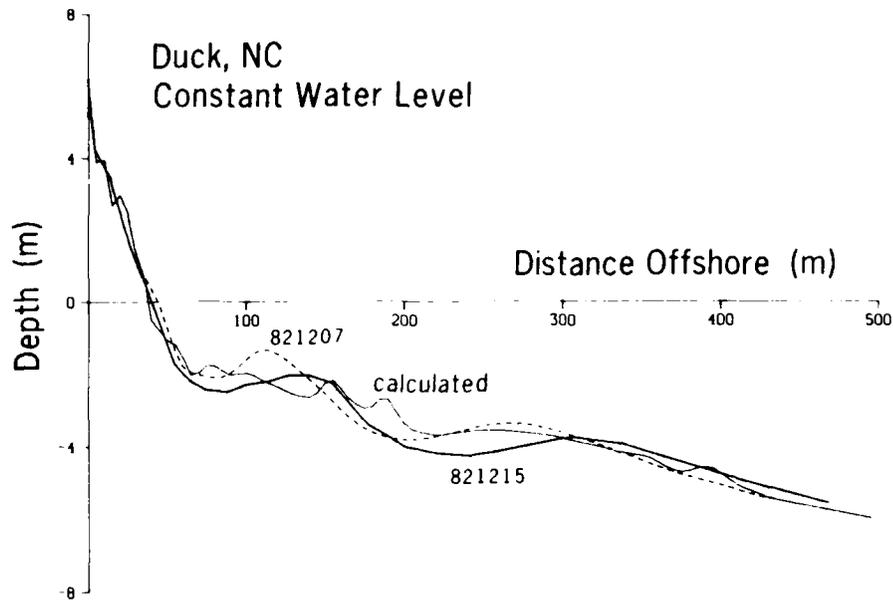
Figure 79. Prediction of numerical model against field data
from profile line 188 at Duck for verification
event (821207-821215) omitting water level
variation

constant at their average values for the verification period, and
no water level change was permitted. The calculated result is
shown in Figure 80, together with the measured initial and final
profiles. The shoreward bar grew very steep and pronounced due
to the constant wave and water level conditions. Also, the
seaward bar did not move since, lacking higher waves, all waves
broke further inshore. This over-simplification of the input
data of wave parameters and neglecting water level variation did
not adequately represent the main features of the driving forces,
viewing the comparison between measured and simulated profile
change. When the wave height and period were held constant, but
the water level was allowed to vary, a pronounced bar developed.

242
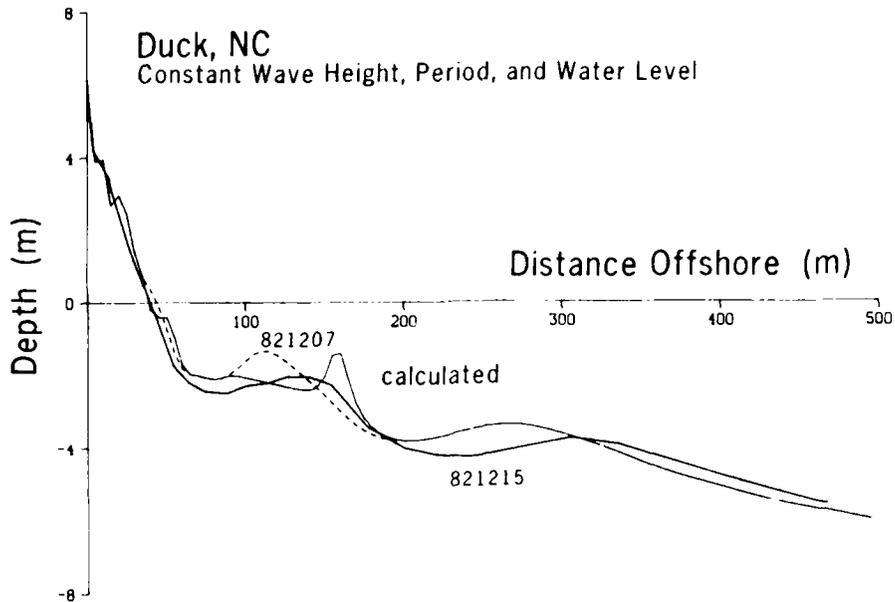
Figure 80. Prediction of numerical model against field data from profile line 188 at Duck for verification event (821207-821215) omitting variation in wave height, wave period, and water level

The main difference compared with the constant water level case was a smoother bar and greater retreat of the shoreline.

Discussion of field simulation

Response of the beach profile to the storm was best reproduced using as much information as possible on wave height, wave period, and water level variation. In order to correctly simulate the behavior of the profile under changing forcing conditions, variation in input data having a time-scale compatible with the profile response must be incorporated. Changes between individual waves is not necessary or meaningful for use of the present model, but differences occurring at a time-scale

243

of about an hour should be represented for best results. Constant wave and water level conditions will produce bars that are too steep, not having the smooth character usually encountered in the field.

The concept of breaking waves as a major cause of bar movement was verified by the model simulation of the field profile change. Locations of the bars were surprisingly well predicted considering the great variability in water level during the several-day storm events. A mass conservation check between measured initial and final profiles showed that none of the cases simulated were free from three-dimensional effects. In Figure 78b the difference in beach volume between initial and final volume was 45 m^3/m (a loss in beach volume, constituting 25% of the total absolute volume moved across the profile). This difference is attributed mainly to differentials in longshore sand transport, and, possibly, to limitations in the surveys (spacing and accuracy). It is speculated that incorporation of longshore sand transport in the numerical model might produce a more pronounced trough, because the maximum longshore sand transport rate is believed to occur somewhat shoreward of the break point.

Although the model was developed using (large-scale) laboratory data for situations with constant wave parameters, the capability to generalize and simulate profile change on natural beaches with variable wave and water level conditions was demonstrated. Steep foreshore and bar slopes that were produced in the wave tanks, well simulated by the numerical model, were a product of monochromatic waves and constant water level. However, the model correctly reproduced essential features of the smoother macroscale field profile change. Consequently, the important effect of variable wave and water level could be represented fairly well by superimposing differing monochromatic waves and stepwise changes in water level. Thus, monochromatic waves and fixed water level serve as elemental conditions that

can be combined in a time series of varying conditions to approximately replicate a random wave and changing water level sea environment.

Comparison With the Kriebel Model

Overview

Presently, there is only one other known numerical model available to the engineering community that allows simulation of time-dependent changes in beach profile produced by breaking waves, that is the model developed by Kriebel (1982, 1986) and Kriebel and Dean (1985a). Simulations were performed with the present model and the Kriebel model for a number of hypothetical cases to evaluate differences in calculated profile response. The Kriebel model does not simulate bar formation and, a priori, is expected to produce more erosion than the present model. Furthermore, the Kriebel model was developed to simulate profile behavior during erosional conditions, particularly dune erosion, and there is no capability for simulating berm build-up in its original formulation.

Since the two models differ in structure and purpose, and contain different numbers of parameters, direct comparison using identical parameter values is not possible. For example, in the present model the wave height distribution is calculated across-shore, requiring specification of two empirical parameters, and is then used to determine transport rates at all points in the surf zone. In the Kriebel model, wave height is assumed to be related to water depth in a fixed ratio. In order to facilitate comparison, parameter values were used as given by calibration against the LWT data for the respective models. Parameter values for the Kriebel model were taken from Kriebel (1986), for which one of the LWT cases were used for the calibration (Case 300).

Calibration

Parameter values in the present model were identical to those obtained from calibration against seven of the LWT cases. Even though the transport relationships are similar in the two models, values of the transport rate coefficient K resulting from the calibration were quite different (in the present model, $K=1.6 \ 10^{-6} \ m^4/N$; in the Kriebel model, $K=8.7 \ 10^{-6} \ m^4/N$). The transport rate coefficient is basically a calibration parameter determining the time scale of profile change, and its value is affected by the amount of smoothing applied in the model. Also, incorporation of a bottom slope-dependent term in the transport rate equation in the present model increases the transport rate on positive slopes. By calculating the wave height distribution in the surf zone with a wave decay model, a more realistic description of the surf zone wave properties is obtained. This also produces a difference in values of the optimum transport rate coefficient.

Comparisons of model simulations

A hypothetical beach profile with a dune having a slope of 1:4, no distinct berm, and a foreshore slope of 1/15 down to 0.6-m depth was used in the model comparison. Seaward from the 0.6-m depth an equilibrium profile according to Bruun (1954) and Dean (1977a) (Equation 1) was used, where the shape parameter A in Equation 1 was chosen from the design curve of Moore (1982) corresponding to a median grain size of 0.25 mm. The water level was varied sinusoidally over a half-period comprising, in total, 48 hr to simulate a storm hydrograph, and wave conditions were held constant with a period of 10 sec and a wave height of 3 m. Figure 81a illustrates the result of simulations with the two numerical models, producing very similar amounts of erosion. (Figure 81b shows a blow-up of the dune and foreshore.)

246
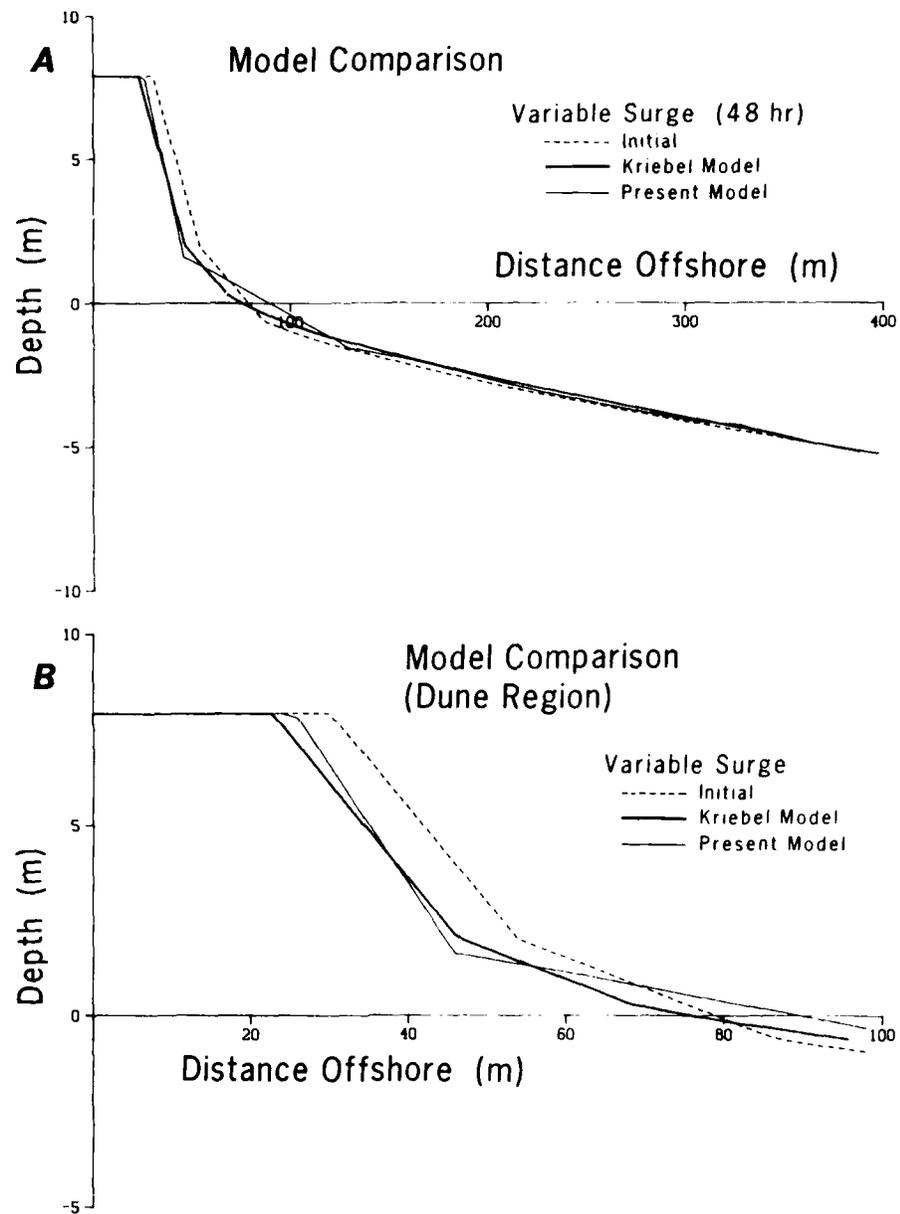
Figure 81. Simulation of hypothetical case with sinusoidal-
ly varying water level with present model and
Kriebel model: (a) full beach profile, and (b)
detail of dune

247

The main difference between model results for this particular case is the area over which material was deposited. The Kriebel model distributed eroded material approximately evenly over the beach profile, whereas the present model tended to deposit sand closer to the toe of the dune. Large wave tank experiments performed by Vellinga (1982) showed a time evolution of the profile qualitatively in agreement with the present model, but for a shorter surge hydrograph.

The dune face of the eroded profile was steeper for the present model, whereas the Kriebel model produced direct translation of the initial profile. Only a low-relief bar feature was developed at the seaward end of the profile in the present model because of the varying water level, causing the break point to move first shoreward and later seaward. Since the break point was not stationary, the maximum transport rate changed location, not giving the bar the required time to evolve.

Wave period does not enter in the Kriebel model, but it is of importance for the shoaling, breaking, and runup of waves in the present model. Therefore, the wave period was changed in the test case to 14 sec to evaluate its effect on the simulation result. The result for the present model was formation of a very smooth, long bar of small height, whereas the amount of dune erosion was approximately the same for both models.

In order to illustrate the difference between the models another case was simulated in which the water level conditions were contrived to promote bar formation. The same initial beach profile and wave conditions were used as for the previous case, but the water level variation consisted of an instantaneous rise of 2 m (surge) at the start of the simulation. The simulation period was 48 hr, and the result is displayed in Figures 82a and 82b. A distinct bar was developed by the present model, reducing the incident wave energy at the dune and thus reducing the amount of dune erosion compared with the Kriebel model.

248
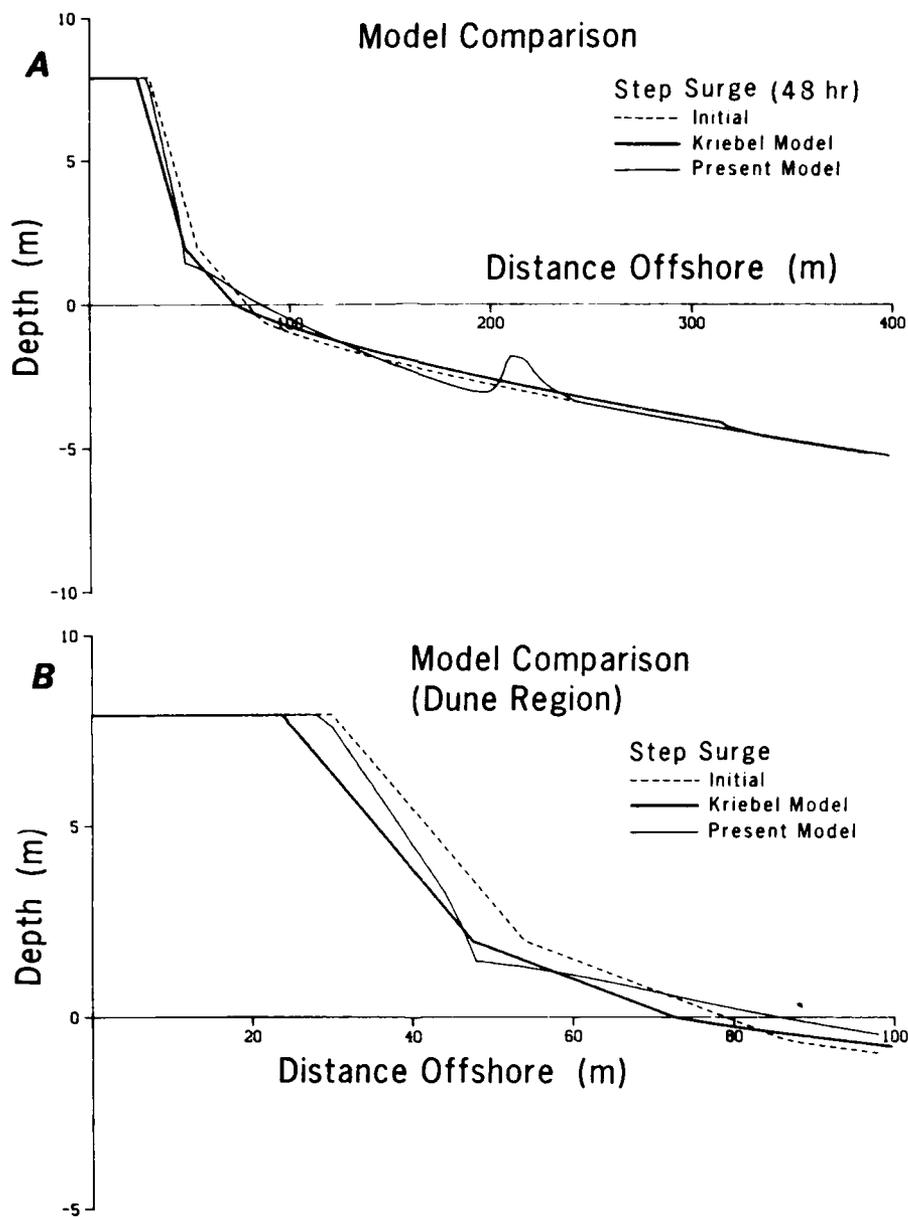
Figure 82. Simulation of hypothetical case with step-
increase in water level with present model and
Kriebel model: (a) full beach profile, and (b)
detail of dune

249

The shoreward slope of the bar is quite steep due to constancy of the incident wave conditions.

In general, the two models appear to produce similar results for dune erosion if the wave and water level conditions are such as to prevent development of a distinct bar. However, if conditions allow a bar to form, the present model will predict a smaller amount of nearshore erosion than the Kriebel model. The beach profile shape seaward of the dune toe is probably more realistically described in the present model, where the area of material deposition is more concentrated, implying a more narrow surf zone as the water level increases.

Numerical Modeling of Beach Profile Accretion

General discussion

Most development work with the numerical model was focused on simulating beach profile response under erosional conditions. Although the characteristics of berm build-up were discussed in the data analysis and related geometric properties quantified, model development was not primarily directed towards simulating accretionary stages of a beach. Transport rates from the LWT experiments showing berm build-up were determined from profile surveys, together with some associated characteristics of the transport rate distribution. However, due to lack of suitable test cases having sufficient information of the wave height distribution across-shore, it was not possible to derive an empirical transport relationship for the surf zone specifically applicable to onshore-directed transport.

The net direction of cross-shore transport may be predicted using Equation 2 in terms of the two quantities of deepwater wave steepness and dimensionless fall velocity. As the grain size increases for a specific wave climate, the tendency for onshore

250

transport becomes stronger. Dean (1973), using the dimensionless fall velocity, explained the criterion for onshore transport in terms of the relation between the height a particle was suspended and the distance it would fall during the passage of a wave. A hydraulically heavy particle would fall to the bottom during the onshore portion of the wave motion because of the rapid settling velocity, resulting in net movement onshore.

The criterion for distinguishing between bar and berm formation is closely related to the transport direction and used in the numerical model for that purpose, as discussed previously. The same basic transport relationship (Equation 33) is used whether onshore or offshore transport occurs. A beach that is not in equilibrium with the wave climate, not being able to dissipate incident wave energy uniformly over its length, will experience transport until equilibrium is attained if exposed to the same wave climate for a sufficiently long time. For onshore transport, the net transport rate in the model is assumed to be proportional to the energy dissipation per unit volume, similar to the situation of offshore transport. Also, the term which modifies the net transport rate due to the local bottom slope is incorporated. Seaward of the breakpoint, an exponential decay (Equation 21) of the transport rate is used with a spatial decay coefficient as given from the LWT experiments. The same value of the spatial decay coefficient is applied independently of wave and sand parameters, namely 0.11 m^{-1}.

Both the location of the plunge point and the spatial decay coefficient between break point and plunge point are determined in the same manner for accretionary and erosional profiles. Since the magnitude and direction of the transport rate seaward of the plunge point depends on the transport rate in the surf zone, the transport will be onshore if the transport is directed onshore in the surf zone. On the foreshore, a linearly decreasing transport rate is applied to the runup limit with the decay starting from the shoreward end of the surf zone. This is

251

identical to the shape chosen for the transport rate distribution on the foreshore for erosional transport conditions. The linear shape of the transport rate on the foreshore was supported by the data analysis for both onshore and offshore transport.

Parameter values used in the breaker decay model are identical to the ones applied for erosional conditions and these values are considered to be representative averages for various slopes. Also, the same criterion for incipient breaking is applied for both erosional and accretionary transport conditions, although this was primarily derived from cases showing erosion and having a clear breakpoint bar.

Model calculation

Case 101 from the LWT experiments was simulated to qualitatively evaluate the capability of simulating beach profile accretion with the numerical model. In the numerical model results, a berm rapidly formed on the foreshore by onshore transport from breaking waves, and material was deposited up to the runup limit (Figure 83). As sand was transported onshore, the surf zone and the offshore zone eroded, increasing the depth in this portion of the profile. The increase in depth caused the break point to move onshore and, at about the same time, the berm retreated somewhat at the shoreline while the seaward slope of the berm grew steeper. Continuous onshore movement of the break point made the surf zone become narrower through time, restricting the onshore transport to a smaller area of the profile. The seaward berm slope steepened because of the continuing transport, limited only by the angle of initial yield. The angle of initial yield was reduced somewhat on the foreshore to achieve a less steep slope which should be more realistic because of the strong turbulent conditions prevailing. A large region of erosion appeared immediately seaward of the fore-hore, where a deep trough developed, allowing the waves break at the beach face.

The profile approached equilibrium as time elapsed, exhibiting an unambiguous berm formation with a deep seaward trough, as shown in Figure 83. The measured and simulated berm volume and location are in good agreement. However, the seaward slope of the berm grew too steep in the numerical simulation, and the profile shape in the surf zone was not well predicted. The small bar that developed slightly shoreward of the breakpoint in the wave tank was not obtained with the model. The main zone of erosion in the tank occurred more seaward than what was predicted by the model.
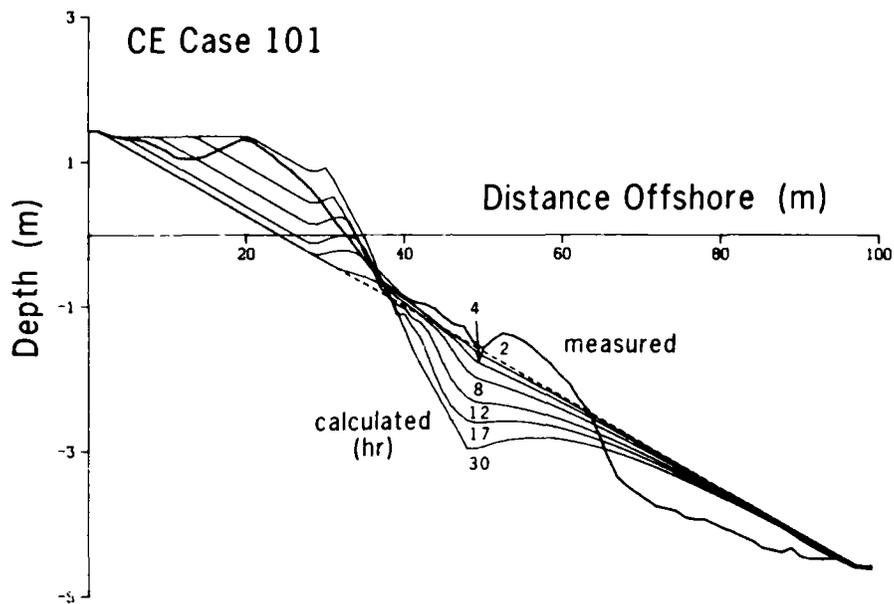
Figure 83. Calibration of numerical model against Case 101 showing berm build-up

In other model simulations of accretion, the zone of fully broken waves became very narrow as the break point moved onshore and the waves directly struck the berm or foreshore. The length of the broken wave zone was by then only one calculation cell wide, and a transport rate equation based on energy dissipation

per unit volume was no longer realistic. In these cases, the transport rate calculated from the energy dissipation was reduced. If no reduction was employed, very local erosion and accretion around the shoreline would occur, giving rise to numerical instability. The value of the reduction constant was typically around 0.2 in these cases. This problem might have been circumvented by using extremely small spatial and temporal steps.

Numerical Modeling of the Influence of a Seawall

The numerical model has the capability of simulating the influence of a seawall on beach profile evolution. The shoreward boundary of the calculation grid is located at the seawall preventing transport of material across this cell. The seawall only affects changes in the beach profile if it is exposed to incident waves. Overtopping is not simulated by the model and it is assumed that the height of the seawall exceeds the runup height (or local wave height).

Profile with seawall

To evaluate the effect of a seawall on beach profile evolution during storm conditions, as predicted by the model, a hypothetical case was simulated. Initial profile and wave data from CE Case 400 were used in the simulation and a seawall was placed on the foreshore, approximately at the still-water shoreline, protecting the subaerial part of the profile from wave attack. The simulation result is displayed in Figure 84, which shows the calculated beach profile at selected time steps with a seawall on the foreshore, and the beach profile at the last time step without a seawall. The wave height distribution across-shore is shown at the last time step for the seawall calculation.

254
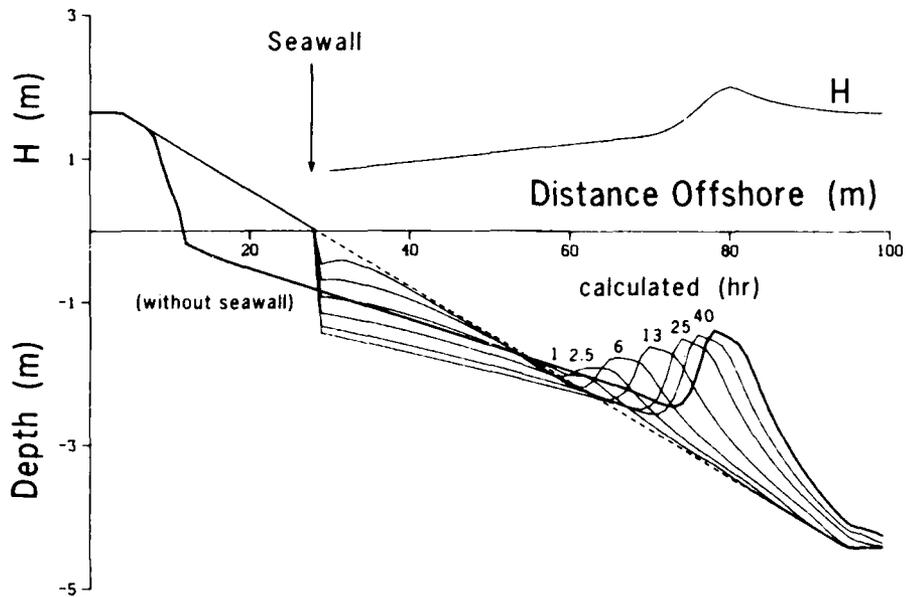
Figure 84. Simulation of hypothetical case with and without
seawall located on the foreshore

The evolution and size of the bar were similar in the
simulation with and without the seawall, the bar being somewhat
larger and more seaward located for the case without seawall.
The main difference was the amount of material eroded in front of
the seawall and shoreward of the bar. In the seawall-case, the
length of the surf zone was much shorter, requiring more material
to be moved before an equilibrium beach shape developed. The
subaerial eroded volume for the case without the seawall ap-
proximately agreed with the extra volume eroded in front of the
seawall.

The approach to equilibrium was more rapid for the seawall-
case, indicated by the slightly more gentle inshore profile
slope. The longer time elapsed for the case without seawall
before equilibrium was attained was caused by a larger extent of

255

the profile involved in the redistribution of sand. Since the depth in front of the seawall was greater than for the case without the wall, the height of the broken waves was correspondingly larger (compare with wave height distribution in Figure 59a).

Profile with seawall and beach fill

In order to evaluate the performance of the model for more complex conditions, a simulation was carried out for a time period involving both mildly erosive or accretionary waves, a storm event, and a recovery period. Furthermore, a seawall was located in the subaerial part of the profile, and the beach profile response was calculated both with and without beach fill. Two different beach fill schemes and grain sizes were evaluated, one case where the material was added as an artificial berm above the still-water level and another case where the material was spread out mainly below the still-water level according to the equilibrium shape associated with the beach sand. The wave height and water level of the simulated event is illustrated in Figure 85 (note that the time scale is distorted).

During the first 21 days the wave height was 0.5 m and the wave period 8 sec, producing mildly erosive or accretionary conditions depending on the grain size. The beach profile was thus allowed to attain its equilibrium shape for the prevailing wave conditions. At day 21 a storm developed which lasted 3 days, and the wave height increased sinusoidally up to a maximum of 2.5 m. Simultaneously a storm surge occurred with a Gaussian shape raising the water level to a maximum of 3 m above the still-water level. The wave period varied sinusoidally between 8 and 12 sec during the storm with the maximum period occurring at the same time as the maximum wave height. After the storm accretionary conditions prevailed with long-period swell of height 0.5 m and period 16 sec, producing beach recovery.

256
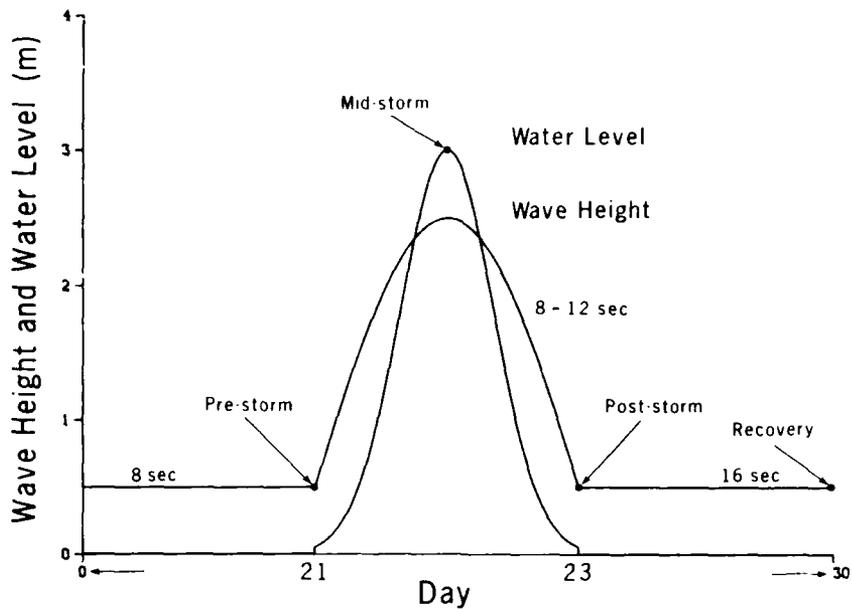
Figure 85. Wave height and water level as a function of elapsed time used in beach fill simulations

At first, model simulations were performed without adding any fill for the two grain sizes 0.25 and 0.40 mm. The initial profile consisted of two linear slopes to a depth of 0.5 m from where an equilibrium profile shape according to Dean (1977a) was employed. Figures 86a and 86b show the beach profiles at selected times during the simulated time period; just before the storm (Day 21), during the storm (middle of Day 22), after the storm (Day 23), and at the end of the simulation period (Day 30).

The initial wave conditions produced erosion for the 0.25-mm grain size (Figure 86a), a small bar developed offshore and the shoreline receded somewhat. As the water level increased during the storm, the beach in front of the seawall was submerged and considerable erosion occurred. The seawall prevented the beach from retreating, thus assuming a height of the seawall exceeding the storm surge height. A long flat bar developed during the peak of the storm which moved offshore with the break point as

257
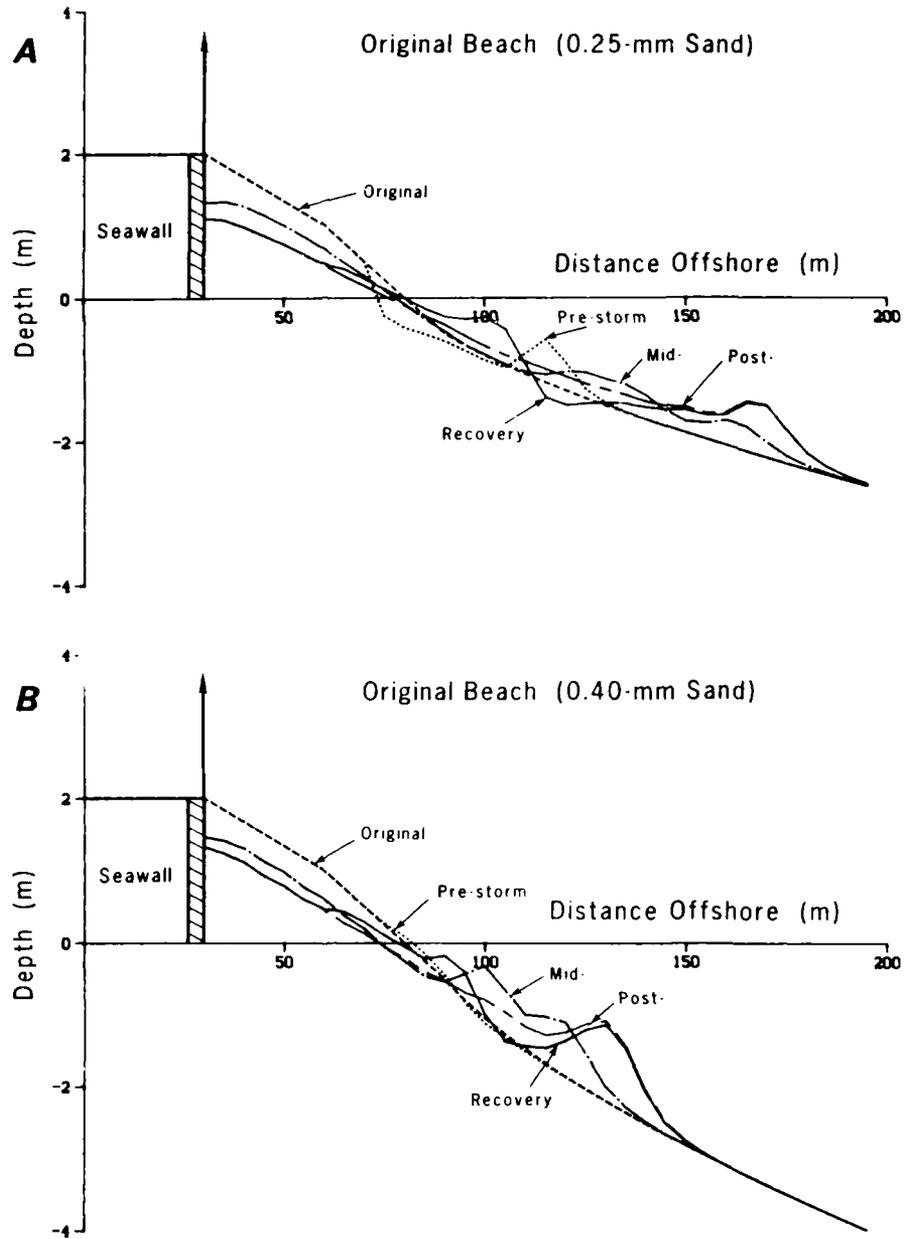
Figure 86. Beach profiles at selected times for hypothetical storm event and original beach without fill: grain size (a) 0.25 mm, and (b) 0.40 mm

258

the water level decreased. After the storm, the inshore portion
of the profile partly recovered producing build-up on the
foreshore and a bar-like feature just below the still-water
level. The main part of the bar, however, did not contribute
material for the recovery process since it was located in too
deep water and far seaward of the breaking waves.

The equilibrium profile of the 0.40-mm sand was much steeper
than the 0.25-mm beach because of the grain-size dependence of
the A-parameter in Equation 1 (Figure 86b). Furthermore, the
mild waves arriving during the initial part of the simulation
period produced onshore transport and a small berm build-up.
During the storm surge the amount of subaerial erosion was
similar to the 0.25-mm profile but the bar did not migrate as far
offshore. The recovery of the 0.40-mm beach did not produce such
a marked trough seaward of the bar-like feature as the 0.25-mm
beach.

The first type of beach fill evaluated was an <u>artificial</u>
<u>berm</u> consisting of approximately 85 m^3/m of material placed on
the subaerial portion of the beach. In the simulations with the
beach fill it was assumed that the fill material was identical to
the natural beach sand. Before the storm a small bar formed,
much in agreement with the case without the fill but closer to
shore. During the storm a large part of the fill eroded and was
deposited offshore. Figures 87a and 87b illustrates the simula-
tion results for the 0.25-mm and 0.40-mm grain size. Although
significant recovery occurred for the 0.25-mm beach, a large
amount of material was trapped offshore. The eroded material
from the artificial berm for the 0.40-mm beach was deposited
closer to shore and during the recovery phase the whole bar moved
slightly onshore.

In the second fill alternative, material was deposited
mostly in the subaqueuos portion of the profile and in accordance
with the equilibrium shape of the beach (called the <u>Bruun beach</u>
<u>fill</u>). The fill volume was 85 m^3/m as for the artificial berm.

259
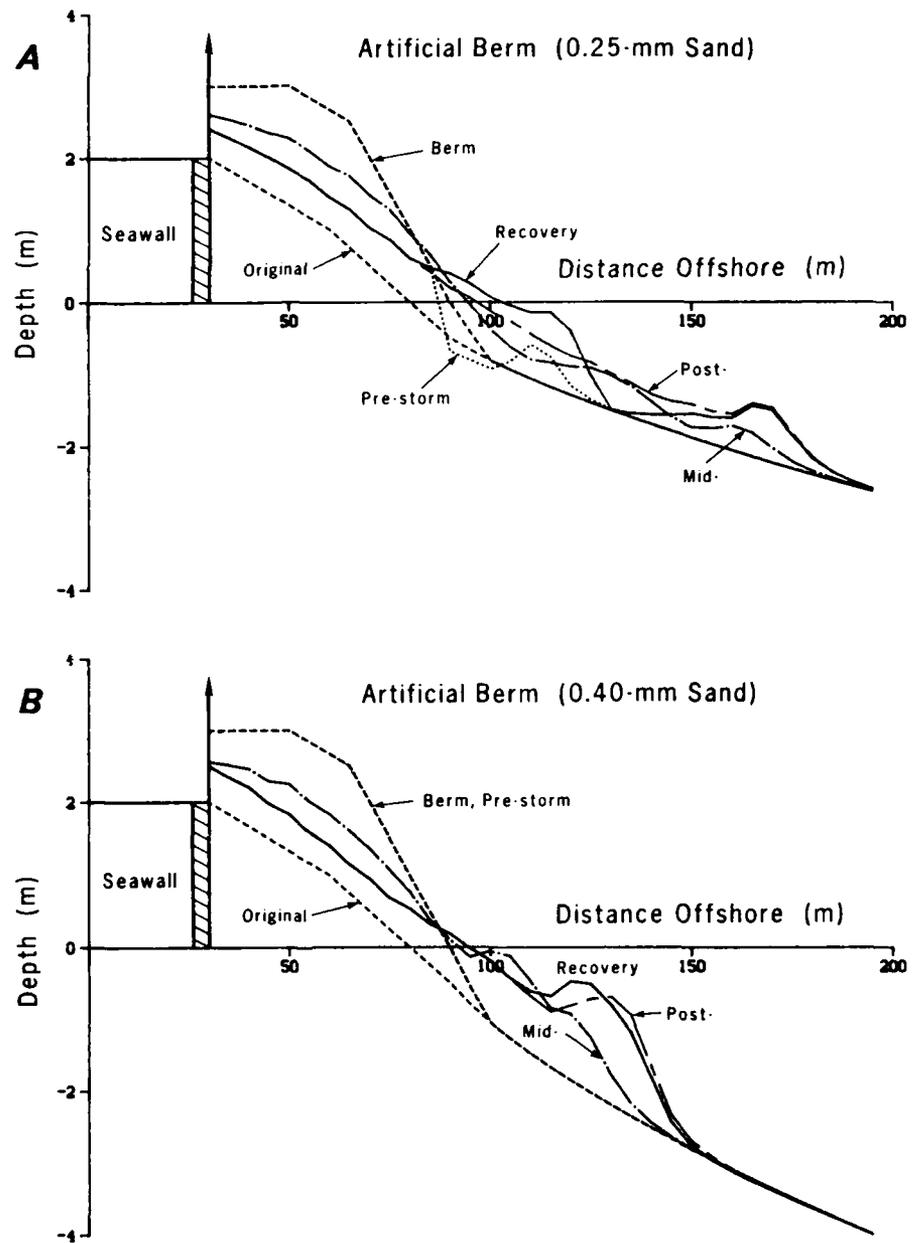
Figure 87. Beach profiles at selected times for hypotheti-
cal storm event and beach with berm fill: grain
size (a) 0.25 mm, and (b) 0.40 mm

260
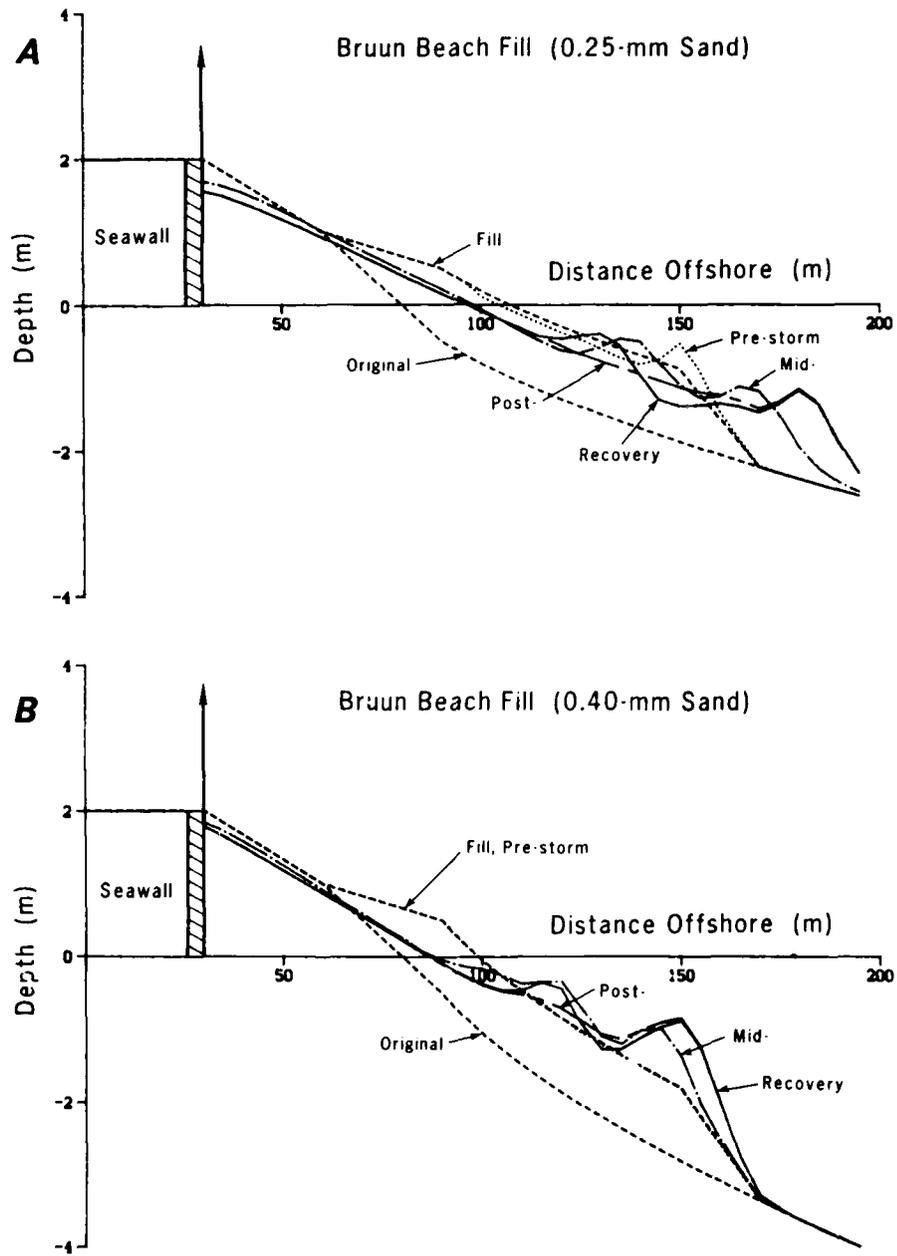
Figure 88. Beach profiles at selected times for hypotheti-
cal storm event and beach with Bruun fill: grain
size (a) 0.25 mm, and (b) 0.40 mm

261

Figures 88a and 88b shows the simulation result for the two grain sizes studied. The amount of subaerial erosion was reduced significantly even though the entire profile was submerged during much of the storm surge. The bar development was less pronounced for the 0.25-mm beach compared to the artificial-berm case, whereas the 0.40 mm-beach showed a stronger bar formation.

In summary, the Bruun fill provided better overall protection of the subaerial beach according to the numerical model, and less material was redistributed within the profile during the storm surge compared to the artificial berm.

PART VIII: SUMMARY AND CONCLUSIONS

The ultimate objective of this study was to develop an
engineering numerical model of beach profile change which has the
capability of simulating formation and movement of major mor-
phologic features of the profile, such as bars and berms. Beach
profile response produced by severe storm or hurricane events,
with large erosion and possible dune retreat, was the principal
target problem of the study, although profile change occurring on
longer time-scales, such as adjustment of beach fill, which
involves accretionary processes as well as erosional, was also of
interest. A basic assumption underlying this work is that major
morphologic change occurring in and around the surf zone is
produced by breaking and broken waves.

As a basis for model development, data sets from two large
wave tank (LWT) experiments were used to understand the fundamen-
tal processes governing beach profile change and to establish
cause and effect relationships between waves, water level, sand
properties, and beach profile response. By using data from LWT
experiments, scaling effects were avoided, yet measurements were
available for controlled conditions with the needed high resolu-
tion in space and time.

Data from two different LWT experiments were used in
development of the numerical model; one experiment performed by
the U.S. Army Corps of Engineers (CE) and the other experiment
carried out by the Central Research Institute of Electric Power
Industry (CRIEPI), Japan. In total, these two experiments
encompassed 42 cases having different wave height, wave period,
water level, grain size, and initial profile slope or shape. The
CRIEPI experiment also included measurements of the wave height
distribution across-shore.

Extensive analysis of morphologic features of the profile
was conducted to provide the foundation for the numerical model,
but the analysis also produced functional relationships between

263

geometric characteristics of the profile and wave and sand properties. Geometric properties of the profile that were quantified were; bar volume, bar height, depth to bar crest, ratio of depth to bar trough and depth to bar crest, distance between break point and trough bottom, movement of mass center of bar, bar migration speed, bar slopes, active profile height, step and terrace slopes, berm volume, berm height, and berm slopes. This type of analysis is expected to stimulate corresponding analysis of field profiles and to aid in setting needed standards for collecting field data.

Regression relationships were established between a number of geometric characteristics of the profile and wave and sand properties. In this process the dimensionless fall velocity (H_o/wT) emerged as an important parameter together with the deepwater wave steepness (H_o/L_o). Quantities that could be related to H_o/wT, H_o/L_o, or both were bar volume, ratio of trough depth to crest depth, bar height, and active profile height, respectively normalized with different wave or sand properties. Distance between break point and trough bottom, normalized with deepwater wavelength, was determined to be a function of the local slope seaward of the break point and H_b/H_o. Average depth to bar crest proved to be directly proportional to the breaking wave height. Profile properties derived from the LWT data sets were found comparable to those in the field, which supported the possibility of generalizing observations from the LWT experiments to field application.

A criterion was developed to delineate between formation of bar and berm profiles in terms of H_o/wT and H_o/L_o. Although several well-known criteria were evaluated using the LWT experiments, the criterion developed in the present study appeared to be the most attractive from a physical point of view and also gave a good delineation between bar and berm profiles. The criterion to distinguish between bar and berm profiles was closely related to the predominant direction of cross-shore

264

transport. A bar formed under mainly offshore-directed transport and a berm formed under mainly onshore-directed transport. The validity of the equilibrium beach profile concept was confirmed by the LWT experiments, which clearly showed a systematic decrease in profile change as time elapsed.

Profile slopes were analyzed for the seaward and shoreward side of the bar, seaward and shoreward side of the berm, inshore step, and terrace. Circumstantial evidence was found for the process of avalanching to occur on the shoreward bar face and on the inshore step as the slopes grew beyond a critical angle. An average estimate of this angle of initial yield was 28 deg, and the slope appeared to reach a stable value of around 20 deg. The average slope on the seaward bar face was typically in the range 8-12 deg and was, in many cases, well approximated by two linear slopes. Bar slopes for the LWT experiments were considerably steeper than corresponding slopes found in the field, attributed to the monochromatic waves and constant water level used in the LWT experiments. Berm face slopes were typically in the range of 6-8 deg on the seaward side and 2-4 deg on the shoreward side.

Properties of the cross-shore transport rate were investigated by integrating the mass conservation equation between consecutive profiles in time. This methodology provided a picture of the net average transport rate distribution between two surveys. The magnitude of the net transport rate distribution decreased with time as the profile approached equilibrium shape and less material moved along the profile. Decrease of peak transport rates was best described by a function which showed an inverse dependence with elapsed time and not with an expected exponential decay with time. This difference was attributed to randomness of microscale processes and slight unsteadiness in forcing conditions, which produce a perturbation on the idealized mean behavior. Decrease of the peak transport rate was more rapid for accretionary profiles than erosional profiles.

265

By comparing the initial and final profile surveys, an "equilibrium transport distribution" was defined and calculated, which indicated how sand was redistributed along the profile to achieve an equilibrium configuration. Equilibrium distribution could be classified into three characteristic shapes in a majority of the experimental cases, called Erosional (Type E), Accretionary (Type A), and mixed Accretionary-Erosional (Type AE). Type E-distributions showed transport directed offshore along the entire profile, whereas Type A-distributions showed transport directed onshore along the entire profile. Type AE-distributions were characterized by a mixed response with offshore transport along the shoreward portion of the profile and onshore transport along the seaward portion of the profile.

The profile was divided into four different zones regarding transport rate properties, in analogy with recent findings from nearshore wave dynamics and characteristics of the transport rate distribution. These zones were: pre-breaking zone (I), breaker transition zone (II), broken wave zone (III), and swash zone (IV). For Zone I, the LWT experiments showed that the transport rate was well approximated by an exponential decay with distance from the break point, with a spatial decay coefficient proportional to D/H for erosional conditions and having an average value of 0.18 m^{-1}. The exponential decay proved to be valid for onshore transport as well, but the spatial decay coefficient was almost constant, with an average value of 0.11 m^{-1}.

For Zone II, which extends over the narrow range from break point to plunge point, it was difficult to extract information on the transport characteristics from the LWT experiments. However, an exponential decay with distance offshore showed good agreement for a small number of available cases, with a spatial decay coefficient that was about 0.20 of the value of the spatial decay coefficient applicable to Zone I. Zone III encompasses the main part of the surf zone, and the transport rate was demonstrated to be closely related to the energy dissipation per unit volume,

266

based on the CRIEPI experiment results involving wave height distributions and profile change. Values of empirical coefficients in the transport equation found through regression analysis were similar to values found by other authors through more indirect numerical modeling.

In Zone IV, the region dominated by runup and backrush, the transport rate is governed by swash dynamics. A transport rate expressed in terms of physical quantities could not be developed for this zone due to lack of measurements of swash wave properties. However, the transport rate showed an approximately linear behavior for both offshore and onshore transport for a wide range of conditions. The extent of Zone IV decreased if the profile eroded and a step evolved; the transport rate simultaneously decreased with time.

A numerical model was developed on the basis of quantitative analysis of the LWT wave and profile change data. The model calculates the wave height distribution across-shore at each time step with linear wave theory up to the break point, and thereafter with a breaker decay model in the surf zone. The break point is determined from an empirical criterion, derived from the CRIEPI data set, relating the breaker ratio to surf similarity parameter in terms of the local slope seaward of the break point and H_o/L_o. A non-linear shoaling theory was applied initially but it overestimated the breaking wave height and did not produce as good agreement as linear wave theory in comparisons with the LWT data.

In the model, the transport rate distribution is determined by using local wave properties along the profile. The profile is divided into four different zones according to findings from the LWT data sets, and the respective transport relationships are used to determine the transport magnitude. Transport direction is determined from an empirical criterion derived from the LWT data sets, which predicts bar or berm profile development. Changes in the profile are determined from the mass conservation

267

equation. The model proved to be numerically stable over a wide range of conditions, and simulated profiles approached an equilibrium configuration if exposed to constant waves and water level.

The model was calibrated against seven cases from the CE and CRIEPI experiments showing foreshore erosion and bar formation. The optimal value of the empirical rate coefficient for the transport relationship applied in zones of broken waves was 1.6 10^{-6} m^4/N. The model was then verified against two independent cases from the CE and CRIEPI experiments with the parameter values given by the calibration. Good agreement was obtained between calculated and measured profiles both regarding the amount of foreshore erosion and the movement and size of the main breakpoint bar. The bar trough was less well reproduced and smaller features inshore of the main breakpoint bar were omitted in the simulations. The model was also tested with one CE case which included a water level variation simulating a tide, and this case was also satisfactorily reproduced.

A number of hypothetical cases were simulated with the numerical model to evaluate the influence of variations in incident wave height, wave period, and water level. Sensitivity analyses were performed for a large number of model parameters to establish their influence on bar formation. A simulation which included a seawall on the foreshore showed that the size of the bar was approximately the same as for simulations without the seawall, but the area immediately seaward of the seawall ex-perienced more erosion. Simulations of beach fill adjustment for use in storm protection design were also performed as an example of the utility of the model.

The process of multiple bar formation was simulated and compared with one case from the CE data set where two bars developed. Multiple bars could be generated in the numerical model through wave reformation and appearance of multiple break points. Data from the LWT experiments gave little guidance about

the cross-shore transport properties in zones of wave reformation. The transport rate in this zone was determined through simple functional relationships based on qualitative observations from the LWT experiments.

The model was also used to simulate onshore transport and berm build-up by using one CE case. The size of the berm was well reproduced, whereas the model failed to adequately describe the seaward berm face slope and inshore profile shape. The seaward berm face slope is only limited by the angle of initial yield in the model because of the crude description of transport in the swash zone.

A comparison between the present model and the Kriebel (1982, 1986) model was conducted to evaluate how bar formation would affect dune erosion. One hypothetical case involved a variation in water level which prevented bar development, and both models gave similar predictions of erosion. The description of the profile at the dune toe was more realistically described by the present model, based on experience with the LWT experiments, than by the Kriebel model, which distributed the eroded material more evenly over the surf zone. Another comparison case involved bar development, giving a significant difference in dune retreat, for which the Kriebel model produced a larger amount of erosion than the present model.

The numerical model was also used to simulate bar movement in the field at the U.S. Army Corps of Engineers Field Research Facility (FRF) at Duck, North Carolina. Four different storm events were used in the calibration that showed erosive profile response and offshore bar movement, and another, independent event was used for verification of the model. Compared to the optimum parameter values given by calibration against the LWT experiments, some parameter values had to be changed to achieve agreement with measured field profiles. In particular, the transport rate coefficient took a smaller value for the field

simulation than for the LWT cases, with an overall best value in a least-square sense of $0.7 \cdot 10^{-6} \, m^4/N$.

Bar movement and location of bar crest was well reproduced by the model both for the field calibration and verification runs. However, bar troughs were not pronounced enough in the model, and bar size was underestimated. Although bar face slopes produced by the model were steep for the LWT cases simulated, in agreement with the experiment data, model simulations for the field data with variable input waves and water level produced more gentle slopes in agreement with the field measurements. This supports the assumption of superposition implicit in the numerical model, where the effect of a random wave climate is simulated as the effect of a number of consecutive individual waves of different height and period.

In conclusion, this study validated the methodology of obtaining information about beach profile response in prototype-sized facilities and generalizing the information to field conditions. The developed numerical model successfully reproduced beach profile change both in large tanks and in the field. The approach of focusing on macro-scale profile features such as bars and berms proved highly productive, both for providing more thorough and quantitative understanding of beach profile change to wave action and for promoting development of numerical models for simulating coastal processes aimed at engineering use.

REFERENCES

Allen, J. R. 1970. "The Avalanching of Granular Solids on Dune and Similar Slopes," Journal of Geology, Vol 78, No 3, pp 326-351.

Aubrey, D. G. 1978. "Statistical and Dynamical Prediction of Changes in Natural Sand Beaches," unpublished Ph.D. thesis, University of California, San Diego, CA.

_____. 1979. "Seasonal Patterns of Onshore/Offshore Sediment Movement," Journal of Geophysical Research, Vol 84, No. C10, pp 6347-6354.

Aubrey, D. G., Inman, D. L., and Nordstrom. C. E. 1977. "Beach Profiles at Torrey Pines, California," Proceedings of the 15th Coastal Engineering Conference, American Society of Civil Engineers, pp 1297-1311.

Aubrey, D. G., Inman, D. L., and Winant, C. D. 1980. "The Statistical Prediction of Beach Changes in Southern California," Journal of Geophysical Research, Vol 85, No. C6, pp 3264-3276.

Aubrey, D. G., and Ross, R. M. 1985. "The Quantitative Description of Beach Cycles," Marine Geology, Vol 69, pp 155-170.

Bagnold, R. A. 1940. "Beach Formation by Waves; Some Model-Experiments in a Wave Tank," Journal of the Institution of Civil Engineers, No. 1, pp 27-52.

_____. 1963. "Mechanics of Marine Sedimentation," In The Sea, Vol 3, editor M. N. Hill, Interscience, New York, pp 507-528.

_____. 1966. "An Approach to the Sediment Transport Problem from General Physics," Geological Survey Professional Paper 422-I, Washington D. C..

Bailard, J. A. 1982. "An Energetics Total Load Sediment Transport Model for a Plane Sloping Beach," Naval Civil Engineering Laboratory, Report No. TN-1626.

Bailard, J. A., and Inman, D. L. 1981. "An Energetics Bedload Model for a Plane Sloping Beach: Local Transport," Journal of Geophysical Research, Vol 86, No. C3, pp 2035-2043.

271

Balsillie, J. H. 1984. "A Multiple Shore-Breaking Wave Trans-formation Computer Model," Florida Department of Natural Resources, Beaches and Shores Technical and Design Memorandum No. 84-4.

Basco, D. R. 1985. "A Qualitative Description of Wave Breaking," Journal of Waterway, Port, Coastal and Ocean Engineering, Vol 111, No. 2, pp 171-188.

Basco, D. R., and Yamashita, T. 1987. "Toward a Simple Model of the Wave Breaking Transition Region in Surf Zones," Proceedings of the 20th Coastal Engineering Conference, American Society of Civil Engineers, pp 955-970.

Bascom, W. N. 1951. "The Relationship Between Sand Size and Beach-Face Slope," Transactions American Geophysical Union, Vol 32, No. 6, pp 866-874.

Battjes, J. A. 1975. "Surf Similarity," Proceedings of the 14th Coastal Engineering Conference, American Society of Civil Engineers, pp 466-480.

Battjes, J. A., and Janssen, J. P. F. M. 1979. "Energy Loss and Set-Up Due to Breaking of Random Waves," Proceedings of the 16th Coastal Engineering Conference, American Society of Civil Engineers, pp 569-587.

Berg, D. W., and Duane, D. B. 1968. "Effect of Particle Size and Distribution on Stability of Artificially Filled Beach, Presque Isle Peninsula, Pennsylvania," Proceedings of the 11th Conference on Great Lakes Research, International Association of Great Lakes Research, pp 161-178.

Birkemeier, W. A. 1985a. "Time Scale of Nearshore Profile Changes," Proceedings of the 19th Coastal Engineering Conference, American Society of Civil Engineers, pp 1507-1521.

_____. 1985b. "Field Data on Seaward Limit of Profile Change," Journal of Waterway, Port, Coastal and Ocean Engineering, Vol 111, No. 3, pp 598-602.

Birkemeier, W. A., Kraus, N. C., Scheffner, N. W., and Knowles, S. C. 1987. "Feasibility Study of Quantitative Erosion Models for Use by the Federal Emergency Management Agency in the Prediction of Coastal Flooding," Technical Report CERC-87-8, Coastal Engineering Research Center, U.S. Army Engineer Waterways Experiment Station, Vicksburg, MS.

Boczar-Karakiewicz, B., and Davidson-Arnott, R. G. D. 1987. "Nearshore Bar Formation by Non-Linear Wave Processes - A Comparison of Model Results and Field Data," Marine Geology, Vol 77, pp 287-304.

Bowen, A. J. 1980. "Simple Models of Nearshore Sedimentation; Beach Profiles and Longshore Bars," In: The Coastline of Canada, editor S. B. McCann, Geological Survey of Canada, Paper 80-10, pp 1-11.

Bruun, P. 1954. "Coast Erosion and the Development of Beach Profiles," Technical Memorandum No. 44, Beach Erosion Board, U.S. Army Corps of Engineers.

_____. 1962. "Sea-Level Rise as a Cause of Shore Erosion," Journal of the Waterways and Harbors Division, American Society of Civil Engineers, Vol 88, No. WW1, pp 117-130.

Buhr Hansen, J., and Svendsen, I. A. 1975. "Laboratory Generation of Waves of Constant Form," Proceedings of the 14th Coastal Engineering Conference, American Society of Civil Engineers, pp 321-339.

Caldwell, J. M. 1959. "Shore Erosion by Storm Waves," Miscellaneous Paper No. 1-59, Beach Erosion Board, U.S. Army Corps of Engineers.

Carter, T. G., Liu, P. L-F., and Mei, C. C. 1973. "Mass Transport by Waves and Offshore Sand Bedforms," Journal of the Waterways, Harbors and Coastal Engineering Division, American Society of Civil Engineers, Vol 99, No. WW2, pp 165-184.

Chappell, J., and Eliot, I. G. 1979. "Surf-Beach Dynamics in Time and Space - An Australian Case Study, and Elements of a Predictive Model," Marine Geology, Vol 32, pp 231-250.

Chiu, T. Y. 1977. "Beach and Dune Response to Hurricane Eloise of September 1975," Proceedings of Coastal Sediments '77, American Society of Civil Engineers, pp 116-134.

Dally, W. R. 1980. "A Numerical Model for Beach Profile Evolution," unpublished M.S. Thesis, University of Delaware, Newark, DE.

_____. 1987. "Longshore Bar Formation - Surf Beat or Undertow," Proceedings of Coastal Sediments '87, American Society of Civil Engineers, pp 71-86.

Dally, W. R., and Dean, R. G. 1984. "Suspended Sediment Transport and Beach Profile Evolution," _Journal of Waterway, Port, Coastal and Ocean Engineering,_ Vol 110, No. 1, pp 15-33.

Dally, W. R., Dean, R. G., Dalrymple, R. A. 1985a. "Wave Height Variation Across Beaches of Arbitrary Profile," _Journal of Geophysical Research,_ Vol 90, No. C6, pp 11917-11927.

Dally, W. R., Dean, R. G., and Dalrymple, R. A. 1985b. "A Model for Breaker Decay on Beaches," _Proceedings of the 19th Coastal Engineering Conference,_ American Society of Civil Engineers, pp 82-98.

Dalrymple, R. A., and Thompson, W. W. 1977. "Study of Equilibrium Beach Profiles," _Proceedings of the 15th Coastal Engineering Conference,_ American Society of Civil Engineers, pp 1277-1296.

Davidson-Arnott, R. G. D. 1975. "Form, Movement and Sedimentological Characteristics of Wave-Formed Bars - A Study of their Role in Nearshore Equilibrium," unpublished Ph.D. thesis, Department of Geography, University of Toronto, Toronto.

_____. 1981. "Computer Simulation of Nearshore Bar Formation," _Earth Surface Processes and Landforms,_ Vol 6, pp 23-34.

Davidson-Arnott, R. G. D., and Pember, G. F. 1980. "Morphology and Sedimentology of Multiple Parallel Bar Systems, Southern Georgian Bay, Ontario," In: _The Coastline of Canada,_ editor S. B. McCann, Geological Survey of Canada, Paper 80-10, pp 417-428.

Davidson-Arnott, R. G. D., and Randall, D. C. 1984. "Spatial and Temporal Variations in Spectra of Storm Waves Across a Barred Nearshore," _Marine Geology,_ Vol 60, pp 15-30.

Davis, R. A., and Fox, W. T. 1972. "Coastal Processes and Nearshore Sand Bars," _Journal of Sedimentary Petrology,_ Vol 42, No. 2, pp 401-412.

Davis, R. A., Fox, W. T., Hayes, M. O., and Boothroyd, J. C. 1972. "Comparison of Ridge and Runnel Systems in Tidal and Non-Tidal Environments," _Journal of Sedimentary Petrology,_ Vol 42, No. 2, pp 413-421.

Dean, R. G. 1973. "Heuristic Models of Sand Transport in the Surf Zone," _Proceedings of the Conference on Engineering Dynamics in the Surf Zone,_ Sydney, Australia, pp 208-214.

_____. 1976. "Beach Erosion: Causes, Processes, and Remedial Measures," CRC Reviews in Environmental Control, CRC Press Inc, Vol 6, Issue 3, pp 259-296.

_____. 1977a. "Equilibrium Beach Profiles: U.S. Atlantic and Gulf Coasts," Department of Civil Engineering, Ocean Engineering Report No. 12, University of Delaware, Newark, DE.

_____. 1977b. "Equilibrium Beach Profiles and Response to Storms," Proceedings of the 15th Coastal Engineering Conference, American Society of Civil Engineers, pp 704-707.

_____. 1984. "Applications of Equilibrium Beach Profile Concepts," Coastal Engineering Abstracts, American Society of Civil Engineers, pp 140-141.

De Best, A., and Bijker, E. W. 1971. "Scouring of a Sand Bed in Front of a Vertical Breakwater," Report No. 71-1, Department of Civil Engineering, Delft University of Technology, The Netherlands.

Deguchi, I., and Sawaragi, T. 1985. "Calculation of the Rate of Net On-Offshore Sediment Transport on the Basis of Flux Concept," Proceedings of the 19th Coastal Engineering Conference, American Society of Civil Engineers, pp 1325-1341.

Dette, H. H. 1986. "Untersuchungen über Dünenabbrüche und Stranderosion im Grossen Wellenkanal," Die Küste, Heft 43, pp 247-282.

Dette, H. H., and Uliczka, K. 1987a. "Prototype Investigation on Time-Dependent Dune Recession and Beach Erosion," Proceedings of Coastal Sediments '87, American Society of Civil Engineers, pp 1430-1444.

_____. 1987b. "Velocity and Sediment Concentration Fields Across Surf Zones," Proceedings of the 20th Coastal Engineering Conference, American Society of Civil Engineers, pp 1062-1076.

Dingler, J. R., and Inman, D. L. 1977. "Wave-Formed Ripples in Nearshore Sands," Proceedings of the 15th Coastal Engineering Conference, American Society of Civil Engineers, pp 2109-2126.

Dolan, T. J. 1983. "Wave Mechanics for the Formation of Multiple Longshore Bars with Emphasis on the Chesapeake Bay," unpublished M.S. thesis, University of Delaware, Newark, DE.

Dolan, T. J., and Dean, R. G. 1984. "Multiple Longshore Sand Bars in the Upper Chesapeake Bay," <u>Estuarine Coastal and Shelf Science,</u> Vol 21, No. 5, pp 727-743.

Dyhr-Nielsen, M., and Sørensen, T. 1971 "Some Sand Transport Phenomena on Coasts with Bars," <u>Proceedings of the 12th Coastal Engineering Conference,</u> American Society of Civil Engineers, pp 855-865.

Eagleson, P. S., Glenne, B., and Dracup, J. A. 1963. "Equilibrium Characteristics of Sand Beaches," <u>Journal of the Hydraulics Division,</u> American Society of Civil Engineers, Vol 89, No. 1, pp 35-57.

Ebersole, B. A. 1987. "Measurements and Prediction of Wave Height Decay in the Surf Zone," <u>Proceedings of Coastal Hydrodynamics,</u> American Society of Civil Engineers, pp 1-16.

Edelman, T. 1969. "Dune Erosion During Storm Conditions," <u>Proceedings of the 11th Coastal Engineering Conference,</u> American Society of Civil Engineers, pp 719-722.

_____. 1973. "Dune Erosion During Storm Conditions," <u>Proceedings of the 13th Coastal Engineering Conference,</u> American Society of Civil Engineers, pp 1305-1311.

Evans, O. F. 1940. "The Low and Ball of the Eastern Shore of Lake Michigan," <u>Journal of Geology,</u> Vol 48, No. 5, pp 476-511.

Exon, N. F. 1975. "An Extensive Offshore Sand Bar Field in the Western Baltic Sea," <u>Marine Geology,</u> Vol 18, pp 197-212.

Fairchild, J. C. 1973. "Longshore Transport of Suspended Sand," <u>Proceedings of the 13th Coastal Engineering Conference,</u> American Society of Civil Engineers, pp 1062-1088.

Felder, W. N. 1978. "Simulation Modeling of Offshore Bars," Department of Environmental Sciences, unpublished Ph.D. thesis, University of Virginia, Charlottesville, VA.

Felder, W. N., and Fisher, J. S. 1980. "Simulation Model Analysis of Seasonal Beach Cycles," <u>Coastal Engineering,</u> Vol 3, pp 269-282.

Fox, W. T., and Davis, R. A. 1973. "Simulation Model for Storm Cycles and Beach Erosion on Lake Michigan," <u>Geological Society of America Bulletin,</u> Vol 84, pp 1769-1790.

Galvin, C. J. 1969. "Breaker Travel and Choice of Design Wave Height," _Journal of Waterways and Harbors Division,_ American Society of Civil Engineers, Vol 95, No. 2, pp 175-200.

_____. 1972. "Wave Breaking in Shallow Water," In: _Waves on Beaches and Resulting Sediment Transport,_ editor R. E. Meyer, Academic Press, pp 413-456.

Gourlay, M. R. 1968 "Beach and Dune Erosion Tests I," Report No. M 935/M 936, Delft Hydraulics Laboratory.

_____. 1981 "Beaches: Profiles, Processes and Permeability," _Proceedings of the 17th Coastal Engineering Conference,_ American Society of Civil Engineers, pp 1320-1339.

_____. 1985. "Beaches: States, Sediments and Set-Up," _Preprints of the Australasian Conference on Coastal and Ocean Engineering,_ Vol 1, pp 347-356.

Greenwood, B., and Davidson-Arnott, R. G. D. 1972. "Textural Variation in Sub-Environments of the Shallow-Water Wave Zone, Kouchibouguac Bay, New Brunswick, _Canadian Journal of Earth Sciences,_ Vol 9, No. 6, pp 679-687.

_____. 1975. "Marine Bars and Nearshore Sedimentary Processes, Kouchibouguac Bay, New Brunswick," In: _Nearshore Sediment Dynamics and Sedimentation,_ An Interdisciplinary Review, John Wiley and Sons, pp 123-150.

_____. 1979. "Sedimentation and Equilibrium in Wave-Formed Bars: A Review and Case Study," _Canadian Journal of Earth Sciences,_ Vol 16, No. 2, pp 312-332.

Greenwood, B., and Mittler, P. R. 1979. "Structural Indices of Sediment Transport in a Straight, Wave-Formed, Nearshore Bar," _Marine Geology,_ Vol 32, pp 191-203.

_____. 1984. "Sediment Flux and Equilibrium Slopes in a Barred Nearshore," _Marine Geology,_ Vol 60, pp 79-98.

Guza, R. T., and Bowen, A. J. 1977. "Resonant Interaction for Waves Breaking on a Beach," _Proceedings of the 15th Coastal Engineering Conference,_ American Society of Civil Engineers, pp 560-579.

Guza, R. T., and Thornton, E. B. 1982. "Swash Oscillations on a Natural Beach," _Journal of Geophysical Research,_ Vol 87, No. C1, pp 483-491.

Hallermeier, R. J. 1979. "Uses for a Calculated Limit Depth to Beach Erosion," Proceedings of the 16th Coastal Engineering Conference, American Society of Civil Engineers, pp 1493-1512.

_____. 1981. "Terminal Settling Velocity of Commonly Occurring Sand Grains," Sedimentology, Vol 28.

_____. 1982. "Oscillatory Bedload Transport: Data Review and Simple Formulation," Continental Shelf Research, Vol 1, pp 159-190.

_____. 1984. "Wave Cuts in Sand Slopes Applied to Coastal Models," Journal of Waterway, Port, Coastal and Ocean Engineering, Vol 110, No. 1, pp 34-49.

_____. 1987. "Applying Large Replicas of Shore Erosion by Storms," Proceedings of Coastal Sediments '87, American Society of Civil Engineers, pp 1415-1429.

Hands, E. B. 1976. "Observations of Barred Coastal Profiles under the Influence of Rising Water Levels, Eastern Lake Michigan, 1967-71," Technical Report 76-1, Coastal Engineering Research Center, U.S. Army Corps of Engineers, Ft. Belvoir, VA.

Hartnack, W. 1924. "Über Sandriffe," Jahrbuch der Geografischen Gesellschaft zu Greifswald, Band XL/XLII, pp 47-70.

Hashimoto, H., and Uda, T. 1980. "An Application of an Empirical Prediction Model of Beach Profile Change to the Ogawara Coast," Coastal Engineering in Japan, Vol 23, pp 191-204.

Hattori, M., and Kawamata, R. 1979. "Restoration of Sandy Beaches Fronting Seawalls," Proceedings of Coastal Structures '79, American Society of Civil Engineers, pp 388-404.

_____. 1981. "Onshore-Offshore Transport and Beach Profile Change," Proceedings of the 17th Coastal Engineering Conference, American Society of Civil Engineers, pp 1175-1193.

Hayden, B., Felder, W., Fisher, J., Resio, D., Vincent, L., and Dolan, R. 1975. "Systematic Variations in Inshore Bathymetry," Department of Environmental Sciences, Technical Report No. 10, University of Virginia, Charlottesville, VA.

Holman, R. A. 1986. "Extreme Value Statistics for Wave Run-Up on a Natural Beach," Coastal Engineering, Vol 9, pp 527-544.

Holman, R. A., and Bowen, A. J. 1982. "Bars, Bumps, and Holes: Models for the Generation of Complex Beach Topography," _Journal of Geophysical Research,_ 87, pp 457-468.

Horikawa, K., and Kuo, C. 1967. "A Study on Wave Transformation Inside the Surf Zone," _Proceedings of the 10th Coastal Engineering Conference,_ American Society of Civil Engineers, pp 217-233.

Howd, P. A., and Birkemeier, W. A. 1987. "Beach and Nearshore Survey Data: 1981-1984 CERC Field Research Facility," Technical Report CERC-87-9, Coastal Engineering Research Center, U.S. Army Engineer Waterways Experiment Station, Vicksburg, MS.

Hughes, S. A. 1983. "Movable-Bed Modeling Law for Coastal Dune Erosion," _Journal of Waterway, Port, Coastal and Ocean Engineering,_ American Society of Civil Engineers, Vol 109, No. 2, pp 164-179.

_____. 1984. "Movable-Bed Modeling Law for Coastal Dune Erosion," _Journal of Waterway, Port, Coastal and Ocean Engineering,_ Closure, Vol 110, No. 4, pp 504-507.

Hughes, S. A., and Chiu, T. Y. 1981. "Beach and Dune Erosion During Severe Storms," Report UFL/COEL-TR/043, Coastal and Oceanographic Engineering Department, University of Florida, Gainesville, FL.

Hughes, M. G., and Cowell, P. J. 1987. "Adjustment of Reflective Beaches to Waves," _Journal of Coastal Research,_ Vol 3, No. 2, pp 153-167.

Hunt, I. A. 1959. "Design of Seawalls and Breakwaters," _Journal of Waterways and Harbors Division,_ Vol 85, pp 123-152.

Hunter, R. E., Clifton, H. E., and Phillips, R. L. 1979. "Depositional Processes, Sedimentary Structures, and Predicted Vertical Sequences in Barred Nearshore Systems, Southern Oregon Coast," _Journal of Sedimentary Petrology,_ Vol 49, No. 3, pp 711-726.

Inman, D. L. 1957. "Wave Generated Ripples in Nearshore Sand," Technical Memorandum No. 100, Beach Erosion Board, U.S. Army Corps of Engineers.

Inman, D. L., and Bagnold, R. A. 1963. "Littoral Processes," In: _The Sea,_ Vol 3, editor M. N. Hill, Interscience, New York, pp 529-553.

279

Ippen, A. I., and Eagleson, P. S. 1955. "A Study of Sediment Sorting by Waves Shoaling on a Plane Beach," Technical Memorandum No. 63, Beach Erosion Board, U.S. Army Corps of Engineers.

Iwagaki, Y., and Noda, H. 1963. "Laboratory Studies of Scale Effects in Two-Dimensional Beach Processes," Proceedings of the 8th Coastal Engineering Conference, American Society of Civil Engineers, pp 194-210.

Jaffe, B. E., Sternberg, R. W., and Sallenger, A. H. 1985. "The Role of Suspended Sediment in Shore-Normal Beach Profile Changes," Proceedings of the 19th Coastal Engineering Conference, American Society of Civil Engineers, pp 1983-1996.

Jansen, P. C. M. 1986. "Laboratory Observations of the Kinematics in the Aerated Region of Breaking Waves," Coastal Engineering, Vol 9, pp 453-477

Johnson, J. W. 1949. "Scale Effects in Hydraulic Models Involving Wave Motion," Transactions of the American Geophysical Union, Vol 30, No. 4, pp 517-525.

Kajima, R., Shimizu, T., Maruyama, K., and Saito, S. 1983a. "Experiments of Beach Profile Change with a Large Wave Flume," Proceedings of the 18th Coastal Engineering Conference, American Society of Civil Engineers, pp 1385-1404.

Kajima, R., Saito, S., Shimizu, T., Maruyama, K., Hasegawa, H., and Sakakiyama, T. 1983b. "Sand Transport Experiments Performed by Using a Large Water Wave Tank," Data Report No. 4-1, Central Research Institute for Electric Power Industry, Civil Engineering Division. (in Japanese)

Kamphuis, J. W., and Bridgeman, S. G. 1975. "Placing Artificial Beach Nourishment," Proceedings of Coastal Engineering in the Oceans III, American Society of Civil Engineers, pp 197-216.

Kana, T. W. 1977. "Suspended Sediment Transport at Price Inlet, S. C.," Proceedings of Coastal Sediments '77, American Society of Civil Engineers, pp 366-382.

Kemp, P. H. 1961. "The Relationship Between Wave Action and Beach Profile Characteristics," Proceedings of the 7th Conference on Coastal Engineering, American Society of Civil Engineers, pp 262-277.

Keulegan, G. H. 1945. "Depths of Offshore Bars," Engineering Notes No. 8, Beach Erosion Board, U.S. Army Corps of Engineers.

_____. 1948. "An Experimental Study of Submarine Sand Bars," Technical Report No. 3, Beach Erosion Board, U.S. Army Corps of Engineers.

King, C. A. M., and Williams, W. W. 1949. "The Formation and Movement of Sand Bars by Wave Action," Geological Journal, Vol 113, pp 70-85.

Kobayashi, N. 1987. "Analytical Solutions for Dune Erosion by Storms," Journal of Waterway, Port, Coastal and Ocean Engineering, Vol 113, No. 4, pp 401-418.

Komar, P. D., and Gaughan, M. K. 1973. "Airy Wave Theory and Breaker Height Prediction," Proceedings of the 13th Coastal Engineering Conference, American Society of Civil Engineers, pp 405-418.

Kraus, N. C. 1987. "The Effects of Seawalls on the Beach: A Literature Review," Proceedings of Coastal Sediments '87, American Society of Civil Engineers, pp 945-960.

_____. 1988. "The Effects of Seawalls on the Beach: An Extended Review," In: The Effects of Seawalls on the Beach, editors N. C. Kraus and O. H. Pilkey, Journal of Coastal Research, in press.

Kraus, N. C., and Dean, J. L. 1987. "Longshore Sediment Transport Rate Distributions Measured by Trap," Proceedings of Coastal Sediments '87, American Society of Civil Engineers, pp 881-896.

Kraus, N. C., and Larson, M. 1988. "Beach Profile Change Measured in the Tank for Large Waves, 1956-1957 and 1962," Technical Report CERC-88-00, Coastal Engineering Research Center, U.S. Army Engineer Waterways Experiment Station, Vicksburg, MS, in press.

Kraus, N. C., Scheffner, N. W., Hanson, H., Chou, L. W., Cialone, M. A., Smith, J. M., and Hardy, T. A. 1986. "Coastal Processes at Sea Bright to Ocean Township, New Jersey, Volume I: Main Text and Appendix A," unpublished Draft Final Report, Coastal Engineering Research Center, U.S. Army Engineer Waterways Experiment Station, Vicksburg, MS.

Kriebel, D. L. 1982. "Beach and Dune Response to Hurricanes," unpublished M.S. Thesis, University of Delaware, Newark, DE.

_____. 1986. "Verification Study of a Dune Erosion Model," Shore and Beach, Vol 54, No. 3, pp 13-21.

_____. 1987. "Beach Recovery Following Hurricane Elena," <u>Proceedings of Coastal Sediments '87,</u> American Society of Civil Engineers, pp 990-1005.

Kriebel, D. L., and Dean, R. G. 1984. "Beach and Dune Response to Severe Storms," <u>Proceedings of the 19th Coastal Engineering Conference,</u> American Society of Civil Engineers, pp 1584-1599.

_____. 1985a. "Numerical Simulation of Time-Dependent Beach and Dune Erosion," <u>Coastal Engineering,</u> Vol 9, pp 221-245.

_____. 1985b. "Estimates of Erosion and Mitigation Requirements under Various Scenarios of Sea Level Rise and Storm Frequency for Ocean City, Maryland," Preliminary Report, Coastal and Oceanographic Department, University of Florida, Gainesville, Fl.

Kriebel, D. L., Dally, W. R., and Dean. R. G. 1986. "Beach Profile Response Following Severe Erosion Events," Report UFL/COEL-86/016, Coastal and Oceanographic Department, University of Florida, Gainesville, Fl.

_____. 1987 "Undistorted Froude Model for Surf Zone Sediment Transport," <u>Proceedings of the 20th Coastal Engineering Conference,</u> American Society of Civil Engineers, pp 1296-1310.

Lau, J., and Travis, B. 1973. "Slowly Varying Stokes Waves and Submarine Longshore Bars," <u>Journal of Geophysical Research,</u> Vol 78, No. 21, pp 4489-4497.

Lehmann, F. W. P. 1884. "Das Küstengebiet Hinterpommerns," <u>Zeitschrift das Gesellschaft für Erdkunde zu Berlin,</u> Band XIX.

Longuet-Higgins, M. S., and Stewart, R. W. 1963. "A Note on Wave Set-up," <u>Journal of Marine Research,</u> Vol 21, pp 4-10.

Madsen, O. S., and Grant, W. D. 1977. "Quantitative Description of Sediment Transport by Waves," <u>Proceedings of the 15th Coastal Engineering Conference,</u> American Society of Civil Engineers, pp 1093-1112.

Mason, C., Sallenger, A. H., Holman, R. A., and Birkemeier, W. A. 1985. "Duck82 - a Coastal Storm Processes Experiment," <u>Proceedings of the 19th Coastal Engineering Conference,</u> American Society of Civil Engineers, pp 1913-1927.

McKee, E. D., and Sterrett, T. S. 1961. "Laboratory Experiments on Form and Structure of Longshore Bars and Beaches," In: Geometry of Sandstone Bodies, editors Peterson, J. A., and Osmond, J. C., American Association of Petroleum Geologists, pp 13-28.

Mei, C. C. 1985. "Resonant Reflection of Surface Water Waves by Periodic Sandbars," Journal of Fluid Mechanics, Vol 152, pp 315-335.

Meyer, R. D. 1936. "A Model Study of Wave Action on Beaches," unpublished M.S. Thesis, Department of Civil Engineering, University of California, Berkeley, CA.

Miller, R. L. 1976. "Role of Vortices in Surf Zone Prediction: Sedimentation and Wave Forces," In: Beach and Nearshore Sedimentation, editors Davis, R. A., and Ethington, R. I., Society of Economic Paleontologists and Mineralogists, Special Publication No. 24, pp 92-114.

Mimura, N., Otsuka, Y., and Watanabe, A. 1987. "Laboratory Study on Two-Dimensional Beach Transformation Due to Irregular Waves," Proceedings of the 20th Coastal Engineering Conference, American Society of Civil Engineers, pp 1393-1406.

Mizuguchi, M. 1981. "An Heuristic Model of Wave Height Distribution in Surf Zone," Proceedings of the 17th Coastal Engineering Conference, American Society of Civil Engineers, pp 278-289.

Moore, B. D., 1982. "Beach Profile Evolution in Response to Changes in Water Level and Wave Height," unpublished M.S. thesis, University of Delaware, Newark, DE.

Mothersill, J. S. 1970. "Relationship of Grain-Size Modes to Nearshore Sedimentary Environments, Lake Superior, Ontario," Canadian Journal of Earth Sciences, Vol 7, pp 522-527.

Nayak, I. V. 1970. "Equilibrium Profiles of Model Beaches," Hydraulic Engineering Laboratory, Technical Report HEL-2-25, University of California, Berkeley, CA.

_____. 1971. "Equilibrium Profiles of Model Beaches," Proceedings of the 12th Coastal Engineering Conference, American Society of Civil Engineers, pp 1321-1340.

Nielsen, P. 1979. "Some Basic Concepts of Wave Sediment Transport," Paper No 20, Technical University of Denmark, Lyngby, Denmark.

Nilsson, H. D. 1979. "Multiple Longshore Sand Bars: Environments of Deposition and a Model for their Generation and Maintenance," unpublished Ph.D. thesis, University of Massachusetts, Amherst, MA.

Nishimura, H., and Sunamura, T. 1987. "Numerical Simulation of Beach Profile Changes," Proceedings of the 20th Coastal Engineering Conference, American Society of Civil Engineers, pp 1444-1455.

Ostle, B., and Mensing, R. W. 1975. Statistics in Research, The Iowa State University Press, Ames, IA.

Otto, T. 1911 "Der Darss und Zingst," Jahrbuch der Geografischen Gesellschaft zu Greifswald, Band XIII, pp 393-403.

Owens, E. H. 1977. "Temporal Variations in Beach and Nearshore Dynamics," Journal of Sedimentary Petrology, Vol 47, No 1, pp 168-190.

Raynor, A. C., and Simmons, G. W. 1964. "Summary of Capabilities," Miscellaneous Paper No. 3-64, Coastal Engineering Research Center, U. S. Army Corps of Engineers.

Rector, R. L. 1954. "Laboratory Study of Equilibrium Profiles of Beaches," Technical Memorandum No. 41, Beach Erosion Board, U.S. Army Corps of Engineers.

Rushu, R., and Liang, W. 1986. "Investigation on Two-Dimensional Transformation of Sandy Beach under Wave Action," Proceedings of the 3th International Symposium on River Sedimentation, The University of Mississippi, pp 378-387.

Sallenger, A. S., Holman, R. A., and Birkemeier, W. A. 1985. "Storm-Induced Response of a Nearshore-Bar System," Marine Geology, 64, pp 237-257.

Sasaki, T. 1983. "Three-Dimensional Topographic Changes on the Foreshore Zone of Sandy Beaches," Science Report, Institute of Geoscience, University of Tsukuba, Section A, Vol 4, pp 69-95.

Sato, S., and Horikawa, K. 1987. "Laboratory Study on Sand Transport over Ripples Due to Asymmetric Oscillatory Flows," Proceedings of the 17th Coastal Engineering Conference, American Society of Civil Engineers, pp 1481-1495.

Savage, R. P. 1959. "Notes on the Formation of Beach Ridges," Annual Bulletin, Beach Erosion Board, U.S. Army Corps of Engineers, pp 31-35.

284

Saville, T. 1957. "Scale Effects in Two Dimensional Beach Studies," Transactions from the 7th General Meeting of the International Association of Hydraulic Research, Vol 1, pp A3-1-A3-10.

Sawaragi, T., and Deguchi, I. 1981. "On-Offshore Sediment Transport Rate in the Surf Zone," Proceedings of the 17th Coastal Engineering Conference, American Society of Civil Engineers, pp 1194-1214

Sayao, O. S. F. J. 1984. "Movable-Bed Modeling Law for Coastal Dune Erosion," Journal of Waterway, Port, Coastal and Ocean Engineering, Discussion, Vol 110, No. 4, pp 493-495.

Saylor, J. H., and Hands, E. B. 1971. "Properties of Longshore Bars in the Great Lakes," Proceedings of the 12th Coastal Engineering Conference, American Society of Civil Engineers, pp 839-853.

Scott, T. 1954. "Sand Movement by Waves," Technical Memorandum No. 48, Beach Erosion Board, U.S. Army Corps of Engineers.

Seelig, W. N. 1983a. "Prediction of Beach Erosion and Accretion," unpublished manuscript, Coastal Engineering Research Center, 42 pp.

_____. 1983b. "Understanding Beach Erosion and Accretion," Journal of Waterway, Port, Coastal and Ocean Engineering, American Society of Civil Engineers, Vol 49, No. 4, pp 490-494.

Seymour, R. J. 1987. "An Assessment of NSTS," Proceedings of Coastal Sediments '87, American Society of Civil Engineers, pp 642-651.

Shepard, F. P. 1950. "Longshore-Bars and Longshore-Troughs," Technical Memorandum No. 15, Beach Erosion Board, U. S. Army Corps of Engineer.

Shibayama, T. 1984. "Sediment Transport Mechanism and Two-Dimensional Beach Transformation Due to Waves," unpublished Ph.D. thesis, University of Tokyo, Tokyo, Japan.

Shibayama, T., and Horikawa, K. 1980a. "Bed Load Measurement and Prediction of Two-Dimensional Beach Transformation Due to Waves," Coastal Engineering in Japan, Vol 23, pp 179-190.

_____. 1980b. "Laboratory Study on Sediment Transport Mechanism Due to Wave Action," Proceedings of the Japanese Society of Civil Engineers, No. 296, April, pp 131-141.

Shimizu, T., Saito, S., Maruyama, K., Hasegawa, H., and Kajima R. 1985. "Modeling of Onshore-Offshore Sand Transport Rate Distribution Based on the Large Wave Flume Experiments," Civil Engineering Laboratory Report No. 384028. (in Japanese)

Shore Protection Manual. 1984. 4th ed., 2 vols, U.S. Army Engineer Waterways Experiment Station, Coastal Engineering Research Center, U.S. Government Printing Office, Washington, DC.

Short, A. D. 1975a. "Offshore Bars Along the Alaskan Arctic Coast," Journal of Geology, Vol 83, pp 209-221.

_____. 1975b. "Multiple Offshore Bars and Standing Waves," Journal of Geophysical Research, Vol 80, No. 27, pp 3838-3840.

_____. 1979. "Three Dimensional Beach-Stage Model," Journal of Geology, Vol 87, pp 553-571.

Shuto, N. 1974. "Nonlinear Long Waves in a Channel of Variable Section," Coastal Engineering in Japan, Vol 17, pp 1-12.

Singamsetti, S. R., and Wind, H. G. 1980. "Breaking Waves. Characteristics of Shoaling and Breaking Periodic Waves Normally Incident to Plane Beaches of Constant Slope," Delft Hydraulics Laboratory, Report M 1371.

Skjelbreia, J. E. 1987. "Observations of Breaking Waves on Sloping Bottoms by Use of Laser Doppler Velocimetry," Report No. KH-R-48, Division of Engineering and Applied Science, California Institute of Technology, Pasadena, CA.

Smith, J., and Kraus, N. C. 1988. "An Analytical Model of Wave-Induced Longshore Current Based on Power Law Wave Height Decay," Miscellaneous Paper CERC-88-3, Coastal Engineering Research Center, U.S. Army Engineer Waterways Experiment Station, Vicksburg, MS.

Sonu, C. J. 1969. "Collective Movement of Sediment in Littoral Environment," Proceedings of the 11th Coastal Engineering Conference, American Society of Civil Engineers, pp 373-400.

_____. 1970. "Beach Changes by Extraordinary Waves Caused by Hurricane Camille," Coastal Studies Institute, Technical Report 77, Louisiana State University, Baton Rouge, LA, pp 33-45.

Stive, M. J. F. 1987. "A Model for Cross-Shore Sediment Transport," Proceedings of the 20th Coastal Engineering Conference, American Society of Civil Engineers, pp 1550-1564.

Stive, M. J. F., and Battjes, J. A. 1985. "A Model for Offshore Sediment Transport," Proceedings of the 19th Coastal Engineering Conference, American Society of Civil Engineers, pp 1420-1436.

Sunamura, T. 1975. "A Study of Beach Ridge Formation in Laboratory," Geographical Review of Japan, 48-11, pp 761-767.

_____. 1981a. "Bedforms Generated in a Laboratory Wave Tank," Science Reports of the Institute of Geoscience, University of Tsukuba, Section A, Vol 2, pp 31-43.

_____. 1981b. "A Laboratory Study of Offshore Transport of Sediment and a Model for Eroding Beaches," Proceedings of the 17th Coastal Engineering Conference, American Society of Civil Engineers, pp 1051-1070.

_____. 1983. "A Predictive Model for Shoreline Changes on Natural Beaches Caused by Storm and Post-Storm Waves," Transactions of the Japanese Geomorphological Union, Vol 4, pp 1-10.

_____. 1984a. "On-Offshore Sediment Transport Rate in the Swash Zone of Laboratory Beaches," Coastal Engineering in Japan, Vol 27, pp 205-212.

_____. 1984b. "Quantitative Predictions of Beach-Face Slopes," Geological Society of America Bulletin, Vol 95, pp 242-245.

_____. 1988. "Sandy Beach Geomorphology as Elucidated by Laboratory Modeling," In: Coastal Modeling: Techniques and Application, Elsevier, in press.

Sunamura, T., and Horikawa, K. 1975. "Two-Dimensional Beach Transformation Due to Waves," Proceedings of the 14th Coastal Engineering Conference, American Society of Civil Engineers, pp 920-938.

Sunamura, T. and Maruyama, K. 1987. "Wave-Induced Geomorphic Response of Eroding Beaches - with Special Reference to Seaward Migrating Bars," Proceedings of Coastal Sediments '87, American Society of Civil Engineers, pp 884-900.

Sunamura, T., and Takeda, I. 1984. "Landward Migration of Inner Bars," Marine Geology, 60, pp 63-78.

Svendsen, I. A. 1984. "Wave Heights and Set-Up in a Surf Zone," Coastal Engineering, Vol 8, pp 303-329.

_____. 1987. "Analysis of Surf Zone Turbulence," Journal of Geophysical Research, Vol 92, No. C5, pp 5115-5124.

Svendsen, I. A., Madsen, P. A., and Buhr Hansen, J. 1979. "Wave Characteristics in the Surf Zone," _Proceedings of the 14th Coastal Engineering Conference,_ American Society of Civil Engineers, pp 520-539.

Swart, D. H. 1975. "A Schematization of Onshore-Offshore Transport," _Proceedings of the 14th Coastal Engineering Conference,_ American Society of Civil Engineers, pp 884-900.

_____. 1977. "Predictive Equations Regarding Coastal Transport," _Proceedings of the 15th Coastal Engineering Conference,_ American Society of Civil Engineers, pp 1113-1132.

Takeda, I. 1984. "Beach Changes by Waves," Science Report, Institute of Geoscience, University of Tsukuba, Japan, Sect A, Vol 5, pp 29-63.

Takeda, I., and Sunamura, T. 1987. "Beach Changes by Storm waves," _Proceedings of the 20th Coastal Engineering Conference,_ American Society of Civil Engineers, pp 1612-1622.

Thomas, K. V., and Baba, M. 1986. "Berm Development on a Monsoon-Influenced Microtidal Beach," _Sedimentology,_ Vol 33, pp 537-546.

Uliczka, K., and Dette, H. H. 1987. "About the Effect of Monochromatic and Irregular Waves on Beach and Dune Profiles," _Proceedings of Seminar on Hydrologie und Küsteningenieurwesen,_ Hannover.

van de Graaff, J. 1983. "Probabilistic Design of Dunes," _Proceedings of Coastal Structures '83,_ American Society of Civil Engineers, pp 820-831.

van Hijum, E. 1975. "Equilibrium Profiles of Coarse Material Under Wave Attack," _Proceedings of the 14th Coastal Engineering Conference,_ American Society of Civil Engineers, pp 939-957.

_____. 1977. "Equilibrium Profiles and Longshore Transport of Coarse Material Under Oblique Wave Attack," _Proceedings of the 15th Coastal Engineering Conference,_ American Society of Civil Engineers, pp 1258-1276.

van Hijum, E., and Pilarczyk, K. W. 1982. "Gravel Beaches - Equilibrium Profile and Longshore Transport of Coarse Material under Regular and Irregular Wave Attack," Delft Hydraulics Laboratory, Publication No. 274.

Vellinga, P. 1982. "Beach and Dune Erosion During Storm Surges," Publication No. 276, Delft Hydraulics Laboratory.

_____. 1983. "Predictive Computational Model for Beach and Dune Erosion During Storm Surges," _Proceedings of Coastal Structures '83_, American Society of Civil Engineers, pp 806-819.

_____. 1984. "Movable-Bed Modeling Law for Coastal Dune Erosion," _Journal of Waterway, Port, Coastal and Ocean Engineering_, Discussion, Vol 110, No. 4, pp 495-504.

_____. 1986. "Beach and Dune Erosion During Storm Surges," Delft Hydraulics Communication No. 372, Delft Hydraulics Laboratory.

Verhagen, H. J. 1985. "Guideline for the Judgement of Safety of Dunes as Coastal Defense," Ministerie van Verkeer en Waterstaat, preliminary version.

Visser, C. 1983. "Design of Dunes as Coastal Protection in the Delta Area of the Netherlands," _Proceedings of Coastal Structures '83_, American Society of Civil Engineers, pp 792-805.

Wang, H., Dalrymple, R. A., and Shiau, J. C. 1975. "Computer Simulation of Beach Erosion and Profile Modification Due to Waves," _Proceedings of the Symposium on Modeling Techniques_, American Society of Civil Engineers, pp 1369-1384.

Watanabe, A. 1982. "Numerical Models of Nearshore Currents and Beach Deformation," _Coastal Engineering in Japan_, Vol 25, pp 147-161.

_____. 1985. "Three-Dimensional Predictive Model of Beach Evolution Around a Structure," _Proceedings of International Symposium on Water Wave Research_, University of Hannover, pp 121-142.

Watanabe, A., Riho, Y., and Horikawa, K. 1981. "Beach Profiles and On-Offshore Sediment Transport," _Proceedings of the 17th Coastal Engineering Conference_, American Society of Civil Engineers, pp 1106-1121.

Waters, C. H. 1939. "Equilibrium Slopes of Sea Beaches," unpublished M.S. thesis, University of California, Berkeley, CA.

Watts, G. M. 1953. "A Study of Sand Movement at South Lake Worth Inlet, Florida," Technical Memorandum No. 42, Beach Erosion Board, U.S. Army Corps of Engineers.

_____. 1954. "Laboratory Study of Effect of Varying Wave Periods on Beach Profiles," Technical Memorandum No. 53, Beach Erosion Board, Corps of Engineers, Department of the Army.

Watts, G. M., and Dearduff, R. F. 1954. "Laboratory Studies of Effect of Tidal Action on Wave-Formed Beach Profiles," Technical Memorandum No. 52, Beach Erosion Board, Corps of Engineers, Department of the Army.

Weggel, R. J. 1972. "Maximum Breaker Height," Journal of the Waterways, Harbors and Coastal Engineering Division, American Society of Civil Engineers, Vol 98, No. 1, pp 529-547.

Wells, D. R. 1967. "Beach Equilibrium and Second-Order Wave Theory," Journal of Geophysical Research, Vol 72, No. 2, pp 497-504.

Winant, C. D., Inman, D. L., and Nordstrom, C. E. 1975. "Description of Seasonal Beach Changes Using Empirical Eigenfunctions," Journal of Geophysical Research, Vol 80, No. 15, pp 1979-1986.

Wright, L. D., Chappel, J., Thom, B. G., Bradshaw, M. P., and Cowell, P. 1979. "Morphodynamics of Reflective and Dissipative Beach and Inshore Systems: Southeastern Australia," Marine Geology, Vol 32, pp 105-140.

Wright, L. D., Nielsen, P., Shi, N. C., and List, J. H. 1986. "Morphodynamics of a Bar-Trough Surf Zone," Marine Geology, Vol 70, pp 251-285.

Wright, L. D., and Short, A. D. 1984. "Morphodynamic Variability of Surf Zones and Beaches: a Synthesis," Marine Geology, Vol 56, pp 93-118.

Wright, L. D., Short, A. D., and Green, M. O. 1985. "Short-Term Change in the Morphodynamic State of Beaches and Surf Zones: An Empirical Predictive Model," Marine Geology, Vol 62, pp 339-364.

Wright, L. D., Short, A. D., Boon, J. D., Hayden, B., Kimball, S., and List, J. H. 1987. "Morphodynamic Responses of an Energetic Beach to Temporal Variations in Wave Steepness, Tide Range, and Incident Wave Groupiness," Marine Geology, 74, pp 1-20.

Zenkovich, V. P. 1967. "Submarine Sand Bars and Related Formations," In: Processes of Coastal Development, editor J. A. Steers, Oliver and Boyd Ltd, New York, pp 219-236.

APPENDIX A: NOTATION

A	Shape parameter for equilibrium beach profile ($m^{-1/3}$)
D	Median grain size of beach sand (m)
D	Wave energy dissipation per unit water volume ($Nm/m^3/sec$)
D_{eq}	Equilibrium energy dissipation per unit water volume ($Nm/m^3/sec$)
g	Acceleration of gravity (m/sec^2)
h	Water depth (m)
h_c	Depth to bar crest (m)
$h_{c,i}$	Calculated profile depth at grid point i (m)
$h_{m,i}$	Measured profile depth at grid point i (m)
h_t	Depth to bar trough (m)
E	Wave energy density (Nm/m^2)
F	Wave energy flux (Nm/m/sec)
F_s	Stable wave energy flux (Nm/m/sec)
C_g	Wave group velocity (m/sec)
H	Wave height (m)
H_{avg}	Mean wave height (m)
H_{mo}	Energy-based significant wave height (m)
K	Transport rate coefficient (m^4/N)
i	Integer number
k	Integer number
l_b	Berm length (m)
l_B	Bar length (m)
l_p	Plunge distance (m)
l_R	Runup length (m)
l_t	Trough length (m)
l_{tc}	Distance between break point and bar trough (m)
L	Wavelength (m)
n	Exponent determining spatial decay of transport rate in wave reformation zones
N	Number of cells where avalanching occurs

q	Cross-shore sand transport rate ($m^3/m/sec$)
q_b	Transport rate at break point ($m^3/m/sec$)
q_m	Peak transport rate ($m^3/m/sec$)
q_m	Minimum transport rate in wave reformation zone ($m^3/m/sec$)
q_{mo}	Peak transport rate at time t=0 ($m^3/m/sec$)
q_r	Transport rate at wave reformation point ($m^3/m/sec$)
Q_A	Average absolute transport rate ($m^3/m/sec$)
r	Correlation coefficient
r^2	Coefficient of determination
R	Sum of squares of difference between measured and calculated beach profile (m^2)
S	Specific gravity of sand
S_{xx}	Radiation stress component directed onshore (N/m)
t	Time (sec)
T	Wave period (sec)
U	Ursell number
V	Bar or berm volume (m^3/m)
w	Sand fall velocity (m/sec)
x	Cross-shore coordinate (m)
x_1	Seaward location of no profile change (m)
x_m	Location of minimum transport rate in wave reformation zone (m)
x_o	Shoreward location of no profile change (m)
x_r	Location of wave reformation point (m)
x_{CM}	Location of bar mass center (m)
z	Depth coordinate (m)
z_b	Maximum berm height (m)
z_B	Maximum bar height (m)
z_R	Height of active subaerial profile
α	Temporal rate coefficient (sec^{-1})
β	Beach slope
β_1	First seaward bar slope
β_2	Second seaward bar slope

β_3 Shoreward bar slope

β_4 Terrace slope

β_5 Step slope

γ Ratio between wave height and water depth at breaking

Γ Stable wave height coefficient

Δ Change in quantity

ϵ Slope-related transport rate coefficient (m^2/sec)

η Wave set-up or set-down (m)

κ Wave decay coefficient

λ Spatial decay coefficient (m^{-1})

ν Spatial decay coefficient (m^{-1})

ρ Density of water (kg/m^3)

ϕ_1 Shoreward berm slope

ϕ_2 Seaward berm slope

Subscripts:

    b   Breaking condition

    eq   Equilibrium condition

    i   Specific value of a variable

    m   Measured quantity

    o   Deepwater condition

    p   Predicted quantity

    1,2   Specific value of a variable

Superscripts:

    k   Specific value of a variable